Adaptive strategies of *Listeria monocytogenes*

Evolved variants with
altered stress resistance and fitness

Xuchuan Ma

Propositions

1. There is another route leading to Sigma B activation apart from the regular RsbV-RsbW partner switching model.
   (This thesis)

2. Losing LacR-mediated lactose utilization capacity contributes to a higher probability of *Listeria monocytogenes* contamination in dairy products.
   (This thesis)

3. Given that a greater emphasis on falsification may accelerate scientific knowledge progress (Rajtmajer et al., 2022, eLife, 11, e78830), publication of reliable negative results is of underestimated value.

4. Studying philosophy aids in relieving stress on the path to a Doctor of Philosophy degree.

5. Artificial intelligence emphasizes human subjectivity.

6. Forgetting old skills is beneficial for learning advanced similar skills.

Propositions belonging to the thesis, entitled

Adaptive strategies of *Listeria monocytogenes*: Evolved variants with altered stress resistance and fitness

Xuchuan Ma

Wageningen, 9 April 2024

Adaptive strategies of *Listeria monocytogenes*

Evolved variants with altered stress resistance and fitness

Xuchuan Ma

Thesis committee

Promotors
Prof. Dr T. Abee
Personal chair at the Laboratory of Food Microbiology
Wageningen University & Research

Prof. Dr H.M.W. den Besten
Personal chair at the Laboratory of Food Microbiology
Wageningen University & Research

Prof. Dr M.H. Zwietering
Professor of Food Microbiology
Wageningen University & Research

Other members
Prof. Dr M. Kleerebezem, Wageningen University & Research
Prof. Dr C. Hill, University College Cork, Ireland
Dr M. Nierop Groot, Wageningen University & Research
Dr A. Zomer, Veterinary Medicine, Utrecht University

This research was conducted under the auspices of the VLAG Graduate School (Biobased, Biomolecular, Chemical, Food and Nutrition Sciences).

Adaptive strategies of *Listeria monocytogenes*
Evolved variants with altered stress resistance and fitness

Xuchuan Ma

Thesis
submitted in fulfilment of the requirements for the degree of doctor
at Wageningen University
by the authority of the Rector Magnificus,
Prof. Dr C. Kroeze,
in the presence of the
Thesis Committee appointed by the Academic Board
to be defended in public
on Tuesday 9 April 2024
at 1.30 p.m. in the Omnia Auditorium.

Xuchuan Ma
Adaptive strategies of *Listeria monocytogenes*: Evolved variants with altered stress resistance and fitness
198 pages

PhD Thesis Wageningen University, Wageningen, the Netherlands (2024)
With references, with summary in English

DOI 10.18174/645586

Table of content

1

General introduction

Xuchuan Ma

1.1 Food safety

As part of the right to an adequate standard of living, the right to food is recognized in the 1948 Universal Declaration of Human Rights and is enshrined in the 1966 International Covenant on Economic, Social and Cultural Rights (United Nations (General Assembly), 1966). The adequacy requires food to be safe for human consumption and free from adverse substances (UN Committee on Economic, 1999). However, the World Health Organization (WHO) estimated that 31 foodborne hazards caused 600 million illnesses, resulting in 420,000 deaths and 33 million disability-adjusted life year (DALY) globally in 2010, demonstrating that the global burden of foodborne disease is of the same order of magnitude as major infectious diseases such as HIV/AIDS, malaria and tuberculosis (Havelaar et al., 2015). Most of these foodborne hazards are foodborne microbial hazards, including norovirus, *Campylobacter* spp., pathogenic *Escherichia coli*, *Salmonella* spp., *Shigella* spp., hepatitis A, and *Listeria monocytogenes* (Havelaar et al., 2015). Among these pathogens, *L. monocytogenes* is notable for its low incidence but high case-fatality rates, ranging from 12 to 41 percent (Huang et al., 2023). Consequently, *L. monocytogenes* emerges as a critical focus in food safety research and is subject to stringent control by food producers and authorities.

1.2 *Listeria monocytogenes*: an important foodborne pathogen

Listeria monocytogenes is a small rod-shaped Gram-positive non-spore forming bacterium firstly isolated from rabbits and guinea pigs in 1924 (Murray et al., 1926). It was recognized as the aetiological agent of a human disease in the 1970s and identified as a foodborne pathogen in the 1980s (Schlech et al., 1983). By 2023, the genus *Listeria* consists of 21 validly published species, of which only *Listeria monocytogenes* and *Listeria ivanovii* are considered pathogenic (Carlin et al., 2022). *L. ivanovii* has been considered to infect mainly ruminants, whereas *L. monocytogenes* infects animals and humans with greatest importance for global public health and economics in its genus (Allerberger and Wagner, 2010; Quereda et al., 2021). *L. monocytogenes* can cause a severe foodborne disease named listeriosis (Buchanan et al., 2017; EFSA and ECDC, 2022).

Listeriosis outbreaks continue to occur globally, with the largest and most deadly one having occurred in South Africa between 2017 and 2018 where 937 laboratory-confirmed cases and 193 deaths were reported (Thomas et al., 2020). This outbreak has been linked to the consumption of ready-to-eat (RTE) meat products (polony) contaminated by *L. monocytogenes* 4b isolates. In the European Union (EU), *L. monocytogenes* was identified in 23 outbreaks in 2021, exhibiting a 13.7% case-fatality rate (EFSA and ECDC, 2022). Notably, for high-risk populations, particularly the elderly, the case-fatality rate can escalate to as high as 39.0% (Huang et al., 2023). Therefore, despite the relatively low annual incidence in high-income countries of around five cases per 1,000,000 population, listeriosis is considered as one of the most important foodborne diseases at the patient level (Allende et al., 2022; EFSA and ECDC, 2021).

Importantly, the incidence of listeriosis has a trend of increasing in Europe and internationally, and several food products have recently been identified as vehicles for human foodborne listeriosis including stone fruit, caramel apples, and plant-based milk alternatives (Desai et al., 2019; EFSA and ECDC, 2021; European Commission, 2023)

1.3 Foods related to listeriosis

L. monocytogenes has been isolated from natural environment, farms, silage, decaying vegetables as well as human and animal feces (Quereda et al., 2021). Due to the ubiquity of *L. monocytogenes*, it can be introduced into foods and food industries as a result of cross-contamination by human carriers, transportation of animals, raw food, and materials from crops, soil and silage (Castro et al., 2018; Grif et al., 2003; Quereda et al., 2021). In addition, the growth capacity at temperatures below 4°C makes refrigeration ineffective to fully restrict the proliferation of *L. monocytogenes* (Quereda et al., 2021; Walker et al., 1990). Foods mostly associated with foodborne listeriosis include industrially processed Ready-to-eat (RTE) foods that: (i) support growth of *L. monocytogenes*, (ii) have a long recommended refrigerated shelf-life, and (iii) are consumed without further bactericidal treatment (e.g. cooking) (FAO/WHO, 2004). Various RTE food groups such as meat, dairy products, (shell)fish and fruits/vegetables are important attributions associated with *L. monocytogenes*, with median estimates of ~40%, ~26%, ~6% and ~8%, respectively (Allende et al., 2022). Notably, different *L. monocytogenes* genotypes are associated with different food groups, which suggests the adaptation of *L. monocytogenes* subspecies to distinct ecological niches and to different food products contamination routes (Maury et al., 2019).

1.4 *L. monocytogenes* biodiversity

L. monocytogenes is ubiquitous in farm environments and animals with high genetic diversity (Castro et al., 2018; Gómez-Laguna et al., 2020). The first method developed for subtype discrimination of *L. monocytogenes* was serotyping, which is based on agglutination of somatic and flagellar antigens and can classify *L. monocytogenes* into at least 13 serotypes (Table 1.1) (Orsi et al., 2011; Paterson, 1940; Seeliger and Höhne, 1979). The serotypes 1/2a, 1/2b, and 4b make up for most of the strains associated with human listeriosis cases and outbreaks (McLauchlin et al., 2004). Further multilocus enzyme electrophoresis and partial sequence data analyses have shown that *L. monocytogenes* isolates represent at least four phylogenetic lineages, and each lineage includes specific serotypes and has distinct characteristics (Piffaretti et al., 1989; Rasmussen et al., 1995; Roberts et al., 2006; Ward et al., 2008). Lineage I or serotype 4b and occurs more often in clinical isolates, and lineage II or serotypes 1/2a and 1/2c are more associated with food products (Gray et al., 2004; Jacquet et al., 2004; McLauchlin, 1990; Ward et al., 2008). In addition, multilocus sequence typing (MLST) based on seven housekeeping genes (length 399–537 bp), which are spread across dispersed genomic locations, further differentiates *L. monocytogenes* on the strain level to clonal complexes (CC) (Ragon et al., 2008). Each CC had a unique or

dominant serotype (4b for CC1, CC2 and CC4, 1/2b for CC3 and CC5, 1/2a for CC7, and 1/2c for CC9) (Ragon et al., 2008). Lineage I CC1, CC2, CC4 and CC6 are strongly associated with clinical origins, which suggests these CCs are potentially hypervirulent, while lineage II CC9 and CC121 are strongly associated with food origins (Maury et al., 2016). Moreover, potentially hypervirulent CC1, CC4 and CC6 are associated with dairy products and exhibit a high adaption to the host environment, reflected by better intestinal colonization and a higher intestinal tissue invasion rate (Maury et al., 2019; Moura et al., 2021). Conversely, the major hypovirulent CC9 and CC121 are associated with meat products and are adapted well to food-processing environment with higher prevalence of genes involved in stress resistance and tolerance to disinfectants (Maury et al., 2019; Moura et al., 2021). Currently, comparative whole genome sequencing (WGS) has been applied for characterization and differentiation on the strain level with higher discriminatory power for *L. monocytogenes*. The WGS approach can simultaneously supply information on serotype, antimicrobial resistant genes, virulence markers, and also allow clustering based on single nucleotide polymorphism (SNP) analysis and core genome and whole genome MLST (cg/wgMLST) (Ribot et al., 2019).

Table 1.1: ***L. monocytogenes* lineages, serotypes and CCs, adapted from Orsi et al. (2011)**

Lineage	Serotypes	Most prevalent CCs	Distribution
I	1/2b, 3b, 3c, 4b	CC1, CC2, CC3, CC4, CC5, CC6	Commonly isolated from various sources; overrepresented among human isolates
II	1/2a, 1/2c, 3a, 3c	CC7, CC8, CC9, CC121, CC14, CC155	Commonly isolated from various sources; overrepresented among food and food-related as well as natural environments
III	4a, 4b, 4c	CC69, CC131, CC641	Most isolates obtained from ruminants
IV	4a, 4b, 4c	CC562	Rarely isolated; most isolates obtained from ruminants

1.5 Population heterogeneity of *L. monocytogenes*

Using the WGS approach, listeriosis outbreaks could be traced to *L. monocytogenes* isolates that persisted in natural, urban and food procession environments for years (Elson et al., 2019; Fagerlund et al., 2022; Holch et al., 2013; Hurley et al., 2019; Li et al., 2017). Persistence is defined as the long-term survival of certain pathogens in specific environments, which may contribute to food contamination and transmission of the pathogen to humans (Ferreira et al., 2014). There are several determinants that contribute to the survival of *L. monocytogenes* in food production environments, including strain diversity and population heterogeneity (Abee et al., 2016; Ferreira et al., 2014; Lake et al., 2021). Population heterogeneity includes genetic and non-genetic population variability, and both can generate phenotypic variation in a population (Davidson and Surette, 2008; Ryall et al., 2012; Smits et al., 2006). During the inactivation of pathogens, the differences in stress resistance between individual cells can make the inactivation deviate from linearity, showing curves with pronounced

tails. Tailing of inactivation curves can result in a higher-than-expected number of surviving cells and selection of stress-resistant variants (Abee et al., 2016; Karatzas and Bennik, 2002; Rajkovic et al., 2009). Several *L. monocytogenes* variants with enhanced multi-stress resistance have been isolated, including *ctsR* and *rpsU* mutants (Karatzas et al., 2003; Metselaar et al., 2016; Van Boeijen et al., 2008). The variants derived from high hydrostatic pressure treatments often carry mutations in the *ctsR* gene. This gene encodes the repressor CtsR, which controls class III heat shock genes such as *clpC*, *clpP*, and *clpE* (Gaballa et al., 2019). The proteins ClpC, ClpP, and ClpE, functioning as proteases, are crucial for degrading damaged or misfolded proteins, thereby aiding *L. monocytogenes* survival under stress. Mutations in *ctsR* disrupt this repression, leading to increased transcription of stress response genes (Abee et al., 2016; Karatzas et al., 2003). The *rpsU* mutants, arising from acid stress treatments, are elaborated upon in the following section.

1.6 *rpsU* mutations lead to stress resistance changes

Previous studies identified 23 stable stress-resistant *L. monocytogenes* variants from acid-treated strain LO28, with 11 harboring mutations in the *rpsU* gene locus, responsible for encoding the 30S ribosomal sub-unit protein S21 (RpsU) (Metselaar et al., 2015; Metselaar et al., 2013). These variants demonstrated a trade-off between reduced growth rates and increased resistance to acid, heat, high hydrostatic pressure, and benzalkonium chloride (Metselaar et al., 2015; Metselaar et al., 2013). Two variants have been selected for further research, namely, variant V14 and variant V15 (Koomen et al., 2018). V14 possesses deletions in *rpsU*, *yqeY*, and part of *phoH*, whereas V15 features a guanine to cytosine nucleotide substitution $rpsU^{\mathrm{G50C}}$, altering the RpsU protein ($\mathrm{RpsU}^{\mathrm{17Arg\text{-}Pro}}$) (Metselaar et al., 2015). Comparative analysis revealed that both V14 and V15 share similar gene expression profiles and phenotypes, such as enhanced stress resistance and glycerol utilization, absence of flagella, and increased attachment and invasion of Caco-2 cells, compared to the wild type (WT) (Koomen et al., 2018). These findings suggest that *rpsU* deletions and the $rpsU^{\mathrm{G50C}}$ mutation may impact the phenotype through a similar mechanism (Koomen et al., 2018). Further mutant construction experiments confirmed that the $rpsU^{\mathrm{G50C}}$ mutation in *L. monocytogenes* WT strains LO28 and EGDe conferred multiple stress resistance and reduced growth rates (Koomen et al., 2021). Evolutionary experiments with variant 15 yielded two evolved variants, 15EV1 and 15EV2, with mutations in the same *rpsU* codon, resulting in $\mathrm{RpsU}^{\mathrm{17Pro\text{-}His}}$ and $\mathrm{RpsU}^{\mathrm{17Pro\text{-}Thr}}$, receptively, and a return to WT-like fitness and stress response. Therefore, single amino acid substitutions in RpsU enable switching between multi-stress resistant and high fitness states in *L. monocytogenes* (Koomen et al., 2021). This raised the follow-up question whether and how V14, with deletion of the whole *rpsU*, could switch between low fitness-high stress resistance and high fitness-low stress resistance, since the known route to WT-like fitness and stress sensitivity via a single point mutation in *rpsU* is effectively blocked.

1.7 SigB mediated stress response in *L. monocytogenes*

The *rpsU* stress-resistant variants V14 and V15 (but not the V15 evolved variants) exhibited strong upregulation of SigB regulon genes and proteins (Koomen et al., 2021; Koomen et al., 2018). In *L. monocytogenes*, SigB is considered as the regulator of general stress response and controls the transcription of approximately 300 genes (Guerreiro et al., 2020a; Liu et al., 2019; O'Byrne and Karatzas, 2008; Toledo-Arana et al., 2009). These genes contribute to the stress response of osmotic, oxidative, acid, antibiotic, bile, alkaline and other stresses (Liu et al., 2019). SigB also regulates virulence genes, including *prfA*, which is the key transcription activator gene of *L. monocytogenes* virulence factors. In addition, SigB is also instrumental in regulating the metabolism of various substances, including carbon, nucleotide, ion, vitamin, and protein (Liu et al., 2019). Therefore, SigB plays a key role in *L. monocytogenes* survival in nature, food processing environment, and in the digestive tract (Guerreiro et al., 2020a; Kazmierczak et al., 2003; NicAogáin and O'Byrne, 2016).

The activation of SigB is controlled at the post-translation level through the stressosome and a series of other Rsb proteins (Figure 1.1) (Becker et al., 1998; Guerreiro et al., 2022a, 2020a). The stressosome is composed of RsbR1 (Lmo0899) and its paralogs (RsbR2 (Lmo0161), RsbL (Lmo0799), and RsbR3 (Lmo1642)), RsbS and RsbT (Impens et al., 2017). RsbT is captured by the stressosome in unstressed cells. Upon environmental stress, RsbR1 and RsbS are phosphorylated, and RsbT is released from the stressosome. The free RsbT can bind to RsbU and stimulate its phosphatase function. Then the anti-sigma factor antagonist RsbV is dephosphorylated by RsbU and binds to anti-sigma factor RsbW, which releases the previously bound SigB, which is then free to bind to RNA polymerase and initiate the transcription of the SigB regulon. Once stress is removed, RsbX, which is co-expressed with SigB, can dephosphorylate RsbR1 and RsbS, and RsbT binds back to the stressosome and inactivates the signal transduction (Guerreiro et al., 2020a; Oliveira et al., 2022).

SigB can be activated via different environmental stresses including osmotic, acid, temperature and oxidative stress (Dorey et al., 2019). SigB can also be activated by blue light irradiation, lactose utilization and *rpsU* mutation (Crespo Tapia et al., 2020; Koomen et al., 2021; Ondrusch and Kreft, 2011). However, only the blue-light sensing mechanism is well understood (Guerreiro et al., 2020a). RsbR paralog RsbL has a light-oxygen-voltage domain that binds flavin mononucleotide (FMN) (Ondrusch and Kreft, 2011). With blue-light irradiation, the FMN forms a covalent adduct with RsbL and produces a local structural rearragenment in RsbL, propagating into the stressosome core and activating the signal transduction (O'Donoghue et al., 2016). Recent studies show that RsbR1 can bind to the small membrane-spanning peptide Prli42, which has been suggested to anchor the stressosome to the cell membrane and to contribute to oxidative stress sensing (Impens et al., 2017; Tran et al., 2023). Further work is required to elucidate the detail mechanisms of the stress sensing and the SigB activation under different conditions, including the *rpsU* mutations. Further work is required to elucidate the detailed mechanisms of stress sensing and SigB activation in different *L. monocytogenes* variants, including those with *rpsU* mutations, and under different conditions.

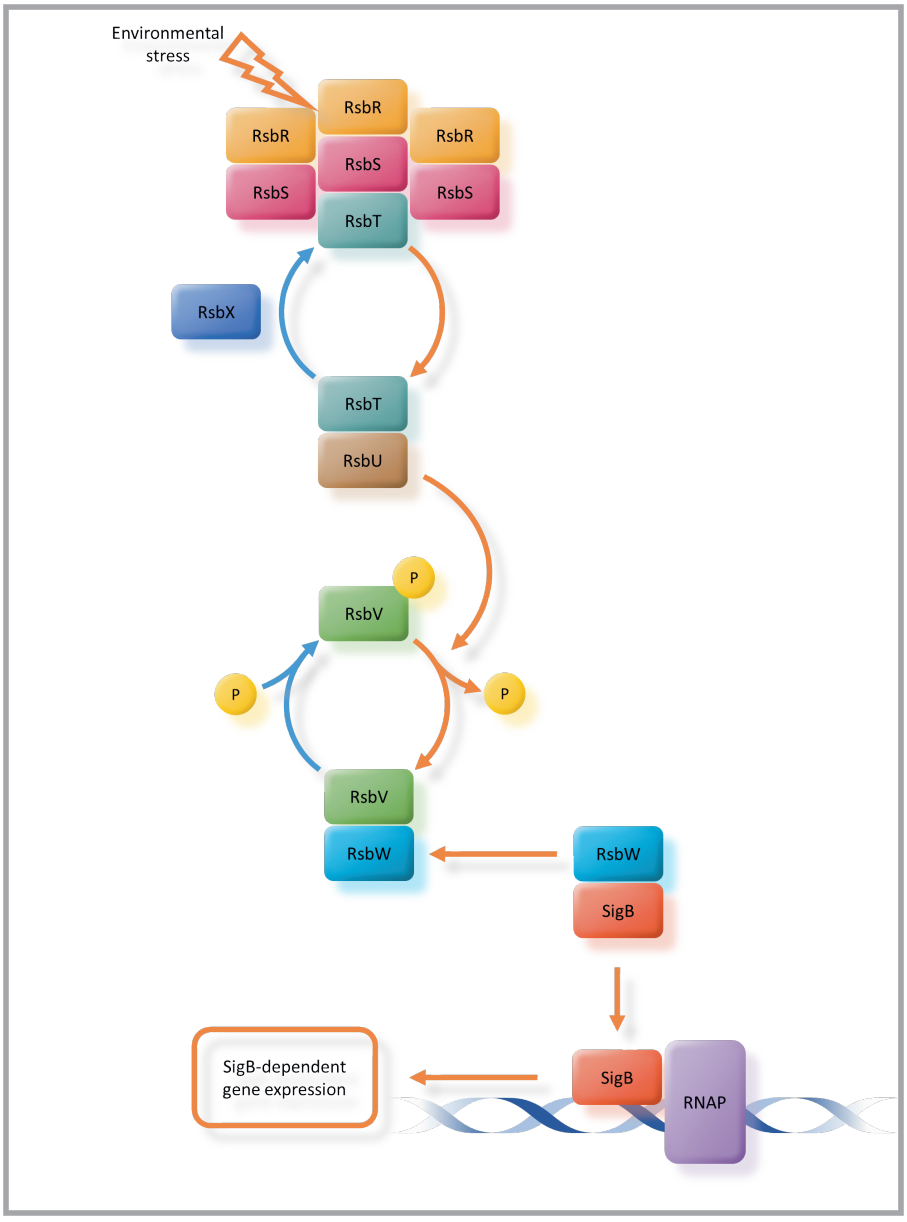

Figure 1.1: **Scheme of SigB activation in *L. monocytogenes*.** See text for details.

1.8 Potential underrepresentation of *rpsU* mutations

The possible activation of the SigB-mediated general stress response, coupled with enhanced multi-stress resistance, suggests that *L. monocytogenes rpsU* mutants likely play a significant role in the overall survival capacity of the total population under different stress conditions, contributing to the adaptation and persistence of *L. monocytogenes* in diverse environments. However, *rpsU* mutations have not been reported in comprehensive whole-genome sequencing studies on persistent *L. monocytogenes* strains (Castro et al., 2021; Cherifi et al., 2018; Lucchini et al., 2023; Palma et al., 2020; Simmons et al., 2014; Stasiewicz et al., 2015). It is noteworthy that the analyzed persistent *L. monocytogenes* strains were predominantly isolated using enrichment-based detection methods, which is required to detect low level of contamination. These procedures favor the growth of the target organism while suppressing other microorganisms, facilitating the isolation of *L. monocytogenes* (Allende et al., 2022). However, they may also introduce a bias in isolating specific *L. monocytogenes* lineages, serotypes, or strains, particularly when there are growth rate differences among them (Bruhn et al., 2005; Gorski et al., 2006; Zilelidou et al., 2016a; Zilelidou et al., 2016b). Given that *rpsU* mutants typically exhibit lower fitness compared to wild-type strains, the probability of detecting *rpsU* variants in food using enrichment-based methods might be lower than that of wild-type strains. Consequently, further research is needed to determine whether enrichment-based detection procedures contribute to a bias in the genetic diversity of deposited *L. monocytogenes* isolates.

1.9 Carbon source utilization of *L. monocytogenes*

Apart from the stress resistance, the ubiquity of *L. monocytogenes* is also due to the ability to utilize a large variety of carbon sources, including glucose, mannose, fructose, glycerol, cellobiose, sucrose, and trehalose (Muchaamba et al., 2019; Wu et al., 2023). This feature is related to the abundance of PEP-dependent phosphotransferase (PTS) system genes in *L. monocytogenes* (Figure 1.2). The *L. monocytogenes* strain EGDe possesses 86 *pts* genes, encoding 29 putative complete PTS systems and additional single PTS components, which can contribute to the transport of carbohydrates and sugar alcohols (Stoll and Goebel, 2010). Screening of 168 *L. monocytogenes* strains and 11 carbon sources on agar-based defined medium demonstrated that when used as the sole carbon source, lactose only modestly supported growth of the tested *L. monocytogenes* isolates, suggesting a low utilization efficiency of lactose (Wu et al., 2023). Lactose is the main available carbon source in dairy products. As previously mentioned, dairy products are significantly associated with *L. monocytogenes* and linked to hypervirulent CCs (Allende et al., 2022; Maury et al., 2019). Moreover, lactose is known to activate general stress response regulator SigB in *L. monocytogenes* resulting in higher stress resistance, biofilm formation and adhesion/invasion capacity (Crespo Tapia et al., 2020). Despite the different roles of (di)saccharides in stress resistance as well as virulence of *L. monocytogenes*, uptake and utilization of lactose are poorly understood. Six putative lactose PTS systems and several additional PTS components have been identified *in silico*, but only one PTS system encoded by *lpo*

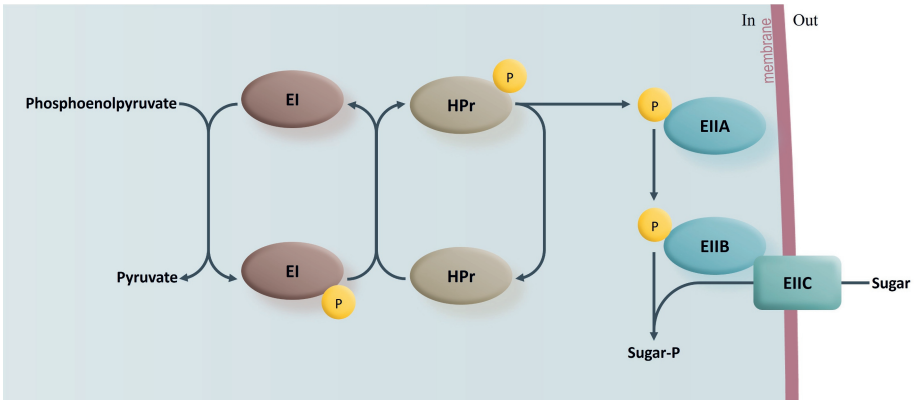

Figure 1.2: **Scheme of sugar phosphotransferase systems.** EI is autophosphorylated by phosphoenolpyruvate and then transfers phosphate group to HPr. HPr subsequently phosporylates EIIA, which is specific for a certain carbohydrate. The P~EIIA transfer the phosphoryl group to the cognate EIIB, which finally phosphorylates the carbohydrate bound to the corresponding membrane-integral EIIC. The phosphorylated carbohydrate is subsequently released into the cytoplasm. Adapted from Galinier and Deutscher (2017).

operon has been analyzed in some detail (Dalet et al., 2003; Stoll and Goebel, 2010). The expression of the *L. monocytogenes lpo* operon has been shown to be induced by the presence of lactose, cellobiose, and chitobiose in the media, and has been found to be controlled by the transcriptional activator LacR (coded by *lmo1721*/*lacR*) together with the transcription factor sigma 54 (Dalet et al., 2003). The *lpo* operon encodes IIA and IIB PTS subunits of the lactose family by *lpoA* and *lpoB* but missed the IIC subunit. Another IIC coding gene *lmo2708* also has sigma 54 promote region and LacR binding upstream activating sequences (UAS), so this gene was hypothesized to produce the IIC protein and functionally linked to *lpo* operon (Dalet et al., 2003). Further work is required to elucidate lactose utilization pathways in *L. monocytogenes* and to assess the impact on stress resistance and virulence.

1.10 Outline of this thesis

Previous evolutionary experiments of variant V15 demonstrated that single amino acid substitutions in RpsU can facilitate a switch between multi-stress resistance and high fitness states in *L. monocytogenes*. In **Chapter 2**, this concept was further explored with the *rpsU* deletion variant V14. We employed an experimental evolution protocol aimed at selecting for increased fitness, defined as a higher maximum specific growth rate compared to the ancestral variant V14, while simultaneously monitoring fitness, stress resistance, and SigB activation of the evolved strains.

In **Chapter 3**, we investigate the molecular mechanism of SigB activation in the *L. monocytogenes* $rpsU^{G50C}$ mutant. Comparing stress resistance and fitness of *L. monocytogenes* WT and single and double mutants, we show that stress resistance in the

rpsU^{G50C} mutant results from SigB activation through an unknown mechanism distinct from the classical stressosome and RsbV/RsbW partner switching model. Moreover, the reduced maximum specific growth rate of the *rpsU*^{G50C} mutant is likely unrelated to SigB activation and potentially linked to impaired ribosomal function.

In **Chapter 4**, we investigate the variation level of *rpsU* in the NCBI *L. monocytogenes* genome database and elucidate whether the detection chance of *rpsU* variants from food differs from WT strains when enrichment-based detection methods are applied. Our observation implies that a bias in the enrichment process used for isolating *L. monocytogenes* could be a factor in the underrepresentation of isolates carrying *rpsU* mutations in the strain collections of publicly accessible genome databases.

In **Chapter 5**, following a screening of a collection of *L. monocytogenes* strains for the capacity to use lactose as a growth substrate, a lactose-negative strain F2365 has been identified, which was previously isolated from the 1985 listeriosis outbreak in California that involved a diary product. Via experimental evolution selecting for enhanced growth with lactose, an alternative PTS-lactose system was discovered. Next to providing evidence for a role of LacR regulated PTS-lactose systems encoded by the *lpo* operon, *lmo2708* and the *lmo2683-2685* operon, the putative regulator Lmo2766 was shown to control expression of another PTS-lactose system formed by the *lmo2761-2765* operon.

Finally, **Chapter 6** provides a comprehensive discussion that integrates findings from the previous chapters. We discuss how the ribosome affects the fitness-stress resistance trade-off and the persistence of *L. monocytogenes*. We also discuss the characteristics of lactose metabolism in shaping *L. monocytogenes*'s adaptability and the impact on food safety. This thesis provides insights into the biodiversity of *L. monocytogenes* for understanding the persistence of this foodborne pathogen in various environments.

2

Ribosomal mutations enable a switch between high fitness and high stress resistance in *Listeria monocytogenes*

Jeroen Koomen, Xuchuan Ma, Alberto Bombelli, Marcel H. Tempelaars, Sjef Boeren, Marcel H. Zwietering, Heidy M.W. den Besten, Tjakko Abee

Under review

Abstract

Multiple stress resistant variants of *Listeria monocytogenes* with mutations in *rpsU* encoding ribosomal protein RpsU have previously been isolated after a single exposure to acid stress. These variants, including *L. monocytogenes* LO28 variant V14 with a complete deletion of the *rpsU* gene, showed upregulation of the general stress sigma factor Sigma B-mediated stress resistance genes and had a lower maximum specific growth rate than the LO28 WT, signifying a trade-off between stress resistance and fitness. In the current work we have subjected V14 to an experimental evolution regime, selecting for higher fitness in two parallel evolving cultures. This resulted in two evolved variants with WT-like fitness: 14EV1 and 14EV2. Comparative analysis of growth performance, acid and heat stress resistance, in combination with proteomics and RNA-sequencing, indicated that in both lines reversion to WT-like fitness also resulted in WT-like stress sensitivity, due to lack of Sigma B-activated stress defence. Notably, genotyping of 14EV1 and 14EV2 provided evidence for unique point-mutations in the ribosomal *rpsB* gene causing amino acid substitutions at the same position in RpsB, resulting in RpsB$^{22\text{Arg-His}}$ and RpsB$^{22\text{Arg-Ser}}$, respectively. Combined with data obtained with constructed RpsB$^{22\text{Arg-His}}$ and RpsB$^{22\text{Arg-Ser}}$ mutants in the V14 background, we provide evidence that loss of function of RpsU resulting in the multiple stress resistant and reduced fitness phenotype, can be reversed by single point mutations in *rpsB* leading to arginine substitutions in RpsB at position 22 into histidine or serine, resulting in a WT-like high fitness and low stress resistance phenotype. This demonstrates the impact of genetic changes in *L. monocytogenes*' ribosomes on fitness and stress resistance.

2.1 Introduction

Listeria monocytogenes is a foodborne pathogen that can cause the infrequent but high-mortality disease listeriosis (Allerberger and Wagner, 2010). *L. monocytogenes* is generally considered to be a robust microorganism, capable of growing in and surviving a wide range of adverse conditions such as low pH, low temperature and low a_w (NicAogáin and O'Byrne, 2016). Microbial populations are innately heterogenous, which contributes to the spread of *L. monocytogenes* in different environmental niches, from soil to man (Abee et al., 2016; Maury et al., 2016). When a population of cells is exposed to stress, population heterogeneity can lead to the differential survival of a subset of cells, resulting in tailing of the inactivation curve. Previously, Metselaar et al. (2015) described stress resistant *L. monocytogenes* variants, acquired after a single exposure to acid stress, with a mutation in the ribosomal *rpsU* gene, encoding small ribosomal protein S21. Additional genotypic and phenotypic studies focussed on variant V14, with a deletion that covers the entire *rpsU* gene as well as *yqeY* and half of *phoH*, and on V15 that harbours a point mutation in *rpsU* resulting in an amino acid substitution from arginine to proline in the RpsU protein, $RpsU^{17Arg\text{-}Pro}$ (Koomen et al., 2018). Gene expression data of *L. monocytogenes* LO28 wild type (WT) and multiple-stress resistant variants V14 and V15 revealed an upregulation of 116 genes (Koomen et al., 2018), including a large fraction of genes controlled by the alternative stress sigma factor SigB, which are known to be involved in providing multiple-stress resistance (Liu et al., 2019).

In a follow-up study (Koomen et al., 2021), we subjected *L. monocytogenes* LO28 V15, with its single $RpsU^{17Arg\text{-}Pro}$ point mutation, to an experimental evolution protocol where we selected for increased fitness, defined as a higher maximum specific growth rate (μ_{max}) compared to V15. Both evolved variants fixed mutations in *rpsU* (resulting in $RpsU^{17Pro\text{-}His}$ and $RpsU^{17Pro\text{-}Thr}$) and reverted back to WT-like high maximum specific growth rate and relative low stress resistance. The potentially disruptive effect of random insertion of a proline residue is known to alter the stability or function of proteins (Chou and Fasman, 1974). Consequently, we hypothesized that replacing the putative disruptive proline at position 17 in *L. monocytogenes* V15 with amino acids that do not have such strong disruptive effects, i.e., threonine or histidine, can restore WT-like functioning of the RpsU protein with originally an arginine at position 17. This was confirmed by using targeted mutants in *L. monocytogenes* LO28 and type strain EGDe, showing that single amino acid substitutions in RpsU enabled *L. monocytogenes* to switch between high fitness-low stress resistance and low fitness-high stress resistance.

This raised the follow-up question whether and how *L. monocytogenes* V14 could switch between low fitness-high stress resistance and high fitness-low stress resistance, since the whole *rpsU* gene is deleted and thus the known route to WT-like fitness and stress sensitivity via a single point mutation in *rpsU* is effectively blocked. Therefore, in the current study we subjected V14 to an experimental evolution regime and used a complementary genotypic, proteomic and phenotypic approach to evaluate how ribosomal mutations in *L. monocytogenes* enable a switch between fitness and stress resistance.

2.2 Materials and Methods

2.2.1 Bacterial strains and culture conditions

Listeria monocytogenes LO28 wild type (from the strain collection of Wageningen Food & Biobased Research, The Netherlands), stress resistant ancestor V14 (Koomen et al., 2018; Metselaar et al., 2013), and evolved variants (this study) were used for all genotypic, proteomic and phenotypic analyses. All cultures were grown as described elsewhere (Metselaar et al., 2013). In brief, cells from -80°C stocks were incubated at 30°C for 48 hours on brain heart infusion (BHI, Oxoid, Hampshire), supplemented with agar (1.5 % [w/w], bacteriological agar no. 1 Oxoid, Hampshire). A single colony was used for inoculation of 20 mL of BHI broth in a 100 mL Erlenmeyer flask (Fisher, USA). After overnight (ON, 18-22 hours) growth at 30°C under shaking at 160 rpm, (Innova 42, New Brunswick Scientific, Edison, NJ) 0.5% (v/v) inoculum was added to fresh BHI broth. Cells were grown under constant shaking at 160 rpm in BHI at 30°C until the late-exponential growth phase (OD_{600} = 0.4-0.5).

2.2.2 Experimental evolution

Experimental evolution was performed as described in Koomen et al. (2021). Briefly, we inoculated two parallel lines with 1% (v/v) of ON culture of *L. monocytogenes* LO28 V14 in 20 mL BHI broth in 100 mL Erlenmeyer flasks. The cultures were then incubated for 24 hours at 20°C with continuous shaking at 160 rpm (Innova 42, New Brunswick Scientific, Edison, NJ). For each parallel line, 44 consecutive transfers were made from 24 hours-cultures, where 1% (v/v) inoculum was used to inoculate fresh BHI, resulting in about 290 generations for each of the two evolution lines (6.6 generations per culture). From every second transfer, a 700 μL culture sample was taken, mixed with glycerol (Sigma, 25% v/v final concentration), flash frozen in liquid nitrogen, and stored at -80°C, resulting in 22 stocks for both evolution lines. These stocks were revived by streaking on BHI-agar plates, from which a single colony was used to inoculate 20 mL of BHI broth in a 100 mL Erlenmeyer flask. After ON culturing at 30°C with shaking at 160 rpm, the culture was diluted 100,000 times in fresh BHI broth, and 200 μL of culture was inoculated in duplicate in wells of a honeycomb plate. The plate was incubated in a Bioscreen C (Oy growth Curves AB Ltd, Helsinki, Finland) at 30°C and the respective growth curves were determined by measuring OD_{600} over time. All growth experiments were performed with biologically independent triplicates. Stock number 14 of the first evolution line and stock number 22 of the second evolution line were streaked on BHI agar, and respective single colonies were selected to prepare -80°C stocks of 14EV1 and 14EV2.

2.2.3 Estimation of μ_{max}

The maximum specific growth rate μ_{max} (h^{-1}) was determined at 30°C following the procedure as described previously by Biesta-Peters et al. (2010) and Koomen et al. (2021). This method is based on the time-to-detection (TTD) of five serially two-fold

diluted cultures, of which the initial bacterial concentration is known. In this setup μ_{max} equals ln(2)/generation time (i.e., $\mu_{max} = 1$ represents a generation (doubling) time of approximately 0.7 h or 42 minutes). Three biologically independent experiments were performed to estimate the mean and standard deviation of μ_{max}.

2.2.4 Inactivation kinetics at low pH

Acid inactivation experiments were performed as described previously (Metselaar et al., 2013). Briefly, 100 mL of late-exponential phase culture was pelleted in a fixed-angle rotor (5804 R, Eppendorf) for 5 minutes at 2,880 x *g*. Pellets were washed using 10 mL BHI broth and pelleted again at 5 min at 2,880 x *g*. The pellet was resuspended in 1 mL PPS, which was pre-warmed to 37°C and adjusted to pH 3.0 using 10 M of HCl, and placed in a 100 mL Erlenmeyer flask in a shaking water bath at 37°C. At appropriate time intervals, samples were taken, decimally diluted in BHI broth and plated on BHI agar using an Eddy Jet spiral plater (Eddy Jet, IUL S.A.). Plates were incubated at 30°C for 4 to 6 days for full recovery of damaged cells. Data of at least three biologically independent experiments were used for analysis.

2.2.5 Inactivation kinetics at high temperature

Heat inactivation experiments were performed as described before (Metselaar et al., 2015). Briefly, 400 μL of late-exponential phase culture was added to 40 mL of fresh BHI broth that was pre-heated to 55°C ± 0.3°C. For the determination of the initial microbial concentration, a separate Erlenmeyer with BHI at room temperature was used. Samples were taken after various timepoints and were decimally diluted in Peptone Physiological Salt (PPS). Appropriate dilutions were plated on BHI agar using an Eddy Jet spiral plater and incubated at 30°C for 4-6 days. Combined data of at least three biologically independent experiments were used for analysis.

2.2.6 Proteomic analysis

Proteomic analysis was performed on late-exponentially growing cells (OD_{600} between 0.4-0.5) of V14 and evolved variants 14EV1 and 14EV2 as described before (Koomen et al., 2021). Briefly, 2 mL of late-exponentially growing cells (OD_{600} of 0.4-0.5) cultures of the LO28 WT, V14 and evolved 14EV1 and 14EV2 were flash frozen in liquid nitrogen and stored. Samples were thawed on ice, pelleted at 17,000 x *g*, and subsequently washed twice with 100 mM Tris (pH 8). Resuspended pellets were sonicated, and samples were prepared according to the filter assisted sample preparation protocol (FASP) (Wiśniewski et al., 2009). Each prepared peptide sample was analysed by injecting (18 μL) into a nanoLC-MS/MS (Thermo nLC1000 connected to an LTQ-Orbitrap XL) as described previously (Feng et al., 2022; Lu et al., 2011; Wendrich et al., 2017). nLC-MSMS system quality was checked with PTXQC (Bielow et al., 2016) using the MaxQuant result files. LCMS data with all MS/MS spectra were analysed with the MaxQuant quantitative proteomics software package (Cox et al., 2014) as described before (Smaczniak et al., 2012; Wendrich et al., 2017). Filtering

and further bioinformatics and statistical analysis of the MaxQuant ProteinGroups file was performed with Perseus (Tyanova et al., 2016). Reverse hits and contaminants were filtered out. In cases where intensity values were zero, a pseudo-value of 5 was added to prevent indefinite fold changes during the t-test. Proteins were considered differentially expressed if the $\log_{10}$ transformed ratio of variant over WT ($\log_{10}$(protein ratio)) was below -1 or above 1, with a negative $\log_{10}$ transformed Benjamini–Hochberg corrected p-value (-$\log_{10}$(p-value)) above 2. The proteins that belonged to the SigB regulon were identified according to previous research (Guariglia-Oropeza et al., 2018; Hain et al., 2008; Kazmierczak et al., 2003; Liu et al., 2017; Mattila et al., 2020; Oliver et al., 2010; Ollinger et al., 2009). Proteins associated with the gene ontology terms "bacterial-type flagellum" or "chemotaxis" according to GOA database were identified as being linked to motility (Huntley et al., 2015). Data visualization was performed using the statistical programming language R (4.3.0).

2.2.7 RNA-sequencing

Total RNA was isolated from late-exponentially growing cells (OD_{600} between 0.4-0.5) of V14 and evolved variants 14EV1 and 14EV2. Briefly, 100 mL of late-exponential phase culture was pelleted for 1 min at room temperature (RT) at 11,000 × *g* in a fixed-angle rotor (5804 R, Eppendorf). The pellet was resuspended in TRI-reagent (Ambion) in a beat-beater tube (lysing matrix A) by vortexing and tubes were snap frozen in liquid nitrogen until use. Cells were disrupted using a beat-beater (MP Fast Prep-24, MP Biomedicals GmbH, Eschwege, Germany) set at 6 m/s for 4 times 20 seconds with two minutes of intermittent air cooling per cycle. Twenty percent of the starting volume of chloroform was added, mixed and incubated at RT for 10 min. Subsequently, samples were centrifuged at 17,000 x *g* and 4°C for 15 min. The upper aqueous phase (approximately 700 μL) was transferred to an RNase free Eppendorf tube, where 600 μL of isopropanol was added, mixed and incubated at RT for 10 min. Next, the samples were centrifuged at 17,000 x *g* and 4°C for 15 min. The pellet was washed with 700 μL of ice-cold 75% ethanol, after which the pellet was centrifuged again at 17,000 x *g* for 5 min at 4°C. The pellet was resuspended in 90 μL of nuclease-free water and incubated at 60°C for 2 minutes to finalize RNA isolation. RNA integrity was checked using gel electrophoresis, after which the RNA was stored by adding 0.1 volume of 3M sodium acetate at pH 5.2 with 2.5 volumes of ethanol absolute and kept at -80°C. Before shipping the samples were centrifuges at 13,000 x *g* and 4°C for 10 minutes, and the supernatant was removed. The pellet was washed with 80% ethanol and centrifuged again at 13,000 x *g* and 4°C for 10 minutes. After removal of the supernatant and air drying, the RNA was dissolved in 90 μL of nuclease-free water and shipped on dry ice. Ribo-Zero rRNA depletion and the generation of paired-end reads using a MiSeq system was done by BaseClear B.V. (Leiden, The Netherlands). QC and read mapping against the LO28 reference genome (NCBI accession: PRJNA664298) was performed via in-house methods by BaseClear. Counting of reads was done by htseq-count (version 0.11.1) (Anders et al., 2015). Differential expression analysis was performed using the DEseq2 package (version 1.24.0) in the statistical programming language R (version 3.6.0). Genes were considered differential expression if $\log_2$(Fold Change) was below -1.58 or above 1.58, with a Benjamini–Hochberg corrected p-value below 0.01. The SigB regulon genes and motility related genes were annotated as

described in Section 2.2.6.

2.2.8 SNP analysis of evolved variants

Ancestor V14 and evolved variants 14EV1 and 14EV2 obtained in the evolution experiment were sequenced using Illumina chemistry as described before (Koomen et al., 2021). Briefly, cells were pelleted and resuspended in 450 μL DNA/RNA Shield (Zymo Research) at 4°C until DNA extraction. The DNA was extracted by BaseClear (Leiden, the Netherlands) and paired-end 2 × 150bp short-reads were generated using a Nextera XT library preparation (Illumina). A NovaSeq 6000 system (Illumina) was used to generate paired-end reads. Raw reads were trimmed and de novo assembled using CLC Genomics Workbench v 10.0 (Qiagen, Hilden, Germany). SNIPPY 3.2 (Torsten, 2015), and Pilon using the "--changes" argument (Walker et al., 2014) were used for SNP analysis of evolved variants against the LO28 WT as reference.

2.2.9 Mutant construction

Mutant strains 14RpsB$^{22\text{Arg-His}}$ and 14RpsB$^{22\text{Arg-Ser}}$ were constructed in the V14 genetic background using the temperature sensitive suicide plasmid pAULA (Chakraborty et al., 1992). The *rpsB* gene from either variant 14EV1 or 14EV2 was amplified from genomic DNA by KAPA HiFi Hotstart ReadyMix (KAPA Biosystems, USA), using the primers listed in Supplemental Table 2.1. The resulting fragments were ligated in frame to the pAULA multiple cloning site via EcoR1 and Sal1 restriction that were introduced to the fragments by the respective primers. The resulting plasmid was electroporated (2.5 kV, 25 μF, 200 W), in a 0.2 cm cuvette using a BIO-RAD GenePulser, to the appropriate *L. monocytogenes* cells and plated on BHI agar at 30°C with 5 μg/mL erythromycin to select for transformants.

Two erythromycin resistant colonies per construct were inoculated in separate tubes in BHI broth supplemented with 5 μg/mL erythromycin and grown overnight at 42°C to select for plasmid integration. Selected strains resulting from a single cross-over integration event were grown overnight in BHI at 30°C to induce double crossover events and were subsequently plated on BHI agar at 30°C. Resulting colonies were replica plated on BHI with and without 5 μg/mL erythromycin and incubated at 30°C. Colonies sensitive to erythromycin were selected. PCR using the primers listed in Supplemental Table 2.1 and subsequent DNA sequencing of the products (BaseClear B.V. Leiden, The Netherlands) of erythromycin sensitive colonies confirmed the correct point mutation in the respective genes and the lack of additional mutations in the targeted region.

2.2.10 Statistical testing

Comparing $\mu_{\max}$ or $\log_{10}$CFU between different strains was performed in the statistical programming language R (version 3.6.0) using the t.test() and var.test() functions (α = 0.05).

2.3 Results

2.3.1 Growth kinetics of evolved variants

The experimental evolution regime was set up using two parallel cultures of *L. monocytogenes* LO28 V14. After 28 and 44 daily transfers, implicating ~186 and ~292 generations, respectively, this regime resulted in the selection of two evolved variants, 14EV1 and 14EV2, that showed different growth kinetics compared to the ancestor V14 (Figure 2.1 **A**). The μ_{max} at 30°C of both evolved variants was significantly higher than that of V14, but just significantly lower than the μ_{max} of the original LO28 WT strain (Figure 2.1 **B**). This indicated that the fitness of the evolved variants was increased compared to the ancestor V14 and almost similar to that of the WT strain.

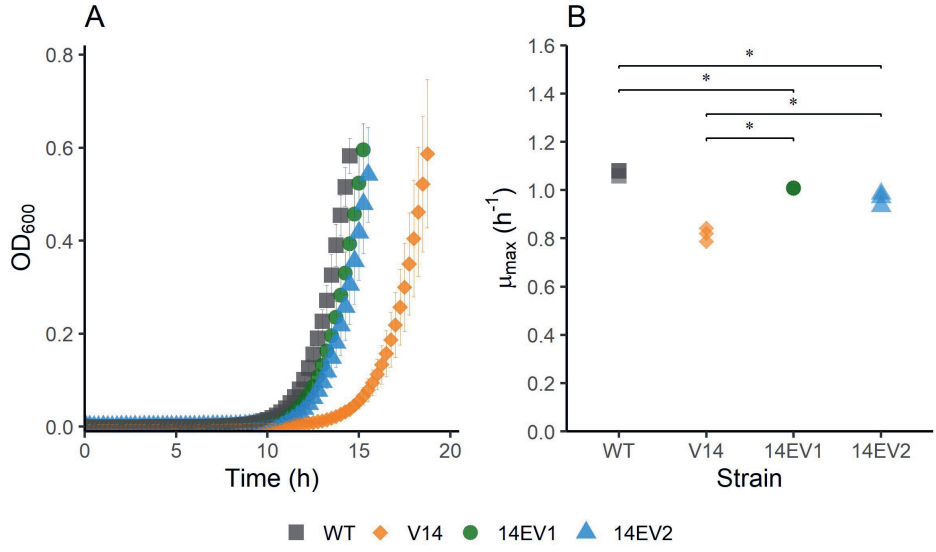

Figure 2.1: **Growth performance of *L. monocytogenes* LO28 WT, V14, 14EV1, and 14EV2 at 30°C . (A)** growth curves for LO28 WT, V14, 14EV1, and 14EV2. **(B)** Maximum specific growth rates (μ_{max}) for *L. monocytogenes* LO28 WT, V14, 14EV1, and 14EV2. The wild type is represented by squares, V14 is represented by diamonds, and variants 14EV1 and 14EV2 are represented by circles and triangles respectively. Significant differences are indicated by an asterisk.

2.3.2 Multiple-stress resistance of evolved variants

Since the evolved variants 14EV1 and 14EV2 showed increased fitness, we compared their heat and acid stress resistance to that of V14 (Figure 2.2). In the heat stress experiments (Figure 2.2 **A**), V14 started with approximately 6.8 $\log_{10}$CFU/mL and showed little inactivation after 20 minutes of exposure with a final concentration of

around 6 $\log_{10}$CFU/mL. In contrast, after 20 minutes of exposure the concentrations of both evolved variants 14EV1 and 14EV2 decreased and were not significantly different from the LO28 WT strain with concentrations of around 2.5 $\log_{10}$CFU/mL. For acid stress experiments (Figure 2.2 **B**), V14 again only showed a small (< 1.0 $\log_{10}$CFU/mL) decrease in cell counts after 20 minutes, while both evolved variants and also the LO28 WT strain showed more than 5 $\log_{10}$CFU/mL reduction after 20 minutes. These data indicated that both evolved variants 14EV1 and 14EV2 lost their high resistance to heat stress and acid stress when compared to V14.

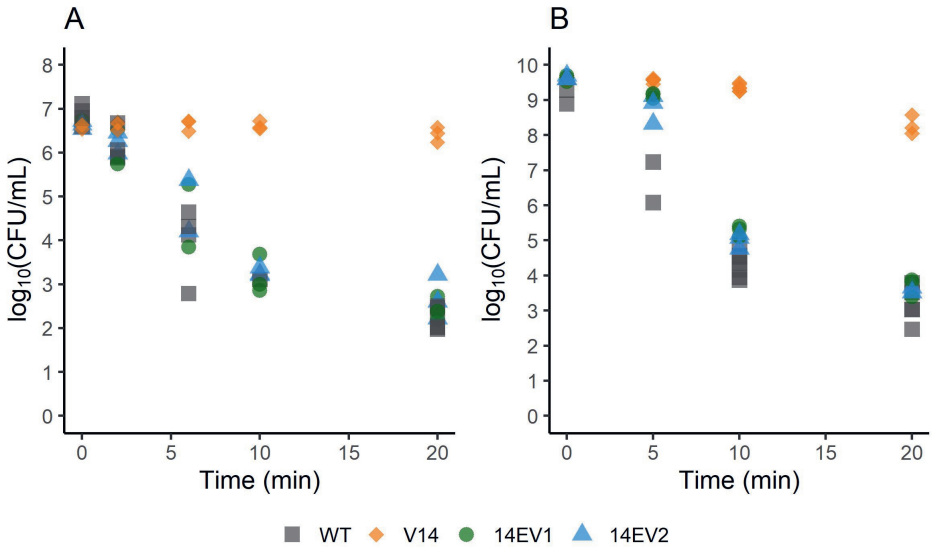

Figure 2.2: **Survival of *L. monocytogenes* LO28 WT, V14, 14EV1, and 14EV2 after exposure to heat (55°C) (A) or acid stress (pH 3.0) (B).** The wild type is represented by squares, V14 is represented by diamonds, and variants 14EV1 and 14EV2 are represented by circles and triangles respectively.

2.3.3 Proteomic and RNAseq analysis of WT and variants V14, 14EV1, and 14EV2

Comparative analysis of proteomes of late-exponential phase cells of *L. monocytogenes* LO28 WT, V14 and evolved variants 14EV1 and 14EV2 showed significant differences for V14 compared to WT and evolved variants (Figure 2.3). There were 28 proteins significantly higher expressed in V14 compared to LO28 WT, of which 25 proteins belonged to the SigB regulon (Figure 2.3 and Supplemental Table 2.2). Upregulated proteins included the general stress marker Ctc (lmo0211) (Ferreira et al., 2004; Kazmierczak et al., 2003; Oliver et al., 2010; Raengpradub et al., 2008) and subunits of the known OpuC glycine betaine osmolyte transporter OpuCA (lmo1428) and OpuCC (lmo1426). SigB (lmo0895) itself was upregulated but did not pass the stringent cut-off values applied to the proteomics data (>1 or <-1 $\log_{10}$(protein ratio), with adjusted -$\log_{10}$(p-value) < 2). Comparative proteome analysis identified in total

17 proteins that were downregulated in V14 compared to the WT (Supplemental Table 2.2). In line with previously obtained gene expression data and the non-motile phenotype of V14 (Koomen et al., 2018), 7 of these 17 downregulated proteins are involved in motility and chemotaxis, such as MotA (lmo0685), CheA (lmo0692), and chemotaxis response regulators CheY (lmo0691) and CheV (lmo0689). Only four and five proteins were differentially expressed in 14EV1 and 14EV2 compared to the WT, respectively (Supplemental Table 2.2). These results indicated that in line with the return to WT-like growth kinetics of 14EV1 and 14EV2, the proteomic profiles of the two evolved variants were highly similar to that of the WT.

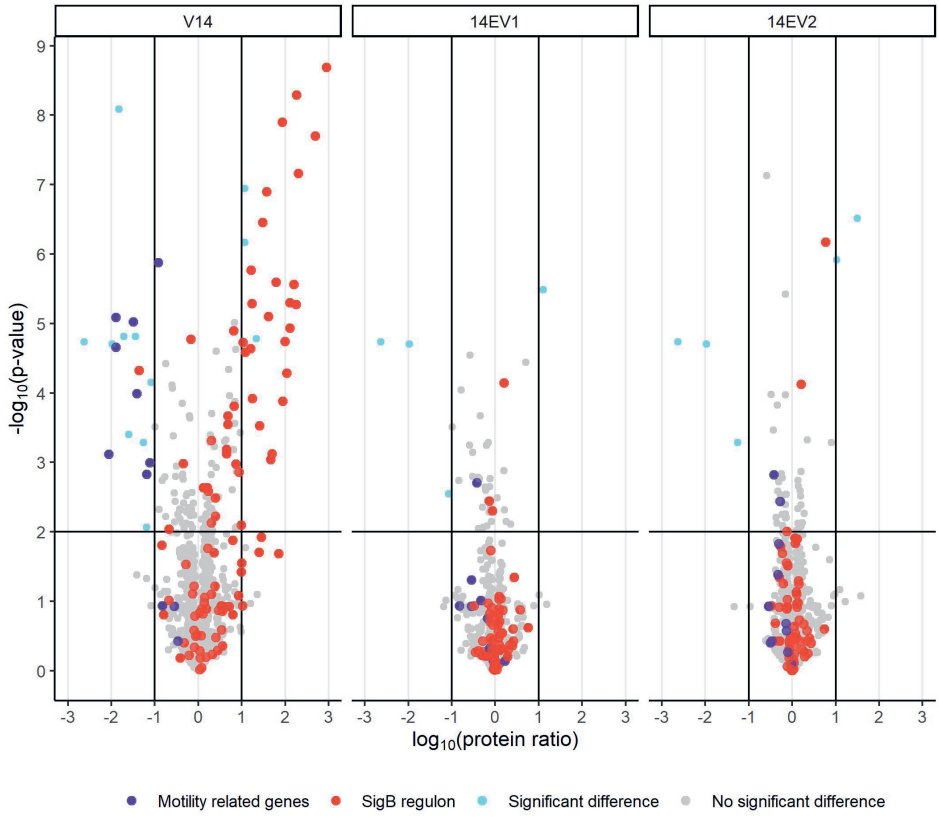

Figure 2.3: **Volcano plot of proteomic data comparing *L. monocytogenes* V14, 14EV1, and 14EV2 to the wild type.** The $-\log_{10}$(p-value) is plotted against the $\log_{10}$(protein ratio: variant over WT). The horizontal line represents the cutoff for $-\log_{10}$(p-value), vertical lines represent $\log_{10}$(protein ratio) cutoff. Red dots indicate proteins regulated by SigB; purple dots indicate proteins involved in motility.

RNAseq data were in line with the observed results in proteomes of ancestor V14, 14EV1 and 14EV2 compared to that of the WT. In total, 281 genes were differentially expressed in V14 compared to the WT, whileas only 15 and 24 genes were differentially expressed in 14EV1 and 14EV2, respectively (Supplemental Figure 2.1). Due to the higher sensitivity of our RNAseq approach, we found 117 genes belonging to

the SigB regulon as significantly upregulated in V14 when compared to the WT (Supplemental Table 2.3). This is in line with the 70% upregulation of the SigB regulon we reported previously based on DNA-micro array data (Koomen et al., 2018). The upregulated genes included all *opuCABCD* genes (lmo1425-1428), glutamate decarboxylase (lmo2434), and *spxA* (ArsC family transcriptional regulator, lmo2191). Other genes upregulated in the RNAseq analyses included the virulence regulator *prfA* (lmo0200), *inlA* (lmo0433) and *inlB* (lmo0434), which encode internalin A and B involved in human epithelial cell adhesion. Genes *sigB* and *rsbX*, (serine phosphatase; indirect negative regulation of sigma B dependent gene expression) were upregulated in V14, but not in 14EV1 and 14EV2 (see Supplemental Table 2.4 for an overview of differential expression level of SigB regulator genes). In addition, for V14, RNAseq and proteomics analysis indicated (slight) upregulation of anti-sigma factor antagonist *rsbV* (lmo0893), anti-sigma factor *rsbW* (lmo0894) and *rsbX* (lmo0896). Notably, RsbS (lmo0890), one of the main components of the stressosome "signal integration hub" (Guerreiro et al., 2020a) was approximately 67-fold downregulated ($\log_{10}$(protein ratio) -1.83, adjusted -$\log_{10}$(p-value) > 2) in V14 compared to the WT at protein level, but the RNAseq analyses did not show a significant difference in expression of *rsbS* between the four strains, which suggests that the observed low RsbS level in V14 is due to posttranslational regulation.

2.3.4 Whole genome sequencing of 14EV1 and 14EV2

Since V14 lacks the *rpsU* gene, single or multiple compensatory mutations could be expected in 14EV1 and 14EV2. Strikingly, whole genome sequencing of 14EV1 and 14EV2 revealed that both evolved lines only fixed a single nonsynonymous mutation. Both evolved variants fixed this mutation in another ribosomal protein, ribosomal protein S2 (RpsB). In the *rpsB* gene of line 14EV1, the Guanine on nucleotide position 65 mutated to Adenine (codon CGT to CAT, NC_003210.1:g.1707853G>A p.(Arg22His)), leading to an amino acid change from Arginine to Histidine on amino acid position 22 of RpsB (RpsB$^{22\text{Arg-His}}$), while in 14EV2, the Cytosine on nucleotide position 64 mutated into Adenine (codon CGT to AGT, NC_003210.1:g.1707854C>A p.(Arg22Ser)), resulting in a substitution from Arginine to Serine on amino acid position 22 (RpsB$^{22\text{Arg-Ser}}$). Proteomic analysis revealed no significant shifts in the levels of RpsB in V14 compared to WT, and also no significant shifts were observed in the levels of RpsB$^{22\text{Arg-His}}$ and RpsB$^{22\text{Arg-Ser}}$ in the evolved variants compared to the WT (data not shown). Combining these results suggests that short term evolution experiments selecting for enhanced fitness, resulted in the isolation of 14EVs with mutations in *rpsB* to compensate for reduced fitness resulting from the loss of *rpsU*.

2.3.5 Fitness and stress resistance of constructed mutants

To assess the effect of the substitutions that were selected during experimental evolution, we introduced RpsB$^{22\text{Arg-His}}$ and RpsB$^{22\text{Arg-Ser}}$ into the V14 genetic background. We measured $\mu_{\max}$ as a proxy for fitness and found that both constructed mutants of V14 had indeed a maximum specific growth rate that was significantly higher than that of V14 (Figure 2.4). With that of V14 carrying the RpsB$^{22\text{Arg-His}}$

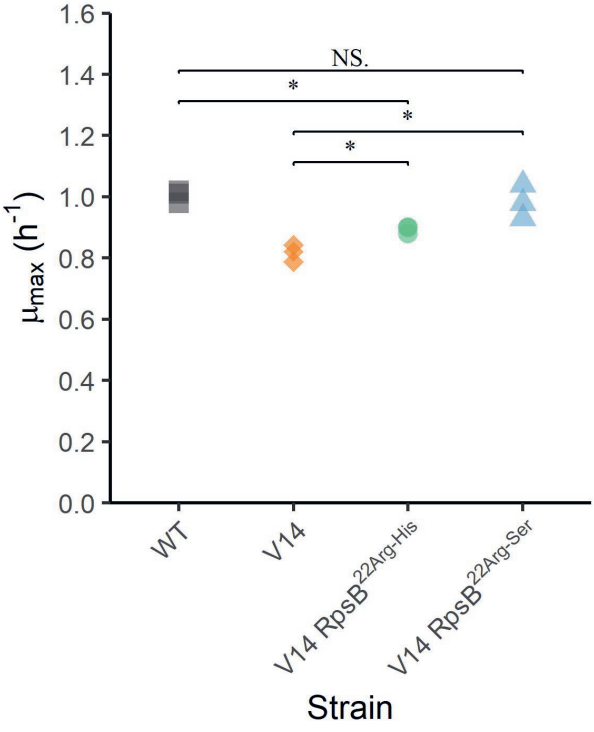

Figure 2.4: **Maximum specific growth rates (μ_{max}) at 30°C for *L. monocytogenes* LO28 WT, V14, and constructed mutants.** Significant differences are indicated by an asterisk, and no significant differences are indicated by NS.

mutation significantly lower than that of LO28 WT (p-value = 0.001), while that of V14 carrying RpsB$^{22\text{Arg-Ser}}$ was not significantly different from the LO28 WT (Figure 2.4). Subsequently, we tested the stress response of these constructed mutants, by exposure to heat (Figure 2.5 **A**) and acid stress (Figure 2.5 **B**). As expected, both constructed mutants were significantly less resistant to heat and acid stress after 20 minutes of exposure compared to V14 (p-value < 0.05), although their resistance was still higher than LO28 WT at this timepoint.

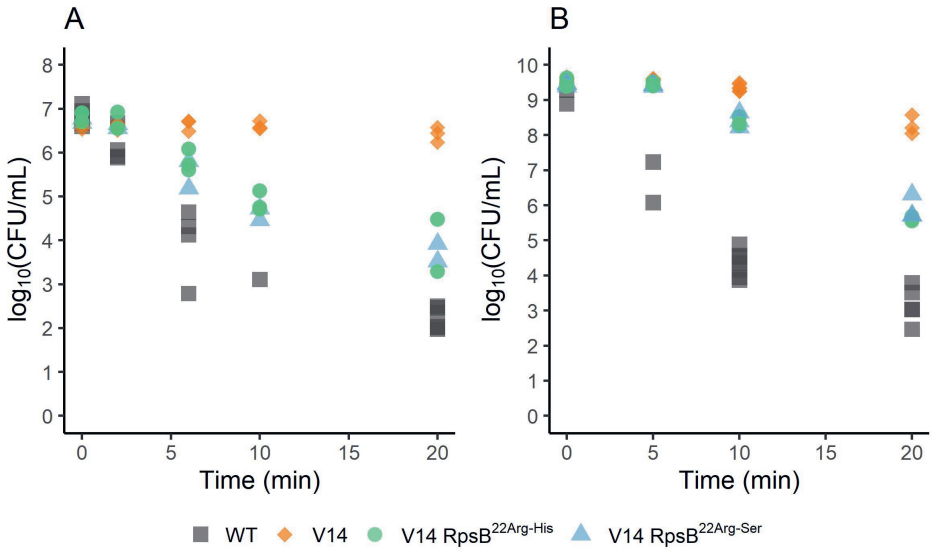

Figure 2.5: **Survival of *L. monocytogenes* LO28 WT, V14, and constructed mutants, during heat (55°C) (A) or acid (pH 3.0) (B) stress.** The wild type is represented by squares, V14 is represented by diamonds, and constructed mutants 14RpsB$^{22\text{Arg-His}}$ and 14RpsB$^{22\text{Arg-Ser}}$ are represented by circles and triangles respectively.

2.4 Discussion

Previously, we described multiple stress resistance of *L. monocytogenes* LO28 variants V14 and V15 isolated after a single exposure to acid stress (Koomen et al., 2018). We linked stress resistance in variants V14 and V15, with a complete gene deletion or point mutation in *rpsU* respectively, to induction of the SigB regulon and showed the correlation between increased stress resistance and reduced fitness. By using experimental evolution to select for increased fitness in V15 in two parallel lines, we were previously able to show that this trade-off was reversible (although not fully) via point mutations in RpsU at the same codon of the initial mutation: RpsU$^{17\text{Pro-His}}$ and RpsU$^{17\text{Pro-Thr}}$, respectively (Koomen et al., 2021). Here, we applied a similar experimental evolution approach using *L. monocytogenes* LO28 V14, which has a complete deletion of *rpsU*. By selecting for higher fitness in two parallel lines, we were

able to select two evolved variants of V14 (14EV1 and 14EV2). Both evolved variants had higher fitness, lower stress resistance, severely reduced induction of SigB regulon members compared to V14 and a single non-synonymous mutation in the ribosomal gene *rpsB* (lmo1658). Our RNA analysis indicated that both *sigB* and *rsbX* were actively transcribed in V14. RsbX is a SigB regulated feedback phosphatase (Xia et al., 2016) and is thought to reset the stressosome after induction, to prevent a positive feedback loop in the absence of a stress signal. In the current stressosome model (Williams et al., 2019), the phosphatase activator RsbT is released from the stressosome after phosphorylation of RsbS and acts on the signalling cascade of RsbU, RsbV, RsbW, ending in the activation of SigB. The downregulation of RsbS in V14 may have affected signaling via the stressosome. Notably, in our whole genome sequencing data of the evolved strains, we did not find (additional) mutations that resulted in premature stop codons within the genes of the *sigB* operon that regulate SigB activity as previously described (Guerreiro et al., 2020b). These authors showed that such mutations leading to the loss of SigB function confer a competitive advantage manifested in an increased growth rate under conditions of sublethal heat stress, at 42°C, but not in non-stressed conditions. The fact that evolved variants with higher fitness originate in our study from slow growing, multiple stress resistant V14 under non-stressed conditions, while no mutation(s) were found within genes of the SigB operon, suggests that the apparent activation of SigB regulon in V14 and loss of SigB regulon activation in 14EV1 and 14EV2, originates from alterations in ribosome functioning.

One of the stresses that can induce SigB and its operon, is nutrient stress. In addition, nutritional stress can indirectly effect ribosome functioning through uncharged tRNA's, leading to the stringent response via RelA (Taylor et al., 2002). Notably, we find significant upregulation of genes involved in metabolism of branched chain amino acids (BCAA) in V14. Although *relA* (lmo1523) is not differentially expressed in our RNAseq or proteomics data, activation of the indicated pathway may point to an interplay between the SigB activation and the stringency that is affected by ribosome functioning and the mutations in the *rpsU* and *rpsB* genes. Nutrient stress-induced SigB activation has been described for *L. monocytogenes*, but how the *L. monocytogenes* stressosome and other regulator proteins respond to metabolic stress is currently unknown (Guerreiro et al., 2020a; Williams et al., 2019). The signal of energy/nutrient stress enters the SigB activation pathway probably downstream from RsbU (Shin et al., 2010). Our recent study also showed that the SigB activation in RpsU$^{17\text{Arg-Pro}}$ mutants is independent from the stressosome and the anti-sigma factor antagonist RsbV (under review). Nevertheless, whether the ribosomal mutations lead to SigB activation via nutritional stress requires further study.

When assessing fitness and stress resistance of the constructed mutants (V14RpsB$^{22\text{Arg-His}}$ and V14RpsB$^{22\text{Arg-Ser}}$), we found that WT stress sensitivity was not fully restored in the constructed mutants. While no further mutations were identified in the sequenced genome, we must consider potential influences undetectable by Illumina DNA-sequencing, such as DNA methylation, which has been known to impact translation initiation and elongation in bacteria (Wang et al., 2020). Additionally, the modulation of protein activity through (de)phosphorylation reactions, particularly involving Rsb proteins that form the stressosome and regulate SigB activation, cannot be overlooked (Guerreiro et al., 2020a; Williams et al., 2019).

The role of individual small (S30) and large (S50) subunit ribosomal proteins in *L.*

monocytogenes has not been studied, but due to high conservation of S70 ribosome functioning, possible effects of *rpsU* and *rpsB* mutations can be discussed based on structural and functional data in well studied bacteria, including *Escherichia coli*. In *E. coli*, ribosomal protein S21 (RpsU) is part of the so-called ribosomal platform, together with S6, S11, S15, and S18 (Culver and Kirthi, 2008; Jagannathan and Culver, 2003), that functions in the initial steps of the translation process. Ribosomal protein S2 (RpsB) and the adjacent S1 (RpsA) are connected to the platform region of the 30S ribosome and are crucial in translation initiation and translation efficiency (Duval et al., 2013; Marzi et al., 2007), which can vary over two orders of magnitude (Espah Borujeni et al., 2014). The correct binding of RpsB to the 30S subunit is critical for the association of RpsA to the platform region and a fully competent 30S ribosome. This could indicate that the compensatory mutations in RpsB have a positive effect on binding of RpsA to the pre-initiation complex, which enhances translation efficiency and presumably results to reversion of the trade-off between growth and stress resistance in 14EV1 and 14EV2.

Here, we show that the apparent trade-off between increased stress resistance and lower fitness that has been described before in *L. monocytogenes* LO28 RpsU deletion mutant V14 and RpsU$^{17\text{Arg-Pro}}$ mutant V15 (Abee et al., 2016; Koomen et al., 2018; Metselaar et al., 2015) can be reversed by compensatory mutations in *rpsB* and *rpsU*, respectively (Figure 2.6). Studies in yeast and higher eukaryotes have indicated that ribosomes may provide an additional layer of fine-tuning in protein expression in response to environmental factors (Gerst, 2018). However, the possibility of a dynamic ribosome, with shifts in ribosome composition and/or functionality of ribosomal proteins, via phosphorylation as a function of the environment, has mainly received attention in eukaryotes (Genuth and Barna, 2018). The results presented in the current study suggest that the 70S ribosome is involved in a signalling cascade to the SigB activation. Further work is required to elucidate in more detail the underlying mechanisms of this signaling cascade and the components involved in 70S ribosome-induced modulation of *L. monocytogenes* fitness and stress resistance.

2.5 Funding

Xuchuan Ma was supported by a grant from the China Scholarship Council (File No. 201907720086).

2.6 Data Availability Statement

The mass spectrometry proteomics data have been deposited to the ProteomeXchange Consortium via the PRIDE (Perez-Riverol et al., 2022) partner repository with the dataset identifier PXD022732, in which the labels of LO28 WT, V14, V14EV1 and V14EV2 are WT (TA31-33), V14_AN (TA49-51), V14_1_S2 (TA34-36) and V14_2_S2 (TA37-39), respectively. The whole genome sequencing and RNA-sequencing datasets generated for this study can be found in the NCBI, BioProject: PRJNA1032842.

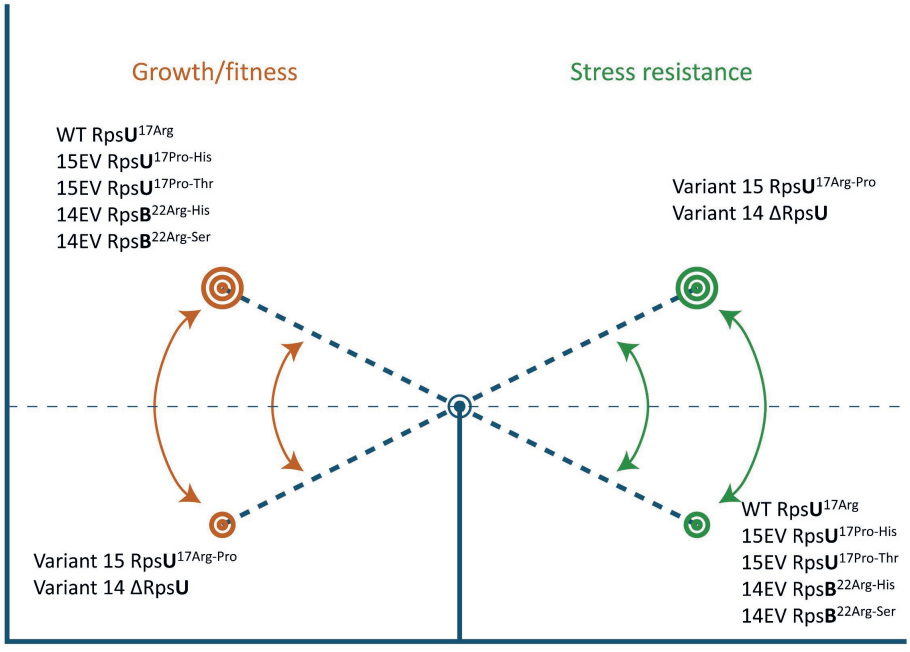

Figure 2.6: **Ribosomal mutations enable a switch between high fitness and multiple-stress resistance.** See text for details.

2.7 Acknowledgments

The authors would like to thank Angela van Hoek of the Dutch National Institute for Public Health and the Environment (RIVM) for assistance with sequencing the evolved variants.

2.8 Supplementary Material

Supplemental Table 2.1: **Primers used in construction of *rpsB* mutants**

Name	Sequence (5'to 3', restriction site underlined)	Source
rpsB-F	TTATGAATTCTTATGACAAGAGCGAGAGCACCAA	This study
rpsB-R	ACTTGTCGACTAGCGTCAGCCATTTTAGCAGTTA	This study

Supplemental Table 2.2: **Proteins above or below the cut off in *L. monocytogenes* V14, 14EV1, and 14EV2 over the wild type.** The p-value and $\log_{10}$(protein ratio) in bold are considered significant

gene ID	protein ID	EGDe locus	gene name	protein name	V14/LO28 WT		14EV1/LO28 WT		14EV2/LO28 WT	
					p-value	$\log_{10}$ ratio	p-value	$\log_{10}$ ratio	p-value	$\log_{10}$ ratio
IEJ01_00215	NP_463576.1	lmo0043	-	arginine deiminase	**0.000**	**1.21**		0.00		0.00
IEJ01_00550	NP_463643.1	lmo0110	-	lipase	**0.000**	**1.33**	**0.000**	**1.11**	**0.000**	**1.03**
IEJ01_00670	NP_463667.1	lmo0134	-	hypothetical protein lmo0134	**0.000**	**1.57**		0.00		0.00
IEJ01_01045	NP_463742.1	lmo0211	ctc	50S ribosomal protein L25	**0.000**	**1.03**	0.270	0.07	0.438	0.04
IEJ01_01390	NP_463796.1	lmo0265	-	succinyl-diaminopimelate desuccinylase	**0.000**	**1.48**		0.00		0.00
IEJ01_01435	NP_463805.1	lmo0274	-	hypothetical protein lmo0274	**0.000**	**1.07**		0.00		0.00
IEJ01_02640	NP_464043.1	lmo0515	-	hypothetical protein lmo0515	**0.000**	**1.08**		0.00		0.00
IEJ01_02760	NP_464067.1	lmo0539	-	tagatose 1,6-diphosphate aldolase	**0.001**	**1.67**	0.483	0.14	0.212	0.27
IEJ01_02960	NP_464107.1	lmo0579	-	hypothetical protein lmo0579	**0.000**	**1.41**		0.00	0.374	0.34
IEJ01_03340	NP_464181.1	lmo0654	-	hypothetical protein lmo0654	**0.000**	**2.04**	0.045	0.44	0.766	0.04
IEJ01_03415	NP_464196.1	lmo0669	-	oxidoreductase	**0.000**	**2.69**		0.00		0.00
IEJ01_03490	NP_464211.1	lmo0684	-	hypothetical protein lmo0684	**0.000**	**-1.60**	0.834	-0.03	0.935	-0.01
IEJ01_03495	NP_464212.1	lmo0685	-	flagellar motor protein MotA	**0.000**	**-1.42**	0.680	-0.05	0.264	-0.13
IEJ01_03500	NP_464213.1	lmo0686	motB	flagellar motor rotation MotB	**0.000**	**-1.08**	0.754	-0.04	0.271	-0.12
IEJ01_03515	NP_464216.1	lmo0689	-	chemotaxis protein CheV	**0.000**	**-1.90**	0.097	-0.33	0.208	-0.15
IEJ01_03520	NP_464217.1	lmo0690	flaA	flagellin	**0.000**	**-1.90**	0.002	-0.43	0.002	-0.42
IEJ01_03525	NP_464218.1	lmo0691	cheY	chemotaxis response regulator CheY	**0.000**	**-1.50**	0.815	0.01	0.810	-0.02
IEJ01_03530	NP_464219.1	lmo0692	cheA	two-component sensor histidine kinase CheA	**0.001**	**-1.19**	0.470	-0.13	0.540	-0.11
IEJ01_03590	NP_464231.1	lmo0704	-	hypothetical protein lmo0704	**0.009**	**-1.18**	0.014	-0.15	0.454	-0.08
IEJ01_03640	NP_464241.1	lmo0714	fliG	flagellar motor switch protein FliG	**0.001**	**-1.12**	0.174	-0.18	0.004	-0.28
IEJ01_03680	NP_464249.1	lmo0722	-	pyruvate oxidase	**0.000**	**2.26**		0.00		0.00

Continued on next page

Supplemental Table 2.2 continued from previous page

gene ID	protein ID	EGDe locus	gene name	protein name	V14/LO28 WT		14EV1/LO28 WT		14EV2/LO28 WT	
					p-value	$\log_{10}$ ratio	p-value	$\log_{10}$ ratio	p-value	$\log_{10}$ ratio
IEJ01_03685	NP_464250.1	lmo0723	-	metyl-accepting chemotaxis protein	**0.001**	**-2.06**	0.727	-0.05	0.041	-0.33
IEJ01_03985	NP_464311.1	lmo0784	-	PTS mannose transporter subunit IIB	**0.000**	**1.21**		0.00		0.00
IEJ01_04515	NP_464416.1	lmo0890	rsbS	negative regulation of sigma-B activity	**0.000**	**-1.83**	0.049	-0.13	0.027	-0.07
IEJ01_04655	NP_464439.1	lmo0913	-	succinate semialdehyde dehydrogenase	**0.000**	**2.95**		0.00		0.00
IEJ01_04890	NP_464485.1	lmo0960	-	protease	**0.000**	**-1.45**	0.017	-0.23	0.124	-0.15
IEJ01_04895	NP_464486.1	lmo0961	-	protease	**0.000**	**-1.71**	0.178	-0.14	0.068	-0.21
IEJ01_06620	NP_464783.1	lmo1258	-	hypothetical protein lmo1258		0.00		0.00	**0.000**	**1.49**
IEJ01_07445	NP_464947.1	lmo1422	-	glycine/betaine ABC transporter permease	**0.000**	**1.24**	0.374	0.42		0.00
IEJ01_07465	NP_464951.1	lmo1426	opuCC	glycine/betaine ABC transporter substrate-binding protein	**0.000**	**1.94**		0.00		0.00
IEJ01_07475	NP_464953.1	lmo1428	opuCA	glycine/betaine ABC transporter ATP-binding protein	**0.000**	**2.26**		0.00		0.00
IEJ01_07675	NP_464993.1	lmo1468	-	hypothetical protein lmo1468	**0.000**	**-1.98**	**0.000**	**-1.98**	**0.000**	**-1.98**
IEJ01_07680	NP_464994.1	lmo1469	rpsU	30S ribosomal protein S21	**0.000**	**-2.63**	**0.000**	**-2.63**	**0.000**	**-2.63**
IEJ01_07970	NP_465051.1	lmo1526	-	hypothetical protein lmo1526	**0.000**	**1.99**		0.00		0.00
IEJ01_08600	NP_465176.1	lmo1651	-	ABC transporter ATP-binding protein	**0.000**	**1.07**		0.00		0.00
IEJ01_08935	NP_465219.1	lmo1694	-	CDP-abequose synthase	**0.000**	**1.62**		0.00		0.00
IEJ01_09635	NP_465355.1	lmo1830	-	short-chain dehydrogenase	**0.000**	**2.11**		0.00		0.00
IEJ01_11125	NP_465650.1	lmo2126	-	maltogenic amylase	**0.001**	**-1.26**	0.090	-0.88	**0.001**	**-1.26**
IEJ01_11305	NP_465681.1	lmo2157	sepA	hypothetical protein lmo2157	**0.000**	**2.31**		0.00		0.00
IEJ01_11545	NP_465729.1	lmo2205	-	phosphoglyceromutase	**0.000**	**1.94**	0.913	-0.02	0.922	-0.02
IEJ01_11585	NP_465737.1	lmo2213	-	hypothetical protein lmo2213	**0.000**	**2.11**		0.00		0.00
IEJ01_12355	NP_465883.1	lmo2360	-	transmembrane protein	0.009	0.86	**0.003**	**-1.07**	0.977	-0.01

Continued on next page

Supplemental Table 2.2 continued from previous page

gene ID	protein ID	EGDe locus	gene name	protein name	V14/LO28 WT		14EV1/LO28 WT		14EV2/LO28 WT	
					p-value	$\log_{10}$ ratio	p-value	$\log_{10}$ ratio	p-value	$\log_{10}$ ratio
IEJ01_12600	NP_465914.1	lmo2391	-	hypothetical protein lmo2391	**0.001**	**1.69**	0.133	0.57	0.122	-0.30
IEJ01_12965	NP_465986.1	lmo2463	-	multidrug transporter	**0.000**	**1.79**		0.00		0.00
IEJ01_13505	NP_466092.1	lmo2569	-	peptide ABC transporter substrate-binding protein	**0.000**	**-1.36**	0.196	-0.12	0.056	-0.21
IEJ01_13525	NP_466096.1	lmo2573	-	zinc-binding dehydrogenase	**0.000**	**1.25**		0.00		0.00
IEJ01_14510	NP_466270.1	lmo2748	-	hypothetical protein lmo2748	**0.000**	**2.20**		0.00		0.00

Supplemental Table 2.3: **Genes with RNAseq expression levels above or below the cut off in *L. monocytogenes* V14, 14EV1, and 14EV2 over the wild type.** The p-value and $\log_2$(Fold change) in bold are considered significant

gene ID	protein ID	EGDe locus	gene name	protein name	V14/LO28 WT		14EV1/LO28 WT		14EV2/LO28 WT	
					p-value	$\log_2$(Fold change)	p-value	$\log_2$(Fold change)	p-value	$\log_2$(Fold change)
IEJ01_00095	NP_463552.1	lmo0019	-	hypothetical protein lmo0019	**0.000**	**6.49**	0.087	0.33	0.353	-0.13
IEJ01_00125	NP_463558.1	lmo0025	-	phosphoheptose isomerase	**0.000**	**3.78**	0.598	0.05	0.429	0.10
IEJ01_00190	NP_463571.1	lmo0038	-	agmatine deiminase	**0.000**	**1.67**	0.916	-0.02	0.649	-0.08
IEJ01_00195	NP_463572.1	lmo0039	-	carbamate kinase	**0.000**	**1.88**	0.939	0.02	0.890	-0.03
IEJ01_00215	NP_463576.1	lmo0043	-	arginine deiminase	**0.000**	**4.22**	0.697	0.07	0.952	0.01
IEJ01_00485	NP_463630.1	lmo0097	-	PTS mannose transporter subunit IIC	**0.000**	**-1.71**	0.000	-0.47	0.000	-1.04
IEJ01_00525	NP_463638.1	lmo0105	-	chitinase B	0.015	-0.70	0.002	-0.93	**0.000**	**-1.94**
IEJ01_00665	NP_463666.1	lmo0133	-	hypothetical protein lmo0133	**0.000**	**7.24**	0.014	1.12	0.249	0.17
IEJ01_00670	NP_463667.1	lmo0134	-	hypothetical protein lmo0134	**0.000**	**6.01**	0.044	0.50	0.513	0.11
IEJ01_00765	NP_463686.1	lmo0153	-	zinc ABC transporter substrate-binding protein	**0.000**	**-2.21**	0.764	-0.05	0.572	-0.09
IEJ01_00845	NP_463702.1	lmo0169	-	glucose transporter	**0.000**	**4.36**	0.952	-0.01	0.490	-0.10
IEJ01_00850	NP_463703.1	lmo0170	-	hypothetical protein lmo0170	**0.000**	**2.79**	0.933	0.02	0.860	0.03
IEJ01_00990	NP_463731.1	lmo0200	prfA	listeriolysin positive regulatory protein	**0.000**	**1.73**	0.653	0.07	0.060	0.34
IEJ01_01045	NP_463742.1	lmo0211	ctc	50S ribosomal protein L25	**0.000**	**2.74**	0.287	0.15	0.738	0.05
IEJ01_01380	NP_463794.1	lmo0263	inlH	internalin H	**0.000**	**7.58**	0.000	1.61	0.175	0.25
IEJ01_01390	NP_463796.1	lmo0265	-	succinyl-diaminopimelate desuccinylase	**0.000**	**7.37**	0.000	1.41	0.664	0.07
IEJ01_01435	NP_463805.1	lmo0274	-	hypothetical protein lmo0274	**0.000**	**2.44**	0.040	0.28	0.000	0.47
IEJ01_01520	NP_463822.1	lmo0291	-	hypothetical protein lmo0291	**0.000**	**1.81**	0.765	0.05	0.983	0.00

Continued on next page

Supplemental Table 2.3 continued from previous page

gene ID	protein ID	EGDe locus	gene name	protein name	V14/LO28 WT		14EV1/LO28 WT		14EV2/LO28 WT	
					p-value	$\log_2$(Fold change)	p-value	$\log_2$(Fold change)	p-value	$\log_2$(Fold change)
IEJ01_06335	NP_463822.1	lmo0291	-	hypothetical protein lmo0291	**0.000**	**-1.67**	0.624	0.06	0.547	0.10
IEJ01_01525	NP_463823.1	lmo0292	-	heat-shock protein htrA serine protease	**0.000**	**1.85**	0.432	-0.08	0.000	-0.34
IEJ01_01570	NP_463832.1	lmo0301	-	PTS beta-glucoside transporter subunit IIA	**0.000**	**-1.96**	0.929	-0.01	0.567	-0.08
IEJ01_01670	NP_463851.1	lmo0321	-	hypothetical protein lmo0321	**0.000**	**5.57**	0.197	0.21	0.185	-0.25
IEJ01_01675	NP_463852.1	lmo0322	-	hypothetical protein lmo0322	**0.000**	**3.07**	0.272	-0.11	0.890	-0.02
IEJ01_01690	NP_463855.1	lmo0325	-	transcriptional regulator	**0.000**	**1.86**	0.769	-0.05	0.452	0.10
IEJ01_01695	NP_463856.1	lmo0326	-	transcriptional regulator	**0.003**	**2.38**	0.804	-0.01		0.00
IEJ01_01810	NP_463881.1	lmo0351	-	phosphotransferase mannnose-specific family component IIA	**0.000**	**1.88**	0.658	-0.06	0.129	-0.30
IEJ01_01985	NP_463914.1	lmo0384	-	IolB protein	**0.006**	**-1.85**	0.745	-0.02		-0.07
IEJ01_02060	NP_463929.1	lmo0399	-	PTS fructose transporter subunit IIB	**0.000**	**-1.96**	0.884	-0.02	0.080	-0.37
IEJ01_02090	NP_463935.1	lmo0405	-	phosphate transporter	**0.000**	**3.58**	0.693	0.07	0.996	0.00
IEJ01_02115	NP_463940.1	lmo0411	-	phosphoenolpyruvate synthase	**0.000**	**1.63**	0.873	0.03	0.219	0.13
IEJ01_02190	NP_463955.1	lmo0426	-	PTS fructose transporter subunit IIA	**0.000**	**-1.64**	0.963	-0.01	0.663	0.07
IEJ01_02225	NP_463962.1	lmo0433	inlA	internalin A	**0.000**	**4.01**	0.140	-0.20	0.044	-0.26
IEJ01_02230	NP_463963.1	lmo0434	inlB	internalin B	**0.000**	**2.12**	0.055	-0.28	0.630	-0.07
IEJ01_02245	NP_463966.1	lmo0437	-	hypothetical protein lmo0437	**0.000**	**-2.07**	0.929	0.02	0.003	0.39
IEJ01_02250	NP_463967.1	lmo0438	-	hypothetical protein lmo0438	**0.000**	**5.20**	0.073	0.13	0.008	1.69
IEJ01_02255	NP_463968.1	lmo0439	-	hypothetical protein lmo0439	**0.000**	**5.48**	0.135	0.25	0.987	0.00
IEJ01_02285	NP_463974.1	lmo0445	-	transcripitonal regulator	**0.000**	**4.63**	0.510	0.10	0.498	0.11
IEJ01_02590	NP_464033.1	lmo0505	-	ribulose-5-phosphate 3-epimerase	**0.000**	**1.60**	0.785	0.03	0.218	0.21

Continued on next page

Supplemental Table 2.3 continued from previous page

gene ID	protein ID	EGDe locus	gene name	protein name	V14/LO28 WT		14EV1/LO28 WT		14EV2/LO28 WT	
					p-value	$\log_2$(Fold change)	p-value	$\log_2$(Fold change)	p-value	$\log_2$(Fold change)
IEJ01_02640	NP_464043.1	lmo0515	-	hypothetical protein lmo0515	**0.000**	**5.45**	0.000	1.02	0.146	0.26
IEJ01_02685	NP_464052.1	lmo0524	-	sulfate transporter	**0.000**	**2.27**	0.619	0.07	0.363	0.10
IEJ01_02760	NP_464067.1	lmo0539	-	tagatose 1,6-diphosphate aldolase	**0.000**	**4.58**	0.020	0.28	0.217	0.16
IEJ01_02835	NP_464082.1	lmo0554	-	NADH-dependent butanol dehydrogenase	**0.000**	**3.59**	0.957	-0.01	0.179	-0.17
IEJ01_02840	NP_464083.1	lmo0555	-	di-tripeptide transporter	**0.000**	**2.29**	0.988	0.00	0.741	-0.04
IEJ01_02960	NP_464107.1	lmo0579	-	hypothetical protein lmo0579	**0.000**	**2.10**	0.285	0.14	0.189	0.17
IEJ01_02965	NP_464108.1	lmo0580	-	hypothetical protein lmo0580	**0.000**	**2.07**	0.559	0.08	0.417	0.09
IEJ01_02985	NP_464112.1	lmo0584	-	hypothetical protein lmo0584	**0.000**	**1.61**	0.720	0.05	0.904	-0.02
IEJ01_03010	NP_464117.1	lmo0589	-	hypothetical protein lmo0589	**0.000**	**3.87**	0.596	-0.07	0.452	-0.13
IEJ01_03015	NP_464118.1	lmo0590	-	hypothetical protein lmo0590	**0.000**	**3.27**	0.989	0.00	0.055	-0.36
IEJ01_03020	NP_464119.1	lmo0591	-	hypothetical protein lmo0591	**0.000**	**3.18**	0.796	0.04	0.486	-0.12
IEJ01_03045	NP_464124.1	lmo0596	-	hypothetical protein lmo0596	**0.000**	**7.54**	0.000	1.36	0.142	0.25
IEJ01_03075	NP_464129.1	lmo0602	-	transcripitonal regulator	**0.000**	**6.86**	0.000	1.03	0.097	0.29
IEJ01_03090	NP_464132.1	lmo0605	-	hypothetical protein lmo0605	**0.000**	**1.81**	0.171	0.16	0.010	0.27
IEJ01_03100	NP_464134.1	lmo0607	-	ABC transporter ATP-binding protein	**0.000**	**1.62**	0.841	-0.03	0.996	0.00
IEJ01_03105	NP_464135.1	lmo0608	-	ABC transporter ATP-binding protein	**0.000**	**1.94**	0.868	-0.03	0.861	0.02
IEJ01_03115	NP_464137.1	lmo0610	-	internalin	**0.000**	**4.68**	0.005	0.44	0.117	0.23
IEJ01_03205	NP_464155.1	lmo0628	-	hypothetical protein lmo0628	**0.000**	**6.18**	0.316	0.10	0.007	0.94
IEJ01_03210	NP_464156.1	lmo0629	-	hypothetical protein lmo0629	**0.000**	**2.63**	0.323	0.15	0.227	0.18

Continued on next page

Supplemental Table 2.3 continued from previous page

gene ID	protein ID	EGDe locus	gene name	protein name	V14/LO28 WT		14EV1/LO28 WT		14EV2/LO28 WT	
					p-value	$\log_2$(Fold change)	p-value	$\log_2$(Fold change)	p-value	$\log_2$(Fold change)
IEJ01_03280	NP_464169.1	lmo0642	-	hypothetical protein lmo0642	**0.000**	**1.93**	0.121	-0.20	0.127	-0.19
IEJ01_03305	NP_464174.1	lmo0647	-	hypothetical protein lmo0647	**0.000**	**3.04**	0.000	0.62	0.000	0.50
IEJ01_03310	NP_464175.1	lmo0648	-	hypothetical protein lmo0648	**0.000**	**3.49**	0.967	0.01	0.957	0.01
IEJ01_03315	NP_464176.1	lmo0649	-	transcriptional regulator	**0.000**	**2.15**	0.775	0.05	0.861	-0.03
IEJ01_03320	NP_464177.1	lmo0650	-	hypothetical protein lmo0650	**0.000**	**1.81**	0.782	-0.04	0.198	-0.14
IEJ01_03340	NP_464181.1	lmo0654	-	hypothetical protein lmo0654	**0.000**	**3.67**	0.000	0.62	0.608	0.08
IEJ01_03345	NP_464182.1	lmo0655	-	phosphoprotein phosphatase	**0.000**	**3.63**	0.001	0.49	0.713	0.06
IEJ01_03415	NP_464196.1	lmo0669	-	oxidoreductase	**0.000**	**7.23**	0.041	0.52	0.260	-0.19
IEJ01_03420	NP_464197.1	lmo0670	-	hypothetical protein lmo0670	**0.000**	**7.44**	0.477	0.07	0.872	-0.02
IEJ01_03460	NP_464205.1	lmo0678	fliR	flagellar biosynthesis protein FliR	**0.000**	**-6.03**	0.004	-0.39	0.000	-0.58
IEJ01_03465	NP_464206.1	lmo0679	flhB	flagellar biosynthesis protein FlhB	**0.000**	**-5.70**	0.004	-0.33	0.000	-0.52
IEJ01_03470	NP_464207.1	lmo0680	flhA	flagellar biosynthesis protein FlhA	**0.000**	**-5.48**	0.055	-0.32	0.000	-0.69
IEJ01_03475	NP_464208.1	lmo0681	-	flagellar biosynthesis regulator FlhF	**0.000**	**-5.61**	0.089	-0.28	0.000	-0.71
IEJ01_03480	NP_464209.1	lmo0682	flgG	flagellar basal body rod protein FlgG	**0.000**	**-5.87**	0.112	-0.25	0.000	-0.72
IEJ01_03485	NP_464210.1	lmo0683	-	chemotaxis protein CheR	**0.000**	**-5.60**	0.026	-0.33	0.000	-0.69
IEJ01_03490	NP_464211.1	lmo0684	-	hypothetical protein lmo0684	**0.000**	**-5.19**	0.013	-0.41	0.000	-0.65
IEJ01_03495	NP_464212.1	lmo0685	-	flagellar motor protein MotA	**0.000**	**-5.43**	0.018	-0.36	0.000	-0.71
IEJ01_03500	NP_464213.1	lmo0686	motB	flagellar motor rotation MotB	**0.000**	**-5.92**	0.019	-0.35	0.000	-0.67

Continued on next page

Supplemental Table 2.3 continued from previous page

gene ID	protein ID	EGDe locus	gene name	protein name	V14/LO28 WT		14EV1/LO28 WT		14EV2/LO28 WT	
					p-value	$\log_2$(Fold change)	p-value	$\log_2$(Fold change)	p-value	$\log_2$(Fold change)
IEJ01_03505	NP_464214.1	lmo0687	-	hypothetical protein lmo0687	**0.000**	**-5.58**	0.006	-0.36	0.000	-0.58
IEJ01_03510	NP_464215.1	lmo0688	-	hypothetical protein lmo0688	**0.000**	**-5.30**	0.006	-0.38	0.000	-0.59
IEJ01_03515	NP_464216.1	lmo0689	-	chemotaxis protein CheV	**0.000**	**-5.51**	0.034	-0.35	0.001	-0.57
IEJ01_03520	NP_464217.1	lmo0690	flaA	flagellin	**0.000**	**-7.43**	0.413	-0.05	0.134	-0.14
IEJ01_03525	NP_464218.1	lmo0691	cheY	chemotaxis response regulator CheY	**0.000**	**-5.99**	0.433	-0.10	0.220	-0.22
IEJ01_03530	NP_464219.1	lmo0692	cheA	two-component sensor histidine kinase CheA	**0.000**	**-5.95**	0.566	-0.06	0.286	-0.16
IEJ01_03535	NP_464220.1	lmo0693	-	flagellar motor switch protein FliY	**0.000**	**-5.64**	0.556	-0.08	0.196	-0.24
IEJ01_03540	NP_464221.1	lmo0694	-	hypothetical protein lmo0694	**0.000**	**-5.65**	0.436	-0.10	0.165	-0.26
IEJ01_03545	NP_464222.1	lmo0695	-	hypothetical protein lmo0695	**0.000**	**-5.86**	0.028	-0.39	0.001	-0.57
IEJ01_03550	NP_464223.1	lmo0696	flgD	flagellar basal body rod modification protein	**0.000**	**-5.61**	0.302	-0.12	0.104	-0.34
IEJ01_03555	NP_464224.1	lmo0697	flgE	flagellar hook protein FlgE	**0.000**	**-5.92**	0.297	-0.11	0.089	-0.37
IEJ01_03560	NP_464225.1	lmo0698	-	flagellar motor switch protein	**0.000**	**-6.16**	0.000	-0.55	0.000	-0.76
IEJ01_03565	NP_464226.1	lmo0699	fliM	flagellar motor switch protein FliM	**0.000**	**-5.91**	0.000	-0.62	0.000	-0.80
IEJ01_03570	NP_464227.1	lmo0700	-	flagellar motor switch protein FliY	**0.000**	**-5.91**	0.131	-0.25	0.033	-0.58
IEJ01_03575	NP_464228.1	lmo0701	-	hypothetical protein lmo0701	**0.000**	**-5.91**	0.000	-0.72	0.000	-0.89
IEJ01_03580	NP_464229.1	lmo0702	-	hypothetical protein lmo0702	**0.000**	**-5.92**	0.037	-0.51	0.002	-0.79
IEJ01_03585	NP_464230.1	lmo0703	-	hypothetical protein lmo0703	**0.000**	**-5.60**	0.001	-0.52	0.000	-0.67
IEJ01_03590	NP_464231.1	lmo0704	-	hypothetical protein lmo0704	**0.000**	**-5.66**	0.160	-0.20	0.034	-0.56

Continued on next page

Supplemental Table 2.3 continued from previous page

gene ID	protein ID	EGDe locus	gene name	protein name	V14/LO28 WT		14EV1/LO28 WT		14EV2/LO28 WT	
					p-value	$\log_2$(Fold change)	p-value	$\log_2$(Fold change)	p-value	$\log_2$(Fold change)
IEJ01_03595	NP_464232.1	lmo0705	flgK	flagellar hook-associated protein FlgK	**0.000**	**-5.44**	0.002	-0.57	0.000	-0.78
IEJ01_03600	NP_464233.1	lmo0706	flgL	flagellar hook-associated protein FlgL	**0.000**	**-5.55**	0.000	-0.55	0.000	-0.74
IEJ01_03605	NP_464234.1	lmo0707	fliD	flagellar capping protein FliD	**0.000**	**-5.50**	0.087	-0.35	0.013	-0.60
IEJ01_03610	NP_464235.1	lmo0708	-	flagellar protein	**0.000**	**-5.58**	0.123	-0.28	0.041	-0.48
IEJ01_03615	NP_464236.1	lmo0709	-	hypothetical protein lmo0709	**0.000**	**-5.64**	0.000	-0.59	0.000	-0.64
IEJ01_03620	NP_464237.1	lmo0710	flgB	flagellar basal-body rod protein FlgB	**0.000**	**-5.67**	0.003	-0.50	0.000	-0.66
IEJ01_03625	NP_464238.1	lmo0711	flgC	flagellar basal body rod protein FlgC	**0.000**	**-5.65**	0.001	-0.55	0.000	-0.75
IEJ01_03630	NP_464239.1	lmo0712	fliE	flagellar hook-basal body protein FliE	**0.000**	**-5.30**	0.027	-0.35	0.000	-0.57
IEJ01_03635	NP_464240.1	lmo0713	fliF	flagellar MS-ring protein FliF	**0.000**	**-4.86**	0.006	-0.53	0.001	-0.63
IEJ01_03640	NP_464241.1	lmo0714	fliG	flagellar motor switch protein FliG	**0.000**	**-4.70**	0.000	-0.52	0.000	-0.72
IEJ01_03645	NP_464242.1	lmo0715	fliH	flagellar assembly protein H	**0.000**	**-4.70**	0.000	-0.54	0.000	-0.62
IEJ01_03650	NP_464243.1	lmo0716	fliI	flagellum-specific ATP synthase	**0.000**	**-4.57**	0.004	-0.40	0.000	-0.49
IEJ01_03655	NP_464244.1	lmo0717	-	transglycosylase	**0.000**	**-4.64**	0.000	-0.41	0.000	-0.44
IEJ01_03660	NP_464245.1	lmo0718	-	hypothetical protein lmo0718	**0.000**	**-4.46**	0.060	-0.22	0.004	-0.32
IEJ01_03680	NP_464249.1	lmo0722	-	pyruvate oxidase	**0.000**	**5.71**	0.043	0.37	0.214	0.21
IEJ01_03685	NP_464250.1	lmo0723	-	metyl-accepting chemotaxis protein	**0.000**	**-2.58**	0.000	-0.59	0.000	-1.11
IEJ01_03690	NP_464251.1	lmo0724	-	hypothetical protein lmo0724	**0.000**	**-2.52**	0.000	-0.46	0.000	-0.80
IEJ01_03865	NP_464287.1	lmo0760	-	hypothetical protein lmo0760	**0.000**	**1.68**	0.013	-0.40	0.286	-0.16

Continued on next page

Supplemental Table 2.3 continued from previous page

gene ID	protein ID	EGDe locus	gene name	protein name	V14/LO28 WT		14EV1/LO28 WT		14EV2/LO28 WT	
					p-value	$\log_2$(Fold change)	p-value	$\log_2$(Fold change)	p-value	$\log_2$(Fold change)
IEJ01_03970	NP_464308.1	lmo0781	-	PTS mannose transporter subunit IID	**0.000**	**5.08**	0.403	-0.11	0.000	-0.52
IEJ01_03975	NP_464309.1	lmo0782	-	PTS mannose transporter subunit IIC	**0.000**	**5.20**	0.335	-0.13	0.000	-0.44
IEJ01_03980	NP_464310.1	lmo0783	-	PTS mannose transporter subunit IIB	**0.000**	**4.60**	0.983	-0.01	0.000	-0.64
IEJ01_03985	NP_464311.1	lmo0784	-	PTS mannose transporter subunit IIB	**0.000**	**4.34**	0.933	0.02	0.000	-0.53
IEJ01_04035	NP_464321.1	lmo0794	-	hypothetical protein lmo0794	**0.000**	**4.83**	0.905	-0.03	0.873	-0.03
IEJ01_04045	NP_464323.1	lmo0796	-	hypothetical protein lmo0796	**0.000**	**3.66**	0.155	-0.19	0.000	-0.47
IEJ01_04235	NP_464362.1	lmo0835	-	peptidoglycan binding protein	**0.000**	**-2.03**	0.000	-1.05	0.072	-0.29
IEJ01_04355	NP_464385.1	lmo0859	-	sugar ABC transporter substrate-binding protein	**0.000**	**-2.02**	0.164	-0.21	0.086	-0.37
IEJ01_04465	NP_464406.1	lmo0880	-	wall associated protein precursor	**0.000**	**9.70**	0.000	2.31	0.022	0.75
IEJ01_04540	NP_464421.1	lmo0895	sigB	RNA polymerase sigma factor SigB	**0.000**	**1.68**	0.113	0.14	0.001	0.27
IEJ01_04545	NP_464422.1	lmo0896	rsbX	indirect negative regulation of sigma B dependant gene expression (serine phosphatase)	**0.000**	**1.93**	0.000	0.27	0.000	0.35
IEJ01_04550	NP_464423.1	lmo0897	-	transporter	**0.000**	**-1.89**	0.731	-0.06	0.050	-0.31
IEJ01_04610	NP_464430.1	lmo0904	-	hypothetical protein lmo0904	**0.000**	**1.74**	0.384	0.12	0.029	0.29
IEJ01_04645	NP_464437.1	lmo0911	-	hypothetical protein lmo0911	**0.000**	**3.75**	0.033	0.26	0.980	0.00
IEJ01_04655	NP_464439.1	lmo0913	-	succinate semialdehyde dehydrogenase	**0.000**	**8.58**	0.000	1.60	0.584	0.08
IEJ01_04725	NP_464453.1	lmo0928	-	3-methyladenine DNA glycosylase	**0.000**	**1.97**	0.841	0.04	0.020	0.33

Continued on next page

Supplemental Table 2.3 continued from previous page

gene ID	protein ID	EGDe locus	gene name	protein name	V14/LO28 WT		14EV1/LO28 WT		14EV2/LO28 WT	
					p-value	$\log_2$(Fold change)	p-value	$\log_2$(Fold change)	p-value	$\log_2$(Fold change)
IEJ01_04775	NP_464462.1	lmo0937	-	hypothetical protein lmo0937	**0.000**	**6.19**	0.000	1.18	0.092	0.26
IEJ01_04805	NP_464468.1	lmo0943	fri	non-heme iron-binding ferritin	**0.000**	**2.32**	0.000	0.40	0.001	0.36
IEJ01_04855	NP_464478.1	lmo0953	-	hypothetical protein lmo0953	**0.000**	**5.66**	0.000	1.05	0.000	0.61
IEJ01_04890	NP_464485.1	lmo0960	-	protease	**0.000**	**-1.85**	0.376	-0.12	0.006	-0.37
IEJ01_04895	NP_464486.1	lmo0961	-	protease	**0.000**	**-2.10**	0.213	-0.18	0.001	-0.50
IEJ01_05065	NP_464519.1	lmo0994	-	hypothetical protein lmo0994	**0.000**	**8.59**	0.000	2.25	0.071	0.40
IEJ01_05070	NP_464520.1	lmo0995	-	hypothetical protein lmo0995	**0.000**	**7.50**	0.000	1.15	0.054	0.33
IEJ01_05700	NP_464665.1	lmo1140	-	hypothetical protein lmo1140	**0.000**	**5.16**	0.002	0.67	0.236	0.20
IEJ01_06525	NP_464766.1	lmo1241	-	hypothetical protein lmo1241	**0.000**	**5.81**	0.002	0.54	0.408	0.13
IEJ01_06635	NP_464786.1	lmo1261	-	hypothetical protein lmo1261	**0.000**	**3.28**	0.189	0.15	0.802	0.03
IEJ01_06795	NP_464818.1	lmo1293	glpD	glycerol-3-phosphate dehydrogenase	**0.000**	**1.86**	0.166	-0.20	0.079	-0.25
IEJ01_06805	NP_464820.1	lmo1295	-	host factor-1 protein	**0.000**	**2.51**	0.189	0.17	0.879	-0.02
IEJ01_07030	NP_464865.1	lmo1340	-	hypothetical protein lmo1340	**0.000**	**1.89**	0.857	0.03	0.608	0.07
IEJ01_07210	NP_464900.1	lmo1375	-	aminotripeptidase	**0.000**	**2.32**	0.846	-0.03	0.951	0.01
IEJ01_07440	NP_464946.1	lmo1421	-	glycine/betaine ABC transporter ATP-binding protein	**0.000**	**4.12**	0.951	0.01	0.841	0.03
IEJ01_07445	NP_464947.1	lmo1422	-	glycine/betaine ABC transporter permease	**0.000**	**3.85**	0.359	-0.13	0.316	-0.14
IEJ01_07460	NP_464950.1	lmo1425	opuCD	glycine/betaine ABC transporter permease	**0.000**	**7.16**	0.000	1.25	0.024	0.39
IEJ01_07465	NP_464951.1	lmo1426	opuCC	glycine/betaine ABC transporter substrate-binding protein	**0.000**	**7.04**	0.000	1.03	0.135	0.27

Continued on next page

Supplemental Table 2.3 continued from previous page

gene ID	protein ID	EGDe locus	gene name	protein name	V14/LO28 WT		14EV1/LO28 WT		14EV2/LO28 WT	
					p-value	$\log_2$(Fold change)	p-value	$\log_2$(Fold change)	p-value	$\log_2$(Fold change)
IEJ01_07470	NP_464952.1	lmo1427	opuCB	glycine/betaine ABC transporter permease	**0.000**	**6.52**	0.013	0.51	0.713	-0.06
IEJ01_07475	NP_464953.1	lmo1428	opuCA	glycine/betaine ABC transporter ATP-binding protein	**0.000**	**6.57**	0.000	0.85	0.895	-0.02
IEJ01_07500	NP_464958.1	lmo1433	-	glutathione reductase	**0.000**	**3.77**	0.899	-0.03	0.603	0.08
IEJ01_07670	NP_464992.1	lmo1467	-	phosphate starvation-induced protein PhoH	**0.000**	**-2.34**	**0.000**	**-1.86**	**0.000**	**-1.92**
IEJ01_07675	NP_464993.1	lmo1468	-	hypothetical protein lmo1468	**0.000**	**-20.08**	**0.000**	**-19.89**	**0.000**	**-20.24**
IEJ01_07680	NP_464994.1	lmo1469	rpsU	30S ribosomal protein S21	**0.000**	**-19.80**	**0.000**	**-19.62**	**0.000**	**-19.96**
IEJ01_07970	NP_465051.1	lmo1526	-	hypothetical protein lmo1526	**0.000**	**4.43**	0.892	-0.02	0.885	0.02
IEJ01_08030	NP_465063.1	lmo1538	glpK	glycerol kinase	**0.000**	**2.34**	0.659	0.06	0.723	0.04
IEJ01_08035	NP_465064.1	lmo1539	-	glycerol transporter	**0.000**	**3.09**	0.632	0.08	0.936	0.01
IEJ01_08240	NP_465105.1	lmo1580	-	hypothetical protein lmo1580	**0.000**	**2.56**	0.220	0.17	0.910	0.02
IEJ01_08290	NP_465115.1	lmo1590	argJ	bifunctional ornithine acetyltransferase/N-acetylglutamate synthase	**0.002**	**-2.30**	0.608	0.03	0.890	-0.01
IEJ01_08295	NP_465116.1	lmo1591	argC	N-acetyl-gamma-glutamyl-phosphate reductase	**0.000**	**-2.26**	0.739	0.02	0.870	-0.02
IEJ01_08350	NP_465126.1	lmo1601	-	general stress protein	**0.000**	**2.69**	0.000	0.41	0.237	0.13
IEJ01_08355	NP_465127.1	lmo1602	-	hypothetical protein lmo1602	**0.000**	**2.59**	0.000	0.51	0.013	0.22
IEJ01_08360	NP_465128.1	lmo1603	-	aminopeptidase	**0.000**	**-1.61**	0.000	-0.63	0.000	-0.85
IEJ01_08585	NP_465173.1	lmo1648	-	hypothetical protein lmo1648	**0.000**	**1.79**	0.272	0.14	0.000	0.42
IEJ01_08595	NP_465175.1	lmo1650	-	hypothetical protein lmo1650	**0.000**	**1.83**	0.272	0.15	0.899	0.02
IEJ01_08600	NP_465176.1	lmo1651	-	ABC transporter ATP-binding protein	**0.000**	**2.26**	0.229	0.16	0.705	-0.05

Continued on next page

Supplemental Table 2.3 continued from previous page

gene ID	protein ID	EGDe locus	gene name	protein name	V14/LO28 WT		14EV1/LO28 WT		14EV2/LO28 WT	
					p-value	$\log_2$(Fold change)	p-value	$\log_2$(Fold change)	p-value	$\log_2$(Fold change)
IEJ01_08605	NP_465177.1	lmo1652	-	ABC transporter ATP-binding protein	**0.000**	**1.63**	0.793	-0.04	0.242	-0.16
IEJ01_08675	NP_465191.1	lmo1666	-	peptidoglycan-linked protein	**0.000**	**2.12**	0.763	0.05	0.481	-0.09
IEJ01_08935	NP_465219.1	lmo1694	-	CDP-abequose synthase	**0.000**	**6.67**	0.000	0.97	0.748	0.06
IEJ01_08960	NP_465224.1	lmo1699	-	chemotaxis protein	**0.000**	**-5.89**	0.053	-0.33	0.000	-0.62
IEJ01_08965	NP_465225.1	lmo1700	-	hypothetical protein lmo1700	**0.000**	**-6.12**	0.169	-0.20	0.001	-0.55
IEJ01_09030	NP_465238.1	lmo1713	-	rod shape-determining protein MreB	**0.000**	**1.92**	0.184	0.14	0.671	0.05
IEJ01_09320	NP_465295.1	lmo1770	purL	phosphoribosylformylglycinamidine synthase I	**0.000**	**1.61**	0.960	-0.01	0.634	-0.08
IEJ01_09425	NP_465313.1	lmo1788	-	transcriptional regulator	**0.000**	**2.15**	0.992	0.00	0.933	-0.02
IEJ01_09430	NP_465314.1	lmo1789	-	hypothetical protein lmo1789	**0.000**	**1.90**	0.967	-0.01	0.967	-0.01
IEJ01_09435	NP_465315.1	lmo1790	-	hypothetical protein lmo1790	**0.000**	**2.30**	0.583	0.09	0.743	0.05
IEJ01_09475	NP_465323.1	lmo1798	-	hypothetical protein lmo1798	**0.000**	**1.87**	0.717	0.06	0.167	0.26
IEJ01_09480	NP_465324.1	lmo1799	-	peptidoglycan binding protein	**0.000**	**2.69**	0.866	0.03	0.033	0.44
IEJ01_09635	NP_465355.1	lmo1830	-	short-chain dehydrogenase	**0.000**	**6.77**	0.000	1.04	0.989	0.00
IEJ01_09825	NP_465393.1	lmo1868	-	hypothetical protein lmo1868	**0.000**	**1.59**	0.502	0.10	0.677	0.07
IEJ01_09895	NP_465407.1	lmo1883	-	chitinase	**0.000**	**3.06**	0.713	-0.05	0.397	-0.14
IEJ01_10400	NP_465507.1	lmo1983	ilvD	dihydroxy-acid dehydratase	**0.000**	**2.06**	0.314	0.14	0.103	0.32
IEJ01_10405	NP_465508.1	lmo1984	ilvB	acetolactate synthase	**0.000**	**1.95**	0.216	0.20	0.005	0.51
IEJ01_10410	NP_465509.1	lmo1985	ilvH	acetolactate synthase small subunit	**0.000**	**2.05**	0.562	0.07	0.137	0.30
IEJ01_10415	NP_465510.1	lmo1986	ilvC	ketol-acid reductoisomerase	**0.000**	**2.05**	0.287	0.16	0.001	0.58
IEJ01_10420	NP_465511.1	lmo1987	leuA	2-isopropylmalate synthase	**0.000**	**2.40**	0.057	0.39	0.000	0.80

Continued on next page

Supplemental Table 2.3 continued from previous page

gene ID	protein ID	EGDe locus	gene name	protein name	V14/LO28 WT		14EV1/LO28 WT		14EV2/LO28 WT	
					p-value	$\log_2$(Fold change)	p-value	$\log_2$(Fold change)	p-value	$\log_2$(Fold change)
IEJ01_10425	NP_465512.1	lmo1988	leuB	3-isopropylmalate dehydrogenase	**0.000**	**2.48**	0.002	0.86	0.000	0.96
IEJ01_10430	NP_465513.1	lmo1989	leuC	isopropylmalate isomerase large subunit	**0.000**	**2.68**	0.001	0.76	0.000	1.34
IEJ01_10435	NP_465514.1	lmo1990	leuD	isopropylmalate isomerase small subunit	**0.000**	**2.62**	0.009	0.94	0.002	1.09
IEJ01_10440	NP_465515.1	lmo1991	ilvA	threonine dehydratase	**0.000**	**2.66**	0.001	0.91	0.000	1.04
IEJ01_10820	NP_465591.1	lmo2067	-	bile acid hydrolase	**0.000**	**5.30**	0.000	0.55	0.940	-0.01
IEJ01_10915	NP_465609.1	lmo2085	-	peptidoglycan binding protein	**0.000**	**5.90**	0.000	0.86	0.010	0.46
IEJ01_10940	NP_465614.1	lmo2090	argG	argininosuccinate synthase	**0.000**	**-3.05**	0.502	0.04	0.894	0.02
IEJ01_10945	NP_465615.1	lmo2091	argH	argininosuccinate lyase	**0.000**	**-3.17**	0.481	0.03	0.737	-0.02
IEJ01_10985	NP_465623.1	lmo2099	-	transcriptional antiterminator	**0.000**	**-1.67**	0.019	-0.57	0.001	-0.79
IEJ01_11020	YP_008475638.1	lmo2104a	-	hypothetical protein lmo2104a	**0.000**	**-1.63**	0.846	0.02	0.422	-0.11
IEJ01_11100	NP_465645.1	lmo2121	-	maltose phosphorylase	**0.000**	**-2.42**	0.000	-1.42	0.000	-1.16
IEJ01_11105	NP_465646.1	lmo2122	-	maltodextrose utilization protein MalA	**0.000**	**-2.28**	0.000	-1.43	0.000	-1.33
IEJ01_11110	NP_465647.1	lmo2123	-	sugar ABC transporter permease	**0.000**	**-2.87**	0.000	-1.35	0.000	-1.40
IEJ01_11115	NP_465648.1	lmo2124	-	sugar ABC transporter permease	**0.000**	**-2.69**	0.000	-0.90	0.000	-1.21
IEJ01_11120	NP_465649.1	lmo2125	-	sugar ABC transporter substrate-binding protein	**0.000**	**-2.39**	0.653	-0.05	0.013	-0.79
IEJ01_11125	NP_465650.1	lmo2126	-	maltogenic amylase	**0.000**	**-1.78**	0.384	-0.10	0.023	-0.62
IEJ01_11175	NP_465655.1	lmo2131	-	hypothetical protein lmo2131	**0.000**	**2.53**	0.700	0.05	0.059	0.47
IEJ01_11180	NP_465656.1	lmo2132	-	hypothetical protein lmo2132	**0.000**	**4.52**	0.960	0.01	0.214	0.22
IEJ01_11305	NP_465681.1	lmo2157	sepA	hypothetical protein lmo2157	**0.000**	**6.67**	0.000	0.75	0.414	0.12
IEJ01_11310	NP_465682.1	lmo2158	-	hypothetical protein lmo2158	**0.000**	**6.36**	0.047	0.33	0.005	-0.48

Continued on next page

Supplemental Table 2.3 continued from previous page

gene ID	protein ID	EGDe locus	gene name	protein name	V14/LO28 WT		14EV1/LO28 WT		14EV2/LO28 WT	
					p-value	$\log_2$(Fold change)	p-value	$\log_2$(Fold change)	p-value	$\log_2$(Fold change)
IEJ01_11325	NP_465685.1	lmo2161	-	hypothetical protein lmo2161	**0.000**	**-1.67**	0.014	-0.87	0.007	-0.90
IEJ01_11335	NP_465687.1	lmo2163	-	oxidoreductase	**0.000**	**-2.17**	0.001	-0.99	0.000	-1.26
IEJ01_11390	NP_465698.1	lmo2174	-	hypothetical protein lmo2174	**0.000**	**2.41**	0.868	-0.03	0.589	-0.08
IEJ01_11475	NP_465715.1	lmo2191	spxA	ArsC family transcriptional regulator	**0.000**	**2.02**	0.721	0.06	0.917	-0.02
IEJ01_11545	NP_465729.1	lmo2205	-	phosphoglyceromutase	**0.000**	**3.01**	0.227	0.14	0.165	0.15
IEJ01_11560	NP_465732.1	lmo2208	-	hypothetical protein lmo2208	0.000	0.42	0.000	0.56	**0.000**	**1.81**
IEJ01_11570	NP_465734.1	lmo2210	-	hypothetical protein lmo2210	0.538	0.13	0.148	-0.23	**0.000**	**-2.43**
IEJ01_11585	NP_465737.1	lmo2213	-	hypothetical protein lmo2213	**0.000**	**6.92**	0.000	1.73	0.591	0.09
IEJ01_11670	NP_465754.1	lmo2230	-	arsenate reductase	**0.000**	**6.95**	0.002	1.26	0.795	0.04
IEJ01_11675	NP_465755.1	lmo2231	-	hypothetical protein lmo2231	**0.000**	**3.88**	0.710	0.06	0.705	-0.07
IEJ01_11770	NP_465774.1	lmo2250	arpJ	amino acid ABC transporter permease	**0.000**	**-3.07**	0.620	0.04	0.895	0.02
IEJ01_11775	NP_465775.1	lmo2251	-	amino acid ABC transporter ATP-binding protein	**0.000**	**-3.28**	0.569	0.03	0.806	-0.02
IEJ01_11780	NP_465776.1	lmo2252	-	aspartate aminotransferase	**0.000**	**-2.21**	0.710	0.05	0.818	-0.04
IEJ01_11865	NP_465793.2	lmo2269	-	hypothetical protein lmo2269	**0.000**	**7.41**	0.135	0.12	0.625	-0.06
IEJ01_11870	NP_465794.1	lmo2270	comK'	competence protein ComK	**0.000**	**3.67**	0.123	0.26	0.524	0.11
IEJ01_11950	NP_465813.1	lmo2289	-	protein gp14	0.002	0.73	0.998	0.00	**0.000**	**-1.94**
IEJ01_11960	NP_465815.1	lmo2291	-	major tail shaft protein	0.000	0.95	0.526	-0.10	**0.000**	**-2.13**
IEJ01_11965	NP_465816.1	lmo2292	-	protein gp11	0.000	0.85	0.260	-0.17	**0.000**	**-1.93**
IEJ01_11970	NP_465817.1	lmo2293	-	protein gp10	0.004	0.76	0.736	-0.05	**0.000**	**-1.59**
IEJ01_11975	NP_465818.1	lmo2294	-	protein gp9	0.009	0.70	0.780	-0.04	**0.000**	**-1.86**
IEJ01_11980	NP_465819.1	lmo2295	-	protein gp8	0.009	0.64	0.580	-0.08	**0.000**	**-1.90**
IEJ01_11985	NP_465820.1	lmo2296	-	phage coat protein	0.000	1.03	0.655	0.07	**0.000**	**-1.66**
IEJ01_11995	NP_465822.1	lmo2298	-	protein gp4	0.008	0.53	0.590	-0.08	**0.000**	**-1.81**

Continued on next page

Supplemental Table 2.3 continued from previous page

gene ID	protein ID	EGDe locus	gene name	protein name	V14/LO28 WT		14EV1/LO28 WT		14EV2/LO28 WT	
					p-value	$\log_2$(Fold change)	p-value	$\log_2$(Fold change)	p-value	$\log_2$(Fold change)
IEJ01_12335	NP_465879.1	lmo2356	-	hypothetical protein lmo2356	**0.000**	**3.15**	0.886	-0.02	0.759	0.04
IEJ01_12355	NP_465883.1	lmo2360	-	transmembrane protein	**0.000**	**2.70**	0.256	0.13	0.108	0.33
IEJ01_12360	NP_465884.1	lmo2361	-	hypothetical protein lmo2361	**0.000**	**2.64**	0.340	0.09	0.063	0.45
IEJ01_12575	NP_465909.1	lmo2386	-	hypothetical protein lmo2386	**0.000**	**2.43**	0.335	0.13	0.006	0.35
IEJ01_12580	NP_465910.1	lmo2387	-	hypothetical protein lmo2387	**0.000**	**4.38**	0.047	0.32	0.139	0.23
IEJ01_12600	NP_465914.1	lmo2391	-	hypothetical protein lmo2391	**0.000**	**5.18**	0.165	0.22	0.364	-0.14
IEJ01_12640	NP_465921.1	lmo2398	ltrC	hypothetical protein lmo2398	**0.000**	**3.77**	0.743	0.05	0.996	0.00
IEJ01_12645	NP_465922.1	lmo2399	-	hypothetical protein lmo2399	**0.000**	**1.76**	0.396	-0.11	0.959	-0.01
IEJ01_12820	NP_465957.1	lmo2434	-	glutamate decarboxylase	**0.000**	**4.67**	0.193	0.20	0.996	0.00
IEJ01_12835	NP_465960.1	lmo2437	-	hypothetical protein lmo2437	**0.000**	**2.31**	0.142	0.22	0.005	0.41
IEJ01_12925	NP_465977.1	lmo2454	-	hypothetical protein lmo2454	**0.000**	**3.53**	0.989	0.00	0.062	-0.24
IEJ01_12965	NP_465986.1	lmo2463	-	multidrug transporter	**0.000**	**3.72**	0.679	-0.06	0.448	-0.10
IEJ01_06420	NP_465991.1	lmo2468	clpP	ATP-dependent Clp protease proteolytic subunit	**0.000**	**-2.58**	0.096	-0.23	0.693	-0.06
IEJ01_13075	NP_466007.1	lmo2484	-	hypothetical protein lmo2484	**0.000**	**2.36**	0.311	-0.13	0.412	-0.12
IEJ01_13080	NP_466008.1	lmo2485	-	hypothetical protein lmo2485	**0.000**	**3.70**	0.653	-0.07	0.155	-0.23
IEJ01_13125	NP_466017.1	lmo2494	-	PhoU family transcriptional regulator	**0.000**	**3.15**	0.019	0.47	0.001	0.64
IEJ01_13130	NP_466018.1	lmo2495	-	phosphate ABC transporter ATP-binding protein	**0.000**	**3.86**	0.002	0.96	0.038	0.52

Continued on next page

Supplemental Table 2.3 continued from previous page

gene ID	protein ID	EGDe locus	gene name	protein name	V14/LO28 WT		14EV1/LO28 WT		14EV2/LO28 WT	
					p-value	$\log_2$(Fold change)	p-value	$\log_2$(Fold change)	p-value	$\log_2$(Fold change)
IEJ01_13135	NP_466019.1	lmo2496	-	phosphate ABC transporter ATP-binding protein	**0.000**	**1.95**	0.369	0.11	0.070	0.41
IEJ01_13140	NP_466020.1	lmo2497	-	phosphate ABC transporter permease	**0.000**	**1.89**	0.419	0.09	0.139	0.29
IEJ01_13145	NP_466021.1	lmo2498	-	phosphate ABC transporter permease	**0.000**	**2.01**	0.196	0.18	0.582	0.09
IEJ01_13150	NP_466022.1	lmo2499	-	phosphate ABC transporter substrate-binding protein	**0.000**	**2.71**	0.000	1.07	0.000	1.01
IEJ01_13210	NP_466034.1	lmo2511	-	hypothetical protein lmo2511	**0.000**	**1.94**	0.569	0.09	0.141	-0.20
IEJ01_13265	NP_466045.1	lmo2522	-	cell wall-binding protein	**0.000**	**1.65**	0.131	0.19	0.018	0.28
IEJ01_13505	NP_466092.1	lmo2569	-	peptide ABC transporter substrate-binding protein	**0.000**	**-1.78**	0.694	0.06	0.894	-0.02
IEJ01_13510	NP_466093.1	lmo2570	-	hypothetical protein lmo2570	**0.000**	**4.86**	0.166	0.22	0.894	0.02
IEJ01_13515	NP_466094.1	lmo2571	-	nicotinamidase	**0.000**	**4.91**	0.615	0.08	0.043	-0.37
IEJ01_13520	NP_466095.1	lmo2572	-	dihydrofolate reductase subunit A	**0.000**	**4.66**	0.697	-0.06	0.108	-0.30
IEJ01_13525	NP_466096.1	lmo2573	-	zinc-binding dehydrogenase	**0.000**	**5.31**	0.016	0.37	0.444	-0.12
IEJ01_13600	NP_466110.1	lmo2587	-	hypothetical protein lmo2587	**0.000**	**1.67**	0.004	0.37	0.085	0.22
IEJ01_13710	NP_466125.1	lmo2602	-	hypothetical protein lmo2602	**0.000**	**4.62**	0.999	0.00	0.625	-0.08
IEJ01_13715	NP_466126.1	lmo2603	-	hypothetical protein lmo2603	**0.000**	**3.47**	0.482	0.11	0.725	0.06
IEJ01_13925	YP_008475644.1	lmo2644a	-	hypothetical protein lmo2644a	0.213	0.57	**0.000**	**1.94**	**0.000**	**2.05**
IEJ01_13930	NP_466168.1	lmo2646	-	hypothetical protein lmo2646	0.638	0.25	**0.002**	**1.73**	**0.000**	**2.09**
IEJ01_13935	NP_466169.1	lmo2647	-	creatinine amidohydrolase	0.066	1.27	**0.001**	**3.15**	**0.001**	**2.85**
IEJ01_13940	NP_466170.1	lmo2648	-	phosphotriesterase	0.008	1.42	**0.000**	**3.29**	**0.000**	**3.33**

Continued on next page

Supplemental Table 2.3 continued from previous page

gene ID	protein ID	EGDe locus	gene name	protein name	V14/LO28 WT		14EV1/LO28 WT		14EV2/LO28 WT	
					p-value	$\log_2$(Fold change)	p-value	$\log_2$(Fold change)	p-value	$\log_2$(Fold change)
IEJ01_13945	NP_466171.1	lmo2649	ulaA	PTS system ascorbate transporter subunit IIC	0.835	-0.08	**0.000**	**2.64**	**0.000**	**1.72**
IEJ01_13950	NP_466172.1	lmo2650	-	MFS transporter	0.453	-0.41	**0.000**	**3.55**	**0.000**	**2.17**
IEJ01_13955	NP_466173.1	lmo2651	-	PTS mannitol transporter subunit IIA	0.848	0.06	**0.000**	**3.58**	**0.000**	**2.16**
IEJ01_14040	NP_466190.1	lmo2668	-	transcriptional antiterminator BglG	**0.000**	**-1.74**	0.595	-0.08	0.001	-0.67
IEJ01_14050	NP_466192.1	lmo2670	-	hypothetical protein lmo2670	**0.000**	**2.05**	0.996	0.00	0.904	-0.02
IEJ01_14055	NP_466193.1	lmo2671	-	hypothetical protein lmo2671	**0.000**	**1.67**	0.956	-0.02	0.660	-0.08
IEJ01_14060	NP_466194.1	lmo2672	-	AraC family transcriptional regulator	**0.000**	**2.92**	0.812	-0.04	0.464	-0.11
IEJ01_14065	NP_466195.1	lmo2673	-	hypothetical protein lmo2673	**0.000**	**6.28**	0.186	0.13	0.660	-0.06
IEJ01_14180	NP_466205.1	lmo2683	-	PTS cellbiose transporter subunit IIB	**0.000**	**-1.65**	0.145	-0.26	0.000	-0.93
IEJ01_14185	NP_466206.1	lmo2684	-	PTS cellbiose transporter subunit IIC	**0.000**	**-2.12**	0.137	-0.14	0.006	-1.13
IEJ01_14245	NP_466217.1	lmo2695	-	dihydroxyacetone kinase subunit DhaK	**0.000**	**4.97**	0.329	0.15	0.017	-0.43
IEJ01_14250	NP_466218.1	lmo2696	-	dihydroxyacetone kinase	**0.000**	**5.86**	0.131	0.26	0.932	-0.02
IEJ01_14255	NP_466219.1	lmo2697	-	PTS mannose transporter subunit IIA	**0.000**	**6.43**	0.001	0.74	0.011	0.53
IEJ01_14310	NP_466230.1	lmo2708	-	PTS cellbiose transporter subunit IIC	**0.000**	**-1.92**	0.135	-0.17	**0.000**	**-1.67**
IEJ01_14390	NP_466246.1	lmo2724	-	hypothetical protein lmo2724	**0.000**	**3.63**	0.933	0.02	0.215	-0.17
IEJ01_14475	NP_466263.1	lmo2741	-	multidrug transporter	**0.000**	**1.64**	0.911	0.02	0.547	-0.10
IEJ01_14510	NP_466270.1	lmo2748	-	hypothetical protein lmo2748	**0.000**	**7.20**	0.000	1.09	0.581	0.10
IEJ01_14780	NP_466322.1	lmo2800	-	dehydrogenase	**0.000**	**-1.99**	0.008	0.70	0.477	0.12
IEJ01_14785	NP_466323.1	lmo2801	-	N-acetylmannosamine-6-phosphate 2-epimerase	**0.000**	**-2.41**	0.057	0.38	0.876	0.03

Continued on next page

Supplemental Table 2.3 continued from previous page

gene ID	protein ID	EGDe locus	gene name	protein name	V14/LO28 WT		14EV1/LO28 WT		14EV2/LO28 WT	
					p-value	$\log_2$(Fold change)	p-value	$\log_2$(Fold change)	p-value	$\log_2$(Fold change)
IEJ01_00725	WP_015084540.1				**0.002**	**2.38**	0.027	0.13		1.88
IEJ01_12015	WP_012582399.1				0.274	0.34	0.873	-0.03	**0.000**	**-1.76**
IEJ01_06405	WP_009917708.1			terminase large subunit	**0.000**	**-1.63**	0.272	-0.16	0.339	0.14
IEJ01_06450	WP_003731642.1			DUF3168 domain-containing protein	**0.000**	**-2.10**	0.418	-0.12	0.904	-0.02
IEJ01_06455	WP_012581455.1			phage tail protein	**0.000**	**-2.13**	0.179	-0.19	0.621	-0.07
IEJ01_06470	WP_012951553.1			phage tail tape measure protein	**0.000**	**-2.16**	0.001	-0.50	0.130	-0.22
IEJ01_06480	WP_012951555.1			phage tail protein	**0.000**	**-2.16**	0.167	-0.22	0.809	-0.04
IEJ01_06465	WP_009931626.1			hypothetical protein	**0.000**	**-2.23**	0.653	-0.05	0.524	-0.09
IEJ01_06430	WP_015987290.1			hypothetical protein	**0.000**	**-2.29**	0.516	-0.06	0.842	-0.03
IEJ01_06390	WP_014930130.1			hypothetical protein	**0.000**	**-2.36**	0.983	0.01	0.567	0.10
IEJ01_06460	WP_014930131.1			hypothetical protein	**0.000**	**-2.41**	0.104	-0.32	0.565	-0.10
IEJ01_06475	WP_014601422.1			phage tail family protein	**0.000**	**-2.49**	0.007	-0.47	0.026	-0.36
IEJ01_06400	WP_014929542.1			P27 family phage terminase small subunit	**0.000**	**-2.53**	0.824	-0.03	0.772	0.05
IEJ01_06385	WP_010991275.1			DUF559 domain-containing protein	**0.000**	**-2.54**	0.830	-0.04	0.086	0.22
IEJ01_06395	WP_000988331.1			HNH endonuclease	**0.000**	**-2.58**	0.670	-0.05	0.928	-0.02
IEJ01_06415	WP_014929544.1			phage portal protein	**0.000**	**-2.59**	0.050	-0.27	0.953	-0.01
IEJ01_06440	WP_014929549.1			phage head-tail adapter protein	**0.000**	**-2.66**	0.514	-0.10	0.890	0.03
IEJ01_06425	WP_012581458.1			phage major capsid protein	**0.000**	**-2.75**	0.005	-0.41	0.339	-0.14
IEJ01_06445	WP_009917701.1			hypothetical protein	**0.000**	**-2.81**	0.171	-0.21	0.648	-0.07
IEJ01_06435	WP_012951549.1			phage gp6-like head-tail connector protein	**0.000**	**-3.07**	0.139	-0.26	0.944	0.01

Supplemental Table 2.4: **Expression of genes involved in the SigB activation in variants V14, 14EV1, 14EV2 when compared to *Listeria monocytogenes* LO28 WT.** The p-value, $\log_2$(Fold change), and $\log_{10}$(protein ratio) in bold are considered signifant

EGDe locus	gene name	RNAseq						Proteomics					
		V14/LO28 WT		14EV1/LO28 WT		14EV2/LO28 WT		V14/LO28 WT		14EV1/LO28 WT		14EV2/LO28 WT	
		p-value	$\log_2$(Fold change)	p-value	$\log_2$(Fold change)	p-value	$\log_2$(Fold change)	p-value	$\log_{10}$ ratio	p-value	$\log_{10}$ ratio	p-value	$\log_{10}$ ratio
lmo0799	rsbL	0.186	0.16	0.454	-0.10	0.413	0.10						
lmo0889	rsbR1	0.847	0.02	0.836	0.03	0.904	-0.01	0.563	-0.07	0.602	0.05	0.955	0.00
lmo0161	rsbR2	0.000	-0.83	0.748	0.04	0.040	0.23	0.596	-0.06	0.565	0.05	0.212	0.18
lmo1642	rsbR3	0.272	0.10	0.698	0.05	0.356	0.09						
lmo1842	rsbR4	0.693	-0.09	0.287	0.16	0.045	0.35						
lmo0890	rsbS	0.028	-0.26	0.370	-0.12	0.204	-0.15	**0.000**	**-1.83**	0.049	-0.13	0.027	-0.07
lmo0891	rsbT	0.029	-0.20	0.866	-0.03	0.553	-0.07						
lmo0892	rsbU	0.365	-0.08	0.989	0.00	0.256	0.11	0.069	0.63	0.374	-0.25	0.374	-0.25
lmo0893	rsbV	0.000	1.39	0.648	-0.06	0.091	0.17	0.001	0.65	0.760	0.03	0.105	0.13
lmo0894	rsbW	0.000	1.26	0.794	0.04	0.058	0.17	0.000	0.68	0.000	0.20	0.000	0.21
lmo0895	sigB	**0.000**	**1.68**	0.113	0.14	0.001	0.27	0.013	0.79	0.422	0.09	0.329	0.05
lmo0896	rsbX	**0.000**	**1.93**	0.000	0.27	0.000	0.35						

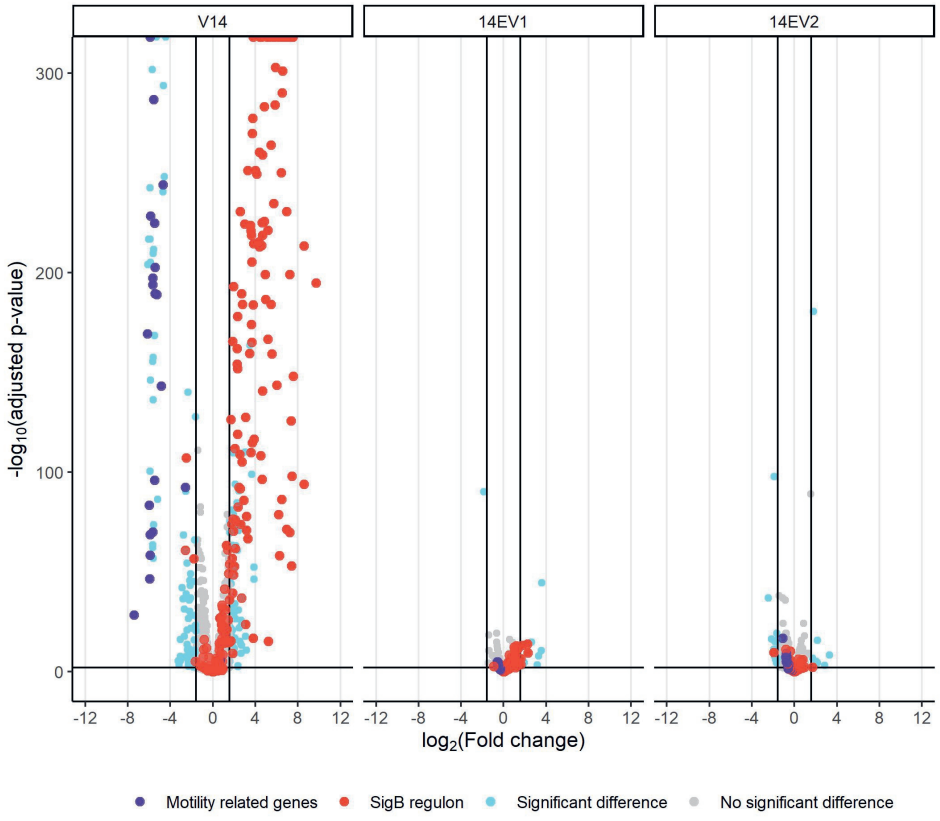

Supplemental Figure 2.1: **Volcano plot of RNAseq data comparing *L. monocytogenes* V14, 14EV1, and 14EV2 compared to the wild type.** The $-\log_{10}$(Benjamini–Hochberg corrected p-value) is plotted against the $\log_2$(Fold change: variant over WT). The horizontal line represents the cutoff for $-\log_{10}$(p-value), vertical lines represent $\log_2$(Fold change) cutoff. Red dots indicate proteins regulated by SigB; purple dots indicate proteins involved in motility.

3

A single point mutation in the *Listeria monocytogenes* ribosomal gene *rpsU* enables SigB activation independently of the stressosome and the anti-sigma factor antagonist RsbV

Xuchuan Ma, Marcel H. Tempelaars, Marcel H. Zwietering, Sjef Boeren, Conor O'Byrne, Heidy M.W. den Besten, Tjakko Abee

Accepted for publication in *Frontiers in Microbiology*

Abstract

Microbial population heterogeneity leads to different stress responses and growth behavior of individual cells in a population. Previously, a point mutation in the *rpsU* gene ($rpsU^{G50C}$) encoding ribosomal protein S21 was identified in a *Listeria monocytogenes* LO28 variant, which leads to increased multi-stress resistance and a reduced maximum specific growth rate. However, the underlying mechanisms of these phenotypic changes remain unknown. In *L. monocytogenes*, the alternative sigma factor SigB regulates the general stress response, with its activation controlled by a series of Rsb proteins, including RsbR1 and anti-sigma factor RsbW and its antagonist RsbV. We combined a phenotype and proteomics approach to investigate the acid and heat stress resistance, growth rate, and SigB activation of *L. monocytogenes* EGDe wild type and the Δ*sigB*, Δ*rsbV* and Δ*rsbR1* mutant strains. While the introduction of $rpsU^{G50C}$ in the Δ*sigB* mutant did not induce a SigB-mediated increase in robustness, the presence of $rpsU^{G50C}$ in the Δ*rsbV* and the Δ*rsbR1* mutants led to SigB activation and concomitant increased robustness, indicating an alternative signaling pathway for the SigB activation in $rpsU^{G50C}$ mutants. Interestingly, all these $rpsU^{G50C}$ mutants exhibited reduced maximum specific growth rates, independent of SigB activation, possibly attributed to compromised ribosomal functioning. In summary, the increased stress resistance in the $rpsU^{G50C}$ mutant results from SigB activation through an unknown mechanism distinct from the classical stressosome and RsbV/RsbW partner switching model. Moreover, the reduced maximum specific growth rate of the $rpsU^{G50C}$ mutant is likely unrelated to SigB activation and potentially linked to impaired ribosomal function.

3.1 Introduction

Listeria monocytogenes is a ubiquitous foodborne pathogen, which can cause the disease listeriosis typically caused by ingestion of contaminated food (Radoshevich and Cossart, 2018). To adapt to and survive harsh environmental conditions during the transmission from the soil to the human body, *L. monocytogenes* has applied many protective strategies including population heterogeneity (Abee et al., 2016). Population heterogeneity includes genetic and non-genetic population variability, and both can generate phenotypic variation in a population and contribute to the overall fitness, adaptation, and survival capacity of the population (Davidson and Surette, 2008; Ryall et al., 2012; Smits et al., 2006). Pathogens may be inactivated during food processing, and differences in stress resistance between individual cells can result in a higher-than-expected number of surviving cells and selection of stress-resistant variants (Metselaar et al., 2016).

Previously, 23 stable stress resistance *L. monocytogenes* variants have been isolated upon acid treatment of *L. monocytogenes* strain LO28 (Metselaar et al., 2013). These variants showed a trade-off between reduced maximum specific growth rate and increased resistance against acid, heat, high hydrostatic pressure and benzalkonium chloride (Metselaar et al., 2015; Metselaar et al., 2013). Whole genome sequencing analysis showed that 11 of the 23 variants had mutations in the *rpsU* gene locus, which encodes the ribosome 30S small sub-unit protein S21 (RpsU) (Metselaar et al., 2015). Two variants have been selected for further research, namely, variant V14 and variant V15 (Koomen et al., 2018). Variant V14 has a deletion of the whole *rpsU* and *yqeY* genes and half of *phoH* gene, while variant V15 has a nucleotide substitution from G to C in *rpsU* at position 50 (NC_003210.1:g.1501930G>C p.(Arg17Pro), designated as $rpsU^{\mathrm{G50C}}$ in this study), which may lead to an amino acid substitution from arginine to proline in the RpsU protein (marked as $\mathrm{RpsU}^{\mathrm{17Arg\text{-}Pro}}$ in this study) (Koomen et al., 2021; Metselaar et al., 2015). Comparative transcriptomic and phenotypic studies showed that variants V14 and V15 have a large overlap in the gene expression profiles and similar phenotypic results including increased stress resistance, higher glycerol utilization rates, flagella absence and higher Caco-2 cells attachment and invasion levels compared to the wild type (Koomen et al., 2018). These results suggest that the deletion of the whole *rpsU* and point mutation $rpsU^{\mathrm{G50C}}$ may affect the phenotype by the same mechanism (Koomen et al., 2018). Additional studies following introduction of the $rpsU^{\mathrm{G50C}}$ mutation into *L. monocytogenes* LO28 and EGDe wild type strains, confirmed that this mutation results in multiple stress resistance and reduced maximum specific growth rate in both mutant strains (Koomen et al., 2021).

SigB is considered as the regulator of general stress response and controls the transcription of approximately 300 genes that contribute to the stress response and virulence of *L. monocytogenes* (Guerreiro et al., 2020a; Liu et al., 2019; O'Byrne and Karatzas, 2008; Toledo-Arana et al., 2009). Indeed, previous transcriptomic and proteomic analyses showed that many SigB regulon genes and proteins were strongly upregulated in the *rpsU* variants, which suggests that the activation of SigB-mediated stress may explain the multiple stress resistance phenotype of *rpsU* variants (Koomen et al., 2021; Koomen et al., 2018). Generally, the activation of SigB is controlled at

the post-translation level through the stressosome and a series of other Rsb proteins (Supplemental Figure 3.1) (Becker et al., 1998; Guerreiro et al., 2022a, 2020a). Briefly, RsbT is captured by the stressosome which is composed of RsbS, RsbR1 and RsbR1 paralogues in unstressed cells. Upon environmental stress, RsbR1 and RsbS are phosphorylated, and RsbT is released from the stressosome. The free RsbT can bind to RsbU and stimulate its phosphatase function. Then anti-sigma factor antagonist RsbV is dephosphorylated by RsbU and binds to anti-sigma factor RsbW, which releases the previously bound SigB, which is then free to bind to RNA polymerase and initiate the transcription of the SigB regulon. Once stress is removed, RsbX, which is co-expressed with SigB, can dephosphorylate RsbR1 and RsbS, and RsbT binds back to the stressosome and inactivates the signal transduction (Guerreiro et al., 2020a; Oliveira et al., 2022). To date, it is unknown whether this stressosome-mediated signaling pathway is involved in SigB activation in the *L. monocytogenes* $rpsU^{G50C}$ mutant, and whether SigB activation leads to reduced fitness of this mutant.

Therefore, in the current study we aim to investigate first whether the stressosome and/or the anti-sigma factor antagonist RsbV are involved in activation of SigB in the $rpsU^{G50C}$ mutant, or if other factors may contribute to (indirect) activation of SigB in the $rpsU^{G50C}$ mutant. Second, we sought to evaluate whether the activation of SigB and its regulon lead to reduced fitness of the $rpsU^{G50C}$ mutant. To address these questions, the $rpsU^{G50C}$ mutation was introduced in *L. monocytogenes* EGDe wild type (WT), and in the RsbR1, RsbV and SigB deletion mutants, previously used to study stressosome structure and functionality (Dessaux et al., 2020; Guerreiro et al., 2020b; Utratna et al., 2012). Comparative phenotypic and proteomic study of the *L. monocytogenes* EGDe WT, $rpsU^{G50C}$, Δ*rsbR1*, Δ*rsbV* and Δ*rsbV* single mutant strains, and Δ*rsbR1*-$rpsU^{G50C}$, Δ*rsbV*-$rpsU^{G50C}$ and Δ*sigB*-$rpsU^{G50C}$ double mutant strains will shed light on the interaction between the ribosome and stressosome-dependent SigB activation and the fitness effect in cells with and without functional RpsU, and whether additional factors are involved.

3.2 Materials and Methods

3.2.1 Bacterial strains, plasmids and mutant construction

The bacterial strains, plasmids, and primers used in this study are described in Table 3.1 and Table 3.2. The shuttle vector pAULA-$rpsU^{G50C}$ and pKSV7-Δ*pstS* were used for introducing the *pstS* gene deletion and the $rpsU^{G50C}$ point mutation in the target *L. monocytogenes* strains, respectively. The pKSV7-Δ*pstS* was constructed as described previously with modification (Rychli et al., 2021). The upstream and down region from *pstS* gene was amplified from gDNA of EGDe WT with the up region primers (*pstS*-Up-EcoRI-F and *pstS*-Up-NotI-R) and the down region primers (*pstS*-Down-NotI-F and *pstS*-Down-SalI-R), respectively. The resulting fragments were fused and ligated into the pKSV7 multiple cloning site. The resulting construct was confirmed by PCR and sequencing using primers M13-F and M13-R. To construct $rpsU^{G50C}$ mutants, pAULA-$rpsU^{G50C}$ was transformed into *L. monocytogenes* competent cells by electroporation (2.5 kV, 25 μF, 200 D) and plated on Brain Heart Infusion (BHI) agar plates at 30°C with 5 μg/mL erythromycin to

select for transformants. The erythromycin-resistant colonies were inoculated in BHI broth with 5 μg/mL erythromycin and grown at 42°C overnight. The 42°C-grown overnight cultures were inoculated into fresh BHI for overnight culture at 30°C and subsequently plated on BHI agar plates at 30°C. The resulting colonies were replica plated on BHI with and without 5 μg/mL erythromycin and incubated at 30°C. The erythromycin-sensitive colonies were selected and the *rpsU*^{G50C} point mutation was verified by PCR and Sanger sequencing with primers *rpsU*-EcoRI-F and *rpsU*-SalI-R. To construct Δ*pstS* mutants, the same process has been performed with pKSV7-Δ*pstS*, and the colonies were selected by chloramphenicol (10 μg/mL) and verified by PCR and sequencing with primers *pstS*-Flank-F, *pstS*-Flank-R *pstS*-Flank-F, *pstS*-Flank-R, *pstS*-Up-Check-F, and *pstS*-Down-Check-R. Single nucleotide polymorphism (SNP) analysis was performed on all constructed mutants as described in the following section and confirmed the absence of any other significant undesired mutations (Supplemental Table 3.1).

Table 3.1: The plasmids and strains used in this study

Plasmid or Strain	Description	Source or reference
Plasmids		
pAULA-*rpsU*^{G50C}	pAULA containing the *rpsU*^{G50C} DNA point mutation cassette	Koomen et al. (2021)
pKSV7	Temperature sensitive suicide plasmid	Smith and Youngman (1992)
pKSV7-Δ*pstS*	pKSV7 containing Δ*pstS* DNA deletion cassette	This study
Strain		
EGDe WT	*L. monocytogenes* EGDe wild type	C. O'Byrne, University of Galway, Ireland
EGDe Δ*sigB*	*L. monocytogenes* EGDe WT with Δ*sigB* deletion	Guerreiro et al. (2020b)
EGDe Δ*rsbV*	*L. monocytogenes* EGDe WT with Δ*rsbV* deletion	Utratna et al. (2012)
EGDe Δ*rsbR1*	*L. monocytogenes* EGDe WT with Δ*rsbR1* deletion	Dessaux et al. (2020)
EGDe-*rpsU*^{G50C}	*L. monocytogenes* EGDe WT with *rpsU*^{G50C} mutation	This study
EGDe Δ*sigB*-*rpsU*^{G50C}	*L. monocytogenes* EGDe double mutant (Δ*sigB*; *rpsU*^{G50C})	This study
EGDe Δ*rsbV*-*rpsU*^{G50C}	*L. monocytogenes* EGDe double mutant (Δ*rsbV*; *rpsU*^{G50C})	This study
EGDe Δ*rsbR1*-*rpsU*^{G50C}	*L. monocytogenes* EGDe double mutant (Δ*rsbR1*; *rpsU*^{G50C})	This study
EGDe Δ*pstS*	*L. monocytogenes* EGDe WT with Δ*pstS* deletion	This study
EGDe Δ*pstS*-*rpsU*^{G50C}	*L. monocytogenes* EGDe double mutant (Δ*pstS*; *rpsU*^{G50C})	This study

Table 3.2: The primers used in this study

Name	Sequence (5'to 3', restriction site underlined)
rpsU-EcoRI-F	GAAGGAATTCCCAGAGAAGGCGAGGATAGTG
rpsU-SalI-R	TGGTGTCGACTCAGCTTTGCCCTTTACTTTAG
pstS-Flank-F	ACACATTGGCAGAAAGTTTGGA
pstS-Up-EcoRI-F	CTAAGAATTCAATCAAGCAGAATGAACAACGA
pstS-Up-Check-F	TGGGGCGATAATTTACCAGT
pstS-Up-NotI-R	ACTAGCGGCCGCATTATCTTATTCCCACCTTGTT
pstS-Down-NotI-F	ACATGCGGCCGCTAACTGACGTAAAATAAAAAGAATGA
pstS-Down-Check-R	CTCTAGTTTCTAGATGCGCCTT
pstS-Down-SalI-R	GATCGTCGACAGCTTGGAACGACTGTGGT
pstS-Flank-R	TAGTGTAAGCGCCCCAGAAA
M13-F	CAGGAAACAGCTATGAC
M13-R	GTTTTCCCAGTCACGAC

3.2.2 Whole genome sequencing and SNP analysis

The genomic DNA was isolated for sequencing using DNeasy Blood and tissue kit (Qiagen). Two times 2 mL of overnight culture was centrifuged (17,000 x *g*), washed by 1 mL PPS, resuspended in 1 mL lysis buffer (20 mM Tris-HCl, 2 mM EDTA, 1.2% (w/v) Triton X-100, 20 mg/mL lysozyme, pH 8.0), and incubated at 37°C for 1 h. Then, 10 μL RNAse (10 mg/mL) was added and incubated for 30 min at room temperature. Subsequently, 62.5 μL proteinase K and 500 μL AL buffer were added and incubated at 56°C for 1 h. Then, 500 μL absolute ethanol was added. The suspension was transferred to a spin column provided by the kit and centrifuged for 1 min at 6000 x *g*. The filters were washed two times with 500 μL buffer AW1 and AW2 at 6000 x *g*. Then, the columns were centrifuged at 17,000 x *g* for 3 min. Subsequently, 50 μL of AE buffer was added to the center of the column. The column was centrifuged at 6,000 x *g* to collect the target sample. Samples were stored at -20°C. Library preparation and paired-end 2 × 150 bp short-reads were generated using the INVIEW resequencing of bacteria service from Eurofins GmbH (Constance, Germany) using Illumina technology. On Galaxy platform, read quality control was performed using FastQC (0.73+galaxy0), and SNPs were identified using snippy (4.6.0+galaxy0) with reference genome of EGDe (ASM19603v1) (Andrews, n.d.; Galaxy Community, 2022; Torsten, 2015).

3.2.3 Culture conditions

For stress resistance experiments and proteomics experiments, the *L. monocytogenes* strains were cultured as described previously (Metselaar et al., 2013). Briefly, stock cultures were grown for 1 to 2 days at 30°C on BHI agar plates. One single colony was then inoculated in 20 mL BHI broth and cultured at 30°C overnight under shaking at 160 rpm. A 0.5% (v/v) inoculum was added to fresh BHI broth and cells were grown at 30°C at 160 rpm until the late-exponential growth phase (OD_{600} = 0.4-0.5).

3.2.4 Acid and heat resistance experiment

Acid and heat inactivation experiments were performed as described before (Metselaar et al., 2013). Briefly, 100 mL late-exponential phase culture was harvested by centrifuging for 5 min at 2,880 x *g*, followed by resuspension in 10 mL BHI broth, centrifugation again for 5 min at 2,880 x *g*, and resuspension in 1.1 mL 0.1% peptone physiological salt solution (PPS). For acid inactivation, 1 mL suspension was added to a 100 mL Erlenmeyer flask with 9 mL BHI broth (pre-warmed at 37°C, adjusted to pH 3.00 ± 0.01 with 10 M HCl) placed in a shaking water bath at 37°C. At the beginning and after 15 min, 100 μL samples were taken. For heat inactivation, 0.1 mL suspension was diluted in PPS and plated to determine the concentration before inactivation, and the remaining 1 mL suspension was added to 19 mL BHI broth which was preheated to 60°C and sampled 1 mL after 5 min. All the samples were decimally diluted and plated on BHI agar plates in duplicate, using a spiral plater or by spread plating when no dilution steps were needed. Plates were incubated at 30°C and counted after 4 to 6 days to allow recovery of all cells. The experiment was done with at least three independent biological replicates.

3.2.5 Estimation of the maximum specific growth rate

The maximum specific growth rate μ_{max} was determined by using the 2-fold dilution method as described previously (Biesta-Peters et al., 2010). Briefly, the overnight culture was diluted, plated on BHI agar plate, and incubated at 30°C for 2 days. In parallel, the culture was 10,000 times diluted, and 400 μL of the diluted culture was added to the first well of a 100-well honeycomb plate in duplicate. Subsequently, four times two-fold dilution series was made by mixing 200 μL diluted bacterial culture and 200 μL fresh BHI in honeycomb plates. The plates were incubated in the Bioscreen at 30°C or 37°C with constant medium shaking. The OD_{600} was measured every 10 min to determine the time-to-detection (TTD) of each well, which was defined as the time OD_{600} reaching 0.2. The μ_{max} (h^{-1}) of each culture was calculated by taking the negative reciprocal of the slope between the TTD and the natural logarithm of the initial concentration N_0 ($\ln(N_0)$) of the five wells. The experiment was done with independent biological triplicates.

3.2.6 Proteomic analysis

The strains for proteomic analysis were cultured as described in Section 3.2.3. For proteomic analysis, 4-mL aliquots of late-exponential phase culture were centrifuged for 1 min at 12,800 x *g* in two 2-mL LoBind Eppendorf tubes, resuspended in 200 μL ice-cold 100 mM Tris (pH 8), pooled together in one tube, and centrifuged again for 1 min at 12,800 x *g*. The pellets were washed using 100 mM Tris, centrifuged for 1 min at 12,800 x *g*, resuspended in 50 μL 100 mM Tris (pH 8), and lysed by sonication for 45 s on ice at maximum power twice (MSE Soniprep 150). Samples were prepared according to the universal solid-phase protein preparation protocol (Dagley et al., 2019) with doubled washing steps (washing with 70% ethanol and 100% acetonitrile). For each prepared peptide sample, 5 μL sample was injected into a nanoLC-MS/MS (Thermo nLC1000 connected to an Exploris 480 with FAIMS at CV=-45V) for further analyzing as described previously (Feng et al., 2022; Wendrich et al., 2017). nLC-MSMS system quality was checked with PTXQC using the MaxQuant result files (Bielow et al., 2016). LCMS data with all MS/MS spectra were analyzed with the MaxQuant quantitative proteomics software package as described before (Bielow et al., 2016; Cox et al., 2014). The reference proteome database used for *L. monocytogenes* EGD-e (Proteome ID: UP000000817) was downloaded from UniProt. Perseus was used for filtering and further bioinformatics and statistical analysis of the MaxQuant ProteinGroups file (Tyanova et al., 2016). Reverse hits and contaminants were filtered out. Significant upregulation or downregulation was defined as a change in protein abundance relative to the parent strains of at least two-fold with a p-value less than 0.05. The proteins that belonged to SigB regulon were identified according to previous research (Guariglia-Oropeza et al., 2018; Hain et al., 2008; Kazmierczak et al., 2003; Liu et al., 2017; Mattila et al., 2020; Oliver et al., 2010; Ollinger et al., 2009). Data visualization was performed using the statistical programming language R (4.0.3). KEGG analysis was performed with R package "clusterProfiler" (4.1.2) (Wu et al., 2021).

3.2.7 Statistical testing

Statistical significance analysis of phenotypic data analysis was performed in JASP (0.11.1) by using an independent samples t-test.

3.3 Results

3.3.1 *rpsU*^{G50C} mutation leads to increased acid and heat stress resistance independently from RsbR1 and RsbV

It has been reported that the *rpsU*^{G50C} mutation in *L. monocytogenes* can lead to a multi-stress resistance phenotype (Koomen et al., 2021). To confirm that the *rpsU*^{G50C} mutation can lead to increased acid stress resistance of the *L. monocytogenes* EGDe strain used in the current study, the wild-type strain EGDe WT and the EGDe-*rpsU*^{G50C} mutant were exposed to pH 3.0 for 15 min. As expected, the EGDe WT had a significantly higher log-reduction than the EGDe-*rpsU*^{G50C} mutant after exposure to acid (p-value < 0.05), which indicates that the EGDe WT had lower acid resistance than the EGDe-*rpsU*^{G50C} mutant (Figure 3.1, A). Then, to explore the effect of SigB on the acid stress resistance of *rpsU*^{G50C} mutants, the EGDe Δ*sigB* mutant and the Δ*sigB*-*rpsU*^{G50C} double mutant were exposed to acid stress. No significant differences were observed between the Δ*sigB* and the Δ*sigB*-*rpsU*^{G50C} mutants, which indicates that SigB is essential, to a large extent, for the increased acid resistance of the *rpsU*^{G50C} mutant (Figure 3.1 A). In *L. monocytogenes*, SigB controls the general stress response, and is activated by a stress sensing stressosome that is responsible for orchestrating the activation of a signal transduction pathway resulting in the activation of the sigma factor (Guerreiro et al., 2020a). To test whether the stressosome was also involved in the SigB-mediated stress resistance of the *rpsU*^{G50C} mutant, we also introduced the *rpsU*^{G50C} mutation into the EGDe WT and the Δ*rsbR1* mutant. The Δ*rsbR1* mutant does not have a functional stressosome, and therefore the signaling pathway is interrupted. Acid stress resistance data show that the Δ*rsbR1*-*rpsU*^{G50C} double mutant is significantly more acid-stress resistant than the Δ*rsbR1* mutant, with comparable stress resistance as the single *rpsU*^{G50C} mutant (Figure 3.1 A). This indicates that the stressosome is not involved in the increased acid stress resistance of the *rpsU*^{G50C} mutant. Apart from the stressosome, there are several other regulators in the SigB activation pathway, in which anti-sigma factor antagonist RsbV is the most downstream positive regulator. To investigate whether RsbV and upstream SigB activation pathway regulators were involved in the increased acid stress resistance of the *rpsU*^{G50C} mutant, the *rpsU*^{G50C} mutation was also introduced in the EGDe Δ*rsbV* mutant. Interestingly, the EGDe Δ*rsbV*-*rpsU*^{G50C} double mutant still had higher acid stress resistance than the Δ*rsbV* mutant, indicating that the SigB-related acid stress resistance of the *rpsU*^{G50C} mutant was independent of RsbV. The EGDe WT strain and the single and double mutant strains were also tested for heat stress resistance by exposure to 60°C for 5 min. Again, the *rpsU*^{G50C} mutant strains except the Δ*sigB*-*rpsU*^{G50C} mutant were more resistant than their counterpart, underlining that the mutation confers SigB-dependent resistance to multiple stresses (Figure 3.1 B). Combining the results, we can conclude that the *rpsU*^{G50C} mutation can lead to

increased multi-stress resistance of *L. monocytogenes*, which requires SigB but not RsbR1 nor RsbV. This suggests that an additional signaling pathway is involved in preventing binding of anti-sigma factor RsbW to SigB in the *rpsU*^{G50C} mutant.

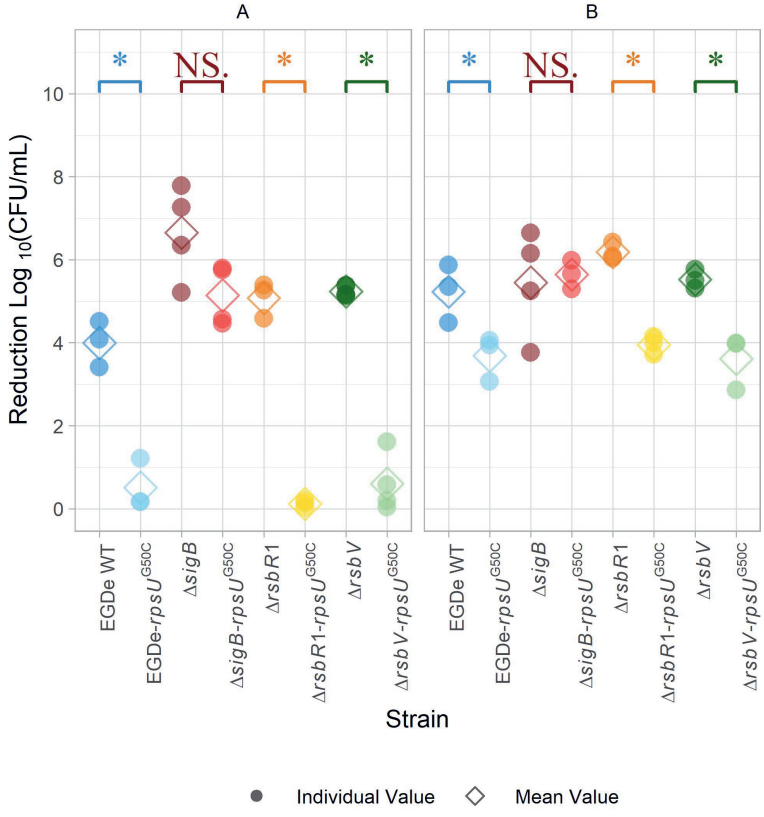

Figure 3.1: **Stress resistance of late-exponential phase cells of *L. monocytogenes* EGDe WT, Δ*sigB*, Δ*rsbV* and Δ*rsbR1* mutants and their *rpsU*^{G50C} mutants in BHI broth.** Late-exponential phase cells were exposed to pH 3.0 for 15 min at 37°C **(A)** and 5 min at 60°C **(B)**. Results are expressed as reduction in $\log_{10}$(CFU/mL) after exposure compared to $\log_{10}$(CFU/mL) before exposure. Significant differences are indicated by an asterisk, and no significant differences are indicated by NS.

3.3.2 *rpsU*^{G50C} mutation can lead to reduced growth rate independently from SigB, RsbR1 and RsbV

In previous research, *rpsU*^{G50C} mutants showed increased stress resistance and lower maximum specific growth rates (Koomen et al., 2021; Metselaar et al., 2016, 2013; Metselaar et al., 2015). Previous research suggested that the reduced growth ability

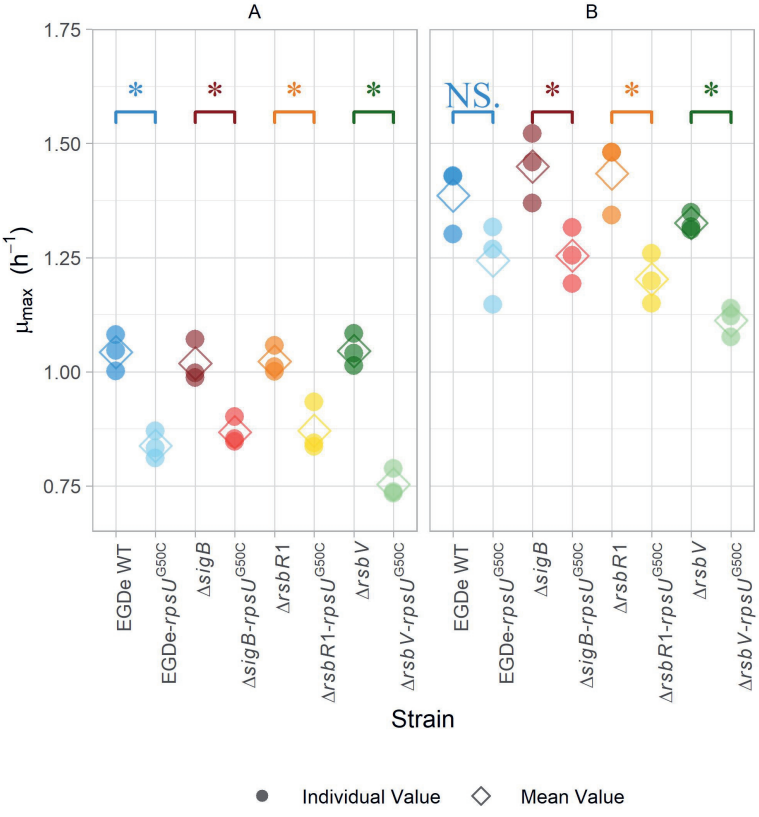

Figure 3.2: **Maximum specific growth rate of *L. monocytogenes* EGDe WT, Δ*sigB*, Δ*rsbV* and Δ*rsbR1* mutants and their *rpsU*^{G50C} mutants in BHI broth at 30°C (A) and 37°C (B), determined by the two-fold dilution method.** Significant differences are indicated by an asterisk, and no significant differences are indicated by NS.

might be the trade-off for the increased resistance (Metselaar et al., 2015). To further investigate this trade-off, the maximum specific growth rate (μ_{max}) of EGDe WT, the Δ*sigB* mutant, the Δ*rsbR1* mutant and the Δ*rsbV* mutant and their *rpsU*^{G50C} mutants were estimated. Since the previous stress resistance experiments were performed using 30°C-grown cultures and 37°C is the optimal growth temperature of *L. monocytogenes*, the μ_{max} was estimated in BHI at both 30°C and 37°C. As expected, the EGDe WT had higher μ_{max} than the EGDe-*rpsU*^{G50C} mutant at both temperatures, although the difference was not statistically significant at 37°C (p-value > 0.05) (Figure 3.2). This is in line with previous data that the growth difference was more pronounced at lower temperature (Metselaar et al., 2016). In addition, the Δ*rsbR1*-*rpsU*^{G50C} and the Δ*rsbV*-*rpsU*^{G50C} mutants, which both had increased stress resistance, had significantly lower μ_{max} than the Δ*rsbR1* and the Δ*rsbV* mutants at 30°C and 37°C (Figure 3.2). However, the Δ*sigB*-*rpsU*^{G50C} mutant, which had similar low stress resistance levels as the Δ*sigB* mutant, still had significantly lower μ_{max} than the Δ*sigB* mutant. This observation provides evidence that the *rpsU*^{G50C} mutation leads to reduced growth rate independently from RsbR1, RsbV and SigB.

3.3.3 *rpsU*^{G50C} mutation leads to increased stress resistance via SigB activation but independent from RsbV

Previously, it has been shown that SigB-regulated genes and proteins are upregulated in *L. monocytogenes* LO28 *rpsU*^{G50C} mutant V15 (Koomen et al., 2021; Koomen et al., 2018). In line with these data, our proteomic data showed that 106 proteins were significantly higher expressed in the EGDe-*rpsU*^{G50C} mutant compared to EGDe WT, and 54 of these higher expressed proteins belonged to SigB regulon (Figure 3.3 A and Supplemental Table 3.2). In addition, the proteomic data showed that only two SigB regulon proteins were significantly upregulated in the Δ*sigB*-*rpsU*^{G50C} mutant compared to the Δ*sigB* mutant (Figure 3.3 B and Supplemental Table 3.2). Since the EGDe-*rpsU*^{G50C} mutant, but not the Δ*sigB*-*rpsU*^{G50C} mutant, has increased stress resistance (Figure 3.1), these proteomic data confirmed that the *rpsU*^{G50C} mutation resulted in SigB activation and the upregulation of SigB regulon proteins, which caused the increased multi-stress resistance of the *rpsU*^{G50C} mutant. For the Δ*rsbV*-*rpsU*^{G50C} mutant, which lacks the anti-sigma factor antagonist RsbV, SigB should not be activated in this mutant and the SigB regulon should not be upregulated. However, our phenotypic data showed that the Δ*rsbV*-*rpsU*^{G50C} mutant still had increased stress resistance, which implies an RsbV-independent SigB activation in the Δ*rsbV*-*rpsU*^{G50C} mutant (Figure 3.1). Indeed, of the 113 proteins that were significantly higher expressed in the Δ*rsbV*-*rpsU*^{G50C} mutant compared to the Δ*rsbV* mutant, 65 proteins belonged to the SigB regulon (Figure 3.3 C and Supplemental Table 3.2). These results provide further evidence that in contrast to the traditional model, RsbV is not involved in the SigB activation and upregulation of regulon members in the *rpsU*^{G50C} mutant.

To further investigate these significantly upregulated or downregulated proteins, the numbers of differentially expressed proteins in each *rpsU*^{G50C} mutant are shown in Figure 3.4. There were 65 proteins that were upregulated in both EGDe-*rpsU*^{G50C} and Δ*rsbV*-*rpsU*^{G50C} mutants compared to their parent strains, of which 46 proteins

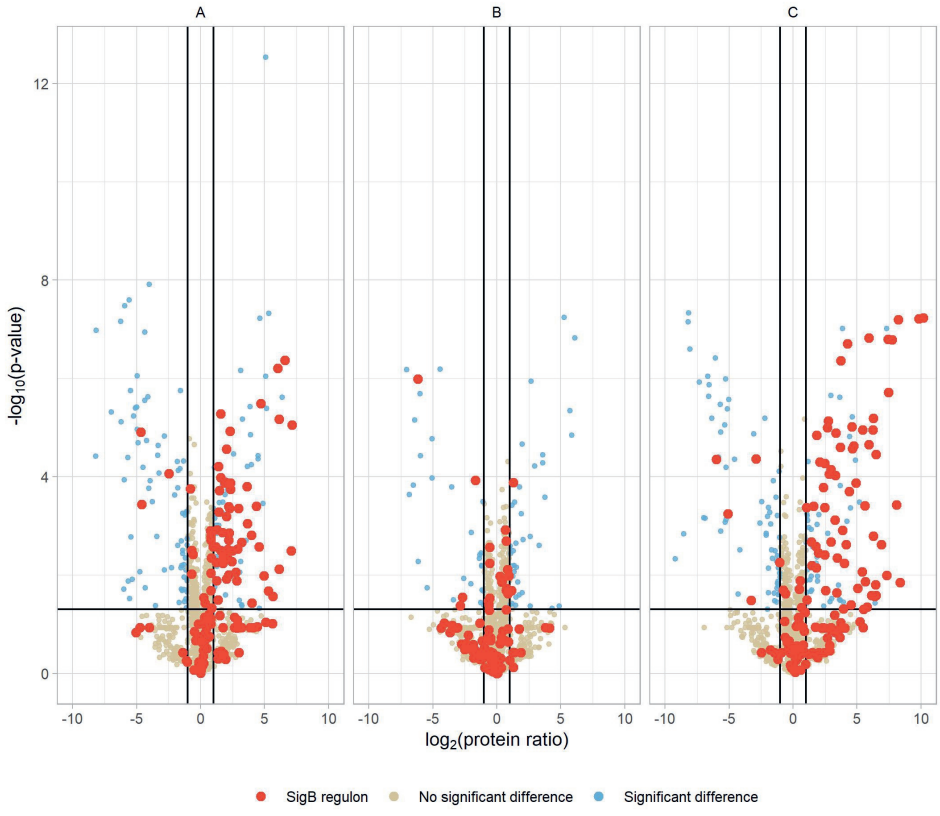

Figure 3.3: **Volcano plot of proteomic data comparing *L. monocytogenes* EGDe WT (A), Δ*sigB* (B) and Δ*rsbV* (C) mutants with their *rpsU*^{G50C} mutants EGDe-*rpsU*^{G50C}, Δ*sigB*-*rpsU*^{G50C} and Δ*rsbV*-*rpsU*^{G50C}, respectively.** The -$\log_{10}$(p-value) is plotted against the $\log_2$(protein ratio: *rpsU*^{G50C} mutants over parent strains). The horizontal line represents the cutoff of the p-value (0.05), and the vertical lines represent the cutoff of $\log_2$ (protein ratio) (± 1). Blue dots represent significantly upregulated or downregulated proteins. Red dots represent the proteins belonging to the SigB regulon.

belonged to the SigB regulon (Figure 3.4 A). Also, there were 36 proteins that were downregulated in both EGDe-$rpsU^{G50C}$ and $\Delta rsbV$-$rpsU^{G50C}$ mutants compared to their parent strains (Figure 3.4 B). KEGG pathway over-representation analysis (p-value < 0.05) of these 36 proteins showed that three enriched terms were found including flagellar assembly, bacterial chemotaxis and two-component systems, which was in line with previous proteomic and electron microscopy study of the $rpsU^{G50C}$ mutant V15 that showed absence of flagella (Koomen et al., 2021; Koomen et al., 2018). The $\Delta sigB$-$rpsU^{G50C}$ mutant had less proteins that were significantly upregulated or downregulated compared to the EGDe-$rpsU^{G50C}$ and the $\Delta rsbV$-$rpsU^{G50C}$ mutants (Figure 3.4), indicating that the $\Delta sigB$-$rpsU^{G50C}$ mutant had a rather similar proteomic profile as its parent strain the $\Delta sigB$ mutant, and this is in line with the observed similar reduced stress resistant phenotype.

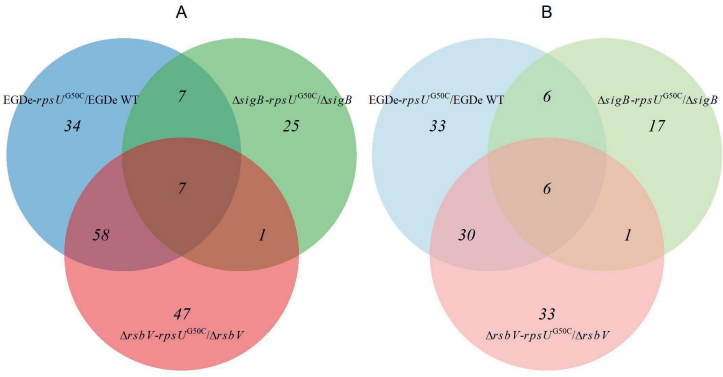

Figure 3.4: **Venn graph of differentially expressed proteins by comparing *L. monocytogenes* EGDe WT, $\Delta sigB$ and $\Delta rsbV$ mutants with their $rpsU^{G50C}$ mutants EGDe-$rpsU^{G50C}$, $\Delta sigB$-$rpsU^{G50C}$ and $\Delta rsbV$-$rpsU^{G50C}$, respectively.** The panel **(A)** and panel **(B)** represent the upregulated and downregulated proteins, respectively. (Light) blue, (light) green and (light) red circles represent the upregulated or downregulated proteins when comparing EGDe-$rpsU^{G50C}$, $\Delta sigB$-$rpsU^{G50C}$ and $\Delta rsbV$-$rpsU^{G50C}$ mutants to their parent strains, respectively.

3.3.4 RsbV-independent SigB activation in $rpsU^{G50C}$ mutants could not be explained by the RsbW:SigB ratio decrease

The activation of SigB requires the release of SigB from the anti-SigB factor RsbW. Interestingly, our proteomic data showed that both RsbW and SigB were upregulated in the EGDe-$rpsU^{G50C}$ and the $\Delta rsbV$-$rpsU^{G50C}$ mutants, but to slightly different levels, which might lead to changes in the protein abundance ratio between RsbW and SigB (Supplemental Table 3.2 and Supplemental Figure 3.2). A possible lower ratio of RsbW:SigB in the $rpsU^{G50C}$ mutant strains may make SigB more available for binding with the RNA polymerase. To evaluate this, the LFQ data from MaxQuant ProteinGroups file were used to calculate the protein ratio of RsbW:SigB for the EGDe WT, the EGDe-$rpsU^{G50C}$, the $\Delta rsbV$ and the $\Delta rsbV$-$rpsU^{G50C}$ mutants (Figure 3.5).

The RsbW:SigB ratio was not significantly lower in the EGDe-*rpsU*^{G50C} mutant than the EGDe WT, and additionally, the ratio was still 2:1, which is the ratio previously determined for the RsbW:SigB complex in *B. subtilis* (Pathak et al., 2020). With the deletion of RsbV, there should be more RsbW available for SigB in Δ*rsbV*-*rpsU*^{G50C}. However, the Δ*rsbV*-*rpsU*^{G50C} mutant had an even higher RsbW:SigB ratio than the EGDe-*rpsU*^{G50C} mutant. Therefore, the RsbV-independent SigB activation in the *rpsU*^{G50C} mutant could not be explained by a reduced RsbW:SigB ratio in the *rpsU*^{G50C} mutant.

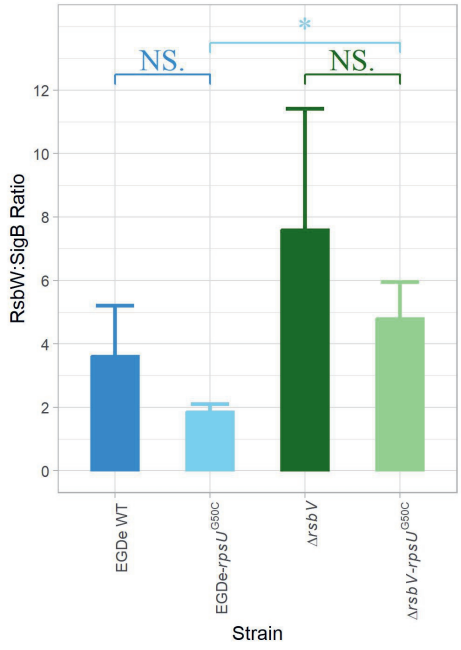

Figure 3.5: **RsbW:SigB protein abundance ratio.** The protein abundance ratio between RsbW:SigB in *L. monocytogenes* EGDe WT, Δ*rsbV* mutant and their *rpsU*^{G50C} mutants, which is calculated based on proteomic data. Significant differences are indicated by an asterisk, and no significant differences are indicated by NS.

3.3.5 PstS is upregulated in the *rpsU*^{G50C} mutant, but does not contribute to phenotypic changes

Since the combined data on RsbW:SigB ratios could not explain the SigB activation in the *rpsU*^{G50C} mutant, proteins whose expression levels were affected by the *rpsU*^{G50C} mutation but independent from the presence of SigB or RsbV should be considered. In all three *rpsU*^{G50C} mutants, seven proteins were significantly upregulated and six proteins were significantly downregulated (Figure 3.4, Supplemental Table 3.3 and Supplemental Table 3.4).

Among these proteins, Lmo2499 was the highest differentially expressed. Lmo2499, a protein homologous to the periplasmic phosphate sensory binding protein PstS, might

be related to inorganic phosphate (Pi) transport and phosphorus (Pho) metabolism, regulated by the Pho regulon (Hsieh and Wanner, 2010; Vaestermark and Saier, 2014). In the case of phosphate limitation, PstS binds inorganic phosphate (Pi) and facilitates transport across the cytoplasmic membrane in combination with an ABC transporter (Vaestermark and Saier, 2014). Interestingly, Pi starvation can also activate the SigB regulon in *B. subtilis* via the SigB regulator RsbP phosphatase, which is activated upon energy stress (Allenby et al., 2005; Vijay et al., 2000). *L. monocytogenes* does not have RsbP, and the mechanisms underlying SigB activation under nutrient and/or energy limitation remain to be elucidated (Shin et al., 2010). To further analyze the possible role of PstS in SigB activation in the *rpsU*^{G50C} mutant, the *pstS* gene was deleted in the EGDe WT and the EGDe-*rpsU*^{G50C} mutant (Table 3.1). The acid and heat stress resistance and the maximum specific growth rate of the Δ*pstS* mutant and the Δ*pstS*-*rpsU*^{G50C} double mutant were then tested. The acid resistance and heat resistance of the Δ*pstS* mutant was lower compared to the Δ*pstS*-*rpsU*^{G50C} mutant, although the difference was not significant for heat resistance (Supplemental Figure 3.3). Also, the Δ*pstS* mutant had a significantly higher μ_{max} than the Δ*pstS*-*rpsU*^{G50C} mutant at 30°C and not significantly higher μ_{max} at 37°C (Supplemental Figure 3.4). Comparative WGS showed an additional mutation in the double mutant (Supplemental Table 3.1), but based on the observed stress resistance and fitness phenotypes, it can be concluded that PstS did not directly contribute to increased robustness and reduced fitness of the rpsU mutants. *rpsU* mutants.

3.4 Discussion

The aim of this study was to examine how the *rpsU*^{G50C} mutation influences the stress resistance and the maximum specific growth rate of *L. monocytogenes*. The phenotypic and proteomic data showed that SigB was activated in the *rpsU*^{G50C} mutant, which led to SigB regulon upregulation and concomitant increased stress resistance. Based on the current knowledge of the SigB controlling pathway, the activation of SigB requires the presence of RsbR1 and RsbV (Supplemental Figure 3.1) (Guerreiro et al., 2020a). However, both the Δ*rsbR1*-*rpsU*^{G50C} and the Δ*rsbV*-*rpsU*^{G50C} mutants surprisingly had higher stress resistance than their parent strains, indicating that the SigB-mediated increased stress resistance in the *rpsU*^{G50C} mutant was independent of RsbR1, i.e., a functional stressosome, and the anti-sigma factor antagonist RsbV. The proteomic analysis also shows that the SigB regulon was still induced in the Δ*rsbV*-*rpsU*^{G50C} mutant, in which SigB was expected to be inactive due to binding to RsbW. As shown in Supplemental Figure 3.1, RsbW is the only SigB regulator downstream of RsbV in the SigB regulation pathway. Hence, the activation signal in the *rpsU*^{G50C} mutant must enter the SigB activation pathway downstream from RsbV, so the mutation in the ribosome may induce an alternative signaling pathway that reduces or prevents the binding between RsbW and SigB, which leads to the RsbV-independent SigB activation.

Previously, activation of SigB at low or high temperature has been observed in growing cells of *B. subtilis* (16°C or 51°C) and *L. monocytogenes* (4°C) wild type and respective *rsbV* mutants (Brigulla et al., 2003; Holtmann et al., 2004; Utratna et al., 2014). It was hypothesized that key physical interactions between RsbW and SigB or between

SigB and core RNA polymerase might change at low or high temperatures, but this hypothesis cannot explain the RsbV-independent SigB activation in the current study, since the *L. monocytogenes* strains were cultured at optimal temperature (30°C) in rich media (BHI). Another explanation may involve changes in the RsbW:SigB ratio of 2:1, which was previously determined in *B. subtilis* based on protein quantification and 3D structural modeling (Pathak et al., 2020). Based on our proteomic results, the respective RsbW:SigB ratios were 2:1 or even higher in the tested *rpsU*^{G50C} mutants (Figure 3.5). Therefore, RsbV-independent SigB activation could not be explained by a decrease in the RsbW:SigB ratio.

Another hypothesis suggested in previous studies was that signaling proteins acting independently from RsbV to RsbW could disrupt the inhibitory RsbW-SigB complex and allow activation of SigB (Brigulla et al., 2003). In the current study, the Pi sensory binding protein PstS has been investigated, since the proteomic data showed that PstS was upregulated more than 4-fold with a p-value less than 0.01 in all three *rpsU*^{G50C} mutants, namely, the EGDe-*rpsU*^{G50C}, the Δ*sigB*-*rpsU*^{G50C} and the Δ*rsbV*-*rpsU*^{G50C} mutants (Supplemental Table 3.2). PstS is involved in phosphate (Pi) transport and Pho regulon regulation (Hsieh and Wanner, 2010; Santos-Beneit, 2015). In *B. subtilis*, both the Pho regulon and the SigB regulon can be activated by Pi starvation, and the signal of Pi starvation is transmitted to SigB via SigB regulator RsbP (Allenby et al., 2005). For *B. subtilis* SigB activation, RsbP is also required in response to energy stress, and another SigB regulator, RsbU, is required for response to environmental stress (Vijay et al., 2000). *L. monocytogenes* only has RsbU but not RsbP, and the energy stress-triggered activation pathway remains to be elucidated (Shin et al., 2010). To our knowledge, there is no research about the *L. monocytogenes* Pi starvation reaction or the activation mechanism of SigB by Pi starvation yet. Since SigB can be activated by Pi starvation in *B. subtilis*, it is possible that SigB can also be activated by Pi starvation in *L. monocytogenes*. However, the phenotypic characterization of the Δ*pstS* and the Δ*pstS*-*rpsU*^{G50C} mutants showed that the Δ*pstS*-*rpsU*^{G50C} mutant still had higher acid and heat stress resistance than the Δ*pstS* mutant (Supplemental Figure 3.3), excluding a direct link of PstS with SigB activation in the mutant strains for the tested conditions. Whether the upregulation of PstS signifies changes in intracellular Pi concentrations in *rpsU*^{G50C} mutant strains, resulting in possible effects on (cross-reacting) kinase activity in other regulatory networks (Shi et al., 2014), that subsequently affect RsbW and SigB interaction in *rpsU*^{G50C} mutants, remains to be studied.

Apart from the stress resistance, we have also tested the fitness of each strain to investigate the stress resistance-fitness trade-off of the *rpsU*^{G50C} mutant. Generally, there is a trade-off between stress resistance and growth rate for bacteria, and this phenomenon has also been reported in *rpsU*^{G50C} mutants in previous studies (Koomen et al., 2021; Koomen et al., 2018; Metselaar et al., 2016, 2013; Nystrom, 2004). This may be due to the competition between SigB and housekeeping SigA for the RNA polymerase, with the latter responsible for the transcription of growth-related genes (Nystrom, 2004; Österberg et al., 2011). In addition, activation of SigB and its regulon conceivably consumes energy, resulting in a negative impact on growth (Guerreiro et al., 2020a; Xia et al., 2016). Indeed, studies have shown that mutations in SigB can increase fitness under sub-optimal conditions, including 0.5 M NaCl, 42°C and blue light (Abram et al., 2008; Guerreiro et al., 2022b, 2020b; O'Donoghue et al., 2016). However, our previous evolution experiments with *rpsU*^{G50C} mutants resulted in the

selection of evolved variants with enhanced fitness (Koomen, 2022). The fact that no variants were obtained with mutations in *sigB* or genes of the SigB operon suggested that the major negative effect on fitness did not derive from SigB activation. Indeed, in the current study, all these *rpsU*^{G50C} mutants, including the Δ*sigB-rpsU*^{G50C} mutant, had lower maximum specific growth rates than their respective parent strains in BHI at 30°C (Figure 3.2). Therefore, the growth rate decrease of the *rpsU*^{G50C} mutant is independent of SigB activation and SigB-mediated stress response. In addition, the Δ*pstS-rpsU*^{G50C} mutant also had a lower specific growth rate than the Δ*pstS* mutant (Supplemental Figure 3.4). Thus, the upregulation of *pstS* in the *rpsU*^{G50C} mutant did not contribute to the reduced fitness either.

In *Escherichia coli* and *B. subtilis*, RpsU (ribosomal protein S21) is involved in translation initiation (Berk et al., 2006; Sohmen et al., 2015; Van Duin and Wijnands, 1981). Combined with the results above, it is conceivable that reduced fitness of *L. monocytogenes rpsU*^{G50C} mutants is linked to decreased translation efficacy and/or the availability of functional 70S ribosomes (Koomen, 2022). The *L. monocytogenes* Lmo0762 protein, HflXr, a homolog of a ribosome-splitting factor, HflX, was also upregulated in all three *rpsU*^{G50C} mutants (Supplemental Table 3.3). HflX belongs to the GTPase OBG-HflX-like superfamily. Another member of this superfamily, Obg (Lmo1537/ObgE), that was detected in the EGDe WT and mutant proteomes, has been reported to play a role in the activation of SigB in *B. subtilis* (Kint et al., 2014; Scott and Haldenwang, 1999; Verstraeten et al., 2011). Whether HflXr and/or ObgE play a role in *L. monocytogenes* RsbV-independent SigB activation and/or fitness modulation in *rpsU*^{G50C} mutants remains to be elucidated.

Taken together, the current study shows that the activation of SigB in the *L. monocytogenes rpsU*^{G50C} mutant resulting in multi-stress robustness and lower maximum specific growth rate is independent of the stressosome protein RsbR1 and anti-sigma factor antagonist RsbV. Although there is generally a trade-off between stress resistance and growth rate for bacteria, we observed that the reduced growth rate is independent of the activation of SigB and its regulon members and conceivably due to reduced ribosomal functioning. Further studies are needed to elucidate the mechanism of RsbV-independent SigB activation and the fitness modulation in *rpsU*^{G50C} mutants.

3.5 Data Availability Statement

The mass spectrometry proteomics data have been deposited to the ProteomeXchange Consortium via the PRIDE (Perez-Riverol et al., 2022) partner repository with the dataset identifier PXD045800.

3.6 Acknowledgments

We thank Jeroen Koomen (Food Microbiology, Wageningen University) for mutant construction support. We thank Chendi Zhang and Kirsten van Kooten (Food Microbiology, Wageningen University) for data collection assistance. We thank Jasper

Bannenberg (Food Microbiology, Wageningen University) for proteomic data analysis assistance. We also thank Oscar van Mastrigt (Food Microbiology, Wageningen University) for SNP analysis support. Xuchuan Ma was supported by a grant from the China Scholarship Council (File No. 201907720086).

3.7 Supplementary Material

Supplemental Table 3.1: **Identified Single nucleotide polymorphisms in the constructed mutants.** The SNPs were shown by comparing the constructed mutants EGDe-*rpsU*^{G50C}, Δ*sigB*-*rpsU*^{G50C}, Δ*rsbV*-*rpsU*^{G50C}, Δ*pstS* and Δ*pstS*-*rpsU*^{G50C} to their parent strains, respectively. COMPARE shows the SNP analysis of the constructed mutants to the parent strains; EFFECT shows the annotated consequence of this SNP; LOCUS_TAG shows the locus tag of the gene; GENE shows the name of the gene; and PRODUCT shows the produced protein by the gene

COMPARE	EFFECT	LOCUS_TAG	GENE	PRODUCT
EGDe-*rpsU*^{G50C} to EGDe WT	missense variant c.50G>C p.Arg17Pro	lmo1469	*rpsU*	30S ribosomal protein S21
Δ*sigB*-*rpsU*^{G50C} to Δ*sigB*	missense variant c.50G>C p.Arg17Pro	lmo1469	*rpsU*	30S ribosomal protein S21
Δ*rsbV*-*rpsU*^{G50C} to Δ*rsbV*	missense variant c.50G>C p.Arg17Pro	lmo1469	*rpsU*	30S ribosomal protein S21
Δ*pstS* to EGDe WT	stop gained c.87C>A p.Tyr29*	lmo1503	*reoM*	hypothetical protein
Δ*pstS*-*rpsU*^{G50C} to Δ*pstS*	missense variant c.50G>C p.Arg17Pro	lmo1469	*rpsU*	30S ribosomal protein S21
Δ*pstS*-*rpsU*^{G50C} to Δ*pstS*	synonymous variant c.1047T>G p.Ala349Ala	lmo1799		peptidoglycan binding protein

Supplemental Table 3.2: **Proteins above or below the cut off in EGDe-*rpsU*^{G50C}, Δ*sigB*-*rpsU*^{G50C} and Δ*rsbV*-*rpsU*^{G50C} mutants compared to EGDe WT, Δ*sigB* and Δ*rsbV* mutants, respectively.** The p-value and $\log_2$ratio in bold are considered significant

Gene locus	Gene name	Uniprot ID	Protein name	SigB regulon	EGDe-*rpsU*^{G50C}/EGDe WT		ΔsigB-*rpsU*^{G50C}/ΔsigB		ΔrsbV-*rpsU*^{G50C}/ΔrsbV	
					p-value	$\log_2$ ratio	p-value	$\log_2$ ratio	p-value	$\log_2$ ratio
lmo0009	-	Q8YAV4	spermidine acetyltransferase	-	**0.000**	**-2.03**	0.065	-3.95	0.201	2.34
lmo0019	-	Q8YAU4	hypothetical protein lmo0019	Yes	**0.000**	**6.05**	-	0.00	**0.000**	**6.23**
lmo0043	arcA	Q8YAS0	arginine deiminase	Yes	**0.009**	**2.75**	0.119	4.12	**0.026**	**6.49**
lmo0092	atpD1	Q8YAM6	ATP synthase F0F1 subunit beta	-	0.116	2.71	-	0.00	**0.011**	**1.44**
lmo0096	-	Q8YAM2	PTS mannose transporter subunit IIAB	-	**0.000**	**-1.56**	**0.000**	**-1.09**	**0.001**	**-1.99**
lmo0098	-	Q8YAM0	PTS mannose transporter subunit IID	-	**0.002**	**-1.76**	**0.006**	**-1.17**	**0.000**	**-2.45**
lmo0117	lmaB	Q7AP94	antigen B	-	0.374	1.03	**0.043**	**4.89**	0.374	-1.80
lmo0119	-	Q7AP92	hypothetical protein lmo0119	-	0.116	-3.25	**0.000**	**5.72**	0.573	-1.56
lmo0120	-	Q8YAK4	hypothetical protein lmo0120	-	0.374	-1.45	**0.000**	**6.09**	0.895	-0.26
lmo0121	-	Q8YAK3	phage tail protein	-	0.227	-2.75	**0.023**	**1.98**	0.264	-2.40
lmo0122	-	Q8YAK2	hypothetical protein lmo0122	-	0.444	0.47	**0.041**	**1.47**	0.425	-1.51
lmo0123	-	Q8YAK1	hypothetical protein lmo0123	-	0.607	0.43	**0.025**	**1.76**	0.131	-1.08
lmo0127	-	Q8YAJ7	hypothetical protein lmo0127	-	0.209	1.03	**0.028**	**1.51**	0.255	-0.70
lmo0129	-	Q8YAJ6	N-acetylmuramoyl-L-alanine amidase	-	0.925	0.08	**0.014**	**1.65**	0.082	-1.03
lmo0169	-	Q8YAF7	glucose transporter	Yes	**0.000**	**7.14**	-	0.00	**0.002**	**6.28**
lmo0170	-	Q8YAF6	hypothetical protein lmo0170	Yes	**0.001**	**1.72**	0.216	-0.48	**0.000**	**2.74**

Continued on next page

Supplemental Table 3.2 continued from previous page

Gene locus	Gene name	Uniprot ID	Protein name	SigB regulon	EGDe-*rpsU*^{G50C}/EGDe WT p-value	EGDe-*rpsU*^{G50C}/EGDe WT log_2 ratio	ΔsigB-*rpsU*^{G50C}/ΔsigB p-value	ΔsigB-*rpsU*^{G50C}/ΔsigB log_2 ratio	ΔrsbV-*rpsU*^{G50C}/ΔrsbV p-value	ΔrsbV-*rpsU*^{G50C}/ΔrsbV log_2 ratio
lmo0177	metG,metS	Q8YAF2	methionyl-tRNA synthetase	-	**0.013**	**-1.06**	0.230	-0.40	**0.019**	**-1.27**
lmo0208	-	P0A4Q8	hypothetical protein lmo0208	-	0.131	0.64	0.386	-2.53	**0.037**	**6.42**
lmo0211	rplY,ctc	Q8YAD3	50S ribosomal protein L25	Yes	**0.000**	**2.34**	0.124	0.86	**0.000**	**2.68**
lmo0235	ispD	Q8YAB5	2-C-methyl-D-erythritol 4-phosphate cytidylyltransferase	-	**0.000**	**4.65**	0.093	2.50	0.127	2.97
lmo0236	ispF	Q8YAB4	2-C-methyl-D-erythritol 2,4-cyclodiphosphate synthase	-	0.095	-2.43	0.116	-3.22	**0.000**	**3.71**
lmo0257	-	Q8YA97	hypothetical protein lmo0257	-	**0.001**	**1.41**	**0.001**	**1.90**	0.589	-0.17
lmo0263	inlH	Q7AP87	internalin H	Yes	0.117	4.03	-	0.00	**0.000**	**7.45**
lmo0265	-	Q7AP85	succinyl-diaminopimelate desuccinylase	Yes	**0.005**	**2.09**	-	0.00	**0.001**	**3.28**
lmo0268	-	Q8YA91	phosphoglycerate mutase	-	**0.001**	**-1.19**	**0.018**	**-5.43**	0.694	0.83
lmo0274	-	Q8YA85	hypothetical protein lmo0274	-	-	0.00	-	0.00	**0.000**	**4.87**
lmo0275	-	Q8YA84	hypothetical protein lmo0275	-	**0.000**	**4.89**	0.914	-0.24	0.010	0.50
lmo0282	-	Q8YA77	hypothetical protein lmo0282	-	0.005	0.47	**0.004**	**1.07**	0.542	0.12
lmo0292	-	Q8YA67	heat-shock protein htrA serine protease	Yes	0.003	0.97	0.387	-0.33	**0.000**	**1.03**
lmo0319	-	Q7AP84	phospho-beta-glucosidase	-	**0.001**	**1.28**	**0.006**	**1.37**	0.002	1.00
lmo0338	-	Q8YA27	hypothetical protein lmo0338	-	**0.001**	**1.12**	0.495	1.52	0.119	3.21
lmo0354	-	Q8YA12	fatty-acid–CoA ligase	-	**0.002**	**-1.52**	0.004	-0.83	**0.009**	**-1.07**
lmo0355	-	Q8YA11	fumarate reductase subunit A	-	**0.004**	**-1.18**	0.074	-0.21	**0.000**	**-1.94**
lmo0368	-	Q8Y9Z9	hypothetical protein lmo0368	-	0.020	1.00	0.142	0.28	**0.032**	**3.70**

Continued on next page

Supplemental Table 3.2 continued from previous page

Gene locus	Gene name	Uniprot ID	Protein name	SigB regulon	EGDe-*rpsU*^{G50C}/EGDe WT		ΔsigB-*rpsU*^{G50C}/ΔsigB		ΔrsbV-*rpsU*^{G50C}/ΔrsbV	
					p-value	$\log_2$ ratio	p-value	$\log_2$ ratio	p-value	$\log_2$ ratio
lmo0387	-	Q8Y9Y0	hypothetical protein lmo0387	Yes	**0.001**	**1.28**	0.147	-3.67	0.139	0.87
lmo0393	-	Q8Y9X5	hypothetical protein lmo0393	-	**0.000**	**-2.82**	0.374	-0.91	-	0.00
lmo0394	-	Q8Y9X4	P60 protein	-	0.374	1.60	**0.000**	**3.76**	0.310	0.35
lmo0411	-	Q8Y9V9	phosphoenolpyruvate synthase	-	0.117	2.31	**0.043**	**2.61**	0.142	2.29
lmo0433	inlA	P0DJM0	internalin A	Yes	0.118	2.66	-	0.00	**0.000**	**4.76**
lmo0437	-	Q8Y9T6	hypothetical protein lmo0437	-	**0.000**	**-5.47**	0.120	-0.80	0.065	-1.06
lmo0443	-	Q8Y9T0	LytR family transcriptional regulator	-	0.022	0.37	**0.041**	**1.04**	0.934	0.02
lmo0445	-	Q8Y9S8	transcripitonal regulator	Yes	**0.000**	**4.70**	-	0.00	**0.000**	**5.94**
lmo0452	-	Q8Y9S1	hypothetical protein lmo0452	-	0.009	0.76	0.015	0.64	**0.013**	**1.92**
lmo0454	-	Q8Y9R9	hypothetical protein lmo0454	-	**0.000**	**6.40**	0.629	-1.03	0.117	-3.48
lmo0480	-	Q8Y9P4	transcriptional regulator	-	**0.000**	**3.13**	0.119	1.81	0.374	1.10
lmo0481	-	Q8Y9P3	hypothetical protein lmo0481	-	**0.005**	**3.14**	-	0.00	**0.000**	**4.57**
lmo0515	-	Q8Y9L2	hypothetical protein lmo0515	Yes	**0.021**	**5.29**	-	0.00	**0.000**	**7.44**
lmo0519	lmrB	Q8Y9K8	multidrug resistance protein	-	**0.021**	**-1.44**	0.374	2.64	**0.023**	**-1.48**
lmo0524	-	Q8Y9K3	sulfate transporter	Yes	0.001	0.76	0.033	-0.67	**0.000**	**1.61**
lmo0539	lacD	Q8Y9I9	tagatose 1,6-diphosphate aldolase	Yes	**0.004**	**1.77**	0.131	-0.62	**0.000**	**3.33**
lmo0554	-	Q8Y9H4	NADH-dependent butanol dehydrogenase	Yes	**0.004**	**1.88**	0.052	-0.58	**0.000**	**2.82**
lmo0560	-	Q8Y9G8	glutamate dehydrogenase	-	0.022	-0.71	**0.004**	**-1.33**	0.048	-0.62
lmo0574	-	Q8Y9F4	beta-glucosidase	-	**0.004**	**1.24**	0.029	0.92	0.003	0.98
lmo0575	-	Q8Y9F3	GntR family transcriptional regulator	-	0.529	1.49	**0.000**	**-6.00**	0.407	1.79

Continued on next page

Supplemental Table 3.2 continued from previous page

Gene locus	Gene name	Uniprot ID	Protein name	SigB regulon	EGDe-*rpsU*^{G50C}/EGDe WT		ΔsigB-*rpsU*^{G50C}/ΔsigB		ΔrsbV-*rpsU*^{G50C}/ΔrsbV	
					p-value	$\log_2$ ratio	p-value	$\log_2$ ratio	p-value	$\log_2$ ratio
lmo0580	-	Q8Y9E9	hypothetical protein lmo0580	Yes	**0.000**	**1.56**	0.095	-4.13	0.268	2.85
lmo0584	-	Q8Y9E6	hypothetical protein lmo0584	-	**0.000**	**1.02**	0.260	0.63	**0.033**	**1.10**
lmo0588	-	Q8Y9E2	DNA photolyase	-	**0.025**	**1.95**	0.201	1.87	**0.020**	**1.47**
lmo0590	-	Q8Y9E0	hypothetical protein lmo0590	Yes	**0.000**	**2.29**	0.912	-0.23	**0.005**	**3.46**
lmo0591	-	Q8Y9D9	hypothetical protein lmo0591	Yes	**0.002**	**2.21**	0.507	-1.14	**0.018**	**5.07**
lmo0606	-	Q8Y9C6	MarR family transcriptional regulator	-	0.028	0.55	-	0.00	**0.000**	**4.41**
lmo0607	-	Q8Y9C5	ABC transporter ATP-binding protein	-	**0.007**	**1.29**	0.118	0.52	**0.006**	**1.80**
lmo0608	-	Q8Y9C4	ABC transporter ATP-binding protein	-	**0.003**	**1.59**	0.170	0.36	**0.001**	**1.89**
lmo0611	azoR1	Q8Y9C1	azoreductase	-	**0.004**	**-1.40**	0.155	-3.36	0.078	-0.48
lmo0617	-	Q8Y9B5	hypothetical protein lmo0617	-	**0.009**	**3.08**	**0.003**	**3.30**	0.973	-0.02
lmo0619	-	Q8Y9B3	hypothetical protein lmo0619	-	0.051	1.65	**0.002**	**2.04**	0.581	-0.30
lmo0623	-	Q8Y9A9	hypothetical protein lmo0623	-	0.060	2.24	**0.000**	**2.70**	0.771	0.50
lmo0650	-	Q8Y983	hypothetical protein lmo0650	-	**0.000**	**1.45**	0.039	0.42	**0.001**	**2.02**
lmo0654	-	Q8Y979	hypothetical protein lmo0654	Yes	0.853	-0.52	-	0.00	**0.002**	**4.13**
lmo0665	-	Q8Y968	hypothetical protein lmo0665	-	-	0.00	-	0.00	**0.000**	**4.50**
lmo0669	-	Q8Y964	oxidoreductase	Yes	**0.000**	**4.35**	-	0.00	**0.000**	**6.48**
lmo0680	-	Q8Y954	flagellar biosynthesis protein FlhA	-	**0.000**	**-5.23**	0.109	0.24	**0.000**	**-5.26**
lmo0681	-	Q8Y953	flagellar biosynthesis regulator FlhF	-	**0.000**	**-5.68**	0.035	0.79	0.060	-4.54

Continued on next page

Supplemental Table 3.2 continued from previous page

Gene locus	Gene name	Uniprot ID	Protein name	SigB regulon	EGDe-*rpsU*^{G50C}/EGDe WT		ΔsigB-*rpsU*^{G50C}/ΔsigB		ΔrsbV-*rpsU*^{G50C}/ΔrsbV	
					p-value	$\log_2$ ratio	p-value	$\log_2$ ratio	p-value	$\log_2$ ratio
lmo0684	-	Q8Y951	hypothetical protein lmo0684	-	**0.000**	**-6.20**	0.329	-2.46	**0.000**	**-5.67**
lmo0685	-	Q7AP82	flagellar motor protein MotA	-	**0.000**	**-3.23**	0.135	0.56	**0.000**	**-8.20**
lmo0686	motB	Q7AP81	flagellar motor rotation MotB	-	**0.000**	**-6.98**	0.203	0.18	**0.001**	**-6.98**
lmo0688	-	Q8Y949	hypothetical protein lmo0688	-	**0.030**	**-5.56**	0.008	-0.36	**0.003**	**-4.17**
lmo0689	-	Q8Y948	chemotaxis protein CheV	-	**0.000**	**-3.78**	0.473	-0.10	**0.001**	**-8.55**
lmo0690	flaA	Q02551	flagellin	-	**0.002**	**-5.46**	0.235	-0.81	**0.005**	**-9.22**
lmo0691	cheY	P0A4H5	chemotaxis response regulator CheY	-	**0.000**	**-4.04**	0.145	-2.53	0.106	-2.71
lmo0692	cheA	Q48768	two-component sensor histidine kinase CheA	-	**0.020**	**-6.01**	0.652	0.05	0.051	-4.90
lmo0695	-	Q8Y945	hypothetical protein lmo0695	-	**0.000**	**-8.18**	0.684	-0.16	0.374	-2.68
lmo0697	-	Q92DV7	flagellar hook protein FlgE	-	**0.000**	**-8.21**	0.439	-2.61	0.374	-2.61
lmo0700	-	Q8Y941	flagellar motor switch protein FliY	-	**0.008**	**-2.84**	0.015	-0.53	**0.000**	**-6.68**
lmo0702	-	Q8Y939	hypothetical protein lmo0702	-	**0.000**	**-3.33**	0.362	0.46	**0.000**	**-6.57**
lmo0704	-	Q8Y937	hypothetical protein lmo0704	-	**0.000**	**-5.98**	**0.000**	**-6.84**	0.374	-1.73
lmo0705	flgK	Q8Y936	flagellar hook-associated protein FlgK	-	**0.009**	**-4.76**	0.106	-0.94	**0.000**	**-5.82**
lmo0706	-	Q8Y935	flagellar hook-associated protein FlgL	-	**0.000**	**-5.59**	0.379	-1.98	**0.001**	**-5.65**
lmo0707	-	Q8Y934	flagellar capping protein FliD	-	**0.000**	**-6.23**	0.433	0.06	**0.000**	**-6.58**
lmo0713	-	Q8Y929	flagellar MS-ring protein FliF	-	**0.018**	**-4.34**	0.213	0.49	**0.000**	**-6.35**
lmo0714	-	Q8Y928	flagellar motor switch protein FliG	-	**0.000**	**-4.87**	0.091	-0.19	**0.000**	**-8.15**

Continued on next page

Supplemental Table 3.2 continued from previous page

Gene locus	Gene name	Uniprot ID	Protein name	SigB regulon	EGDe-*rpsU*^{G50C}/EGDe WT		ΔsigB-*rpsU*^{G50C}/ΔsigB		ΔrsbV-*rpsU*^{G50C}/ΔrsbV	
					p-value	$\log_2$ ratio	p-value	$\log_2$ ratio	p-value	$\log_2$ ratio
lmo0715	-	Q8Y927	flagellar assembly protein H	-	**0.000**	**-4.94**	0.131	-3.41	0.117	-3.05
lmo0716	-	Q8Y926	flagellum-specific ATP synthase	-	**0.042**	**-3.54**	0.059	0.31	0.448	-2.11
lmo0718	-	Q8Y924	hypothetical protein lmo0718	-	**0.013**	**-5.64**	0.134	-0.87	**0.001**	**-5.23**
lmo0722	-	Q8Y920	pyruvate oxidase	Yes	**0.001**	**2.23**	-	0.00	**0.000**	**4.40**
lmo0723	-	Q8Y919	metyl-accepting chemotaxis protein	Yes	**0.000**	**-4.61**	0.504	0.19	**0.001**	**-5.10**
lmo0738	-	Q8Y904	PTS beta-glucoside transporter subunit IIABC	Yes	0.626	0.24	**0.042**	**-2.85**	**0.033**	**-3.29**
lmo0758	-	Q8Y8Y4	hypothetical protein lmo0758	-	**0.000**	**-4.11**	0.374	-1.48	0.374	1.39
lmo0762	hflXr	Q8Y8Y0	ATP/GTP-binding protein	-	**0.000**	**2.09**	**0.002**	**1.50**	**0.001**	**1.43**
lmo0764	-	Q8Y8X8	lipoate-protein ligase	-	**0.006**	**1.31**	0.149	-0.22	0.229	2.61
lmo0770	-	Q8Y8X2	LacI family transcriptional regulator	-	**0.000**	**3.26**	0.542	-1.10	0.374	-1.22
lmo0781	-	Q8Y8W1	PTS mannose transporter subunit IID	Yes	**0.000**	**3.62**	0.125	1.73	**0.000**	**9.83**
lmo0782	-	Q8Y8W0	PTS mannose transporter subunit IIC	Yes	0.092	5.09	-	0.00	**0.000**	**10.18**
lmo0783	-	Q8Y8V9	PTS mannose transporter subunit IIB	Yes	**0.005**	**2.16**	0.770	-0.96	**0.001**	**3.86**
lmo0786	azoR2	Q8Y8V6	ACP phosphodiesterase	-	**0.006**	**-1.30**	0.079	-0.32	0.179	-4.00
lmo0814	-	Q8Y8T0	oxidoreductase	-	**0.007**	**-2.26**	**0.005**	**-1.38**	0.138	-2.66
lmo0819	-	Q8Y8S5	hypothetical protein lmo0819	Yes	**0.003**	**1.18**	0.002	0.74	**0.000**	**1.85**
lmo0820	-	Q8Y8S4	acetyltransferase	-	0.277	0.27	0.903	0.04	**0.022**	**1.38**
lmo0821	-	Q8Y8S3	hypothetical protein lmo0821	Yes	0.107	2.95	0.903	-0.22	**0.000**	**4.26**
lmo0823	-	Q8Y8S1	oxidoreductase	-	**0.017**	**1.12**	0.893	-0.03	0.098	0.40
lmo0829	nifJ	Q8Y8R6	pyruvate-flavodoxin oxidoreductase	-	**0.022**	**-1.04**	0.046	0.51	0.150	-3.12

Continued on next page

Supplemental Table 3.2 continued from previous page

Gene locus	Gene name	Uniprot ID	Protein name	SigB regulon	EGDe-*rpsU*^{G50C}/EGDe WT		ΔsigB-*rpsU*^{G50C}/ΔsigB		ΔrsbV-*rpsU*^{G50C}/ΔrsbV	
					p-value	$\log_2$ ratio	p-value	$\log_2$ ratio	p-value	$\log_2$ ratio
lmo0858	-	Q8Y8N8	LacI family transcriptional regulator	-	**0.036**	**1.44**	0.904	0.04	**0.023**	**1.07**
lmo0880	-	Q8Y8L7	wall associated protein precursor	Yes	0.113	4.43	-	0.00	**0.000**	**8.23**
lmo0882	-	Q8Y8L5	hypothetical protein lmo0882	-	0.500	-0.12	**0.038**	**1.18**	0.092	-0.41
lmo0883	-	Q8Y8L4	hypothetical protein lmo0883	-	0.072	0.54	**0.010**	**1.10**	0.957	0.01
lmo0894	rsbW	Q8Y8K6	serine-protein kinase RsbW	Yes	**0.003**	**1.58**	0.905	-0.13	**0.000**	**2.46**
lmo0895	sigB	Q7AP79	RNA polymerase sigma factor SigB	Yes	**0.005**	**2.46**	0.807	-0.58	**0.002**	**2.98**
lmo0896	rsbX	Q8Y8K5	indirect negative regulation of sigma B dependant gene expression (serine phosphatase)	Yes	**0.000**	**2.04**	**0.000**	**1.29**	0.092	3.74
lmo0899	-	Q8Y8K2	hypothetical protein lmo0899	-	**0.000**	**-3.93**	**0.000**	**-4.42**	-	0.00
lmo0913	-	Q8Y8I9	succinate semialdehyde dehydrogenase	Yes	**0.001**	**3.67**	0.259	-1.87	**0.000**	**5.92**
lmo0919	-	Q8Y8I3	antibiotic ABC transporter ATP-binding protein	-	**0.001**	**1.81**	0.213	0.70	0.020	0.63
lmo0938	-	Q8Y8G6	protein-tyrosine-phosphatase	-	0.374	0.90	-	0.00	**0.016**	**3.54**
lmo0940	-	Q8Y8G4	hypothetical protein lmo0940	-	**0.000**	**-4.51**	0.374	-1.28	-	0.00
lmo0943	dps,flp,fri	Q8Y8G1	non-heme iron-binding ferritin	Yes	0.617	0.22	0.840	-0.63	**0.049**	**5.51**
lmo0955	-	Q8Y8E9	hypothetical protein lmo0955	-	0.001	0.74	0.006	0.76	**0.003**	**1.01**
lmo0956	-	Q8Y8E8	N-acetylglucosamine-6P-phosphate deacetylase	Yes	0.021	0.80	0.220	-1.15	**0.004**	**2.00**
lmo0958	-	Q8Y8E6	GntR family transcirptional regulator	Yes	0.064	0.64	0.286	-2.17	**0.032**	**1.08**

Continued on next page

Supplemental Table 3.2 continued from previous page

Gene locus	Gene name	Uniprot ID	Protein name	SigB regulon	EGDe-*rpsU*^{G50C}/EGDe WT		ΔsigB-*rpsU*^{G50C}/ΔsigB		ΔrsbV-*rpsU*^{G50C}/ΔrsbV	
					p-value	$\log_2$ ratio	p-value	$\log_2$ ratio	p-value	$\log_2$ ratio
lmo0960	-	Q8Y8E4	protease	-	**0.000**	**-1.60**	0.005	-0.71	**0.004**	**-1.24**
lmo0961	-	Q8Y8E3	protease	-	**0.000**	**-1.76**	0.003	-0.52	**0.003**	**-1.66**
lmo0962	lemA	Q8Y8E2	LemA protein	-	**0.031**	**1.46**	**0.009**	**1.35**	**0.004**	**1.87**
lmo0964	spxH	Q8Y8E0	hypothetical protein lmo0964	-	0.558	1.61	**0.000**	**5.86**	0.118	3.73
lmo0974	dltA	Q8Y8D4	D-alanine–poly(phosphoribitol) ligase subunit 1	-	**0.000**	**-1.75**	0.258	0.12	**0.000**	**-3.09**
lmo0978	-	Q8Y8D0	branched-chain amino acid aminotransferase	-	0.071	-0.70	**0.015**	**-2.03**	0.937	-0.06
lmo0983	-	Q8Y8C5	glutathione peroxidase	-	0.459	0.28	**0.037**	**-1.25**	0.234	-0.63
lmo1016	gbuC	Q8Y898	glycine/betaine ABC transporter substrate-binding protein	Yes	**0.000**	**-4.69**	0.116	-3.07	0.187	-0.62
lmo1047	moaA	Q8Y870	molybdenum cofactor biosynthesis protein A	-	-	0.00	0.753	0.44	**0.000**	**2.96**
lmo1066	-	Q8Y852	myo-inositol-1(or 4)-monophosphatase	-	0.668	-1.86	**0.000**	**-6.51**	0.116	-5.18
lmo1100	cadA	P58414	Probable cadmium-transporting ATPase	-	**0.047**	**-1.11**	0.722	0.16	0.019	-0.84
lmo1113	-	Q8Y806	Lmo1113 protein	-	**0.000**	**4.50**	-	0.00	**0.000**	**4.64**
lmo1188	-	Q8Y7T3	hypothetical protein lmo1188	-	0.079	0.99	**0.007**	**1.54**	0.077	0.80
lmo1223	-	Q8Y7Q0	ABC transporter ATP-binding proteins	-	0.118	-1.98	0.327	1.27	**0.043**	**2.42**
lmo1241	-	Q8Y7N3	hypothetical protein lmo1241	Yes	**0.003**	**2.12**	-	0.00	**0.009**	**5.39**
lmo1242	-	Q8Y7N2	hypothetical protein lmo1242	-	0.179	0.97	**0.000**	**-5.05**	0.374	-0.96
lmo1261	-	Q8Y7L6	hypothetical protein lmo1261	Yes	**0.013**	**1.24**	0.374	1.36	**0.021**	**2.54**
lmo1270	-	Q8Y7K7	type I signal peptidase	-	0.477	2.75	**0.000**	**-7.04**	0.278	3.01

Continued on next page

Supplemental Table 3.2 continued from previous page

Gene locus	Gene name	Uniprot ID	Protein name	SigB regulon	EGDe-*rpsU*^{G50C}/EGDe WT		ΔsigB-*rpsU*^{G50C}/ΔsigB		ΔrsbV-*rpsU*^{G50C}/ΔrsbV	
					p-value	$\log_2$ ratio	p-value	$\log_2$ ratio	p-value	$\log_2$ ratio
lmo1292	-	Q8Y7I5	glycerophosphodiester phosphodiesterase	-	0.001	0.77	0.496	-0.22	**0.001**	**1.12**
lmo1293	glpD	Q8Y7I4	glycerol-3-phosphate dehydrogenase	Yes	**0.000**	**1.58**	0.019	0.78	**0.000**	**2.48**
lmo1324	-	Q8Y7F7	hypothetical protein lmo1324	-	**0.012**	**-5.32**	**0.000**	**-6.40**	0.374	-2.50
lmo1354	-	Q8Y7C9	aminopeptidase P	-	0.048	-0.59	**0.004**	**-1.21**	0.018	-0.52
lmo1364	cspLA, cspA, cspL	P0A355	cold-shock protein	-	0.090	0.61	0.352	0.33	**0.011**	**1.91**
lmo1375	-	Q8Y7B1	aminotripeptidase	Yes	**0.012**	**2.02**	0.992	0.02	**0.014**	**5.64**
lmo1378	lisK	Q7AP74	two-component sensor histidine kinase	-	**0.005**	**1.40**	**0.011**	**1.25**	0.013	0.89
lmo1379	yidC1	Q8Y7A9	sporulation protein SpoJ	-	0.012	0.50	**0.000**	**1.19**	0.023	0.88
lmo1406	pflB	Q8Y786	pyruvate formate-lyase	-	**0.003**	**-1.38**	0.012	-0.72	**0.000**	**-1.32**
lmo1419	-	Q8Y777	hypothetical protein lmo1419	-	**0.000**	**-4.38**	0.374	-1.38	0.374	1.32
lmo1421	-	Q7AP69	glycine/betaine ABC transporter ATP-binding protein	Yes	**0.000**	**2.19**	0.726	0.14	**0.006**	**4.01**
lmo1422	-	Q8Y775	glycine/betaine ABC transporter permease	Yes	**0.000**	**2.35**	0.248	0.25	**0.000**	**3.69**
lmo1426	opuCC	Q7AP67	glycine/betaine ABC transporter substrate-binding protein	Yes	**0.000**	**2.27**	0.374	-0.37	**0.000**	**4.61**
lmo1428	opuCA	Q7AP65	glycine/betaine ABC transporter ATP-binding protein	Yes	**0.003**	**2.47**	0.326	-1.75	**0.000**	**4.63**
lmo1432	-	Q8Y769	hypothetical protein lmo1432	Yes	**0.000**	**1.47**	0.024	0.88	**0.006**	**1.47**
lmo1433	-	Q8Y768	glutathione reductase	Yes	**0.002**	**3.21**	-	0.00	**0.023**	**3.41**
lmo1452	-	P53434	hypothetical protein lmo1452	-	0.035	0.63	0.000	0.42	**0.001**	**1.24**
lmo1469	rpsU	P0DJP1	30S ribosomal protein S21	-	**0.002**	**-3.42**	**0.032**	**-3.38**	**0.023**	**-1.92**

Continued on next page

Supplemental Table 3.2 continued from previous page

Gene locus	Gene name	Uniprot ID	Protein name	SigB regulon	EGDe-*rpsU*^{G50C}/EGDe WT		ΔsigB-*rpsU*^{G50C}/ΔsigB		ΔrsbV-*rpsU*^{G50C}/ΔrsbV	
					p-value	$\log_2$ ratio	p-value	$\log_2$ ratio	p-value	$\log_2$ ratio
lmo1470	-	Q7AP62	16S ribosomal RNA methyltransferase RsmE	-	0.961	-0.14	**0.000**	**-5.06**	0.374	-1.71
lmo1474	grpE	P0DJM3	heat shock protein GrpE	-	**0.007**	**-1.54**	0.075	-1.03	0.513	-0.45
lmo1477	-	Q8Y744	oxidoreductase	-	**0.000**	**2.57**	0.374	-0.70	0.374	-0.88
lmo1480	rpsT	P66503	30S ribosomal protein S20	-	**0.019**	**-1.50**	0.290	-0.36	**0.036**	**-1.25**
lmo1508	-	Q8Y718	histidine kinase	-	**0.000**	**3.87**	0.848	0.37	-	0.00
lmo1526	-	Q8Y704	hypothetical protein lmo1526	Yes	**0.008**	**6.14**	0.925	-0.27	**0.045**	**5.80**
lmo1538	glpK	Q8Y6Z2	glycerol kinase	Yes	**0.001**	**1.44**	0.001	0.65	**0.004**	**2.48**
lmo1539	-	Q8Y6Z1	glycerol transporter	Yes	0.521	1.94	0.231	0.89	**0.041**	**4.52**
lmo1540	rpmA	P66125	50S ribosomal protein L27	-	**0.011**	**-1.30**	0.112	-0.55	0.078	-0.67
lmo1545	minC	Q8Y6Y6	septum formation inhibitor MinC	-	0.342	-2.09	**0.000**	**-5.96**	0.491	1.66
lmo1580	-	Q8Y6V1	hypothetical protein lmo1580	Yes	0.077	0.79	0.095	-1.33	**0.007**	**1.80**
lmo1584	-	Q8Y6U7	hypothetical protein lmo1584	-	**0.000**	**5.11**	-	0.00	-	0.00
lmo1601	-	Q7AP59	general stress protein	Yes	**0.000**	**1.89**	0.187	0.35	**0.000**	**2.10**
lmo1602	-	Q8Y6T1	hypothetical protein lmo1602	Yes	**0.001**	**2.03**	**0.021**	**1.15**	**0.000**	**2.35**
lmo1603	-	Q8Y6T0	aminopeptidase	-	**0.000**	**-1.80**	**0.001**	**-2.01**	**0.005**	**-1.61**
lmo1606	-	Q8Y6S7	DNA translocase	Yes	**0.006**	**1.21**	0.008	0.83	**0.002**	**1.43**
lmo1621	-	Q8Y6R3	hypothetical protein lmo1621	-	0.186	-0.77	**0.040**	**-1.04**	0.801	-0.17
lmo1630	trpC	Q8Y6Q4	indole-3-glycerol phosphate synthase	-	**0.000**	**5.10**	0.274	1.86	0.590	-1.36
lmo1638	-	Q8Y6P6	hypothetical protein lmo1638	-	**0.000**	**-3.33**	0.971	0.01	0.735	0.44
lmo1651	-	Q8Y6N3	ABC transporter ATP-binding protein	-	**0.000**	**1.85**	**0.000**	**1.78**	**0.001**	**1.16**
lmo1652	-	Q8Y6N2	ABC transporter ATP-binding protein	-	**0.001**	**1.56**	**0.000**	**1.98**	**0.012**	**1.31**
lmo1666	-	Q8Y6L8	peptidoglycan-linked protein	-	**0.000**	**1.93**	0.041	0.28	**0.000**	**2.62**

Continued on next page

Supplemental Table 3.2 continued from previous page

Gene locus	Gene name	Uniprot ID	Protein name	SigB regulon	EGDe-*rpsU*^{G50C}/EGDe WT		ΔsigB-*rpsU*^{G50C}/ΔsigB		ΔrsbV-*rpsU*^{G50C}/ΔrsbV	
					p-value	$\log_2$ ratio	p-value	$\log_2$ ratio	p-value	$\log_2$ ratio
lmo1694	-	Q8Y6J0	CDP-abequose synthase	Yes	**0.002**	**3.96**	0.374	1.24	**0.014**	**8.35**
lmo1699	-	Q8Y6I5	chemotaxis protein	-	**0.000**	**-5.95**	0.054	-4.65	-	0.00
lmo1712	-	Q8Y6H4	multidrug resistance protein	-	**0.040**	**3.20**	0.116	-2.60	0.951	-0.12
lmo1713	mreB	Q8Y6H3	rod shape-determining protein MreB	-	**0.000**	**1.66**	0.111	0.52	**0.004**	**2.07**
lmo1751	-	Q8Y6D6	hypothetical protein lmo1751	-	0.005	0.90	**0.003**	**1.29**	0.218	0.48
lmo1764	purD	Q8Y6C6	phosphoribosylamine–glycine ligase	-	**0.000**	**1.06**	0.003	0.85	**0.000**	**1.19**
lmo1765	purH	Q8Y6C5	bifunctional phosphoribosylaminoimidazolecarboxamide formyltransferase/IMP cyclohydrolase	-	0.001	0.96	0.028	0.41	**0.003**	**1.52**
lmo1771	purS	Q92AN7	phosphoribosylformylglycinamidine synthase subunit PurS	-	**0.033**	**3.05**	0.992	-0.02	0.116	2.57
lmo1772	purC	Q8Y6B9	phosphoribosylaminoimidazole-succinocarboxamide synthase	-	0.221	2.70	**0.000**	**5.28**	0.200	2.64
lmo1774	purK	Q8Y6B7	phosphoribosylaminoimidazole carboxylase ATPase subunit	-	**0.001**	**1.25**	**0.000**	**1.41**	0.020	0.64
lmo1784	rpmI	P0A491	50S ribosomal protein L35	-	**0.006**	**-1.45**	0.250	-1.07	0.111	-1.20
lmo1785	infC	P0A3L1	translation initiation factor IF-3	-	0.046	-0.32	0.026	-0.72	**0.008**	**1.10**
lmo1792	trmD	Q8Y6A3	tRNA (guanine-N(1)-)-methyltransferase	-	**0.000**	**5.16**	0.914	-0.27	0.988	-0.04
lmo1796	-	P67234	hypothetical protein lmo1796	-	0.117	-4.61	**0.005**	**-6.14**	0.518	-1.81
lmo1810	fapR	Q8Y687	fatty acid biosynthesis transcriptional regulator	-	0.652	0.26	0.936	-0.25	**0.000**	**7.34**
lmo1830	-	Q8Y669	short-chain dehydrogenase	Yes	**0.003**	**4.58**	-	0.00	**0.002**	**6.90**

Continued on next page

Supplemental Table 3.2 continued from previous page

Gene locus	Gene name	Uniprot ID	Protein name	SigB regulon	EGDe-*rpsU*^{G50C}/EGDe WT		ΔsigB-*rpsU*^{G50C}/ΔsigB		ΔrsbV-*rpsU*^{G50C}/ΔrsbV	
					p-value	$\log_2$ ratio	p-value	$\log_2$ ratio	p-value	$\log_2$ ratio
lmo1849	mntB	Q8Y651	metal ABC transporter ATP-binding protein	-	**0.036**	**-1.66**	0.112	-0.24	**0.000**	**-8.05**
lmo1858	-	Q8Y642	dehydrogenase	-	**0.000**	**1.75**	0.019	0.98	0.003	0.75
lmo1894	nth	Q8Y608	endonuclease III (DNA repair)	-	**0.000**	**-4.03**	-	0.00	-	0.00
lmo1913	-	Q8Y5Z0	hypothetical protein lmo1913	-	0.450	-1.39	0.510	1.60	**0.032**	**3.63**
lmo1955	xerD	Q8Y5V0	integrase/recombinase	-	**0.002**	**-1.05**	0.922	0.03	0.059	-4.35
lmo1981	-	Q8Y5S4	hypothetical protein lmo1981	-	0.117	3.04	-	0.00	**0.000**	**5.19**
lmo1982	-	Q8Y5S3	hypothetical protein lmo1982	-	0.147	1.85	0.066	2.29	**0.030**	**3.03**
lmo1986	ilvC	Q8Y5S0	ketol-acid reductoisomerase	-	**0.013**	**1.17**	0.180	-2.04	**0.035**	**2.89**
lmo1987	leuA	Q8Y5R9	2-isopropylmalate synthase	-	**0.000**	**3.97**	0.682	0.69	-	0.00
lmo1991	ilvA	Q8Y5R5	threonine dehydratase	-	0.077	2.14	**0.000**	**3.58**	0.429	1.38
lmo1996	-	Q8Y5R0	DeoR family transcriptional regulator	-	**0.000**	**5.33**	0.117	3.48	0.368	1.75
lmo2006	alsS	Q8Y5Q0	acetolactate synthase	-	**0.001**	**-1.07**	0.026	-0.32	**0.000**	**-2.21**
lmo2029	-	Q8Y5M8	hypothetical protein lmo2029	-	**0.041**	**3.98**	**0.047**	**4.31**	0.481	-1.37
lmo2059	-	Q8Y5K1	potassium channel protein	-	0.610	-0.68	**0.000**	**2.95**	0.374	-0.90
lmo2080	-	Q8Y5I2	hypothetical protein lmo2080	-	0.844	0.35	0.456	1.56	**0.000**	**3.88**
lmo2108	-	Q8Y5F6	N-acetylglucosamine-6-phosphate deacetylase	-	**0.000**	**3.66**	0.925	0.18	0.925	0.19
lmo2130	-	Q8Y5D5	hypothetical protein lmo2130	Yes	0.720	-0.10	**0.000**	**-6.17**	0.374	1.50
lmo2142	-	Q8Y5C3	hypothetical protein lmo2142	-	**0.000**	**-4.95**	-	0.00	0.374	-2.04
lmo2157	sepA	Q8Y5B0	hypothetical protein lmo2157	Yes	**0.000**	**2.98**	0.367	-1.25	**0.000**	**5.63**
lmo2158	-	Q929L4	hypothetical protein lmo2158	Yes	**0.013**	**2.83**	**0.028**	**-2.70**	**0.000**	**4.92**

Continued on next page

Supplemental Table 3.2 continued from previous page

Gene locus	Gene name	Uniprot ID	Protein name	SigB regulon	EGDe-*rpsU*^{G50C}/EGDe WT		ΔsigB-*rpsU*^{G50C}/ΔsigB		ΔrsbV-*rpsU*^{G50C}/ΔrsbV	
					p-value	$\log_2$ ratio	p-value	$\log_2$ ratio	p-value	$\log_2$ ratio
lmo2174	-	Q8Y595	hypothetical protein lmo2174	-	0.383	1.90	-	0.00	**0.035**	**3.92**
lmo2182	-	Q8Y587	ferrichrome ABC transporter ATP-binding protein	-	0.001	0.70	0.013	0.60	**0.013**	**1.02**
lmo2205	gpmA	Q8Y571	phosphoglyceromutase	Yes	**0.006**	**1.75**	0.412	-1.71	**0.000**	**2.96**
lmo2207	-	Q8Y569	hypothetical protein lmo2207	-	**0.000**	**-5.00**	0.191	2.38	0.856	-0.46
lmo2213	-	Q8Y563	hypothetical protein lmo2213	Yes	0.097	5.63	-	0.00	**0.027**	**6.40**
lmo2230	-	Q8Y546	arsenate reductase	Yes	**0.000**	**6.15**	-	0.00	-	0.00
lmo2231	-	Q8Y545	hypothetical protein lmo2231	Yes	-	0.00	-	0.00	**0.000**	**3.74**
lmo2250	arpJ	Q8Y527	amino acid ABC transporter permease	-	**0.001**	**-1.22**	0.009	-0.68	**0.002**	**-2.09**
lmo2251	-	Q8Y526	amino acid ABC transporter ATP-binding protein	-	0.082	-3.26	**0.021**	**-1.04**	0.090	-4.35
lmo2268	addB	Q8Y510	ATP-dependent deoxyribonuclease subunit B	-	0.010	0.88	**0.003**	**1.06**	0.034	0.95
lmo2360	-	Q8Y4S2	transmembrane protein	-	**0.008**	**-1.16**	0.375	0.22	**0.001**	**-2.08**
lmo2391	-	Q8Y4P4	hypothetical protein lmo2391	Yes	**0.003**	**2.88**	0.374	-0.87	**0.010**	**7.31**
lmo2399	-	Q8Y4N6	hypothetical protein lmo2399	Yes	**0.000**	**1.38**	-	0.00	0.066	3.23
lmo2430	-	Q928K8	ferrichrome ABC transporter permease	-	**0.048**	**4.61**	0.095	4.21	0.462	-1.72
lmo2434	-	Q8Y4K4	glutamate decarboxylase	Yes	**0.032**	**1.38**	0.119	-4.35	0.089	5.23
lmo2436	-	Q8Y4K2	transcription antiterminator	-	**0.012**	**1.14**	0.129	-3.08	0.231	2.24
lmo2437	-	Q8Y4K1	hypothetical protein lmo2437	-	**0.042**	**3.24**	0.700	-0.54	-	0.00
lmo2463	-	Q8Y4H8	multidrug transporter	Yes	**0.000**	**1.91**	-	0.00	**0.000**	**3.36**

Continued on next page

Supplemental Table 3.2 continued from previous page

Gene locus	Gene name	Uniprot ID	Protein name	SigB regulon	EGDe-*rpsU*^{G50C}/EGDe WT		ΔsigB-*rpsU*^{G50C}/ΔsigB		ΔrsbV-*rpsU*^{G50C}/ΔrsbV	
					p-value	$\log_2$ ratio	p-value	$\log_2$ ratio	p-value	$\log_2$ ratio
lmo2471	namA	Q8Y4H1	NADPH dehydrogenase	-	0.029	0.92	0.012	0.56	**0.001**	**1.07**
lmo2494	-	Q8Y4F0	PhoU family transcriptional regulator	Yes	**0.010**	**4.95**	0.983	0.04	0.131	2.94
lmo2495	pstB1	P63363	phosphate ABC transporter ATP-binding protein	-	**0.000**	**3.92**	0.982	-0.04	0.374	-1.39
lmo2499	pstS	Q8Y4E7	phosphate ABC transporter substrate-binding protein	-	**0.002**	**3.55**	**0.002**	**2.61**	**0.001**	**2.71**
lmo2501	phoP	Q8Y4E5	two-component response phosphate regulator	-	**0.000**	**4.51**	0.854	-0.32	-	0.00
lmo2511	hpf	Q927Y2	hypothetical protein lmo2511	Yes	0.002	0.82	0.189	-0.48	**0.003**	**1.78**
lmo2516	-	Q8Y4D4	hypothetical protein lmo2516	-	**0.000**	**-4.22**	-	0.00	0.117	-2.65
lmo2569	-	Q8Y486	peptide ABC transporter substrate-binding protein	Yes	**0.000**	**-2.48**	**0.000**	**-1.68**	**0.000**	**-2.90**
lmo2571	-	Q8Y484	nicotinamidase	Yes	0.073	2.64	-	0.00	**0.000**	**5.43**
lmo2572	-	Q8Y483	dihydrofolate reductase subunit A	Yes	**0.010**	**2.18**	0.374	-1.82	**0.000**	**7.74**
lmo2573	-	Q8Y482	zinc-binding dehydrogenase	Yes	**0.037**	**4.01**	0.414	-1.59	**0.016**	**6.44**
lmo2574	-	Q8Y481	hypothetical protein lmo2574	-	0.178	2.18	0.690	-0.85	**0.001**	**4.23**
lmo2607	rpsK	P66352	30S ribosomal protein S11	-	**0.035**	**-1.27**	0.253	-0.21	0.483	-0.33
lmo2621	rplX	Q8Y443	50S ribosomal protein L24	-	**0.020**	**-1.25**	**0.006**	**-1.20**	**0.007**	**-1.14**
lmo2690	-	Q8Y3Y9	TetR family transcriptional regulator	-	**0.000**	**-5.09**	0.319	1.80	0.474	-1.72
lmo2696	-	Q8Y3Y3	dihydroxyacetone kinase	Yes	**0.027**	**5.64**	-	0.00	**0.026**	**6.13**
lmo2697	-	Q8Y3Y2	PTS mannose transporter subunit IIA	Yes	0.118	3.21	-	0.00	**0.000**	**6.29**
lmo2715	cydD	Q8Y3W4	ABC transporter ATP-binding protein	-	**0.001**	**-1.40**	0.312	-0.27	0.004	-0.79
lmo2716	cydC	Q8Y3W3	ABC transporter	-	**0.000**	**-1.32**	0.004	-0.52	**0.015**	**-1.24**

Continued on next page

Supplemental Table 3.2 continued from previous page

Gene locus	Gene name	Uniprot ID	Protein name	SigB regulon	EGDe-*rpsU*^{G50C}/EGDe WT		ΔsigB-*rpsU*^{G50C}/ΔsigB		ΔrsbV-*rpsU*^{G50C}/ΔrsbV	
					p-value	$\log_2$ ratio	p-value	$\log_2$ ratio	p-value	$\log_2$ ratio
lmo2720	-	Q8Y3W1	acetate-CoA ligase	-	0.001	0.85	0.008	0.60	**0.002**	**1.02**
lmo2727	-	Q8Y3V4	hypothetical protein lmo2727	-	**0.001**	**1.24**	0.429	2.26	0.009	0.93
lmo2734	-	Q8Y3U7	sugar hydrolase	Yes	0.404	1.83	0.999	0.00	**0.049**	**3.94**
lmo2736	-	Q8Y3U5	hypothetical protein lmo2736	Yes	**0.000**	**6.58**	-	0.00	0.374	2.43
lmo2739	cobB	Q8Y3U2	NAD-dependent deacetylase	-	0.437	1.45	0.374	-1.45	**0.000**	**3.65**
lmo2743	tal1	Q8Y3T8	translaldolase	-	**0.000**	**-4.34**	0.908	-0.29	0.429	1.44
lmo2748	-	Q8Y3T3	hypothetical protein lmo2748	Yes	**0.003**	**7.10**	-	0.00	**0.000**	**8.08**
lmo2773	-	Q8Y3R0	transcriptional antiterminator	-	0.766	-0.55	**0.000**	**-3.52**	0.374	1.02
lmo2779	ychF	Q926X1	GTP-binding protein EngD	-	**0.002**	**-1.06**	0.017	-0.63	0.003	-0.98
lmo2792	-	Q8Y3P3	hypothetical protein lmo2792	-	**0.001**	**1.20**	**0.007**	**1.23**	0.009	0.78
lmo2825	serC	Q8Y3L0	phosphoserine aminotransferase	-	0.136	3.08	**0.003**	**1.01**	**0.038**	**1.07**
lmo2829	-	Q8Y3K6	nitroreductase	-	**0.031**	**-1.16**	**0.012**	**-2.57**	0.811	-0.13
lmo2844	-	Q8Y3J1	hypothetical protein lmo2844	-	0.075	3.28	**0.000**	**3.59**	0.132	2.39
lmo2853	-	Q8Y3I3	hypothetical protein lmo2853	-	0.038	-0.72	**0.020**	**-1.15**	0.005	-0.50

Supplemental Table 3.3: Proteins that were significantly upregulated in all three $rpsU^{G50C}$ mutants including EGDe-$rpsU^{G50C}$, Δ*sigB*-$rpsU^{G50C}$ and Δ*rsbV*-$rpsU^{G50C}$ mutants

Locus	Gene name	Protein name
lmo0319	-	phospho-beta-glucosidase
lmo0762	*hflXr*	ATP/GTP-binding protein
lmo0962	*lemA*	LemA protein
lmo1602	-	hypothetical protein lmo1602
lmo1651	-	ABC transporter ATP-binding protein
lmo1652	-	ABC transporter ATP-binding protein
lmo2499	*pstS*	phosphate ABC transporter substrate-binding protein

Supplemental Table 3.4: Proteins that were significantly downregulated in all three $rpsU^{G50C}$ mutants including EGDe-$rpsU^{G50C}$, Δ*sigB*-$rpsU^{G50C}$ and Δ*rsbV*-$rpsU^{G50C}$ mutants

Locus	Gene name	Protein name
lmo0096	-	PTS mannose transporter subunit IIAB
lmo0098	-	PTS mannose transporter subunit IID
lmo1469	*rpsU*	30S ribosomal protein S21
lmo1603	-	aminopeptidase
lmo2569	-	peptide ABC transporter substrate-binding protein
lmo2621	*rplX*	50S ribosomal protein L24

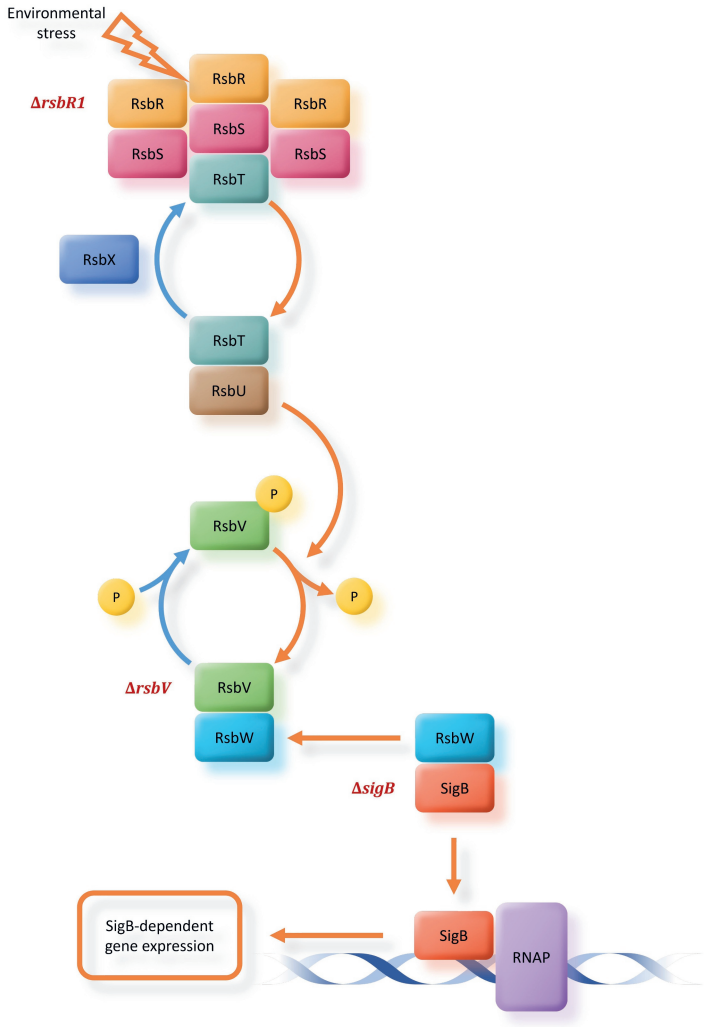

Supplemental Figure 3.1: **Scheme of SigB activation in *L. monocytogenes* wild type and the positions of RsbR1, RsbV and SigB deletion mutations.** Following perception of a stress signal by the stressosome formed by RsbR1 and its paralogues and RsbS, RsbT dissociates from the stressosome and binds to RsbU. Activated RsbU phosphatase removes a phosphate (P) group from anti-anti-sigma factor RsbV. The anti-sigma factor RsbW has a higher affinity for the now dephosphorylated RsbV than for SigB and binds to RsbV resulting in release of SigB allowing it to bind to RNA polymerase and initiate transcription of SigB regulon members. The red labels $\Delta rsbR1$, $\Delta rsbV$ and $\Delta sigB$ indicate the positions of RsbR1, RsbV and SigB, which are absent in the respective single and double mutants. See text for more information.

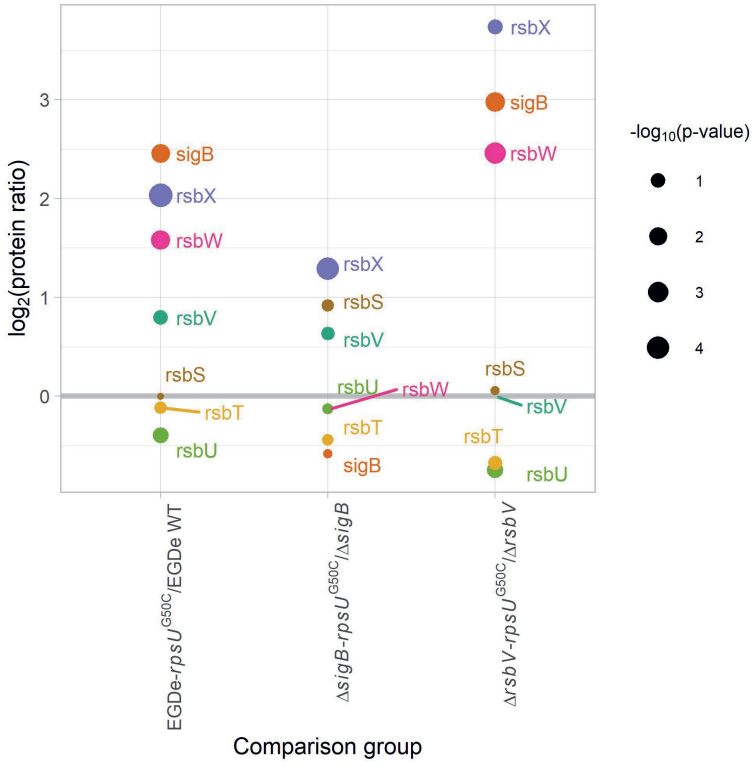

Supplemental Figure 3.2: **Proteomic data of SigB and SigB regulators by comparing EGDe-*rpsU*^{G50C}, Δ*sigB*-*rpsU*^{G50C} and Δ*rsbV*-*rpsU*^{G50C} mutants to their parent strains EGDe WT, Δ*sigB* and Δ*rsbV* mutants, respectively.** The size of the dots represents the -$\log_{10}$(p-value) of the proteomic results.

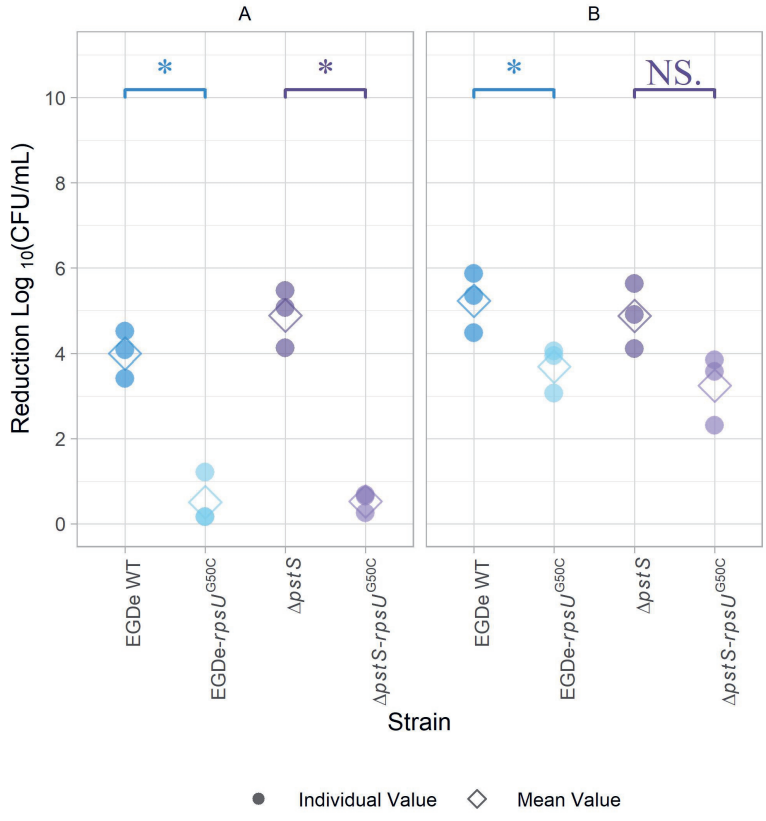

Supplemental Figure 3.3: **Stress resistance of late-exponential phase cells of *L. monocytogenes* EGDe WT, Δ*pstS* mutant and their *rpsU*^{G50C} mutants in BHI broth.** Late-exponential phase cells were exposed to pH 3.0 for 15 min at 37°C **(A)** and 5 min at 60°C **(B)**. Results are expressed as reduction in $\log_{10}$(CFU/mL) after exposure compared to $\log_{10}$(CFU/mL) before exposure. Significant differences are indicated by an asterisk, and no significant differences are indicated by NS.

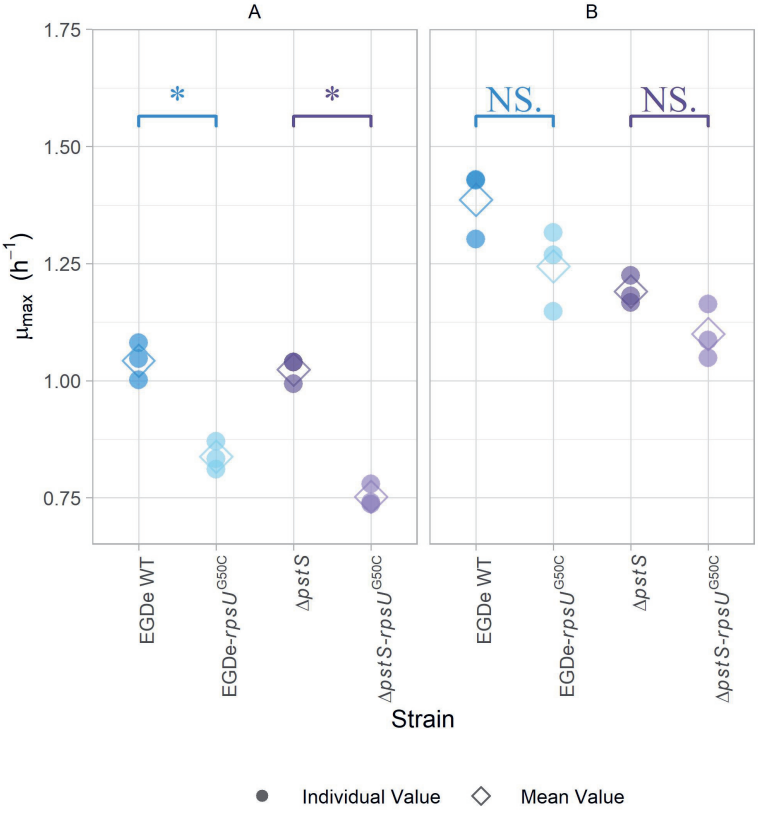

Supplemental Figure 3.4: **Maximum specific growth rate of *L. monocytogenes* EGDe WT, Δ*pstS* mutant and their *rpsU*^{G50C} mutants in BHI broth at 30°C (A) and 37°C (B), determined by the two-fold dilution method.** Significant differences are indicated by an asterisk, and no significant differences are indicated by NS.

4

Stress resistant *rpsU* variants of *Listeria monocytogenes* can become underrepresented due to enrichment bias

Xuchuan Ma, Jingjie Chen, Marcel H. Zwietering, Tjakko Abee, Heidy M.W. den Besten

Accepted for publication in *International Journal of Food Microbiology*

Abstract

Population heterogeneity is an important component of the survival strategy of *Listeria monocytogenes*, leading to cells in a population with diverse stress resistance levels. We previously demonstrated that ribosomal gene *rpsU* mutations enhanced the stress resistance of *L. monocytogenes* and lowered the growth rate at 30°C and lower temperatures. This study investigated whether these switches in phenotypes could result in a bias in strain detection when standard enrichment-based procedures are applied to a variety of strains. Detailed growth kinetics analysis of *L. monocytogenes* strains were performed, including the LO28 wild type (WT) and *rpsU* variants V14 and V15, during two commonly used enrichment-based procedures described in the ISO 11290-1:2017 and the U.S. Food and Drug Administration Bacteriological Analytical Manual. WT had a higher growth rate than the variants during the enrichment processes. Co-culture growth kinetics predictions for WT and *rpsU* variants showed that the detection chances of the *rpsU* mutants were reduced during enrichment, which was validated through subsequent qPCR experiments. Higher heat stress resistance of *rpsU* variants did not lead to faster recovery during enrichment after heat treatment, and different pre-culturing temperatures before heat treatment did not significantly affect the growth kinetics of the WT and *rpsU* variants. Additionally, post-enrichment isolation procedures involving streaking on selective agar plates did not show preferences for isolating WT or *rpsU* variants nor affect the detection chance of *rpsU* variants. The difference in detection chance suggests that the selective enrichment procedures inadequately represent the genotypic diversity present in a sample. Hence, the enrichment bias during the *L. monocytogenes* isolation procedure may contribute to the observed underrepresentation of the *rpsU* mutation in *L. monocytogenes* isolates deposited in publicly available genome databases.

4.1 Introduction

Listeria monocytogenes is a ubiquitous foodborne pathogen that can cause one of the most serious foodborne diseases, listeriosis, with a fatality rate of 13.7% (EFSA and ECDC, 2022). This bacterium can survive in a wide range of stress conditions, such as low pH, high osmotic pressure, and low temperature (Liu et al., 2019). In addition, *L. monocytogenes* can persist in food processing plants and food-associated environments for years or even decades (Ferreira et al., 2014; Harrand et al., 2020; Vongkamjan et al., 2013). The inherent population heterogeneity is one of the factors that contribute to the robustness and persistence of *L. monocytogenes* in food processing environment (Abee et al., 2016).

Population heterogeneity means that individual cells within the population have genotypic and phenotypic diversity including different stress resistance levels. When exposed to lethal stresses, the stress resistant diversity can lead to tailing of the inactivation curve. Tailing may not only lead to a higher than expected number of surviving cells and inaccurate prediction of inactivation procedures but can also lead to the selection of resistant subpopulations. Previous studies reported the identification of stable stress-resistant variants from *L. monocytogenes* by isolating cells from the tail of inactivation curves upon acid, high hydrostatic pressure (HHP) and heat treatment (Metselaar et al., 2013; Van Boeijen et al., 2011; Van Boeijen et al., 2008).

Mutations in the ribosomal protein gene *rpsU* were predominantly present in the acid isolated variants, and mutations in this gene were also found in variants isolated after HHP and heat exposure (Metselaar, 2016). These mutations include missense mutation, frameshift mutation, and deletion of the whole *rpsU* gene. Further studies focusing on the amino acid substitution variant V15 and the *rpsU* deletion variant V14 revealed that these variants have increased multi-stress resistance, reduced motility, and reduced growth rates at temperatures below the optimum temperature and the latter was more pronounced at lower temperatures (Koomen et al., 2018; Metselaar et al., 2016). Interestingly, laboratory evolution study of V15 showed that this variant is able to mutate and revert to the wild type like phenotype (Koomen et al., 2021). The mutation happened in the same codon of the *rpsU* gene for two V15 evolved strains. Hence, mutations in ribosomal genes, especially at *rpsU*, enables switching between multiple-stress resistant and high fitness states in *L. monocytogenes* (Koomen et al., 2021). Since mutations in the *rpsU* gene can be a strategy of *L. monocytogenes* to adapt to different environmental stresses, the *rpsU* gene may be a hot spot of mutation.

Foodborne isolates are often isolated from food using enrichment-based detection procedures. The selective enrichment step of these procedures promotes the growth of the target organism and decreases the growth of background microorganisms, allowing for the isolation of *L. monocytogenes* (Allende et al., 2022). However, the selective enrichment can also lead to an isolation bias of *L. monocytogenes* lineages, serotypes, or strains when growth rate differences exist (Bruhn et al., 2005; Gorski et al., 2006; Zilelidou et al., 2016a; Zilelidou et al., 2016b). Two commonly used *L. monocytogenes* detection standards are the ISO 11290-1:2017 and the U.S. Food and Drug Administration (FDA) Bacteriological Analytical Manual (BAM). The ISO 11290-1:2017 applies a two-step enrichment with two different media, half Fraser broth (HFB) and Fraser broth (FB). The BAM standard uses buffered *Listeria* enrichment

broth (BLEB) for the enrichment. To allow the recovery of stressed cells, the ISO standard uses HFB for the first step, which contains less antibiotics than FB, and the BAM standard applies a four hour incubation before adding the antibiotics in the enrichment culture. Both standards require 48 hours of enrichment using the required media, and the cultures are streaked onto two different selective agar media for isolation after 24 h and 48 h enrichment.

In this study, genome sequences of strains deposited in the National Center for Biotechnology information (NCBI) database were analysed to assess the conservation level of the *rpsU* gene. To elucidate whether the detection chance of *rpsU* variants from food may differ from wild type (WT) strains when enrichment-based detection methods are applied, growth kinetics were determined for *L. monocytogenes* LO28 wild type strain and *rpsU* variants V14 and V15 during the enrichment according to the ISO 11290-1:2017 and BAM methods. This allows to assess whether enrichment-based detection procedures contribute to a bias in the genetic diversity of deposited *L. monocytogenes* isolates.

4.2 Materials and methods

4.2.1 Gene variation level analysis and *rpsU* mutants' isolation origins analysis

A pipeline tool was built (github.com/xchuam/blast_at_local_computer) to construct a genome database at a local computer and run the Basic Local Alignment Search Tool (BLAST). This local analysis was needed because the NCBI online BLAST tool can only display the top 5,000 aligned sequences. By using this pipeline, 51,784 genome assemblies (303 complete genomes, 71 chromosomes, 1,507 scaffolds and 49,903 contigs) were downloaded from the NCBI ftp site. The consistency of the downloaded genomes was checked by the MD5 checksum tool (GNU coreutils, 8.32). Then, BLAST+ (NCBI, 2.13.0) was used to construct the genome database and run BLAST with all the coding sequences from *L. monocytogenes* EGD-e reference genome sequence (NC_003210.1) as queries. The BLAST hit results that were located at the start or the end of the subject sequence were filtered out. The variation level of each gene was estimated by the following equation:

$$Variation = \frac{N_{type}}{N_{total} \cdot Length} \tag{4.1}$$

where N_{type} is the number of DNA sequence types of the gene found by BLAST; N_{total} is the total number of DNA sequences of the gene that were found by BLAST; $Length$ is the maximum length of the gene DNA sequence. Next to the DNA sequence, also the sample attribute information for each genome assembly was downloaded from NCBI, and the sample isolation origin (animal, clinical, food associated environment, other environment, food, feed and unknown) was manually annotated for each genome assembly according to the sample attribute information.

4.2.2 Bacterial strains and mono-culture enrichment conditions

L. monocytogenes strain LO28 WT, *rpsU* deletion variant V14 and *rpsU* point mutation variant V15 were used in this study (Metselaar et al., 2013). Enrichment procedures were followed using the ISO 11290-1:2017 standard and the U.S. Food and Drug Administration (FDA) Bacteriological Analytical Manual (BAM). Cultures were made by inoculating 10 mL of Brain Heart Infusion (BHI, Oxoid, Ltd., Basingstoke, England) broth with a single colony from a BHI agar plate (1.5% (w/w), bacteriological agar no. 1 Oxoid) obtained from -80°C freezer stocks. Cultures were grown at 30°C under shaking at 160 rpm for 17 to 30 h to obtain a working culture. Afterwards, two parallel time-shifted overnight (ON) cultures were made by inoculating 10 μL of the working culture in 10 mL BHI broth in the morning and in the afternoon, respectively. Both parallel ON cultures were grown at 30°C under shaking at 160 rpm for 22 to 24 h and subsequently diluted 1,000,000 times in the enrichment media or exposed to heat treatment as described below (see Section 4.2.6). For the enrichment according to the ISO 11290-1:2017, 5 mL diluted culture or heat-treated culture was added to 45 mL HFB, which was made by supplementing Fraser broth base (Oxoid) with half Fraser supplement (Oxoid). The parallel time-shifted HFB cultures were incubated at 30°C for 24 h and sampled at time points 0, 2, 4, 6, 8, 10, 14, 18, 22, and 24 h. After 24 h enrichment, 0.1 mL of HFB enrichment was transfered into 10 mL FB, which was made by supplementing Fraser broth base with Fraser supplement (Oxoid). The FB cultures were incubated at 37°C for 24 h and sampled at time points 0, 2, 4, 6, 8, 10, 14, 18, 22, and 24 h. For the enrichment according to the BAM standard, a 5 mL diluted culture or heat-treated culture was added to 45 mL BLEB (Oxoid) and cultured at 30°C for 48 h. Listeria Selective Enrichment Supplement (Oxoid) was added to the enrichment culture after 4 h incubation at 30°C. The BLEB enrichment cultures were sampled at time points 0, 2, 4, 8, 12, 16, 20, 24, 28, 32, 40, and 48 h. All the samples were spread-plated on BHI agar plates after appropriately diluting and plates were incubated at 30°C for 24 h before counting. Three independent biological reproductions were carried out.

4.2.3 Growth model fitting

Growth of *L. monocytogenes* LO28 WT, V14 and V15 during mono-culture enrichment was modeled with the three-phase model (Buchanan et al., 1997):

$$y = \begin{cases} \log_{10} N_0 & t \leq \lambda \\ \log_{10} N_0 + \mu(t - \lambda) & \lambda < t < t_s \\ \log_{10} N_{max} & t \geq t_s \end{cases} \tag{4.2}$$

where y is the $\log_{10}$ concentration ($\log_{10}$CFU/mL) at time t (h); $\log_{10} N_0$ is the initial concentration ($\log_{10}$CFU/mL); $\log_{10} N_{max}$ is the concentration at stationary phase ($\log_{10}$CFU/mL); μ is the maximum growth rate ($\log_{10}$/h); λ is the lag time (h); t_s is the time to reach stationary growth phase (h). In some cases, the growth data did not show a clear stationary phase, so a three-phase model without stationary phase was used for model fitting in those cases:

$$y = \begin{cases} \log_{10} N_0 & t \leq \lambda \\ \log_{10} N_0 + \mu(t - \lambda) & t > \lambda \end{cases} \tag{4.3}$$

The model was fitted using an adapted version of the R package biogrowth (0.2.3) (Garre et al., 2023), accessed from https://github.com/xchuam/biogrowth/tree/two_phase_model.

The model was fitted to the biological replicates data together. The fitting results were evaluated to check whether λ was significantly ($\alpha = 0.05$) different from zero. If the λ was not significantly different from zero, the F-test was applied to verify if fixing the λ to zero was statistically acceptable. The f value was calculated by the following equation:

$$f = \frac{(RSS_2 - RSS_1)/(DF_2 - DF_1)}{RSS_1/DF_1} \tag{4.4}$$

where RSS_1 is the residual sum of squares of the full model (i.e., model with λ); RSS_2 is the residual sum of squares of the reduced model (i.e., model without λ); DF_1 and DF_2 are the degrees of freedom for the full and reduced models, respectively. The f value was tested against the F table value (95% confidence, $F_{DF_2}^{DF_2 - DF_1}$). If the f value was smaller than the F table value, the F-test was accepted and the λ was fixed at zero.

To decide the inclusion of the stationary phase in the three-phase model, the adequacy and the fitting performance of the models with determined λ setting was further checked according to Den Besten et al. (2006). The mean square error (MSE_{model}) was used to measure the adequacy of the model to describe the data.

$$MSE_{model} = \frac{RSS}{DF} = \frac{\sum_{i=1}^{n} (\log_{10} N_i^{observed} - \log_{10} N_i^{fitted})^2}{n - p} \tag{4.5}$$

RSS is the residual sum of squares; DF is the degree of freedom; n is the number of data points; p is the number of parameters of the model; $\log_{10} N_i^{observed}$ is the observed population level ($\log_{10}$CFU/mL); $\log_{10} N_i^{fitted}$ is the fitted population level ($\log_{10}$CFU/mL).

The F-test was used to decide if the fitting performance of the model was statistically accepted. The f value was calculated by the following equation:

$$f = \frac{MSE_{model}}{MSE_{data}} \tag{4.6}$$

where MSE_{model} is the mean square error of the model and MSE_{data} is the mean square error of the data for replicate values, which indicates the measuring error. MSE_{data} was calculated by the following equation:

$$MSE_{data} = \frac{RSS}{DF} = \frac{\sum_{i=1}^{m} \sum_{j=1}^{k} (\log_{10} N_i - \log_{10} N_{ij})^2}{n - m} \tag{4.7}$$

where $n = m*k$ is the number of data points; m is the number of time points (sampling times); k is the number of replicates at each time point i; $\log_{10} N_{ij}$ ($\log_{10}$CFU/mL) is the population at time point i for specific replicate j; $\log_{10} N_i$ ($\log_{10}$CFU/mL) is the mean value of the population at time point i.

For the F-test, the f value was tested against F table value (95% confidence, $F_{DF_{data}}^{DF_{model}}$). If the f value was smaller, the F-test was accepted, and the model describes the observed data well.

To compare the differences between each strain, the λ and the μ were estimated by fitting the selected model to each biological replicate, and significant differences between strains were tested and plotted in R with the `ggsignif` package (Ahlmann-Eltze and Patil, 2021).

4.2.4 Co-culture kinetics prediction

The three-phase model was used to predict the growth kinetics of WT and V14 or V15 during co-culture. In the prediction, the initial concentration $\log_{10} N_0$ was assumed the same as the concentration in the quantitative PCR (qPCR) experiment (see Section 4.2.5). The λ and μ were estimated by fitting the selected model to the biological replicates data together of the mono-cultures, and these parameter estimates were used for the prediction of the co-culture growth kinetics. The $\log_{10} N_{max}$ was assumed to be the mean value of the highest concentration from each replicate of mono-culture. Also, it was assumed that when the concentration of one strain reaches $\log_{10} N_{max}$, both strains reach the stationary phase. The lowest and highest confidence interval (95%) value of $\log_{10} N_0$, λ, μ, and $\log_{10} N_{max}$ were used to determine the confidence intervals of each of the strains.

4.2.5 Co-culture kinetics identification by qPCR

Previously reported WT-specific and V14-specific primers (Metselaar et al., 2016) were used for qPCR by targeting the DNA deletion region in V14 (Supplemental Table 4.1). The ON cultures of WT and V14 were made and plated on BHI agar plates after appropriately diluting to determine the initial concentration. Then, WT and V14 ON cultures were diluted 100,000 times in the enrichment media, and 500 μL diluted culture of each strain was added together to the same flask with 49 mL enrichment media and enriched as described previously (see Section 4.2.2). For heat treatment effect investigation, equal amount of WT and V14 ON culture were mixed and exposed to heat treatment as describe below (see Section 4.2.6). Then, a 5 mL heat-treated sample was added to 45 mL enrichment media and enriched as described previously. At time points 24, 36 and 48 h, the co-culture enrichment culture was plated on BHI agar after appropriately diluting , and 2 mL culture was sampled for DNA isolation by the DNeasy blood and tissue kit (Qiagen), using the protocol with pre-treatment for Gram-positive bacteria with lysozyme and proteinase K incubations for 1 h. DNA was stored at -20°C with maximum three times freeze-thaw cycle until qPCR analysis. The BHI agar plates were incubated at 30°C for 24 h before counting. Based on the counting results, the total concentration of WT and V14 during co-culture enrichment could be

determined and used for qPCR results verification. To make the qPCR standard curve suitable for each time point, WT and V14 were also enriched as mono-culture. At time points 24, 36 and 48 h, the mono-culture enrichment cultures of WT and V14 were plated on BHI agar plates after appropriately diluting, and 2 mL culture of each strain were mixed for DNA isolation, using the same protocol as co-culture enrichment. The DNA samples of the co-culture enrichment and standard curve were serially diluted by Milli-Q water, mixed with Power SYBRgreen mastermix (Applied Biosystems), and added to a Hard-Shell 96-well PCR plate (Bio-Rad). The qPCR was done using the qPCR machine CFX96 (Bio-Rad) at an annealing temperature of 60°C. Threshold cycle (C_T) values were determined with automatic baseline settings. The concentration of WT and V14 were calculated based on the standard curve and verified by comparing with the plate counting results of the total concentration. Three independent biological reproductions were carried out for each co-culture experiment.

4.2.6 Heat treatment conditions

Heat treatments were carried out in BHI at 60°C for 8.5 min. For mono-culture enrichment, 0.1 mL WT, V14 or V15 ON culture were added to 9.9 mL 60°C pre-heated BHI (i.e. 1% [v/v]). For co-culture enrichment, equal amount of WT and V14 ON culture were mixed, and 0.4 mL mixed ON culture were added to 19.6 mL 60°C pre-heated BHI (i.e. 1% [v/v] of both WT and V14). After 8.5 min, a 5 mL heat-treated culture was transferred to 45 mL enrichment media immediately and cultured as described previously. At least three independent biological reproductions were carried out for each strain.

4.2.7 Mono-culture enrichment after low pre-culturing temperature and heat treatment

ON cultures of WT, V14 and V15 were inoculated into fresh BHI (0.1% [v/v]) and incubated at 20°C, 10°C or 7°C. The culture was grown under shaking at 160 rpm until the stationary phase (~9 $\log_{10}$CFU/mL). The stationary phase culture was exposed to heat treatment as described previously (see Section 4.2.6). The heat-treated cultures were added to enrichment media and cultured as described in Section 4.2.2 with sampling at time points 0, 24 and 48 h. All the samples were spread plated on BHI agar plates after appropriately diluting and plates were incubated at 30°C for 24 h before counting. Three independent biological reproductions were carried out.

4.2.8 Colony difference identification for *L. monocytogenes* isolation procedure

WT, V14 and V15 were enriched as described in Section 4.2.2. After 24 h of enrichment in HFB, FB, and BLEB and 48 h enrichment in BLEB, the culture was streaked on an ALOA agar plate (BioMérieux), a Rapid' *L. mono* agar plate (Bio-Rad), a PALCAM medium agar plate (Oxoid) and on a OXA plate (Listeria Selective Agar [Oxford], Oxoid). The ALOA plates and Rapid' *L. mono* plates were cultured at 37°C, and the

PALCAM plates and OXA plates were cultured at 35 °C following the recommendations of the suppliers. All the plates were checked after 24 h and 48 h of incubation.

4.3 Results

4.3.1 *rpsU* gene is conserved in the *L. monocytogenes* genome database

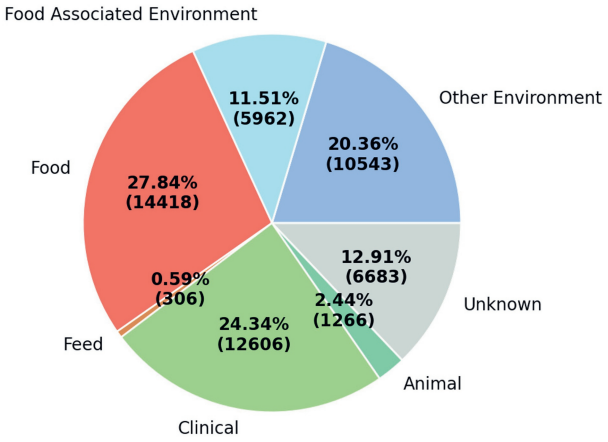

Figure 4.1: **Isolation origins of sequenced *L. monocytogenes* isolates deposited in the NCBI genome database.** The prevalence is shown in percentage with the sample number between brackets.

To analyze the genotype variation of the *L. monocytogenes* genes, a *L. monocytogenes* genome database was constructed, which includes 51,784 genome assemblies for strains isolated from seven main categories: food, feed, clinical, animal, food associated environment, other environment, and unknown (Figure 4.1). For each of the genomes, 2,867 *L. monocytogenes* genes were analyzed, and the gene variation levels are shown in Figure 4.2. Among all the analyzed genes, *rpsU* exhibited the lowest variation level, with a notable distinction from the other genes. The *rpsU* gene has been found in 51,768 genomes, but there were only 49 genomes that showed a mutation in the *rpsU* gene, which was around 0.1% of all the genomes available in the genome database. These 49 genomes with *rpsU* mutations were from clinical isolates (28), food isolates (8), other environment isolates (8), and unknown resource (5). Notably, in the rest 16 genomes without identified *rpsU* sequence, 8 genomes exhibited partial *rpsU* sequences due to their location at the contig edges, while the remaining 8 genomes raised concerns due to low data quality warnings on the NCBI website or their high contig count, exceeding 370. Collectively, these findings suggest that the *rpsU* gene exhibits a remarkable level of conservation within the *L. monocytogenes* genome database.

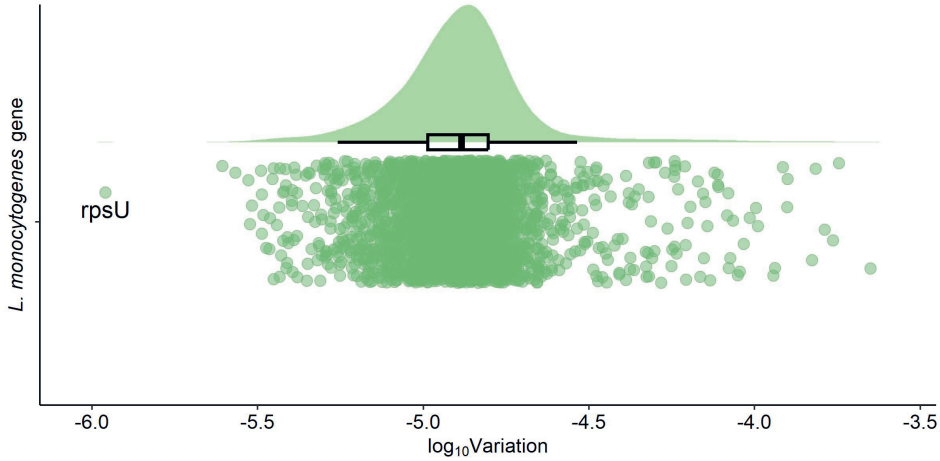

Figure 4.2: **Raincloud plot of *L. monocytogenes* gene variation levels in the genome database.** The point that represents the *rpsU* gene variation level has been labeled.

4.3.2 *rpsU* mutant detection chance reduced during enrichment

Our previous research showed that *rpsU* variants have a stress resistance advantage over the WT strain, and mutations in *rpsU* enables switching between multiple-stress resistant and high fitness states in *L. monocytogenes* (Koomen et al., 2021; Koomen et al., 2018; Metselaar et al., 2015; Metselaar et al., 2013). Therefore, it was expected that *rpsU* mutations were widely spread in *L. monocytogenes*. However, the genome analyses demonstrated that the *rpsU* gene had a high conservation level in the *L. monocytogenes* genome database. A possible explanation may be that the *L. monocytogenes* detection methods may introduce an isolation bias and a reduced detection chance of *rpsU* variants. To further investigate this, the *L. monocytogenes* LO28 WT and *rpsU* variants V14 and V15 were cultured and plated according to two commonly used *L. monocytogenes* detection methods, the ISO 11290-1:2017 standard and the FDA BAM standard.

The *L. monocytogenes* strain LO28 WT and *rpsU* variants V14 and V15 were individually cultured according to the ISO 11290-1:2017 and the BAM methods (Figure 4.3). The three-phase model was used to fit the growth data and the inclusion of lag phase λ and stationary phase $\log_{10} N_{max}$ was tested (Supplemental Table 4.2). In all the enrichment culture media, there was no significant difference in the λ between the WT and the *rpsU* variants (Figure 4.4, A). In FB, λ was not significantly different from zero for each of the strains. The WT had a significantly higher growth rate than the *rpsU* variants in HFB and BLEB (at 30°C) but not in FB (at 37°C) (Figure 4.4, B).

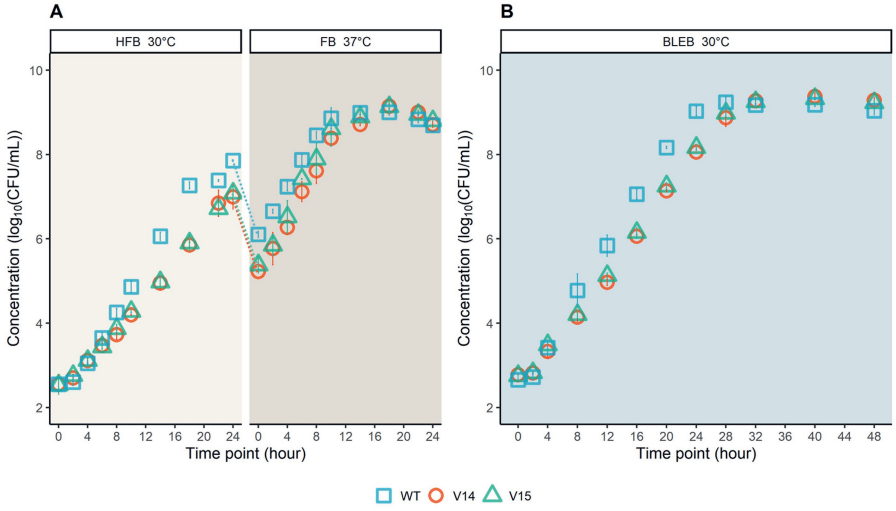

Figure 4.3: **Mono-culture growth kinetics of LO28 WT, V14 and V15 during enrichment by following the ISO standard (A) and the BAM standard (B).** The dotted lines indicate a 1:100 (v/v) inoculation from HFB to FB.

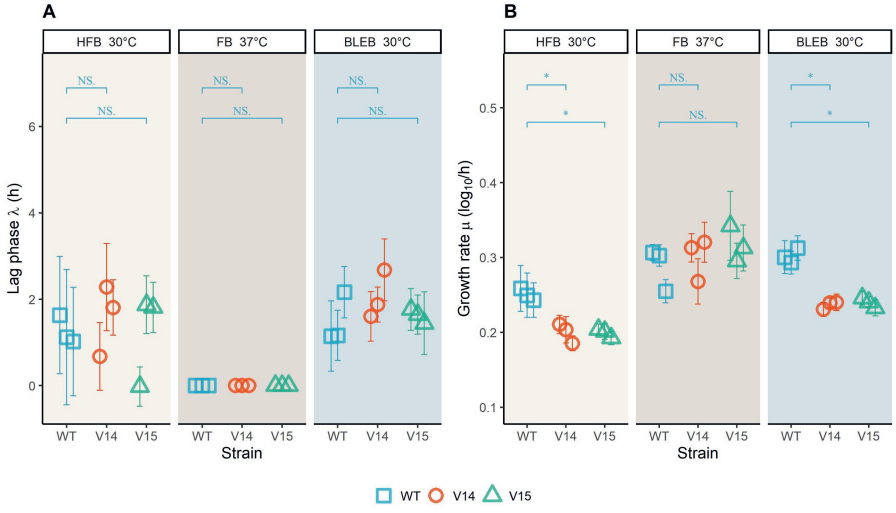

Figure 4.4: **Mono-culture growth parameter estimates of LO28 WT, V14 and V15 in enrichment broth.** Panel (A) and Panel (B) show the fitting results of lag phase (h) and growth rate (log_{10}/h), respectively. The points represent the best estimated values, and the error bars represent the 95% confidence interval. Significant differences are indicated by an asterisk, and no significant differences are indicated by NS.

4.3.2.1 *rpsU* variants detection chance reduced during co-culture enrichment

To investigate how the growth rate differences affected the detection chance of *rpsU* variants after the enrichment, the growth behavior of WT and *rpsU* variant V14 during co-culture were predicted by using the fitted parameters of mono-culture growth data (Figure 4.5). Since the enrichment culture should be sampled after incubation for 24 and 48 h according to the ISO and the BAM detection procedure, the variant detection chances at 24 and 48 h were calculated. The predicted results show that the detection chance of *rpsU* variants reduced from ~52% to ~7% in HFB after 24 h (Supplemental Figure 4.2, A). In BLEB, the detection chance reduced from ~52% to ~3% after 24 and 48 h co-culture (Supplemental Figure 4.2, A). The prediction of WT and V15 co-culture behaviour shows similar results as expected, since the growth parameters were similar between V14 and V15 (Supplemental Figure 4.1 and Supplemental Figure 4.2, A). To verify the prediction results, WT and V14 were co-cultured according to these isolation standards and measured by qPCR (Figure 4.5). Comparing the qPCR results and the prediction results, the qPCR results were mostly found in the confidence interval of the predicted results. The prediction model might however overestimate the growth of V14 in FB and BLEB, since in both media the V14 qPCR results were at the lower end of the confidence interval. Nevertheless, the qPCR results confirmed that the detection chances of V14 were reduced after co-culture enrichment.

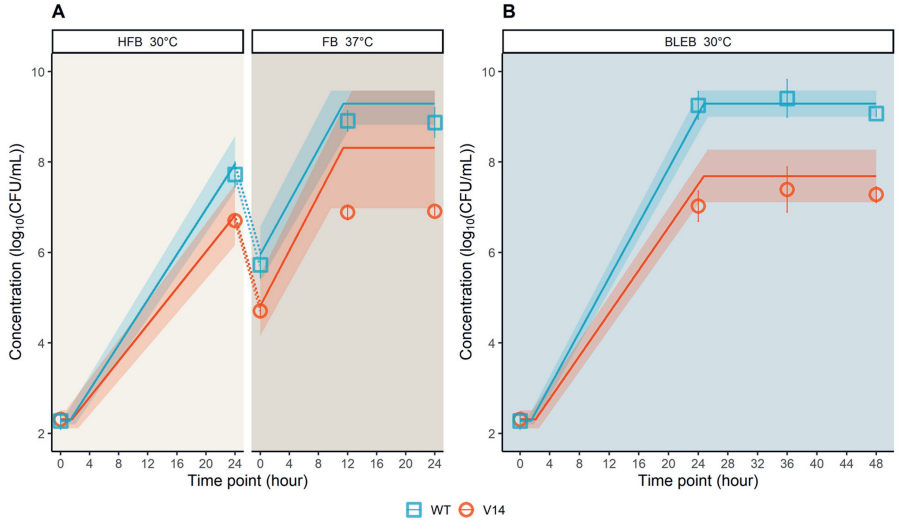

Figure 4.5: **Co-culture growth predictions and validations of LO28 WT and V14 during enrichment by following the ISO standard (A) and the BAM standard (B).** Co-culture growth predictions, which are shown as solid lines with confidence interval as shadow, according to the three-phase model were based on estimated parameters from mono-culture. Validations were done by qPCR (blue square for WT and red circle for V14) of co-culture. The error bars indicate standard deviations. The dotted lines indicate a 1:100 (v/v) inoculation from HFB to FB.

4.3.2.2 Detection chance of heat-treated *rpsU* variants also reduced during co-culture enrichment

L. monocytogenes rpsU variants have higher stress resistance than the LO28 WT (Metselaar et al., 2015). To investigate if the higher stress resistance of *rpsU* variants V14 and V15 results in a faster recovery after heat treatment during enrichment, the *L. monocytogenes* strain LO28 WT and *rpsU* variants V14 and V15 were exposed to 60°C for 8.5 min and then individually cultured according to the ISO 11290-1:2017 and the BAM methods (Supplemental Figure 4.3). The three-phase model was used to fit these growth data (Supplemental Table 4.3). After heat treatment, there were again no significant differences between the lag phase of the WT and the *rpsU* mutants in HFB, and V15 had even a significantly higher lag phase than WT in BLEB (Figure 4.6, A). The growth rate of the WT was again significantly higher compared to the *rpsU* variants in HFB and BLEB but not in FB (Figure 4.6, B). Therefore, high resistance *rpsU* mutants did not have a faster recovery but again had a growth disadvantage during enrichment after heat treatment.

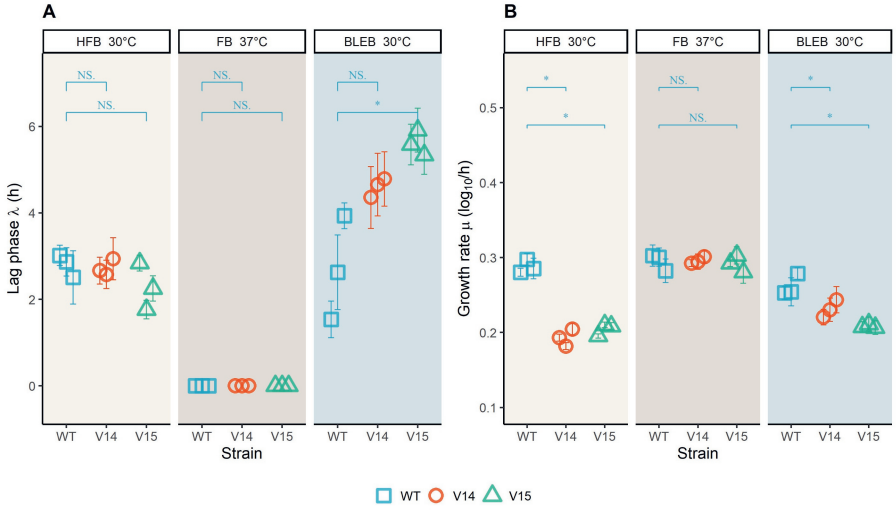

Figure 4.6: **Mono-culture growth model fitting results of heat-treated LO28 WT, V14 and V15.** Panel (A) and Panel (B) show the fitting results of lag phase (h) and growth rate ($\log_{10}$CFU/mL/h), respectively. The points represent the best estimated values, and the error bars represent the 95% confidence interval. Significant differences are indicated by an asterisk, and no significant differences are indicated by NS.

To investigate how the stress resistance difference affected the growth behavior and detection chance of WT and *rpsU* variants during co-culture, the co-culture growth behaviour of WT and V14 were predicted using the fitted parameters of the mono-culture growth data after heat treatment (Figure 4.7, B and C). For prediction, the initial concentration of WT and the *rpsU* variants was assumed to be the same before heat treatment. Since the WT had around 1 $\log_{10}$(CFU/mL) more reduction than V14 after heat treatment (Figure 4.7, A), WT was around 1 $\log_{10}$(CFU/mL)

less than V14 at t0 of the enrichment. The predicted results show that the detection chances were still reduced for V14 in both enrichment methods (Supplemental Figure 4.5, A). The prediction of WT and V15 co-culture behaviour shows similar results (Supplemental Figure 4.4 and Supplemental Figure 4.5, A). To verify the prediction results, WT and V14 ON culture were mixed, exposed to heat treatment, co-cultured according to these isolation standards and measured by qPCR (Figure 4.7, B and C). This confirmed that the detection chance of heat-stressed resistance variants was reduced after the enrichment (Figure 4.7 and Supplemental Figure 4.5, B).

It has been reported that the growth defect of *rpsU* variants was more pronounced at lower temperature (Metselaar et al., 2016). To further investigate the effect of pre-culturing temperature on the growth of *L. monocytogenes* WT and the *rpsU* variants during enrichment, LO28 WT, V14 and V15 were pre-cultured at 7°C, 10°C or 20°C, exposed to heat treatment and then enriched in HFB, FB, or BLEB. The growth kinetic of these cultures during enrichment were rather similar to 30°C pre-cultured cells (Supplemental Figure 4.6), suggesting that the detection chance reduction of the heat treated *rpsU* mutants during enrichment in HFB, FB and BLEB will not be altered by the pre-culturing temperature followed by heat treatment.

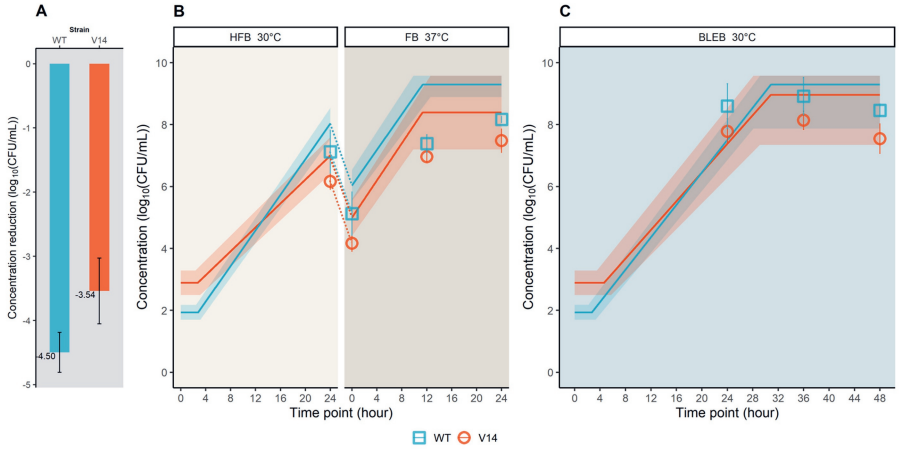

Figure 4.7: **Heat reduction of LO28 WT and V14 (A) and co-culture growth predictions and validations of heat-treated LO28 WT and V14 during enrichment by following the ISO standard (B) and the BAM standard (C).** Heat reductions were measured by exposing stationary phase culture at 60°C in BHI for 8.5 min and shown as bar plot with reduction level and standard deviation. Co-culture growth predictions, which are shown as solid lines with confidence interval as shadow, according to the three-phase model were based on estimated parameters from mono-culture after heat treatment. Validations were done by qPCR results (blue square for WT and red circle for V14) in co-culture. The error bars indicate standard deviations. The dotted lines indicate a 1:100 (v/v) inoculation from HFB to FB.

4.3.2.3 Isolation procedure does not affect the detection chance of *rpsU* variants

After 24 and/or 48 h of enrichment in HFB, FB or BLEB, the enrichment culture should be streaked on two different types of selective agar plates following the isolation procedure according to the ISO 11290-1:2017 and the BAM methods. Colony differences between WT and the *rpsU* variants on selective agar plate might lead to the selection preference of a certain strain. To investigate the colony differences between WT and the *rpsU* variants on the selective agar plates, *L. monocytogenes* LO28 WT, V14 and V15 were enriched and streaked on four different types of selective agar plates including ALOA, Rapid' *L.mono*, PALCAM, and OXA plates. As shown in the Supplemental Figure 4.7, WT and *rpsU* mutants had similar colony shape, size, and color, so it was difficult to distinguish WT and *rpsU* mutants based on the colony characterization on these selective agar plates. Therefore, the isolation procedure seems not to affect the detection chance of *rpsU* variants.

4.4 Discussion

Previous genotyping and phenotyping studies demonstrated that mutations in the *rpsU* enable switching between multi-stress resistant and high fitness phenotypes of *L. monocytogenes* (Koomen et al., 2021; Koomen et al., 2018), and this may point to a mutation hot spot. Our bioinformatics analysis showed, however, that the *rpsU* gene exhibited a high conservation level amongst *L. monocytogenes* strains that are deposited in the NCBI genome database. Here, we demonstrated that the lower fitness of the *rpsU* mutants resulted in a lower detection chance compared to the WT strain when enrichment-based detection procedures are applied to isolate *L. monocytogenes*. Consequently, this approach may underestimate the genotypic diversity of *L. monocytogenes* in a sample for enrichment. Therefore, this phenomenon could contribute to the underrepresentation of *rpsU* mutants in the *L. monocytogenes* genome database. Previous studies reported a bias in the *L. monocytogenes* enrichment procedure at the lineage and strain levels (Bannenberg et al., 2021; Bruhn et al., 2005; Zilelidou et al., 2016a; Zilelidou et al., 2016b), and the current study underlines that such a bias can be extended to the sub-strain level. In line with this, *rpsU* mutations were not identified in studies employing whole-genome sequencing to investigate persistent *L. monocytogenes* strains isolated using enrichment-based methods, including the ISO 11290-1:2017 and the BAM methods (Castro et al., 2021; Cherifi et al., 2018; Lucchini et al., 2023; Palma et al., 2020; Simmons et al., 2014; Stasiewicz et al., 2015). Although stress resistance variants, such as *rpsU* variants, may significantly contribute to the overall stress resistance of the *L. monocytogenes* population, the fraction of these stress resistance variants is generally low in non-stressed populations (Metselaar, 2016). The detection bias induced during enrichment, resulting in infrequent isolation, and their rareness in non-stressed population may have contributed to the observed low prevalence of *rpsU* variants in the genome and phenotype databases.

The WT strain had a higher growth rate than V14 and V15 during the enrichment in HFB and BLEB but not in FB. Notably, the culture temperature is 30°C in HFB and

BLEB but 37°C in FB. Previous research based on nutrient-rich medium BHI showed that the growth rate of *rpsU* variants, relative to the WT, is more significantly reduced at lower temperatures (Supplemental Figure 4.8) (Metselaar et al., 2016). Therefore, the differences in growth rates between the WT and the *rpsU* variants in HFB and BLEB may be attributed to the culture temperature of 30°C rather than the culture media.

In FB with 37°C as culture temperature, the WT strain did not exhibit a significantly higher growth rate than the V14 strain during mono-culture. However, the detection chance of V14 reduced during co-culture enrichment in FB (see Supplemental Figure 4.2, B), suggesting that factors beyond mere differences in mono-culture growth rates contribute to the competitive advantage of the WT over *rpsU* variants in co-culture conditions. Indeed, previous studies have reported that the outgrowth of a strain in co-culture cannot only be explained by growth rate differences during mono-culture (Gorski et al., 2006; Mellefont et al., 2008; Zilelidou et al., 2016b; Zilelidou et al., 2015). This evidence underscores the complexity of competitive dynamics between WT and the *rpsU* variants in co-culture environments.

Also in other *Bacillales* bacteria, *rpsU* mutations have been reported to impact phenotype significantly. In *Bacillus subtilis*, a nonsense mutation in the second codon of *rpsU* led to impaired cell separation, defective motility, and robust biofilm formation (Takada et al., 2014). Furthermore, a study on clinical strains of *Staphylococcus aureus* identified *rpsU* mutants after five days of vancomycin treatment, exhibiting increased resistance to vancomycin and lysostaphin, thicker cell walls, and a reduced growth rate (Basco et al., 2019). These findings highlight the phenotypic alterations associated with *rpsU* mutations across various bacterial species beyond *L. monocytogenes*, underscoring the critical role of *rpsU* mutations in bacterial physiology and adaptation. Notably, the level of *rpsU* variation in the genome databases of *B. subtilis* and *S. aureus* is markedly higher than in *L. monocytogenes*, with $\log_{10} Variation$ values of -4.1, -4.2, and -6.0, respectively, which suggests a higher *rpsU* mutation detection chance for *B. subtilis* and *S. aureus*. The potential link between the higher detection rates of *rpsU* mutations in these two species and the growth behavior of wild type strains and *rpsU* mutants during enrichment requires further investigation.

In conclusion, selective enrichment procedures at 30°C may inadequately represent the genotypic diversity present in a sample. Hence, this enrichment bias contributes to the underrepresentation of natural mutants in the *L. monocytogenes* genome database.

4.5 Declaration of Competing Interest

The authors declare that they have no known competing financial interests or personal relationships that could have appeared to influence the work reported in this paper.

4.6 Acknowledgments

The authors would like to thank Dennis van den Berg (Food Microbiology, Wageningen University) for his assistance in workstation computer assembly for genome data analysis. The authors would like to thank Ziye Chen (Food Microbiology, Wageningen University) for her assistance in data collection. The authors would also like to thank Ingrid Maas (Food Microbiology, Wageningen University) for her help in experiment materials arrangement. Xuchuan Ma was supported by a grant from the China Scholarship Council (File No. 201907720086).

4.7 Supplementary Material

Supplemental Table 4.1: **The primers used in this study**

Primer	sequence (5'to 3')
WT-specific-F	CGCGCTTTCTGGATTCTTGC
WT-specific-R	ACGAATCGCTTGAAGATGCTC
V14-specific-F	CGATGCCCGATGATTAAAA
V14-specific-F	CGATGCCCGATGATTAAAA

Supplemental Table 4.2: **The selected inclusion of parameters for mono-culture growth model fitting of LO28 WT, V14 and V15**

Strain	Media	Include	Include stationary phase
WT	HFB	Yes	No
V14	HFB	Yes	No
V15	HFB	Yes	No
WT	FB	No	Yes
V14	FB	No	Yes
V15	FB	No	Yes
WT	BLEB	Yes	Yes
V14	BLEB	Yes	Yes
V15	BLEB	Yes	Yes

Supplemental Table 4.3: **The selected inclusion of parameters for mono-culture growth model fitting of heat-treated LO28 WT, V14 and V15**

Strain	Media	Include	Include stationary phase
WT	HFB	Yes	No
V14	HFB	Yes	No
V15	HFB	Yes	No
WT	FB	No	Yes
V14	FB	No	Yes
V15	FB	No	Yes
WT	BLEB	Yes	Yes
V14	BLEB	Yes	Yes
V15	BLEB	Yes	Yes

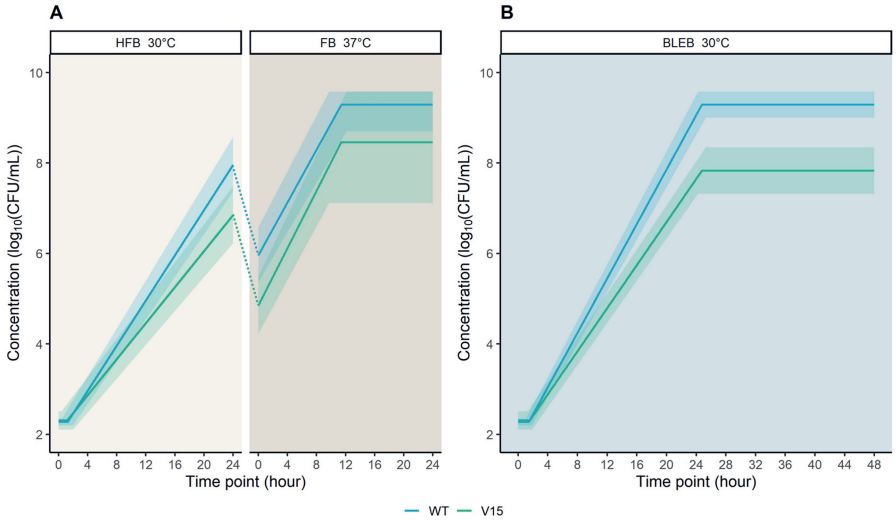

Supplemental Figure 4.1: **Co-culture growth predictions of LO28 WT and V15 during enrichment by following the ISO standard (A) and the BAM standard (B).** Co-culture growth predictions, which are shown as solid lines with confidence interval as shadow, according to the three-phase model were based on estimated parameters from mono-culture. The dotted lines indicate a 1:100 (v/v) inoculation from HFB to FB.

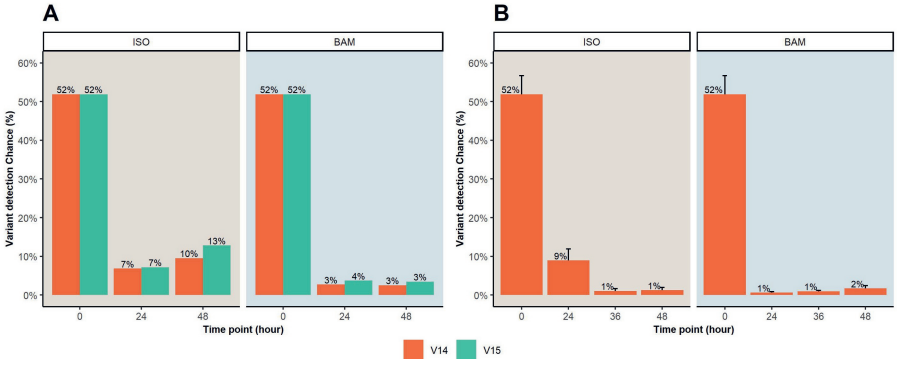

Supplemental Figure 4.2: **Variants detection chance during co-culturing according to prediction (A) and qPCR (B)** Variant detection chances are shown on the top of each bar. The error bars indicate standard deviations.

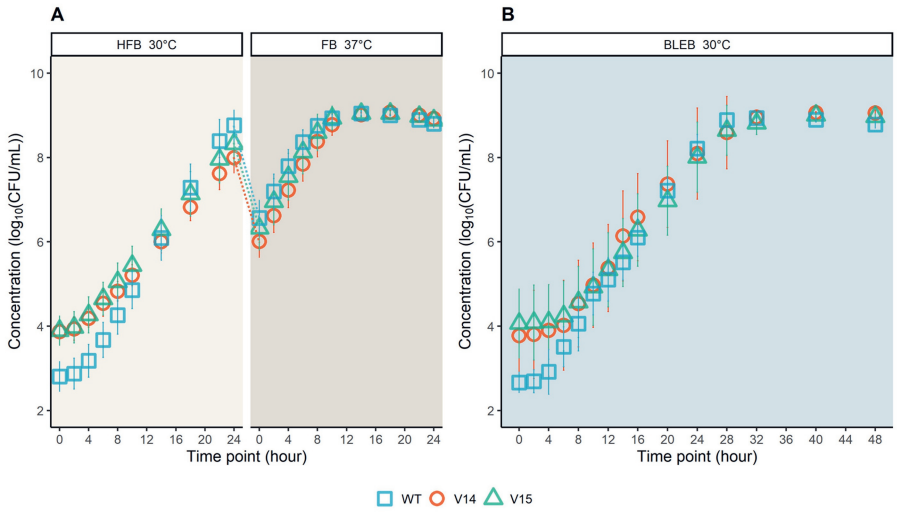

Supplemental Figure 4.3: **Mono-culture growth kinetics of heat-treated LO28 WT, V14 and V15 during enrichment by following the ISO standard (A) and the BAM standard (B).** The dotted lines indicate a 1:100 (v/v) inoculation from HFB to FB.

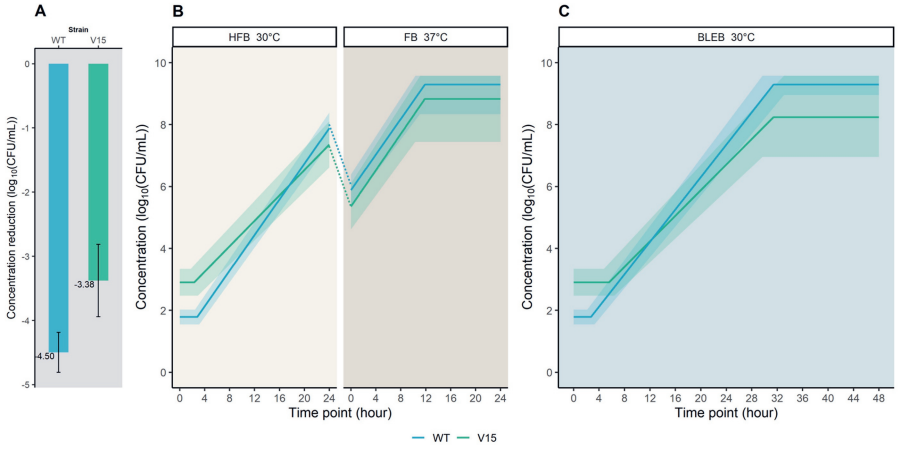

Supplemental Figure 4.4: **Heat reduction of LO28 WT and V15 (A) and co-culture growth predictions of heat-treated LO28 WT and V15 during enrichment by following the ISO standard (B) and the BAM standard (C).** Heat reductions were measured by exposing stationary phase culture at 60°C in BHI for 8.5 min and shown as bar plot with reduction level, and the error bars indicate the standard deviations. Co-culture growth predictions, which are shown as solid lines with confidence interval as shadow, according to the three-phase model were based on estimated parameters from mono-culture after heat treatment. The dotted lines indicate a 1:100 (v/v) inoculation from HFB to FB.

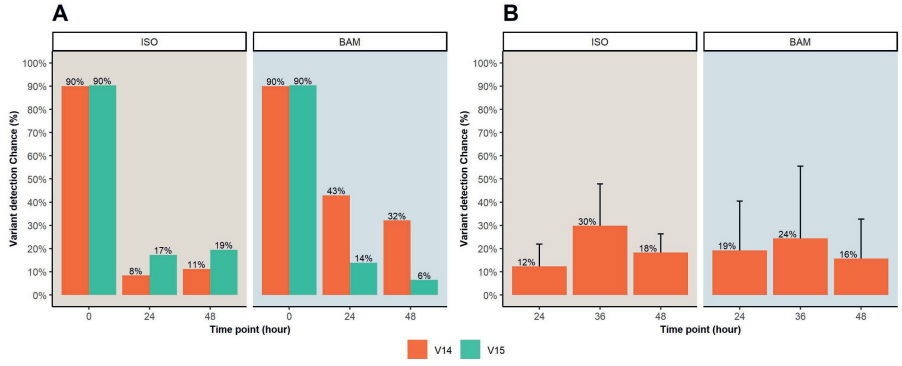

Supplemental Figure 4.5: **Variants detection chance during co-culturing after heat treatment according to prediction (A) and qPCR (B).** Variant detection chances are shown on the top of each bar. The error bars indicate standard deviations.

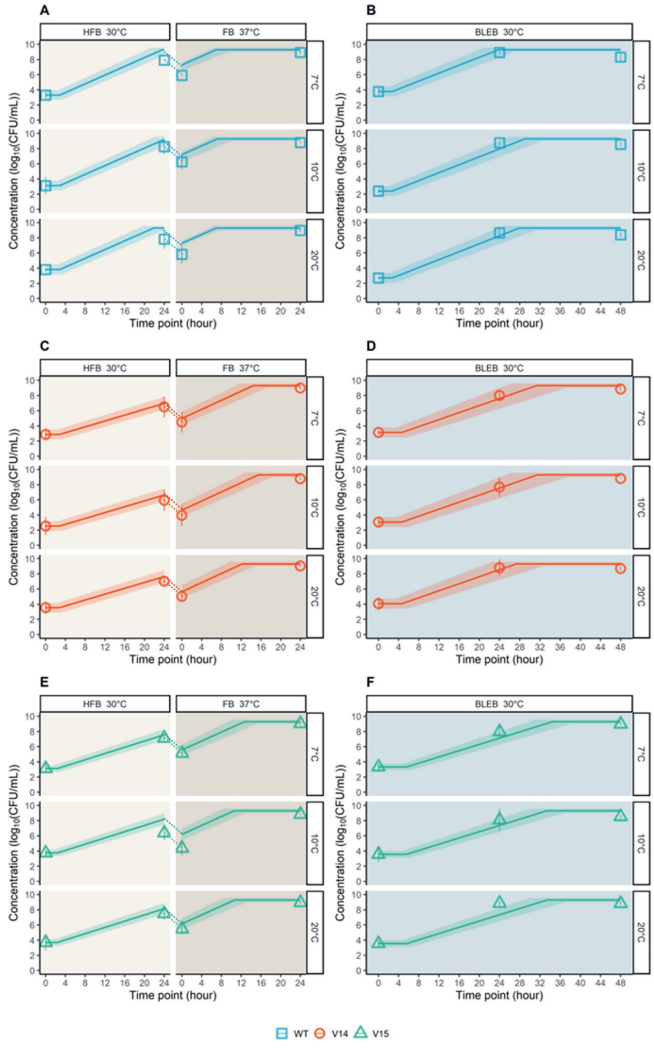

Supplemental Figure 4.6: **After pre-culturing at 7°C, 10°C and 20°C and heat treatment at 60°C for 8.5 min, mono-culture growth kinetics of LO28 WT (green square), V14 (red circle) and V15 (green triangle) during enrichment by following the ISO standard (A, C and E) and the BAM standard (B, D and F).** The solid lines indicate the growth prediction according to the three-phase model based on estimated parameters from mono-culture after 30°C ON culture and heat treatment. The shadow indicates the prediction confidence interval. The dotted lines indicate a 1:100 (v/v) inoculation from HFB to FB. The error bars indicate standard deviations.

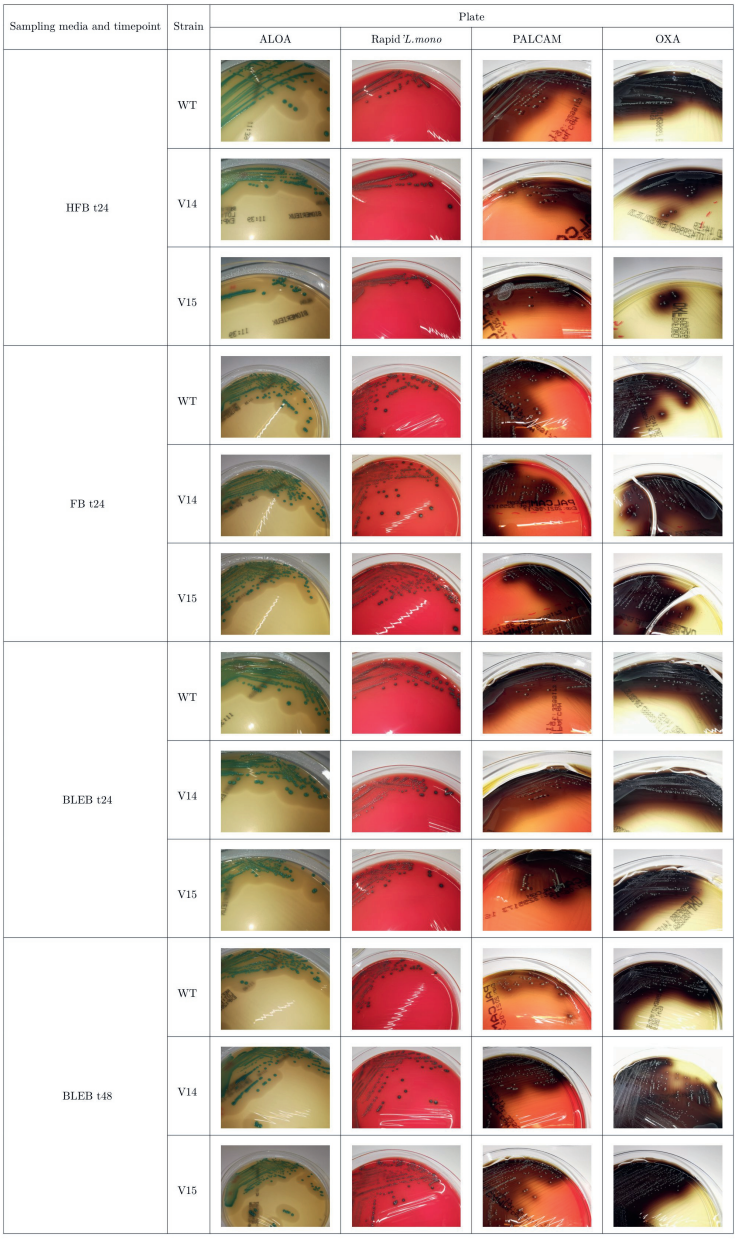

Supplemental Figure 4.7: **The streaking plates of WT, V14 and V15 after 48 h culturing at a designated temperature.** *L. monocytogenes* LO28 WT and *rpsU* variants V14 and V15 were enriched by following the ISO standard or the BAM standard. After 24 and 48 h enrichment, the culture was streaked on ALOA, Rapid' *L.mono*, PALCAM and OXA plates.

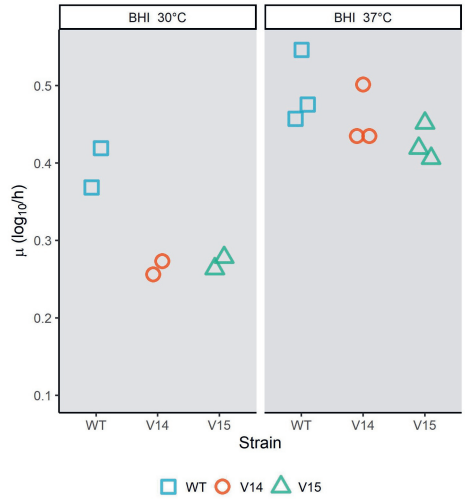

Supplemental Figure 4.8: **Maximum growth rate of LO28 WT, V14 and V15 in BHI at 30°C and 37°C from previous research** (Metselaar et al., 2016).

5

Activation of a silent lactose utilization pathway in an evolved *Listeria monocytogenes* F2365 outbreak isolate

Xuchuan Ma, Natalia Crespo Tapia, Jeroen Koomen, Oscar van Mastrigt, Marcel H. Zwietering, Heidy M.W. den Besten, Tjakko Abee

Under review

Abstract

Listeria monocytogenes, a widespread food-borne pathogen, utilizes diverse growth substrates including mono- and di-saccharides via PEP-phosphotransferase (PTS) systems. We evaluated a collection of *L. monocytogenes* isolates from different origins for the lactose utilization ability, a disaccharide composed of galactose and glucose and the main carbon source in milk and dairy products. Notably, the dairy-associated outbreak strain F2365 could not utilize lactose efficiently. Genome analysis of F2365 revealed a frameshift mutation *lacR*$^{887\text{del}}$, resulting in a truncated LacR. The LacR is a transcription regulator involved in the expression of two PTS systems, encoded by the *lpo* operon *lmo1718-1720* in combination with *lmo2708* and the *lmo2683-2685* operon, and linked to lactose and/or cellobiose metabolism in *L. monocytogenes*. Via experimental evolution of the ancestral strain F2365, an evolved isolate F2365 EV was obtained which showed enhanced growth and metabolism of lactose. Using the lactose-positive model strain *L. monocytogenes* EGDe as a control, HPLC experiments showed that EGDe and F2365 EV could consume lactose and utilize the glucose moiety, while the galactose moiety was exported from the cells. Genome sequencing of F2365 EV found the original *lacR*$^{887\text{del}}$ mutation was still present but an additional point mutation *lmo2766*$^{\text{C415T}}$ had occurred, resulting in an amino acid substitution in the putative regulator Lmo2766. The *lmo2766* gene is located next to a putative PTS operon *lmo2761-2765* in the genome. Notably, comparative RNAseq analysis confirmed that the *lmo2761-2765* operon was strongly upregulated in F2365 EV in the presence of lactose, but not in EGDe and F2365, whereas the LacR regulated *lpo* operon, *lmo2708*, and *lmo2683-2685* operon were upregulated in EGDe but not in F2365 and F2365 EV. Additional growth and HPLC experiments, using mutants constructed in lactose-positive *L. monocytogenes* EGDe, showed reduced growth of the EGDe *lacR*$^{887\text{del}}$ mutant with no utilization of lactose, while the double mutant EGDe *lacR*$^{887\text{del}}$ *lmo2766*$^{\text{C415T}}$ showed enhanced growth and efficient lactose utilization. Hence, these results demonstrate that an amino acid substitution in the Lmo2766 regulator activates a previously silent lactose utilization pathway, encoded by PTS operon *lmo2761-2765*, facilitating the growth and metabolism of *L. monocytogenes* with lactose as a substrate. This finding highlights a specific mechanism of lactose metabolic adaptation in *L. monocytogenes*, providing insight into the association of this pathogen with the dairy-associated outbreak and the evolutionary adaptability in different environments.

5.1 Introduction

Listeria monocytogenes is a Gram-positive foodborne pathogen that is widespread in natural environments, farms, silage, decaying vegetables, as well as in human and animal feces (Quereda et al., 2021). Due to its ubiquity, *L. monocytogenes* can be introduced into foods and food processing environments through cross-contamination by human carriers, transportation of animals, raw foods, and materials from crops, soil, and silage (Castro et al., 2018; Grif et al., 2003; Quereda et al., 2021). The consumption of food contaminated with *L. monocytogenes* can lead to listeriosis, a foodborne disease with low incidence but high case-fatality rates (Buchanan et al., 2017; EFSA and ECDC, 2022). Notably, several listeriosis outbreaks have been linked to the presence of *L. monocytogenes* in dairy products (Carrique-Mas et al., 2003; Castro et al., 2018; Kim et al., 2018; Kiss et al., 2006; Linnan et al., 1988; MacDonald et al., 2005; Sauders and D'Amico, 2016).

Dairy products have been suggested to be associated with hypervirulent *L. monocytogenes* clones based on an extensive comparative whole genome sequence (WGS) analysis of a large collection of food and clinical *L. monocytogenes* isolates (Maury et al., 2019). The metabolism of lactose, the main available carbon sources in dairy products, also links with stress response and biofilm production of *L. monocytogenes* (Crespo Tapia et al., 2020). Lactose is a disaccharide composed of galactose and glucose moieties with a beta-1→4 glycosidic linkage, and it is widely used by many bacterial species as a carbon/energy source. Two main lactose metabolic pathways have been identified in bacteria, the Leloir and the Tagatose-6-P pathways (Iskandar et al., 2019; Solopova et al., 2012). In the Leloir pathway, lactose enters the cell via a lactose-specific permease and is immediately hydrolyzed via a beta-galactosidase into glucose-1-P and beta-galactose, which are further metabolized via the glycolysis pathway (Iskandar et al., 2019; Solopova et al., 2012). The Tagatose-6-P pathway consists of a phosphoenolpyruvate (PEP) sugar phosphotransferase (PTS) system that phosphorylates lactose during uptake, which is later hydrolyzed by a phospho-beta-galactosidase into glucose and galactose-6-P. The glucose moiety enters glycolysis directly, while the galactose-6-P is first transformed into tagatose-6-P and tagatose-1,6-P before entering glycolysis (Iskandar et al., 2019; Solopova et al., 2012). Notably, galactose-6-P isomerase, which transforms galactose-6-P into tagatose-6-P, is not identified in the *L. monocytogenes* BioCyc database (Karp et al., 2019).

Despite the persistence of *L. monocytogenes* in food-processing environments, including dairy industries, and the association of dairy products with listeriosis outbreaks and hypervirulent clones, the uptake and utilization of lactose in *L. monocytogenes* has so far gained limited attention. The expression of the *L. monocytogenes lpo* operon has been shown to be induced by the presence of lactose, cellobiose, and chitobiose in the media, and has been found to be controlled by the transcriptional activator LacR (coded by *lmo1721*/*lacR*) together with the transcription factor sigma 54 (Dalet et al., 2003). The *lpo* operon encodes IIA and IIB PTS subunits of the lactose family by *lpoA* (*lmo1719*) and *lpoB* (*lmo1720*) but misses the IIC subunit, since *lpoO* (*lmo1718*) encodes a putative protein LpoO with unknown function rather than the IIC subunit. Another IIC coding gene *lmo2708* also has a sigma 54 promoter region and LacR

binding upstream activating sequences (UAS), so Dalet et al. (2003) hypothesized that *lmo2708* produces the IIC protein and is functionally linked to the *lpo* operon. Further API 50 CH gallery screening found that *lpoA* and *lpoO* deletion mutants of the *L. monocytogenes* LO28 strain retained the ability to metabolize lactose, cellobiose and chitobiose, to the same degree as the WT strain, which points to the presence of one or more alternative utilization pathways for these carbohydrates in this strain (Dalet et al., 2003). Indeed, *in silico* analysis found several other lactose PTS systems, including a complete IIABC permease coded by *lmo2683-2685*, which may also be controlled by LacR (Stoll and Goebel, 2010). Further analysis based on cellobiose showed that the expression of the *lpo* operon, the *lmo2708*, and the *lmo2683-2685* operon are all controlled by activator LacR (Cao et al., 2019). The IIA/B pairs encoded by *lpoA*/*lpoB* and *lmo2683*/*lmo2685* are similarly efficient as phosphoryl donors in cellobiose transport via IIC coded by *lmo2684*, whereas the Lmo2708 does not significantly contribute to cellobiose transport (Cao et al., 2019). Since the role of these putative lactose PTS systems has not been studied in *L. monocytogenes* grown in lactose-based media, further studies are required.

In this study, we evaluated growth performance and lactose metabolism diversity within a collection of *L. monocytogenes* isolates and uncover an alternative lactose PTS pathway through the experimental evolution of the lactose-negative strain F2365, which was associated with the 1985 Jalisco Cheese outbreak and was previously shown to contain multiple authentic nonsense and frameshift mutations, including a premature stop codon in a DNA repair gene LMOF2365_2275 (Linnan et al. (1988); Nightingale et al. (2007)). Using *L. monocytogenes* EGDe as a model, we comprehensively investigated the regulatory mechanisms and functional implications of both the LacR-regulated PTS systems and the alternative lactose PTS pathway. This investigation encompassed analyses through growth kinetics, WGS, high-performance liquid chromatography (HPLC), RNA sequencing (RNAseq), and targeted mutant construction, offering a broader view on lactose utilization in *L. monocytogenes*.

5.2 Materials and Methods

5.2.1 Bacterial strains and growth conditions

The *L. monocytogenes* strains used in this study are described in Table 5.1, including 20 strains belonging to the FHM collection from different origins, an evolved isolate of strain F2365, and two constructed mutants of strain EGDe. Bacterial stocks were stored at -80°C in Brain Heart Infusion (BHI) broth (Sigma) in cryovials containing 5 mm glass beads and 30% (v/v) glycerol (Fluka). For the preparation of a working culture, *L. monocytogenes* was streaked on BHI agar (1.5% (w/w), bacteriological agar no. 1 Oxoid) plates and incubated at 30°C for 24 h. Plates were kept in the fridge for up to a week. Subsequently, single colonies were inoculated in 50 mL tubes containing 5 mL of BHI broth. Tubes were incubated overnight under shaking conditions (160 rpm) at 30°C. Unless otherwise specified, further experiments were carried out in nutrient broth (NB, Oxoid) supplemented with 1% (w/v) lactose (Sigma-Aldrich) (i.e. NB-lactose medium), 0.5% (w/v) glucose (VWR Chemicals) (i.e. NB-glucose medium), or 0.5% (w/v) galactose (VWR Chemicals) (i.e. NB-galactose medium). Phosphate buffered

saline (PBS) was prepared by dissolving 8.98 g Na_2HPO_4 (Merck), 2.72 g $NaH_2PO_4 \cdot H_2O$ (Merck) and 8.5 g NaCl (Sigma-Aldrich) in 1 L deionized H_2O.

Table 5.1: The strains used in this study

Strain name	Description	Source or reference
AOPM3	Serotype 4b	Human isolate
C5	Serotype 4b	Smoked meat
FBR12	Serotype 1/2a	Frozen vegetable mix
FBR13	Serotype 1/2a	Frozen endive a la creme
FBR14	Serotype 1/2a	Carrot piece
FBR15	Serotype 1/2c	Ice cream packaging machine
FBR16	Serotype 1/2a	Ham (after cutting machine)
FBR17	Serotype 4d	Frozen fried rice
FBR18	Serotype 1/2a	Ice cream
FBR19	Serotype 1/2a	Frozen meat
FBR20	Serotype 1/2a	Frozen vegetables for soup
FBR21	Serotype 4d	Fresh yeast
FBR33	Serotype 1/2c	Pancake
H7764	Serotype 1/2a	Deli turkey
H7962	Serotype 4b	Hotdog
L6	Serotype 1/2b	Milk
LO28	Serotype 1/2c	Healthy pregnant carrier
ScottA	Serotype 4b	Human isolate from Massachusetts milk outbreak
EGDe	Serotype 1/2a	Rabbit
F2365	Serotype 4b	Jalisco cheese
F2365 EV	Serotype 4b	Derived from F2365 in this study
EGDe *lacR*^{887del}	EGDe with *lacR*^{887del} DNA point mutation	This study
EGDe *lacR*^{887del} *lmo2766*^{C415T}	EGDe with *lacR*^{887del} DNA point mutation and *lmo2766*^{C415T} DNA point mutation	This study

5.2.2 Plasmids and mutant construction

The plasmids and primers used in this study are described in Table 5.2. The shuttle vector pKSV7-*lacR*^{887del} and pKSV7-*lmo2766*^{C415T} were used for introducing the *lacR*^{887del} point deletion and the *lmo2766*^{C415T} point mutation in the target *L. monocytogenes* strains, respectively. The pKSV7-*lacR*^{887del} and pKSV7-*lmo2766*^{C415T} were constructed as described previously with modification (Rychli et al., 2021). The sequences of *lacR* or *lmo2766* with mutations were amplified from genomic DNA of F2365 or F2365 EV with the primers with restriction sites, respectively. The resulting fragments were ligated into the pKSV7 multiple-cloning site. The resulting construct was confirmed by PCR and sequencing using primers M13-F and M13-R. To construct the mutants EGDe *lacR*^{887del} and EGDe *lacR*^{887del} *lmo2766*^{C415T}, the pKSV7-*lacR*^{887del} and the pKSV7-*lmo2766*^{C415T} were respectively transformed into *L. monocytogenes* EGDe competent cells respectively by electroporation (2.5 kV, 25 μF, 200 D) and plated on Brain Heart Infusion (BHI) agar plates at 30°C with chloramphenicol (10 μg/mL) to select for transformants. The chloramphenicol-resistant colonies

were inoculated in BHI broth with 10 μg/mL chloramphenicol and grown at 42°C overnight. The 42°C-grown overnight cultures were inoculated into fresh BHI for overnight culturing at 30°C and subsequently plated on BHI agar plates at 30°C. The resulting colonies were replica plated on BHI agar plate with and without 10 μg/mL chloramphenicol and incubated at 30°C to check the chloramphenicol sensitivity of each colony. For the chloramphenicol-sensitive colonies, the planktonic growth curves in NB-lactose were measured as described in Section 5.2.3, using EGDe and F2365 as control. For those cultures that showed an expected growth curve, the constructed mutations were verified by PCR and Sanger sequencing with primers without restriction sites (Table 5.2).

Table 5.2: The plasmids and primers used in this study

Name	Description or sequence (5'to 3', restriction site underlined)	Source or reference
Plasmids		
pKSV7	Temperature sensitive suicide plasmid	Smith and Youngman (1992)
pKSV7-*lacR*^{887del}	pKSV7 containing the *lacR*^{887del} DNA point mutation cassette	This study
pKSV7-*lmo2766*^{C415T}	pKSV7 containing the *lmo2766*^{C415T} DNA point mutation cassette	This study
pKSV7-*lacR*^{887del} construction primers		
lacR-EcoRI-F	CTCAGAATTCCCTCCAGAAGGTCAAGAAATG	This study
lacR-PstI-R	TATTCTGCAGTGGCTTTGTTCACGTCAATC	This study
lacR-F	CTTCAAATGGACAGAGCAAAC	This study
lacR-R	CTTTGGTCCTTCCCTTCTTTC	This study
pKSV7-*lmo2766*^{C415T} construction primers		
lmo2766-PstI-F	TTCACTGCAGTAGACAATTTACAGAGACAG	This study
lmo2766-BamHI-R	TAGTGGATTCTTATTCTTCTTGCTCTTGAT	This study
lmo2766-F	TTAACACAGTTGGTGGTGCAA	This study
lmo2766-R	CGGAAGACTTACTCATCACAA	This study
Plasmid construction checking primers		
M13-F	CAGGAAACAGCTATGAC	
M13-R	GTTTTCCCAGTCACGAC	

5.2.3 Planktonic growth curves

For cell density-based experiments, an ON culture was 1,000 times diluted in NB with and without supplemented sugars to reach an initial OD_{600} of 0.01. Polystyrene 96-well plates (Sigma) and Bioscreen honeycomb plates (Thermofisher) were used for *L. monocytogenes* growth experiment in NB with different supplemented sugars. The 96-well plates and honeycomb plates were filled with 250 μL and 300 μL of the diluted culture per well, respectively. The plates were incubated shaking at 30°C. OD_{600} measurements were taken every 30 min for 20 h in the Spectramax M2 plate reader (Molecular Devices) or every 30 min for 48 h in the Bioscreen C (Oy Growth Curves Ab Ltd). A blank control of the sterile media was included, and its value was

subtracted from the strain's values. The experiment was performed with two and three biologically independent replicates in the Spectramax M2 plate reader and Bioscreen C, respectively.

5.2.4 DNA sequence analysis of the *lpo* operon in the FHM strain collection

The DNA sequences of the *lacR* and *lpo* operon genes (*lpoA*, *lpoB* and *lpoO*) were analyzed by using the FHM strain collection sequenced genomes. The gene sequences were aligned and compared using the EMBL-EBI Clustal Omega web service (Madeira et al., 2022).

5.2.5 Experimental evolution approach

An experimental evolution approach was used to obtain a lactose-positive isolate of the lactose-negative F2365 strain. Briefly, 50 mL tubes containing 5 mL of NB-lactose medium were inoculated with 1% (v/v) of the F2365 ON culture and cultured at 30°C, 160 rpm. Samples of the original inoculum were stored in cryovials as ancestral strain at the beginning of the experiment. Every 24 h 1% (v/v) of the previous culture was transferred into fresh NB-lactose medium, allowing for ~6.6 generations increase each transfer. The experiment was run for three weeks (~140 generations), until a visible change in the turbidity of the culture suggested a change in growth performance of the F2365 strain. The culture was then plated on BHI agar plates, incubated at 30°C overnight, and a single colony was grown at 30°C overnight in BHI three consecutive times to ensure the stability of any potential change in phenotype/genotype by eliminating the selective pressure of lactose in the medium. The growth performance of the resulting evolved isolate (F2365 EV) was compared to the ancestral strain in NB-lactose medium using the Spectramax, and the lactose-positive F2365 EV isolate was stored in a cryovial at -80°C and used in further experiments.

5.2.6 DNA extraction and *lacR* sequencing

The genomic DNA was isolated for sequencing using DNeasy Blood and tissue kit (Qiagen) following the manufacturer's instructions with modifications. Two times 2 mL of overnight culture was centrifuged (17,000 x *g*), washed with 1 mL PPS, resuspended in 1 mL lysis buffer (20 mM Tris-HCl, 2 mM EDTA, 1.2% (w/v) Triton X-100, 20 mg/mL lysozyme, pH 8.0), and incubated at 37°C for 1 h. Then, 10 μL RNAse (10 mg/mL) was added and incubated for 30 min at room temperature. Subsequently, 62.5 μL proteinase K and 500 μL AL buffer were added and incubated at 56°C for 1 h. Then, 500 μL absolute ethanol was added. The suspension was transferred to a spin column provided by the kit and centrifuged for 1 min at 6000 x *g*. The filters were washed two times with 500 μL buffer AW1 and AW2 at 6000 x *g*. Then, the columns were centrifuged at 17,000 x *g* for 3 min. Subsequently, 50 μL of AE buffer was added to the center of the column. The column was centrifuged at 6,000 x *g* to collect the target sample. Samples were stored at -20°C. A high-fidelity PCR was then performed

on the genomic DNA samples following the KAPA HiFi PCR kit (Roche) instructions with primers *lacR*-F and *lacR*-R (Table 5.2) followed by a sample clean up with the PCR purification kit (Qiagen). The concentration of the samples was measured via UV absorbance at 260 nm (BioPhotometer Eppendorf), and the purity of the PCR product was checked via gel electrophoresis. The samples were stored at -80°C until sent for sequencing (BaseClear B.V., the Netherlands). The resulting forward and reverse sequences were combined, and the data of EGDe, F2365 and F2365 EV was aligned and analyzed.

5.2.7 Quantification of lactose metabolism via HPLC

NB-lactose medium was inoculated with 0.01% (v/v) of an ON culture to reach 6 $\log_{10}$CFU/mL, and incubated shaking at 30°C at 160 rpm in 250 mL flasks (total volume 20 mL). Samples of 1 mL were taken for HPLC analysis after 0, 8, 24 and 48 h of incubation and centrifuged at 17,000 x *g* for 1 min. Proteins in the supernatant were removed by addition of Carrez A (0.1 M $K_4[Fe(CN)_6] \cdot 3H_20$, Merck) and B (0.2 M $ZnSO_4 \cdot 7H_20$, Merck) (in ratio 2:1:1, 2-fold dilution), followed by centrifugation at 17,000 x *g* for 1 min and 2-fold dilution with MilliQ. Additionally, a standard curve of 2-fold dilutions of known concentrations of lactose, galactose, glucose, acetate, lactate, and formate were prepared. Compounds were quantified on an UltiMate 3000 HPLC (Dionex) equipped with an autosampler and Aminex HPX – 87H column (7.8 x 300 mm) with a guard column (Bio-Rad, Hercules, CA). Compounds were detected using a refractive index detector (RefractoMax 520). As mobile phase, 5 mM H_2SO_4 was used at a flow rate of 0.6 mL/min, and the column was kept at 40°C. Total run time was 30 min. The injection volume was 10 μL. The experiment was performed in three biological replicates.

5.2.8 Whole genome sequence and protein sequence analysis

BHI streak plates of F2365 and F2365 EV isolates were prepared as described in Section 5.2.1. After 24 h incubation at 30°C, the plates were sealed and sent to RIVM (the Netherlands) for genomic DNA extraction and sequencing. The whole-genome sequences of the F2365 AN and EV isolates were compared to a reference genome of *L. monocytogenes* F2365 strain retrieved from the NCBI Gene Bank (NC_002973.6). SNPs were identified using snippy (4.6.0+galaxy0) on Galaxy platform (Galaxy Community, 2022; Torsten, 2015). DNA sequence visualization and multiple sequence alignment were performed with BioEdit (7.2.5) software (Hall, 1999). For protein sequence, the protein domains and motifs have been scanned by PROSITE (Sigrist et al., 2013). The predicted protein structures have been accessed from the AlphaFold Protein Structure Database (Jumper et al., 2021; Varadi et al., 2022).

5.2.9 RNA sequencing

NB-glucose and NB-lactose media was inoculated with 0.01% (v/v) of an ON culture to reach 6 $\log_{10}$CFU/mL, and incubated shaking at 160 rpm in 250 mL flasks (total

volume 20 mL). Samples of 10 mL were taken after 8 and 24 h of incubation for RNA extraction. The samples were centrifuged at 10,000 x *g* for 2 min and the supernatant was removed completely from the 2 mL tubes. The pellet was then dissolved in 1 mL Tri-reagent, vortexed well and let stand for 5 min at room temperature, after which the samples were snap-frozen with liquid N_2 and stored at -80°C until the RNA extraction day. After all samples were collected, the tubes were defrosted on ice and the total volume was added to tubes containing beads. Cell lysis was performed by bead beating (Fast Prep, settings 4 times 6 m/s for 20 seconds, rest 1 min on ice in between). After that, 200 μL of chloroform was added to the sample, mixed well and centrifuged for 15 min at maximum speed. The aqueous phase of the samples was then carefully removed and transferred to RNase-free 2 mL eppendorf tubes containing 500 μL of isopropanol. After mixing, the tubes were centrifuged for 10 min at maximum speed, the supernatant was removed, and 1 mL of 70% ethanol was added to the samples. After further centrifugation of 5 min at 17,000 x *g* the supernatant was removed, and the tubes were left to air dry in the laminar flow cabinet to completely remove the ethanol from the samples. The pellet was then resuspended in 90 μL RNAse-free water and treated with the Ambion RNase-free DNase kit for genomic DNA removal, following the manufacturer's instructions. The concentration of the samples was measured with the Nanodrop, and the RNA was checked for degradation via agarose gel electrophoresis. After adding 0.1 volume of 3 M sodium acetate and 2.5 volume of absolute ethanol, the samples were store at -80° until sent for sequencing (BaseClear B.V., the Netherlands).

5.3 Results

5.3.1 Strain diversity of *L. monocytogenes* in lactose metabolism

The growth performance of a collection of *L. monocytogenes* strains isolated from different origins was assessed in NB and NB-lactose media (Supplemental Figure 5.1). The growth in NB was comparable for all strains, while F2365 and ScottA showed less enhanced growth performance in NB-lactose compared to the other strains. This observation suggests that F2365 and ScottA have a lower efficiency in utilizing lactose as a carbon source, categorizing them as lactose-negative strains. DNA sequence analysis of the putative lactose PTS system encoded by the *lpo* operon and the activator gene *lacR* identified the presence of a unique 1 bp deletion in the *lacR* gene (NC_003210.1:g.1783453del, marked as $lacR^{887del}$ in this study) of the lactose-negative strain F2365 (Figure 5.1). This deletion conceivably causes a frame shift resulting in a premature stop codon, which impedes the production of a functional LacR protein (Supplemental Figure 5.2). All the other isolates including the ScottA strain showed no unique missense mutation in the *lacR*, the *lpo* operon, the respective promoters, the upstream presumed binding site of LacR, and the ribosomal binding sites (data not shown). Based on this unique mutation in the *lacR* gene and the association with the 1985 Jalisco Cheese outbreak (Linnan et al. (1988)), our further study on lactose utilization is focused on the *L. monocytogenes* F2365 strain.

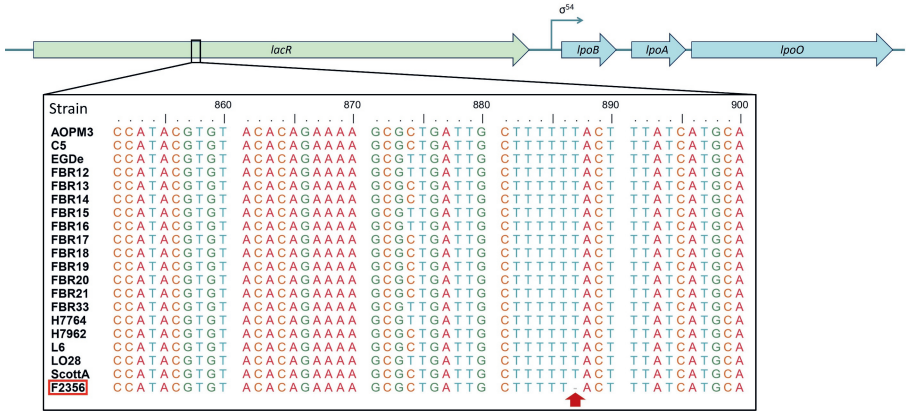

Figure 5.1: **The gene cluster of *lacR* and the *lpo* operon in *L. monocytogenes* and the DNA sequence alignment of *lacR* in 20 *L. monocytogenes* strains.** Numbers above the alignment indicate the nucleotide position in the *lacR* gene. The strain F2365 has been highlighted by a red box, and the point deletion $lacR^{887del}$ in F2365 has been highlighted by a red arrow.

5.3.2 The evolved F2365 EV strain can use lactose as a carbon source

To investigate whether an additional, conceivably silent, lactose utilization pathway(s) exist(s) in F2365, we performed a short term evolution experiment in which the ancestral strain of F2365 was subjected to repeated daily (24 h) transfers in NB-lactose. After 3 weeks of transfers, an evolved isolate of F2365 (F2365 EV) that showed enhanced growth performance in the presence of lactose was obtained. Growth performance and lactose metabolism of the F2365 and F2365 EV strains in NB, NB-lactose, NB-glucose and NB-galactose were assessed (Figure 5.2). In NB, NB-galactose and NB-glucose, the F2365 EV showed similar growth as the ancestral strain F2365, with the highest OD obtained in the NB-glucose (Figure 5.2 **A**). In NB-lactose, only F2365 EV reached OD_{600} values similar to that in NB-glucose, while F2365 only showed a small increase in OD_{600}. For the cell count-based growth curves, both strains reach approximately 8.4 $\log_{10}$(CFU/mL) in NB and 9.0 $\log_{10}$(CFU/mL) in NB-glucose, while in NB-lactose, F2365 attains 8.5 $\log_{10}$(CFU/mL) and F2365 EV 9.0 $\log_{10}$(CFU/mL) (Supplemental Figure 5.3). The HPLC results show that F2365 EV consumed more lactose and secreted more galactose and acetate in the medium than the F2365 ancestral strain (Figure 5.2 **B**). The sole production of acetate as an end product is conceivably due to the presence of oxygen in the shaken cultures (160 rpm) allowing NAD+ regeneration via NADH dehydrogenase (Müller-Herbst et al., 2014). Although the decrease in lactose was slightly greater than the increase in galactose from t0 to t48, primarily because galactose levels remained near 0 mM until t8, the changes in concentrations from t8 to t48 were consistent between lactose and galactose. This suggests that the galactose moiety of the uptaken lactose was not metabolized by *L. monocytogenes* but rather secreted into the medium after several hours of lactose uptake. In total, these results show enhanced growth performance and lactose utilization of the F2365 EV strain while the galactose moiety was conceivably

not used and secreted in the medium.

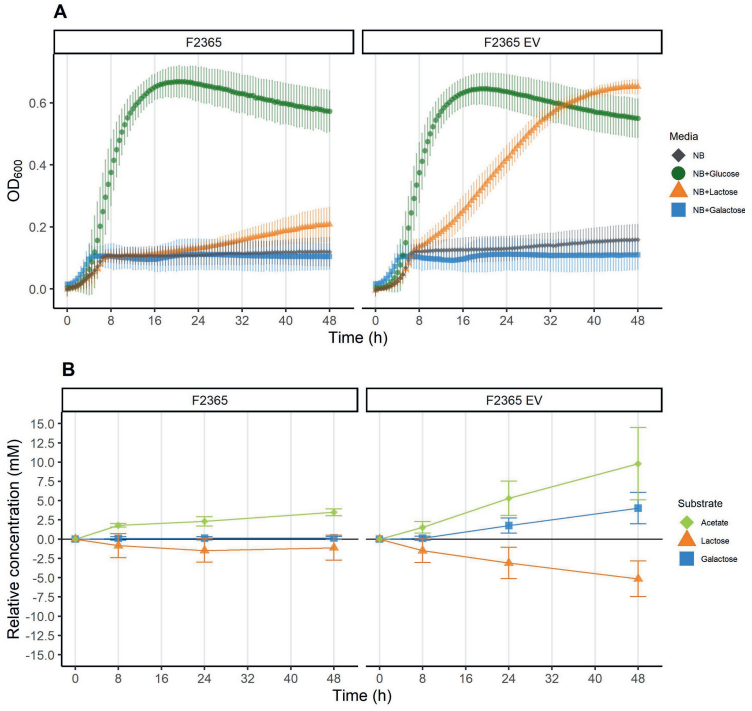

Figure 5.2: **Growth in different media (A) and lactose metabolism (B) of *L. monocytogenes* F2365 and F2365 EV. A**: Cell density growth curves in plain NB (black diamonds), NB-glucose (green circles), NB-lactose (orange triangles), and NB-galactose (blue squares). **B**: HPLC quantification of lactose (orange triangles) consumption and galactose (blue squares) and acetate (light green diamonds) production during growth in NB-lactose. The error bars correspond to the standard deviation of the biological replicates.

5.3.3 F2365 EV has an additional mutation in *lmo2766*

The point deletion *lacR*$^{887\text{del}}$ leads to a premature stop codon in *lacR*, and the loss of LacR activation conceivably contributes to the lactose-negative phenotype of F2365. Notably, DNA sequence analysis showed that the lactose-positive evolved strain F2365 EV obtained a second mutation, next to *lacR*$^{887\text{del}}$ (Supplemental Figure 5.4), in *lmo2766* (NC_003210.1:g.2847159C>T, marked as *lmo2766*$^{\text{C415T}}$ in this study) (Figure 5.3 **B**). The point mutation *lmo2766*$^{\text{C415T}}$ conceivably results in an amino acid substitution from arginine to tryptophan in Lmo2766 at amino acid position 139 (Figure 5.3 **C**). Lmo2766, a putative transcriptional regulator, may influence the expression of the adjacent *lmo2761-2765* operon, encoding a potential lactose PTS uptake system, a beta-glucosidase, and a beta-glucoside kinase (Figure 5.3 **A**). A PROSITE motif scanner found two hits in Lmo2766: a DNA-binding RpiR-type

HTH domain and a phospho-sugar-binding SIS domain, with the identified mutation located in the center region of SIS domain (Figure 5.3, D). It is conceivable that the *lmo2766*^{C415T} mutation affects the function of Lmo2766 resulting in expression of the alternative lactose PTS system encoded by *lmo2762*, *lmo2763* and *lmo2765*.

5.3.4 Lactose-induced genes encoding PTS system in F2365 EV

Comparative RNAseq analysis of *L. monocytogenes* EGDe and F2365 cells grown in NB-lactose and NB-glucose revealed significant upregulation of LacR regulated genes in EGDe, but not in F2365, and a lack of significant upregulation in most genes of the *lmo2761-lmo2765* operon for both strains (Supplemental Figure 5.5). These results underscore the low lactose metabolism efficacy of F2365 conceivably resulting from the mutation in the *lacR* gene described above. Further comparative RNAseq analysis of F2365 EV and F2365 cells grown in NB-lactose showed notable upregulation of the *lmo2761-2765* operon in F2365 EV compared to F2365, with $\log_2$(Fold change) values ranging between 7.58 to 8.15 (Supplemental Figure 5.6 and Table 5.3). In contrast, genes in the *lpo* operon, the *lmo2683-2685* operon, and *lmo2708* exhibited no or only modest upregulation, with $\log_2$(Fold change) values no more than 2.60. Consequently, the PTS system encoded by these genes conceivably did not significantly contribute to lactose utilization in F2365 EV. These findings imply that the *lmo2761-lmo2765* operon encoded EIIABC might serve as an alternative lactose PTS system and be a key factor in F2365 EV's ability to utilize lactose, which requires further elucidation via a mutation construction study.

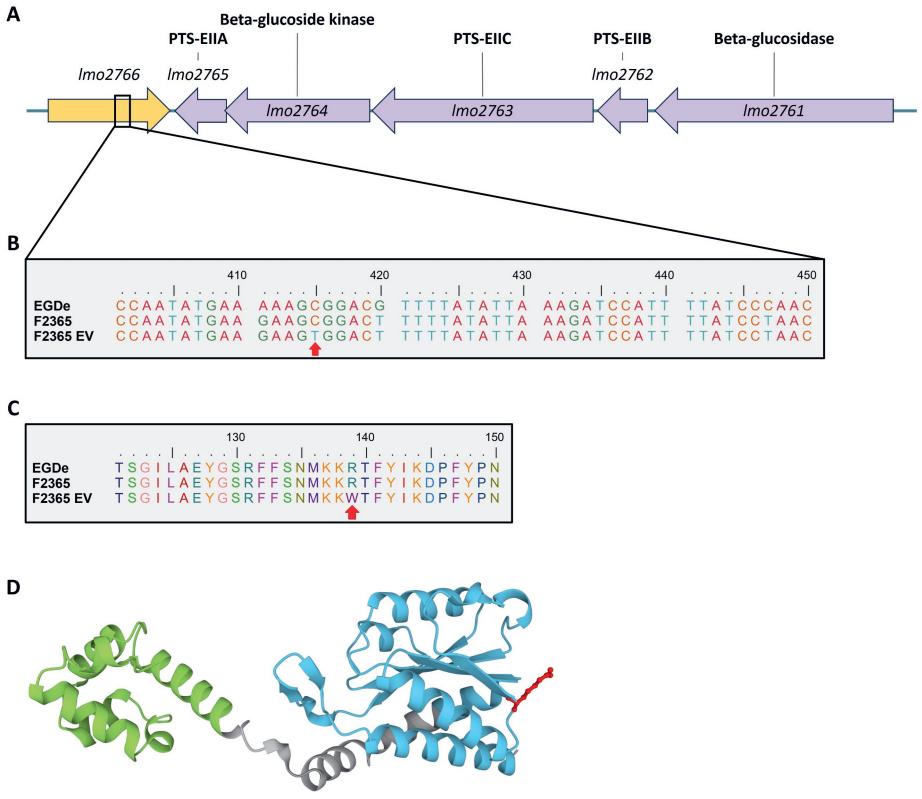

Figure 5.3: **Comparative analysis of *lmo2761-2766* in EGDe, F2365 and F2365 EV. A**: The gene cluster of *lmo2761-2766* with putative functions of encoded proteins indicated. **B**: DNA sequence alignment of *lmo2766* in EGDe, F2365, and F2365 EV with nucleotide positions indicated by numbers, and the point mutation $lmo2766^{C415T}$ in F2365 EV is indicated by a red arrow. **C**: Protein amino acid sequence alignment of Lmo2766 in EGDe, F2365, and F2365 EV with amino acid positions indicated by numbers, and arginine to tryptophan substitution (at amino acid position 139) is highlighted by a red arrow. **D**: The structure of the EGDe Lmo2766 protein in AlphaFoldDB. Green and blue colors represent the PROSITE predicted RpiR-type HTH domain and SIS domain, respectively. The Arginine that is substituted in F2365 EV is highlighted as ball and stick structure in red.

Table 5.3: **The putative LacR and Lmo2766 regulated genes differential expression level comparing F2365 EV to F2365 grown in NB-lactose.** The log_2(Fold change) and adjusted p-value of significantly downregulated genes are highlighted in bold

EGDe orthologs gene locus	Gene locus	Protein name	log_2(Fold change)	Adjusted p-value
LacR regulated genes				
lmo1718	LMOf2365_1742	DUF871 domain-containing protein, LpoO	**2.21**	**0.000**
lmo1719	LMOf2365_1743	PTS sugar transporter subunit IIA, LpoA	**2.60**	**0.000**
lmo1720	LMOf2365_1744	PTS sugar transporter subunit IIB, LpoB	**1.82**	**0.000**
lmo2708	LMOf2365_2688	PTS sugar transporter subunit IIC	-0.13	0.793
lmo2683	LMOf2365_2663	PTS sugar transporter subunit IIB	0.07	0.895
lmo2684	LMOf2365_2664	PTS sugar transporter subunit IIC	**2.25**	**0.000**
lmo2685	LMOf2365_2665	PTS sugar transporter subunit IIA	**2.23**	**0.000**
Lmo2766 regulated genes				
lmo2761	LMOf2365_2751	Beta-glucosidase	**8.15**	**0.000**
lmo2762	LMOf2365_2752	PTS sugar transporter subunit IIB	**7.77**	**0.000**
lmo2763	LMOf2365_2753	PTS sugar transporter subunit IIC	**7.58**	**0.000**
lmo2764	LMOf2365_2754	Beta-glucoside kinase	**8.02**	**0.000**
lmo2765	LMOf2365_2755	PTS sugar transporter subunit IIA	**7.90**	**0.000**

5.3.5 Mutations in transcriptional regulators *lacR* and *lmo2766* alter *L. monocytogenes* lactose utilization capacity

To further confirm the impact of the *L. monocytogenes* F2365 *lacR*^{887del} and *lmo2766*^{C415T} mutations on lactose utilization, we constructed single mutant EGDe *lacR*^{887del} and double mutant EGDe *lacR*^{887del} *lmo2766*^{C415T} strains, comparing their growth in various media. All three strains exhibited comparable growth in NB-glucose (data not shown). For EGDe *lacR*^{887del}, growth in NB and NB-lactose was similar during the first 24 h, but a slight increase in optical density (OD) was observed in the latter over the next 24 hours (Figure 5.4). For EGDe and EGDe *lacR*^{887del} *lmo2766*^{C415T}, better growth in NB-lactose compared to NB was already showed in the first 24 h. Notably, the EGDe *lacR*^{887del} *lmo2766*^{C415T} strain exhibited the most significant growth in NB-lactose. The cell count-based growth results are in line with the cell density growth results (Supplemental Figure 5.3). Combining these results from EGDe WT and mutants, it indicates that the *lacR*^{887del} mutation reduces growth and lactose metabolism in NB-lactose media, whereas the additional *lmo2766*^{C415T} mutation enhances lactose utilization in *L. monocytogenes* via an alternative lactose PTS EIIABC uptake system, beta-glucoside kinase and beta-glucosidase encoded by the *lmo2761-lmo2765* operon.

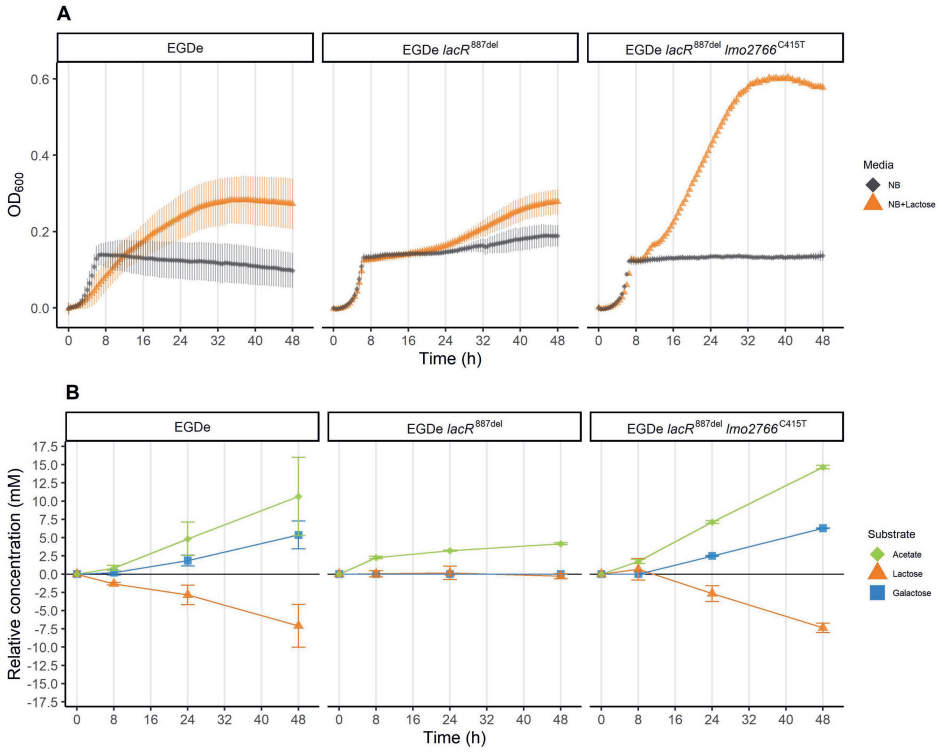

Figure 5.4: **Growth in different media (A) and lactose metabolism (B) of *L. monocytogenes* EGDe WT, EGDe *lacR*^{887del} and EGDe *lacR*^{887del} *lmo2766*^{C415T}.** **A**: Cell density growth curves in plain NB (black diamonds) and NB-lactose (orange triangles). **B**: HPLC quantification of lactose (orange triangles) consumption and galactose (blue squares) and acetate (light green diamonds) production during growth in NB-lactose. The error bars correspond to the standard deviation of the biological replicates.

5.4 Discussion

This study reiterates the diversity in lactose metabolism among *L. monocytogenes* strains, as noted in previous research (Pine et al., 1989). The strain F2365, linked to the 1985 Jalisco Cheese outbreak (Linnan et al. (1988)), exhibited inefficient lactose metabolism due to a truncated LacR. This protein regulates the *lpo* operon, *lmo2708*, and the *lmo2683-2685* operon, which are linked to lactose metabolism (Cao et al., 2019; Dalet et al., 2003; Stoll and Goebel, 2010). In the lactose-positive strain EGDe, a notably higher upregulation of *lmo2683-2685* compared to the *lpo* operon in NB-lactose medium suggests its primary role in lactose transport (Supplemental Figure 5.5). This may also offer an explanation for the earlier observation by Dalet et al. (2003), who reported similar growth in lactose containing medium of the *L. monocytogenes* LO28 wild type strain and its *lpoA* knocked-out strain. Furthermore, introducing the $lacR^{887\text{del}}$ mutation into EGDe resulted in reduced efficacy of lactose metabolism, confirming the role of this mutation in influencing lactose utilization in *L. monocytogenes*.

In an evolution experiment, the lactose-positive strain F2365 EV was derived from F2365, which contained an additional point mutation $lmo2766^{\text{C415T}}$, leading to an arginine to tryptophan substitution in Lmo2766. Growth experiments and HPLC analysis confirmed the lactose metabolism capability of F2365 EV. This was further confirmed in a double mutant EGDe $lacR^{887\text{del}}$ $lmo2766^{\text{C415T}}$ carrying the same mutations. PROSITE scanning revealed that Lmo2766 possesses a DNA-binding RpiR-type HTH domain and a phosphosugar-binding SIS domain. The HTH domain, common in prokaryotic RpiR-type regulators (Brennan and Matthews, 1989), and most RpiR-type HTH regulators typically function in sugar metabolism as a transcription repressor (Kohler et al., 2011; Sørensen and Hove-Jensen, 1996; Zhang et al., 2022), with some acting as activators (Afzal et al., 2015; Aleksandrzak-Piekarczyk et al., 2019; Yamamoto et al., 2001). The SIS domain, harboring the arginine to tryptophan substitution in F2365 EV, is found in phosphosugar isomerases, binding proteins, and regulatory proteins (Bateman, 1999), suggesting that the $lmo2766^{\text{C415T}}$ mutation could affect phosphosugar binding and alter Lmo2766's function as transcriptional regulator. RNAseq analysis showed significant upregulation of the adjacent *lmo2761-2765* operon, encoding a putative lactose PTS system (Stoll and Goebel, 2010), in F2365 EV compared to F2365, implying that Lmo2766 regulates this alternative lactose PTS system, with the $lmo2766^{\text{C415T}}$ mutation enabling lactose metabolism in *L. monocytogenes*. For RpiR-type HTH repressors, phosphosugar binding can attenuate DNA binding (Zhang et al., 2022), suggesting Lmo2766 might function similarly, with the mutation altering its conformation and DNA binding ability. Nevertheless, further research, such as employing *lmo2766* deletion mutants, is essential to determine Lmo2766's role in regulating the *lmo2761-2765* operon.

In NB-lactose medium, both F2365 and EGDe $lacR^{887\text{del}}$ displayed limited lactose utilization and slow growth after 24 hours of incubation (Figure 5.2, Figure 5.4, and Supplemental Figure 5.3). Previous *in silico* analysis identified several putative PTS lactose component genes (Stoll and Goebel, 2010), with genes like *lmo0298/0301*, *lmo0874-0876*, *lmo0914-0916*, *lmo2780/2782/2783*, and *lmo0373/0374* showing significant upregulation in F2365 in NB-lactose compared to NB-glucose after 24 hours

incubation (Supplemental Table 5.1). However, this upregulation did not translate into effective lactose consumption or galactose production, as HPLC results indicated no significant metabolic changes from 24 to 48 hours in NB-lactose for F2365 and EGDe *lacR*$^{887\text{del}}$ (Figure 5.2 and Figure 5.4), thus leaving their physiological roles uncertain in the tested conditions.

Human milk oligosaccharide N-Acetyl-D-Lactosamine (LacNAc) is comprised of an acetylglucosamine and a galactose with the same beta-1→4 glycosidic linkage as lactose (Masi and Stewart, 2021). Since the lactose operon in *Lactobacillus casei* is also involved in the transport and metabolism of LacNAc (Bidart et al., 2018), the lactose PTS systems in *L. monocytogenes* may also be able to utilize LacNAc. Indeed, lactose-positive strains EGDe and F2365 EV, but not F2365, were capable of utilizing LacNAc as shown by growth curves (Supplemental Figure 5.7). Notably, F2365 EV exhibited superior growth in NB-lactose compared to EGDe, yet their growth in NB-lacNAc was comparable. Nevertheless, this suggests that both LacR-regulated PTS systems and the alternative lactose PTS system, encompassing Lmo2762, Lmo2763, and Lmo2765, are implicated in LacNAc utilization.

Based on our results, we present a model for lactose metabolism in *L. monocytogenes* via three PTS systems as shown in Figure 5.5. In strains with a functional LacR, lactose transport is facilitated by two PTS systems: one comprising LpoA and LpoB, potentially with Lmo2708, and another involving Lmo2683-2685. Lactose is transported into the *L. monocytogenes* cell via an integral membrane EIIC porter and phosphorylated by EIIB, utilizing a phosphate group derived from phosphoenolpyruvate (PEP). Once inside, lactose-6-P is cleaved into galactose-6-P and glucose, the latter entering glycolysis as glucose-6-P, in total consuming two NAD^+ and two ATPs, and yielding two PEP molecules and two ATPs. Of these PEP molecules, one is converted to pyruvate, generating one ATP, while another one is employed by the PTS system for lactose phosphorylation, converting into pyruvate without producing ATP. Under our experimental conditions (shaking at 160 rpm) with sufficient oxygen, NAD^+ is regenerated through oxidation of NADH in the electron transport chain, allowing pyruvate to be further metabolized to acetate and CO_2, generating an additional two ATPs. Galactose-6-P needs galactose-6-phosphate isomerase, which is lacking in *L. monocytogenes*, to transform to tagatose-6-P before entering glycolysis. Our HPLC data align with the notion that *L. monocytogenes* consumes lactose and secretes the galactose moiety, as the consumption of lactose corresponds with the production of galactose, indicating that galactose-6-P may be dephosphorylated and exported by an unknown mechanism (Pine et al., 1989). When the *lmo2766*$^{\text{C415T}}$ mutation is present, an alternative PTS system formed by Lmo2762, Lmo2763, and Lmo2765 participates in lactose transport, utilizing the same metabolic pathway as the LacR-regulated systems. These lactose PTS systems, compared to the glucose PTS system that phosphorylates glucose during transport, need an extra ATP to convert glucose into glucose-6-P, which may contribute to the observed slower growth on NB-lactose compared to NB-glucose for *L. monocytogenes*.

5.5 Conclusions

This study provided a detailed study of three PTS systems in *L. monocytogenes* involved in lactose uptake and metabolism. Through an evolutionary experiment, we isolated a lactose-positive variant, F2365 EV, derived from the F2365 strain, which maintained the *lacR*$^{887\text{del}}$ mutation and gained a second mutation, *lmo2766*$^{\text{C415T}}$. Lmo2766 has been demonstrated to regulate an alternative lactose PTS system operon *lmo2761-2765*. In addition, the *lacR*$^{887\text{del}}$ mutation was found to affect the activation levels of two lactose PTS systems, encoded by *lpo* operon, *lmo2708*, and *lmo2683-2685*, which are important determinants of reduced lactose utilization efficiency in *L. monocytogenes*. Furthermore, we confirmed *L. monocytogenes*'s inability to utilize the galactose moiety of lactose, with acetate identified as a lactose metabolic byproduct under aerobic conditions. This research enhances our understanding of the metabolic capabilities and adaptability of *L. monocytogenes*, offering a broader view on lactose utilization in *L. monocytogenes*.

5.6 Declaration of Competing Interest

The authors declare that they have no known competing financial interests or personal relationships that could have appeared to influence the work reported in this paper.

5.7 Acknowledgments

This work was supported by the European Union's Horizon 2020 research and innovation programme under the Marie Sklodowska-Curie (List_MAPS) [grant agreement no 641984]. Xuchuan Ma was supported by a grant from the China Scholarship Council (File No. 201907720086).

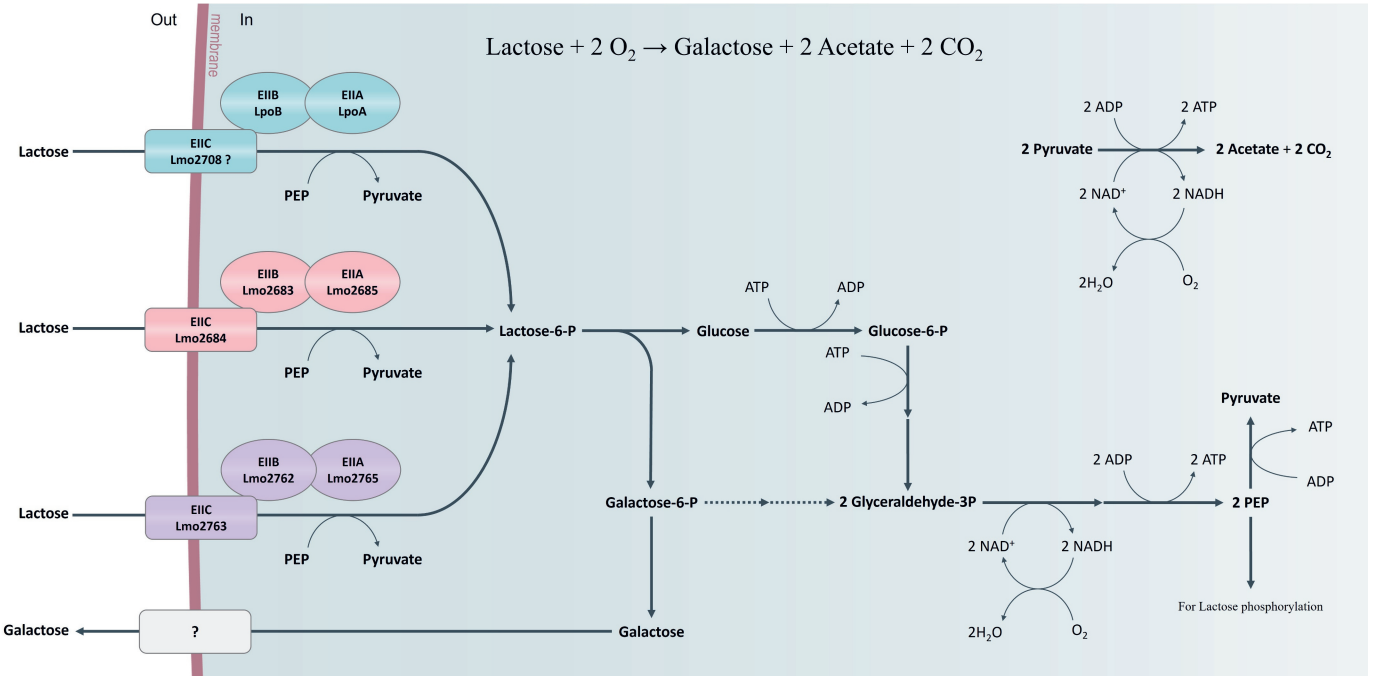

Figure 5.5: **Schematic presentation of lactose transport in *L. monocytogenes*.** With functional LacR, two PTS systems can be formed by LpoA, LpoB, possibly Lmo2708, and Lmo2683-Lmo2685. With the $lacR^{887\text{del}}$ and $lmo2766^{\text{C415T}}$ mutation, another PTS system formed by Lmo2762, Lmo2763, and Lmo2765 becomes the major lactose transport system in *L. monocytogenes*. The PTS systems transport and phosphorylate lactose into *L. monocytogenes* cells using a phosphate group derived from PEP. The lactose-6-P is hydrolyzed intracellularly to galactose-6-P and glucose. Galactose-6-P may not enter glycolysis due to the lack of galactose-6-P isomerase and is conceivably dephosphorylated and transported outside of cells as galactose. The glucose enters glycolysis as glucose-6-P and is metabolized to two PEP molecules resulting in the production of two ATPs. One of the two PEP molecules is converted to pyruvate resulting in the production of one ATP, and the other one is utilized for lactose transportation. The resulting pyruvate is further metabolized to acetate and CO_2 in the presence of oxygen and results in the production of another two ATPs. In total, the consumption of one lactose can yield three ATPs aerobically.

5.8 Supplementary Material

Supplemental Table 5.1: **The differential expression level of putative lactose PTS permease genes in F2365 comparing growing in NB-lactose to growing in NB-glucose.** The putative lactose PTS genes are identified by Stoll and Goebel (2010). The $\log_2$(Fold change) and adjusted p-value of significantly upregulated or downregulated genes are highlighted in bold

EGDe orthologs gene locus	Gene locus	Protein name	$\log_2$(Fold change)	Adjusted p-value
lmo0034	LMOf2365_0043	PTS sugar transporter subunit IIC	**1.95**	**0.001**
lmo0298	LMOf2365_0319	PTS sugar transporter subunit IIC	**2.61**	**0.000**
lmo0299	LMOf2365_0320	PTS sugar transporter subunit IIB	**1.43**	**0.006**
lmo0301	LMOf2365_0322	PTS sugar transporter subunit IIA	**2.41**	**0.003**
lmo0373	LMOf2365_0389	PTS sugar transporter subunit IIC	**3.21**	**0.000**
lmo0374	LMOf2365_0390	PTS sugar transporter subunit IIB	**2.22**	**0.002**
lmo0874	LMOf2365_0893	PTS sugar transporter subunit IIA	**3.68**	**0.001**
lmo0875	LMOf2365_0894	PTS sugar transporter subunit IIB	**8.15**	**0.000**
lmo0876	LMOf2365_0895	PTS sugar transporter subunit IIC	**4.42**	**0.000**
lmo0901	LMOf2365_0922	PTS sugar transporter subunit IIC	0.43	0.363
lmo0914	LMOf2365_0936	PTS sugar transporter subunit IIB	**5.30**	**0.000**
lmo0915	LMOf2365_0937	PTS sugar transporter subunit IIC	**7.91**	**0.000**
lmo0916	LMOf2365_0938	PTS sugar transporter subunit IIA	**4.48**	**0.000**
lmo1095	LMOf2365_1109	PTS sugar transporter subunit IIB	**-1.10**	**0.000**
lmo1719	LMOf2365_1743	PTS sugar transporter subunit IIA	**-2.40**	**0.000**
lmo1720	LMOf2365_1744	PTS sugar transporter subunit IIB	**-1.64**	**0.000**
lmo2259	LMOf2365_2292	PTS sugar transporter subunit IIA	-0.03	0.919
lmo2373	LMOf2365_2344	PTS sugar transporter subunit IIB	**1.26**	**0.000**
lmo2683	LMOf2365_2663	PTS sugar transporter subunit IIB	1.01	0.135
lmo2684	LMOf2365_2664	PTS sugar transporter subunit IIC	**1.44**	**0.006**
lmo2685	LMOf2365_2665	PTS sugar transporter subunit IIA	**1.35**	**0.007**
lmo2708	LMOf2365_2688	PTS sugar transporter subunit IIC	0.80	0.151
lmo2762	LMOf2365_2752	PTS sugar transporter subunit IIB	**3.22**	**0.007**
lmo2763	LMOf2365_2753	PTS sugar transporter subunit IIC	**1.77**	**0.000**
lmo2765	LMOf2365_2755	PTS sugar transporter subunit IIA	1.41	0.073
lmo2780	LMOf2365_2771	PTS sugar transporter subunit IIA	**5.95**	**0.000**
lmo2782	LMOf2365_2773	PTS sugar transporter subunit IIB	**6.28**	**0.000**
lmo2783	LMOf2365_2774	PTS sugar transporter subunit IIC	**6.90**	**0.000**

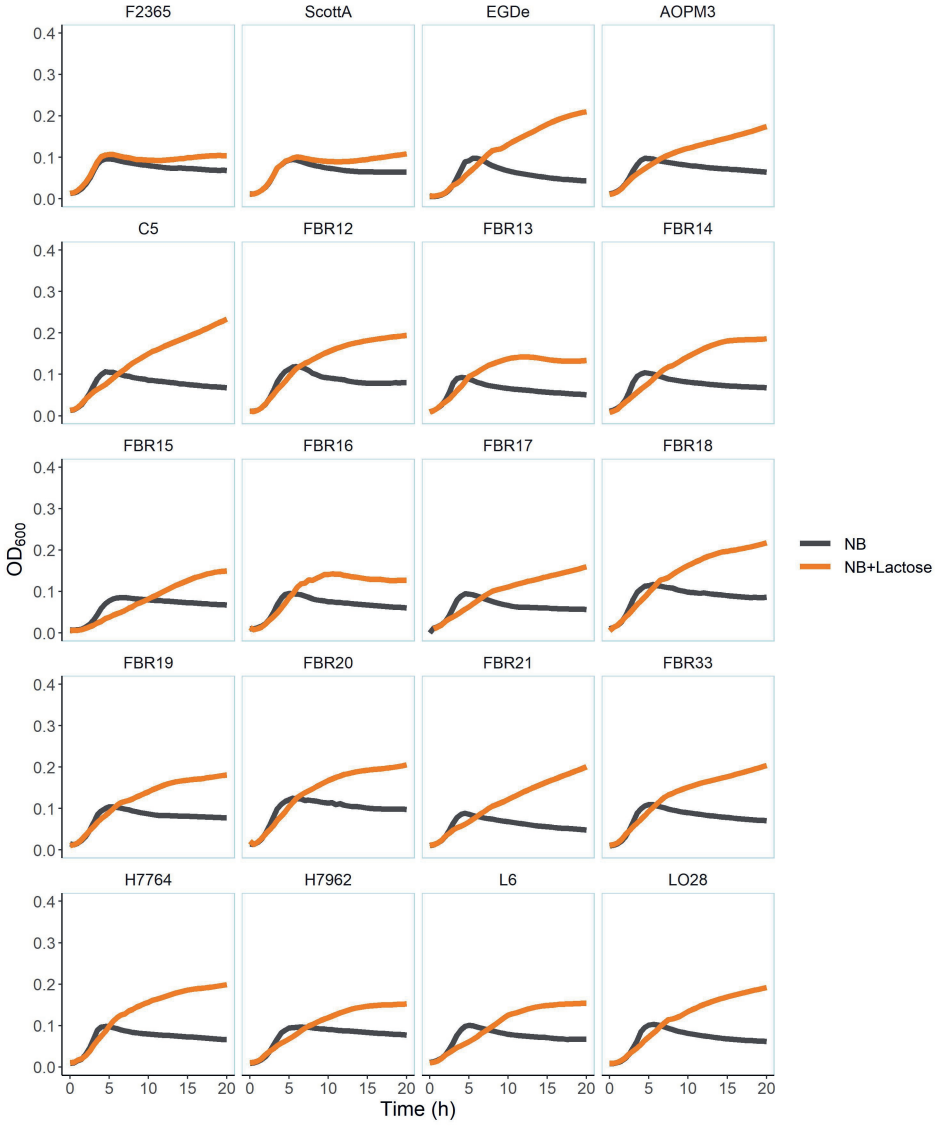

Supplemental Figure 5.1: ***L. monocytogenes* strain diversity in lactose metabolism.** Cell density growth curves in plain NB (black) and NB-lactose (orange) are shown for the 20 strains of the FHM collection. OD_{600} measurements were taken every 30 min in the Spectramax M2 plate reader during incubation at 30°C for 20 h. The data corresponds to the average of two biological replicates with three technical replicates each.

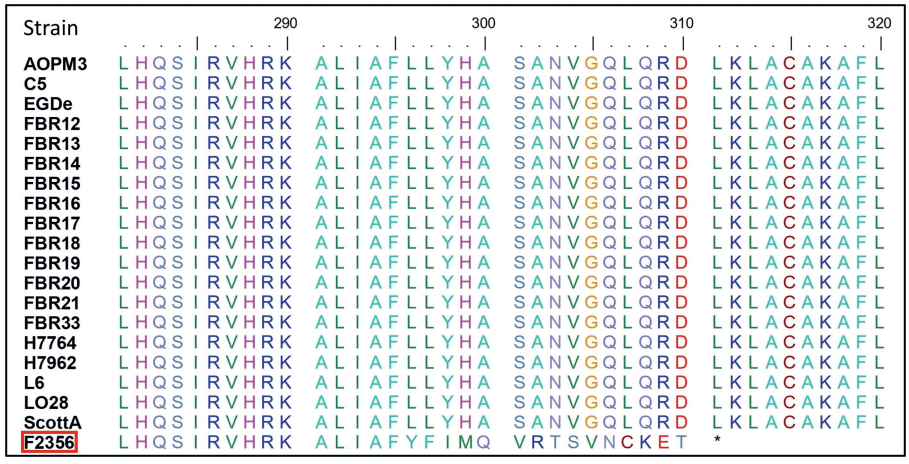

Supplemental Figure 5.2: **The protein amino acid sequence alignment of LacR in 20 strains.** Numbers above the alignment indicate the amino acid position in the LacR protein. The strain F2365 has been highlighted by a red box. The asterisk at amino acid position 311 represents the stop codon.

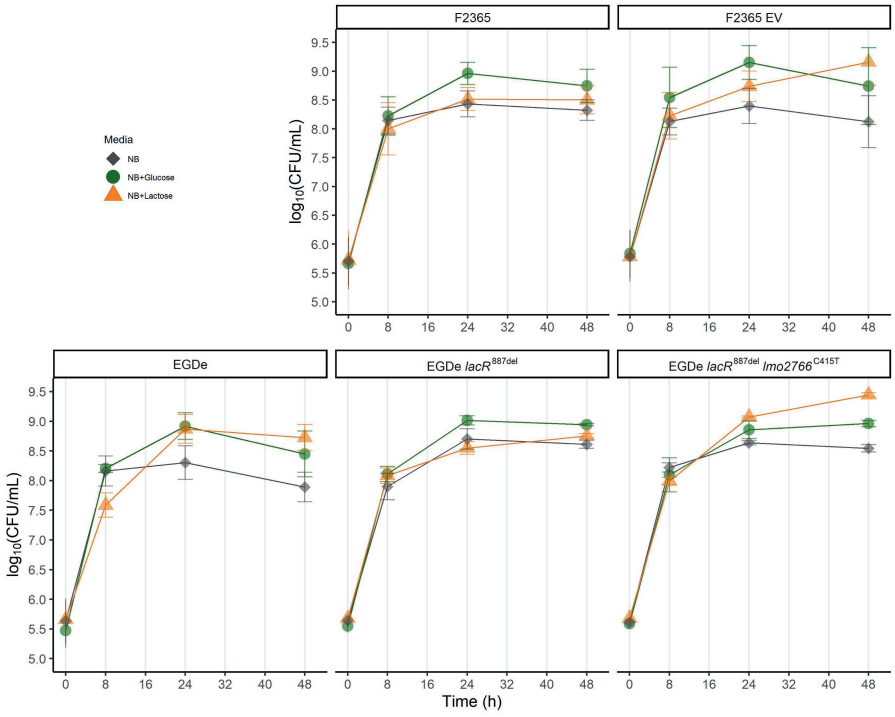

Supplemental Figure 5.3: **CFU-based planktonic growth of *L. monocytogenes* F2365, F2365 EV, EGDe WT, EGDe *lacR*^{887del} and EGDe *lacR*^{887del} *lmo2766*^{C415T} in plain NB (black diamonds), NB-glucose (green circles), and NB-lactose (orange triangles).** The error bars correspond to the standard deviation of the biological replicates.

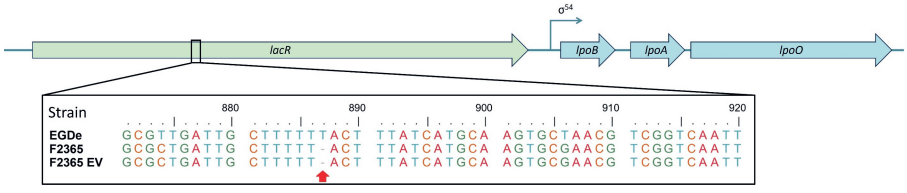

Supplemental Figure 5.4: **The gene cluster of *lacR* and *lpo* operon in *L. monocytogenes* and the DNA sequence alignment of *lacR* in EGDe, F2365, and F2365 EV.** Numbers above the alignment indicate the nucleotide position in the *lacR* gene. The point deletions *lacR*^{887del} in F2365 and F2365 EV have been highlighted by a red arrow.

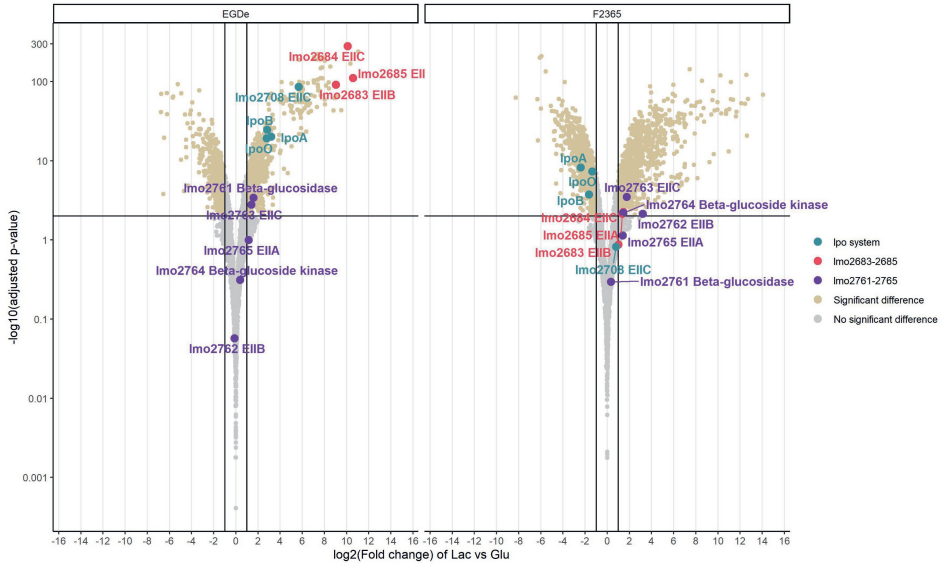

Supplemental Figure 5.5: **Volcano plot of EGDe (left) and F2365 (right) RNAseq data comparing growing in NB-lactose to growing in NB-glucose.** The -$\log_{10}$(p-value) is plotted against the $\log_2$(Fold change of gene expression level in NB-lactose to NB-glucose). The horizontal line represents the cutoff of the p-value (0.01), and the vertical lines represent the cutoff of $\log_2$(Fold change) (i.e. 1 $\log_2$(Fold change)). Light brown dots represent significantly upregulated or downregulated proteins. Cyan, red, and purple dots represent the genes of *lpo* system, *lmo2683-2685* operon, and *lmo2761-2765* operon, respectively.

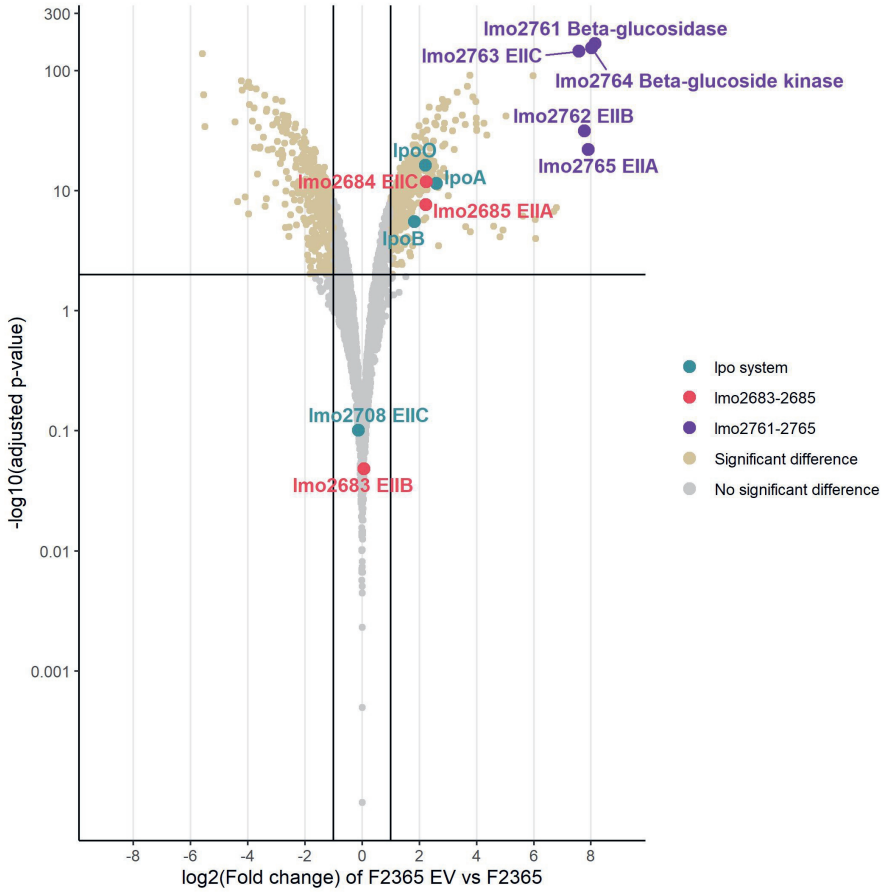

Supplemental Figure 5.6: **Volcano plot of RNAseq data comparing F2365 EV to F2365 growing in NB-lactose.** The -$\log_{10}$(p-value) is plotted against the $\log_2$(Fold change of gene expression level in F2365 EV to F2365). The horizontal line represents the cutoff of the p-value (0.01), and the vertical lines represent the cutoff of $\log_2$(Fold change) (i.e. 1 $\log_2$(Fold change)). Light brown dots represent significantly upregulated or downregulated proteins. Cyan, red, and purple dots represent the genes of *lpo* system, *lmo2683-2685* operon, and *lmo2761-2765* operon, respectively.

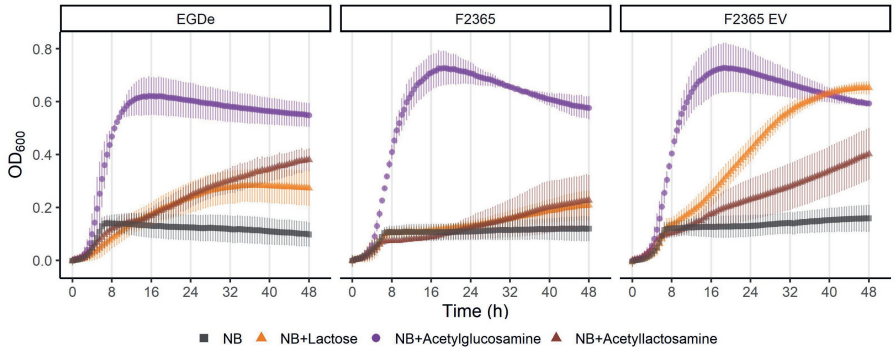

Supplemental Figure 5.7: **Cell density growth curves of *L. monocytogenes* EGDe, F2365 and F2365 EV in plain NB (black diamonds), NB-lactose (orange triangles), NB-Acetylglucosamine (purple circles), and NB-Acetyllactosamine (brown triangles).** The error bars correspond to the standard deviation of the biological replicates.

6

General Discussion

Xuchuan Ma

Strain diversity and population heterogeneity are important in the survival, adaptation, and persistence of *Listeria monocytogenes* across various niches, including those in food production environments. In this thesis, we first focused on *rpsU* mutants, which play a significant role in the overall survival capability of the population under diverse stress conditions. In **Chapter 2**, we presented evidence that loss of RpsU, leading to multiple stress resistance and reduced fitness phenotypes, can be reversed by single-point mutations in *rpsB*. This finding underscores the regulatory role of ribosomal proteins, particularly *rpsU* and *rpsB*, in stress response and fitness of *L. monocytogenes*. To explore the molecular mechanisms underlying phenotypic changes induced by *rpsU* mutations, the *rpsU*^{G50C} mutation was introduced into the *L. monocytogenes* EGDe wildtype (WT) strain and into the Δ*sigB*, Δ*rsbV*, and Δ*rsbR1* mutant strains in **Chapter 3**. Two important results were reported in this chapter: 1., SigB is activated in the *rpsU*^{G50C} mutants but through an unknown mechanism distinct from the classical stressosome and RsbV/RsbW partner switching model; 2., the reduced growth rate is not linked to the SigB activation, even though there is normally a trade-off between growth and SigB-mediated stress protection (Guerreiro et al., 2020a). Thus, the ribosome likely serves as a key regulatory element in *L. monocytogenes* for fitness and stress response.

6.1 RpsU and RpsB functions

Translation in bacteria is conducted by the 70S ribosome, comprising the small 30S subunit and the large 50S subunit (Keiler, 2015). The initiation of this translation process, the rate-limiting step for protein synthesis, depends on the assembly of translation initiation factors (IF) IF1, IF2, IF3, mRNA, and the initiator tRNA on the 30S subunit (Keiler, 2015; Laursen et al., 2005; Shah et al., 2013). This process is driven by the interaction between the mRNA's Shine-Dalgarno (SD) sequence and the anti-SD (aSD) sequence at the 3' end of 16S rRNA (Shine and Dalgarno, 1974; Wen et al., 2021). During the 30S subunit assembly, RpsB (also named uS2) and RpsU (also named bS21) are incorporated into the 30S subunit fraction in the last stage, forming the mRNA exit channel with the 3 end of the 16S rRNA (Sashital et al., 2014). Recent protein structure analysis of *Escherichia coli*'s ribosomes revealed that the RpsU C-terminal residues are near the SD helix formed between the 16S rRNA aSD sequence and the mRNA SD sequence (Watson et al., 2020). Furthermore, RpsB and RpsU anchor and reinforce the binding of the ribosome and 16S rRNA to RpsA (bS1), which acts as a dynamic mesh to modulate the mRNA binding, folding and movement (D'Urso et al., 2023; Loveland and Korostelev, 2018). These findings clarify the role of RpsU during the translation initiation, including promoting base pairing between SD and aSD sequences and reinforcing RpsA's binding to 16S rRNA. Thus, the loss or structural disruption of RpsU can divert the aSD sequence from the mRNA exit pathway, weaken RpsA binding, delay translation initiation, reduce protein synthesis, and ultimately lower growth rates. This mechanism likely underpins the reduced growth rates observed in the *L. monocytogenes rpsU* deletion mutants and *rpsU*^{G50C} mutants. Moreover, this thesis demonstrates that single-point mutations in RpsB can reverse phenotypic changes caused by the loss of RpsU in *L. monocytogenes*. Notably, the maximum specific growth rates of strains 14EV1 and 14EV2, although higher

than that of V14, are still significantly lower than WT (**Chapter 2**, Figure 2.1). A possible reason is that the *rpsB* mutation may only be able to enhance the binding of RpsA but not the paring of the SD-aSD sequences. Therefore, translation initiation affected by *rpsU* or *rpsB* mutations could explain the observed growth rate changing in *L. monocytogenes*. Further structural analyses are needed to elucidate the SD-aSD pairing and RpsA binding states in these *rpsU* and *rpsB* mutants.

6.2 *rpsU* and *rpsB* variants in other bacteria

Table 6.1: **The *rpsU* and *rpsB* variants**

Species	Isolation procedure	Mutation	Phenotypic change	Reference
Bacillus subtilis	isolated from *plsX103* mutant grown on LB plates at 39°C	nonsense mutation in the second codon of *rpsU* (TCA codon to TGA)	cell separation and swimming defects, robust biofilm formation	Takada et al. (2014)
Staphylococcus aureus	isolated from bacteraemic patient undergoing antibiotic treatment with vancomycin	nucleotide insertion in *rpsU* that led to a frameshift mutation from the fourth amino acid onwards in RpsU	slower growth rate, thicker cell walls, increased resistance to lysostaphin-mediated cell wall lysis, and increased resistance to vancomycin	Basco et al. (2019)
Pseudomonas aeruginosa	isolated after infection by podovirus AB09	a single nucleotide deletion resulted in premature stop	resisted infection by phage AB09, very poor growth	Latino et al. (2019)

Apart from the variants discussed in this thesis, variants with mutations in the *rpsU* or *rpsB* genes have been reported in other studies, leading to significant phenotypic changes (Table 6.1). As elaborated in **Chapter 3**, mutations in *rpsU* have been identified in *Bacillus subtilis* and *Staphylococcus aureus*, each inducing distinct phenotypic alterations. In *B. subtilis*, a nonsense mutation at the second codon of *rpsU* results in impaired cell separation, defective motility, and robust biofilm formation (Takada et al., 2014). In *S. aureus*, a frameshift mutation from the fourth amino acid in RpsU leads to increased resistance to vancomycin and lysostaphin, thicker cell walls, and a reduced growth rate (Basco et al., 2019). Similar alterations were observed in the *rpsB* variant of *Pseudomonas aeruginosa* (Latino et al., 2019). In *P. aeruginosa*, a single nucleotide deletion leading to a premature stop codon has been identified in a phage AB09 resistant variant, which exhibited poor growth (Latino et al., 2019). Remarkably, all these variants, including the *L. monocytogenes* variants reported in this thesis, demonstrate altered growth behaviors and stress resistant capacities. This consistent pattern implies that ribosomal proteins, particularly RpsU and RpsB, play a crucial regulatory role in the fitness and resistance trade-off of bacteria.

6.3 RpsU and RpsB may influence SD sequence preference

The regulatory roles of RpsU and RpsB may be linked to their influence on the ribosome's preference for mRNA sequences with varying ribosome-binding sites (RBS). The RBS sequence, extending from the SD sequence to the first 5-6 codons of the coding sequence, plays a crucial role in translation efficiency and fidelity, thereby directly affecting protein abundance and quality (Asahara et al., 2021; Faure et al., 2016; Trabelsi et al., 2021). The SD sequence is particularly influential in this context (Asahara et al., 2021). Recent studies demonstrated that RpsU and RpsB can alter ribosomal preference for different RBS sequences, suggesting their potential regulatory impact on gene expression (Acosta-Reyes et al., 2023; Aseev et al., 2013; Chen et al., 2022; Jha et al., 2021; McNutt et al., 2023; Mizuno et al., 2019; Trautmann et al., 2023; Trautmann and Ramsey, 2022). In *E. coli*, *rpsB* mutants with missense mutations or decreased protein levels exhibit enhanced translation of leaderless mRNAs (lmRNA), which lack the SD sequence (Acosta-Reyes et al., 2023; Aseev et al., 2013). Interestingly, these changes can be reversed by supplementing with an excess of RpsA (Aseev et al., 2013). Protein structural analysis of one such *E. coli rpsB* mutant strain revealed that ribosomes deficient in RpsB also lack RpsU (Acosta-Reyes et al., 2023). In *Flavobacterium johnsoniae*, RpsU is implicated in the sequestration of the aSD sequence in the ribosome, with mutations or depletion of *rpsU* leading to increased translation of genes with strong SD sequences (Jha et al., 2021; McNutt et al., 2023). In *Francisella tularensis*, a homolog of RpsU, bS21-2, enhances translation initiation of mRNAs with imperfect SD sequences, thereby modulating virulence genes (Trautmann et al., 2023; Trautmann and Ramsey, 2022). Furthermore, the *rpsU* gene has been detected in various viruses, encoding RpsU homologs capable of integrating into bacterial ribosomes and competing with native cellular counterparts (Mizuno et al., 2019). These phage-encoded RpsU proteins may hijack the bacterial ribosome, preferentially translating phage mRNA over host transcripts (Chen et al., 2022). Thus, it appears to be a conserved strategy across diverse microorganisms to utilize RpsU or RpsB in regulating gene expression via altering SD sequence preference, thereby modulating fitness and enhancing adaptation.

In the *L. monocytogenes* EGD-e reference genome (NC_003210.1), 197 distinct SD sequences are identified among 2,768 coding sequences (data not shown). The most common SD sequences are AGGAGG, TGGAGG, and AGGAGA, appearing 557, 216, and 204 times, respectively. The 16S rRNA aSD sequence in the EGD-e reference genome is CCUCCU, complementing the most prevalent SD sequence, AGGAGG. Intriguingly, both the *sigB* gene and its antagonist, the anti-SigB factor *rsbW*, exhibit rare SD sequences. The SD sequence of *sigB* is AGCAGG, shared with only six other genes, while *rsbW* possesses the SD sequence AGAGGG, common to 18 genes. To date, there has been no specific research focusing on the SD sequences and translation efficiency in *L. monocytogenes*. However, studies in *E. coli* demonstrate a strong positive correlation between translation efficiency and guanine content, and a negative correlation with cytosine content (Kuo et al., 2020). Given the conservation of the aSD sequence CCUCCU across diverse organisms, including *E. coli* and *L. monocytogenes* (Amin et al., 2018; Shine and Dalgarno, 1974), it is plausible that in

L. monocytogenes, the cytosine content of SD sequences also negatively correlates with translation efficiency. Consequently, *sigB* is likely to have lower translation efficiency compared to *rsbW* when using wild-type ribosomal proteins. As discussed in the previous paragraph, mutations or deletions in *rpsU* might cause the aSD sequence to lack structural support from RpsU, deviating from the normal mRNA exit pathway. This deviation could enhance the translation efficiency of imperfect SD sequences, such as the AGCAGG of *sigB*. In such scenarios, the balance between SigB and the anti-SigB factor RsbW could be disrupted. This effect might be further amplified due to the positive regulation of SigB itself, potentially leading to the SigB activation and upregulation of the SigB regulon. The mutation of RpsB may partially restore the position of aSD, potentially via enhancing the binding of RpsA, and thus restore the translation efficiency of genes including *rsbW*, rebalancing the SigB-RsbW balance. In this manner, mutations in *rpsU* and *rpsB* may fine-tune the translation efficiency of *sigB* and *rsbW*, providing a RsbV-independent SigB activation regulation mechanism. Further research is required to investigate this hypothesis by modifying the SD sequence or RBS of *sigB* and *rsbW* in *rpsU* and *rpsB* mutants.

6.4 Obg: a potential RsbV-independent SigB activator

Another potential RsbV-independent SigB activation mechanism may be linked to GTPase proteins, which interact with both the ribosome and RsbW. The GTPase protein HflXr (Lmo0762) was upregulated in the *rpsU* mutants, including EGDe-*rpsU*^{G50C}, Δ*sigB*-*rpsU*^{G50C}, Δ*rsbV*-*rpsU*^{G50C}, and V14, but not in the *rpsU* and *rpsB* double mutants 14EV1 and 14EV2 (see **Chapter 2** and **Chapter 3**). HflXr, a member of the GTPase OBG-HflX-like superfamily, is known to alter the ribosomal conformation, thereby increasing resistance to macrolide and lincosamide antibiotics (Duval et al., 2018; Koller et al., 2022). Intriguingly, another member of this superfamily, Obg (Lmo1537/ObgE), has been previously linked to SigB activation in various studies (Kint et al., 2014; Scott and Haldenwang, 1999; Verstraeten et al., 2011). In *B. subtilis*, strains depleted of Obg failed to activate SigB in response to environmental stresses, such as ethanol treatment and heat shock (Scott and Haldenwang, 1999). Further research revealed that a substitution in the Obg carboxy terminus blocked sporulation and impaired stress regulon induction in *B. subtilis* (Kuo et al., 2008). This study also indicated that the inhibition of SigB activation occurred downstream of RsbT release in the SigB activation pathway, most likely due to an interaction between Obg and RsbW (Kuo et al., 2008). Interestingly, this interaction is not exclusive to *B. subtilis*, since homologs of Obg have also been found to interact with RsbW homologs in *Mycobacterium tuberculosis* (Kuo et al., 2008; Sasindran et al., 2011; Scott and Haldenwang, 1999). Although the exact mechanism by which Obg modulates the activity state of SigB is not yet certain, this protein may play a crucial role in the SigB activation in the *rpsU* mutants.

To investigate the potential role of Obg in *L. monocytogenes rpsU* mutants, the *obg* gene was deleted in both the EGDe WT and the EGDe-*rpsU*^{G50C} mutant, resulting in the construction of Δ*obg* and the double mutant Δ*obg*-*rpsU*^{G50C}. Interestingly,

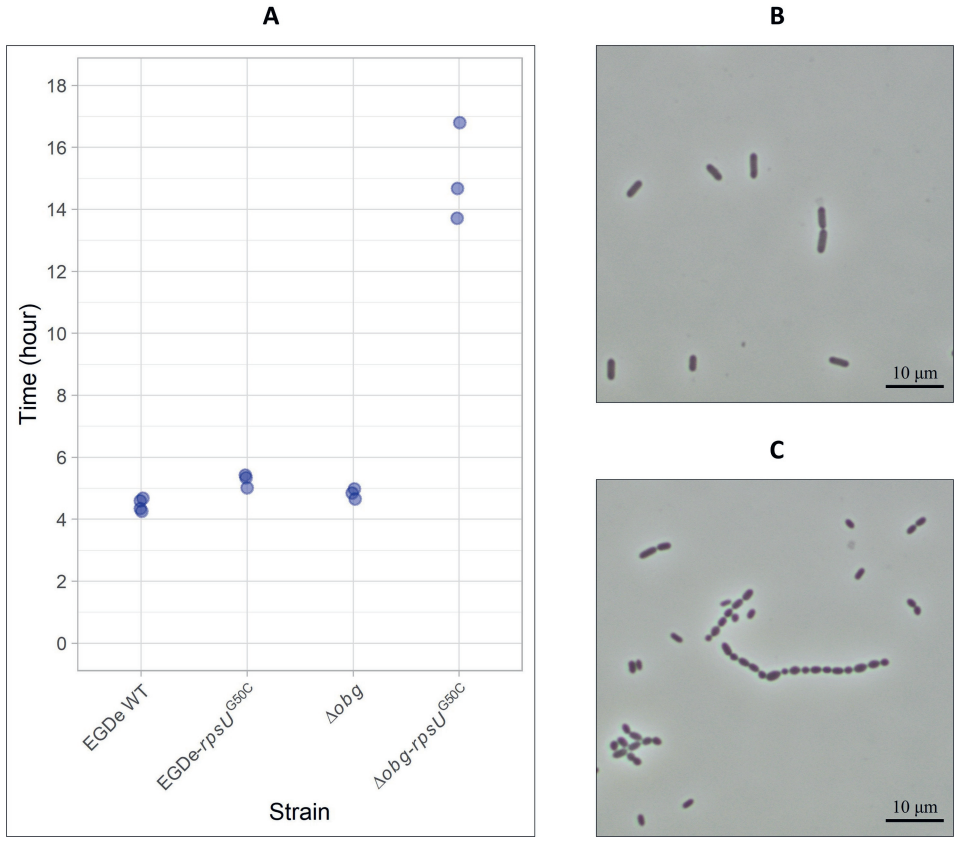

Figure 6.1: **Growth and morphology characteristics of *L. monocytogenes* mutants Δ*obg* and Δ*obg-rpsU*^{G50C}.** **A**, Time of *L. monocytogenes* Δ*obg* and Δ*obg-rpsU*^{G50C} 0.5% (v/v) inoculum to reach late-exponential growth phase in fresh BHI broth at 30°C with 160 rpm shaking. Individual points represent biological reproductions. **B & C**, Microscopic picture of *L. monocytogenes* Δ*obg* (**B**) and Δ*obg-rpsU*^{G50C} (**C**). Unpublished data.

while the Δ*obg* mutant exhibited normal growth, the double mutant Δ*obg-rpsU*^{G50C} demonstrated a significant decrease in growth rate. Inoculating a single colony into 20 mL BHI broth and culturing it at 30°C with shaking at 160 rpm, the Δ*obg-rpsU*^{G50C} required over 40 hours to reach an OD_{600} value typical of a normal overnight (ON) culture. In addition, when fresh BHI broth was inoculated with a 0.5% (v/v) Δ*obg* ON culture, it took approximately 4.5 hours to reach the late-exponential growth phase (OD_{600} = 0.4-0.5) at 30°C and 160 rpm, which is similar to the EGDe WT (Figure 6.1, A). However, under identical conditions, the 0.5% (v/v) Δ*obg-rpsU*^{G50C} culture required more than 13.5 hours to achieve the same growth phase, which is much longer than the single mutant EGDe-*rpsU*^{G50C}. Microscopic examination of the ON cultures revealed that the single mutants Δ*obg* and EGDe-*rpsU*^{G50C} maintained similar cell shape and size to the EGDe WT (Figure 6.1, B). In contrast, the Δ*obg-rpsU*^{G50C} cells displayed considerable size variation and formed long chains that could not be broken by vortexing (Figure 6.1, C). Despite these dramatic changes in the Δ*obg-rpsU*^{G50C} mutant, both Δ*obg* and Δ*obg-rpsU*^{G50C} mutants were subjected to heat stress, following the procedure outlined in **Chapter 3**. The Δ*obg* mutant exhibited a similar reduction level to the EGDe WT, with approximately ~5 $\log_{10}$ CFU/mL, whereas the Δ*obg-rpsU*^{G50C} mutant showed a reduction level comparable to the EGDe-*rpsU*^{G50C} mutant, at around ~4 $\log_{10}$ CFU/mL. However, these results do not necessarily imply that the Δ*obg-rpsU*^{G50C} mutant is more heat-resistant than the Δ*obg* mutant. The cell chaining observed in Δ*obg-rpsU*^{G50C} could lead to an overestimation of stress resistance. Even if only one cell in a chain survives the heat treatment, it could form the same number of colonies as the entire cell chain prior to heat exposure. Nevertheless, the significant growth reduction and cell morphology changes in Δ*obg-rpsU*^{G50C} suggest an interaction between RpsU and Obg in *L. monocytogenes*. Further investigations into the SigB activation level in the double mutant Δ*obg-rpsU*^{G50C} are warranted, potentially using methods such as an EGFP-based reporter with a SigB promoter (Utratna et al., 2012).

6.5 *rpsU* is conserved at both DNA and protein sequence level

Despite the potential fitness and stress resistance regulatory functions of *rpsU* in *L. monocytogenes*, this gene is notably conserved at the DNA level in the NCBI *L. monocytogenes* genome database, as discussed in **Chapter 4**. To further analyze the conservation of *rpsU* at the protein sequence level, the BLAST results for all EGDe coding sequences were translated *in silico*, and protein variation levels were calculated following Equation 6.1, which was similar as the gene variation level calculation equation described in **Chapter 4**.

$$Protein\ Variation = \frac{N_{protein\ type}}{N_{total} \cdot Length_{protein}} \tag{6.1}$$

where $N_{protein\ type}$ is the number of protein sequence types after *in silico* translation of the gene; N_{total} is the total number of protein sequences of the *in silico* translated

genes that were found by BLAST; $Length_{protein}$ is the maximum length of the *in silico* translated protein sequence.

As shown in Figure 6.2, RpsU again emerges as one of the most conserved proteins. However, several other proteins exhibit similar or even lower levels of variation, including the ribosomal protein RpsK, the elongation factor G encoded by *fusA*, and the flotillin-like protein FloA. The low sequence variation in these proteins suggests that changes in their protein sequences may significantly impact the phenotype of *L. monocytogenes*. However, the outstanding DNA conservation level of *rpsU* indicates that synonymous mutations in *rpsU* could also impact the fitness of *L. monocytogenes*. Synonymous mutations, while not altering the protein's primary structure, can modify mRNA sequences. These alterations can influence translation elongation rates, co- and post-translational protein folding, and ultimately affect bacterial fitness (Hunt et al., 2019; Jiang et al., 2023; O'Brien et al., 2014; Walsh et al., 2020; Yu et al., 2015). The pronounced conservation of the *rpsU* gene at the DNA level suggests that the folding and function of the RpsU protein may be sensitive to changes in the mRNA sequence and subsequent alterations in the elongation rate. This hypothesis warrants further investigation, potentially by introducing synonymous mutations into the *L. monocytogenes rpsU* gene.

6.6 *rpsU* mutation present in *L. monocytogenes* persistent strain

To further analyze the variation of *rpsU* and the origins of related variants, a phylogenetic analysis was performed for all unique *rpsU* DNA and protein sequence types. Additionally, the prevalence and origin of each DNA and protein sequence type were annotated, except for the most abundant unique sequence type (Figure 6.3 and Supplemental Figure 6.1). Out of the 51,784 analyzed *L. monocytogenes* genomes, including 49 genomes with an *rpsU* mutation, there are ten different *rpsU* gene sequence types (type A to J in Figure 6.3) and six protein sequence types (type A to F in Supplemental Figure 6.1)). The gene sequence type A and the protein sequence type A are the same as the EGDe *rpsU* gene sequence and protein sequence, respectively. Notably, the synonymous mutation $rpsU^{C149T}$ (sequence type E in Figure 6.3) is present in 28 samples, the majority of which are clinical isolates. To further explore the relationship among these 28 samples, core genome single nucleotide polymorphism (SNP) analysis was conducted together with the reference genomes of EGDe and 10403S. Detailed sample information was annotated on the SNP matrix heatmap (Figure 6.4). Interestingly, 18 of these clinical isolates, which were isolated in Germany, Austria, Italy, and Denmark from 2013 to 2020, exhibit few SNPs (<21) among themselves. Further maximum likelihood phylogenetic tree analysis of these 18 strains also showed that these strains were clustered in a monophyletic clade with a bootstrap more than 90% (Figure 6.4). Therefore, these strains meet the criteria to be considered as originated from the same source of contamination (Pightling et al., 2018). BioProject information (PRJEB48063) suggests that these samples most likely related to smoked and graved salmon products. The variation in isolation times suggests that these strains from the same source might have persisted in the

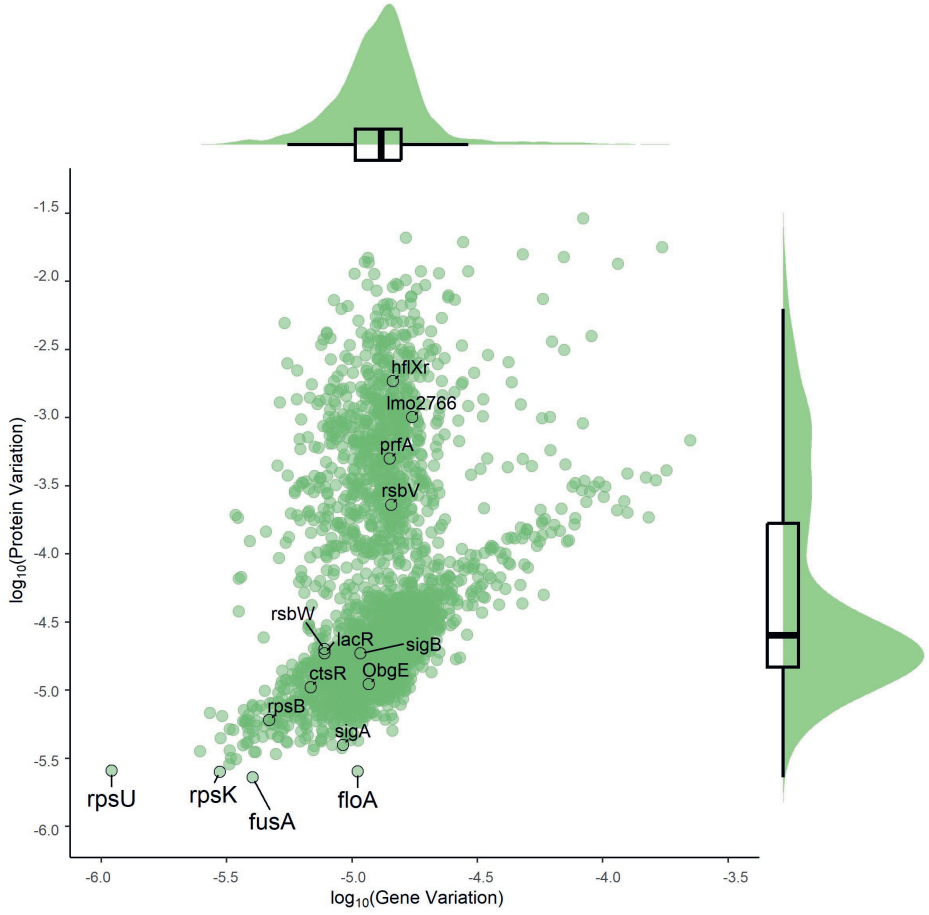

Figure 6.2: ***L. monocytogenes* gene and protein variation levels in the genome database.** The gene variation was calculated based on the BLAST results of the *L. monocytogenes* genome database by using coding sequences of *L. monocytogenes* EGD-e reference genome (NC_003210.1) as queries. The gene BLAST results were *in silico* translated and the resulted protein sequences were used to calculated the protein variation. The genes that are discussed in this thesis are labeled. The genes with similar or lower protein variation level than *rpsU* are labeled with larger text.

salmon production environment for several years. Furthermore, if the synonymous mutation in *rpsU* affects the phenotype as discussed previously, it may contribute to the persistence of these clinical isolates. In addition, a similar analysis was performed for the five environmental variants with the mutation $rpsU^{C34T}$ (sequence type I in Figure 6.3), leading to the amino acid substitution $RpsU^{L12F}$ (protein sequence type E in Supplemental Figure 6.1). All five environmental samples, isolated from water or water sediment in Salinas, California, USA, from 2013 to 2016, had few SNPs (<17) among themselves and also were clustered in a monophyletic clade with a bootstrap more than 90%. (Supplemental Figure 6.2). Therefore, although *rpsU* mutations have not been identified in previous studies investigating persistent *L. monocytogenes* strains (Castro et al., 2021; Cherifi et al., 2018; Lucchini et al., 2023; Palma et al., 2020; Simmons et al., 2014; Stasiewicz et al., 2015), current results indicate that some *rpsU* mutants may persist in certain environments and may repeatedly contaminate food.

6.7 Lactose utilization and dairy product contamination

As discussed in **Chapter 5**, strain F2365, linked to the 1985 Jalisco Cheese outbreak (Linnan et al., 1988), exhibited inefficient lactose metabolism due to a truncated LacR. The $lacR^{887del}$ mutation was found to affect the activation levels of two lactose PTS systems, encoded by the *lpo* operon, *lmo2708*, and *lmo2683-2685*, which are important determinants of reduced lactose utilization efficiency in *L. monocytogenes*. This finding prompts further investigation into the prevalence of mutations in the transcriptional regulator LacR within the *L. monocytogenes* genome database and the potential connection to the source of the isolates. Leveraging the genome database construction pipeline from **Chapter 4**, a *L. monocytogenes* food isolates genome database was compiled, encompassing 14,457 genome records. Within this dataset, 2.3% (326) genomes were identified with truncated LacR, which was defined as less than 80% protein sequence length compared to the EGDe LacR. (Table 6.2). Surprisingly, this incidence of truncated LacR was higher in a subset of 1,741 dairy product isolates, where 11.2% (195) genomes exhibited this feature. Fisher's Exact test confirmed that truncated LacR was significantly ($P < 0.001$) over-represented in dairy product isolates. Consequently, the prevalent association between truncated LacR and *L. monocytogenes* dairy isolates suggests that the loss of LacR-mediated lactose utilization capacity might lead to a fitness advantage in lactose-rich environments.

Table 6.2: **The prevalence of truncated and not truncated LacR in food isolates.** The percentage of truncated and not truncated LacR within each category of food isolates is indicated in brackets

	Dairy isolates	Non-Dairy isolate	Unknown category food isolates	total
LacR truncated	195 (11.2%)	54 (0.8%)	77 (1.3%)	326 (2.3%)
LacR not truncated	1546 (88.8%)	6762 (99.2%)	5823 (98.7%)	14131 (97.7%)
total	1741 (100%)	6816 (100%)	5900 (100%)	14457 (100%)

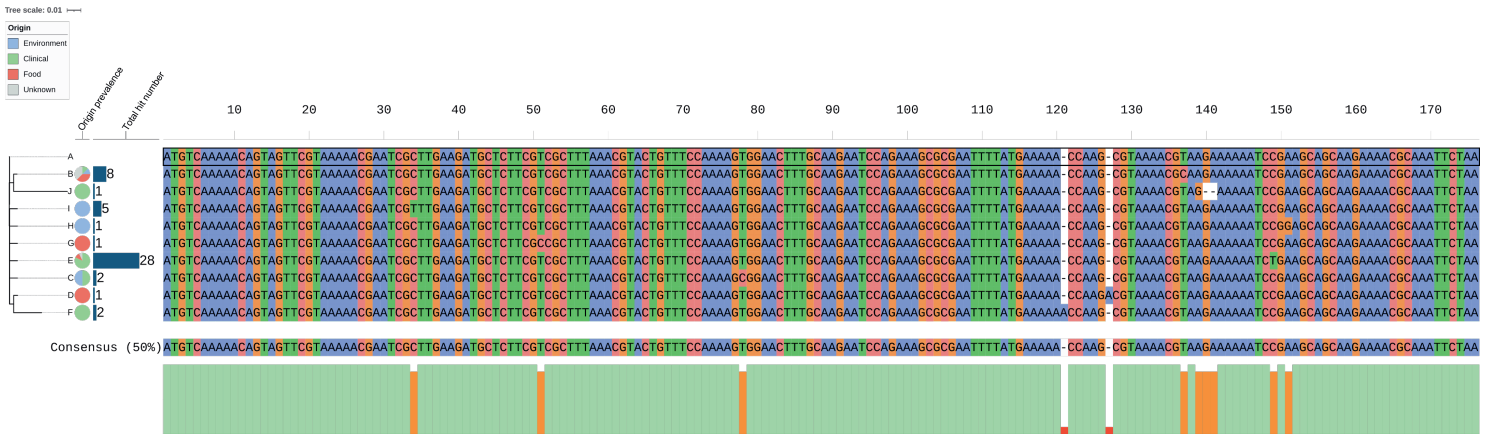

Figure 6.3: **Neighbour-joining tree based on *rpsU* BLAST results.** Each tip of the tree represents one *rpsU* unique sequence type, and type A is the same as EGDe *rpsU* sequence. For each *rpsU* unique sequence type except type A, isolation origin prevalence (pie chart) and total BLAST hit number (bar chart) are annotated next to the tree. The sequence alignment is also annotated with a consensus sequence and conservation barplot (below the alignment). The conservation barplot is colored based on conservation value with green (>95%), orange (>30%) and red (<30%).

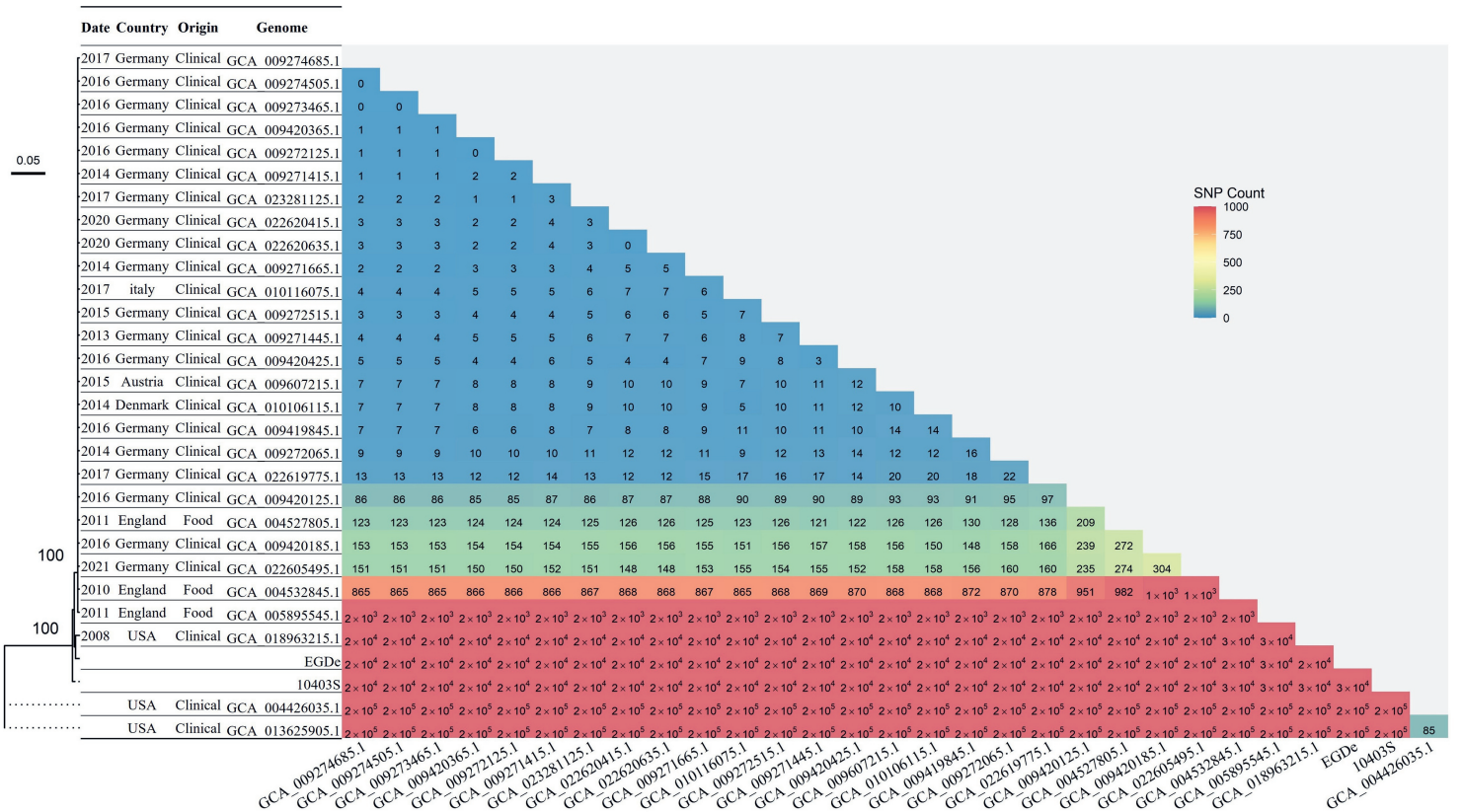

Figure 6.4: **Phylogenetic analysis and core genome SNP matrix of EGDe, 10403S and twenty eight samples with the same mutation *rpsU*$^{\mathbf{C149T}}$.** Maximum likelihood phylogenetic tree was constructed by using the program RAxML (8.2.12) with GTRCAT model and 1,000 rapid bootstraps. Branch labels indicate support values in percentage for 1,000 bootstrap replicates. Bootstrap values less than 90% are not shown. The number and color in the core genome SNP matrix heatmap represent the amount of core genome SNPs between the samples indicated at the row and column. The attribution data of each genome, except reference genome EGDe and 10403S, are annotated between the phylogenetic tree and the heatmap.

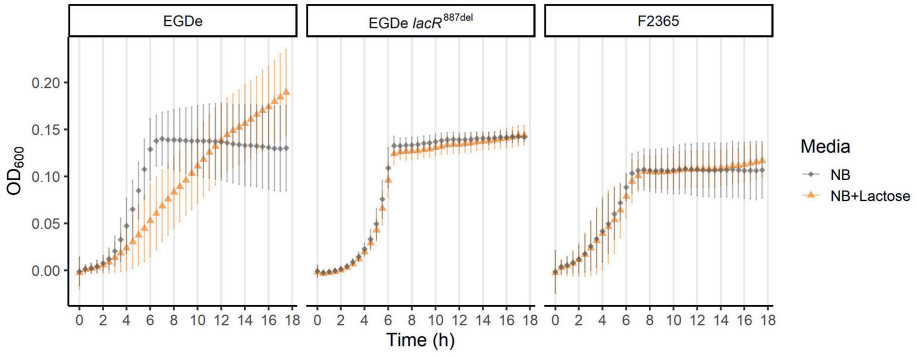

Figure 6.5: **Cell density growth curves of *L. monocytogenes* EGDe, EGDe *lacR*^{887del} and F2365 in plain NB (black diamonds) and NB-Lactose (orange triangles) in the first 18 hours.** The error bars correspond to the standard deviation of the biological replicates.

A possible explanation is that the presence of a functional LacR, leading to lactose consumption, may disrupt the utilization of other carbon sources in *L. monocytogenes*, affecting its fitness. In plain NB medium, all strains used in **Chapter 5** reached an OD_{600} of approximately 0.13, indicating the presence of a low concentration of carbon sources, likely from yeast extract. Interestingly, while the lactose-positive strain EGDe eventually attained a higher OD_{600} in 1% (w/v) lactose-supplemented NB (NB-lactose) compared to NB (**Chapter 5**, Figure 5.4), it exhibited slower growth in NB-lactose during the initial 12 hours of growth (Figure 6.5). To reach an OD_{600} of approximately 0.13 in NB-lactose, EGDe required around 12 hours, whereas the lactose-negative strain EGDe *lacR*^{887del} only needed about 6 hours. In contrast, the lactose-negative strains EGDe *lacR*^{887del} and F2365 showed similar growth patterns in both NB and NB-lactose during the first 12 hours. The Supplemental Figure 5.1 in **Chapter 5** further illustrates that all lactose-positive strains exhibit slower growth in NB-lactose compared to NB during the initial five hours, while lactose-negative strains demonstrate similar growth in both media during this period. This leads to the formulation of the following hypothesis. Compared to the *L. monocytogenes* lactose-negative strains, the lactose positive strain could use lactose as an extra carbon source and eventually reach higher cell densities. However, the using of lactose might also disturb the utilization of other available carbon sources, resulting in slower early growth. Before exhausting the background carbon sources, the lactose negative strains might have faster growth than the lactose positive strains. Thus, lactose utilization capacity does not necessarily confer a fitness advantage in lactose-rich environments. Notably, another lactose-negative strain, ScottA, is also associated with dairy products, having been isolated from the 1983 Massachusetts milk outbreak (Fleming et al., 1985). In dairy products, although lactose is the major carbon source, other carbon sources, including glucose, may also be present at low concentrations (Larsen and Moyes, 2015; Ohlsson et al., 2017). These alternative carbon sources could provide a fitness advantage to lactose-negative *L. monocytogenes* strains in case of dairy product contamination. Further studies are needed to test this hypothesis by determining the growth kinetics of lactose-positive and negative strains in mono and co-culture in dairy-based media.

In conclusion, this thesis provides insights into the biodiversity of *L. monocytogenes* in terms of stress resistance, growth performance, and carbon source utilization at the population and strain levels. Through evolutionary experiments and mutant construction, the molecular mechanisms driving this phenotypic heterogeneity have been investigated. Furthermore, bioinformatic analysis and mathematical modeling revealed that current approaches to investigating and controlling this pathogen may underestimate its diversity. A deeper understanding of the genotype and phenotype diversity of *L. monocytogenes* can contribute to a better controlling of this foodborne pathogen and improvement of food safety.

6.8 Supplementary Material

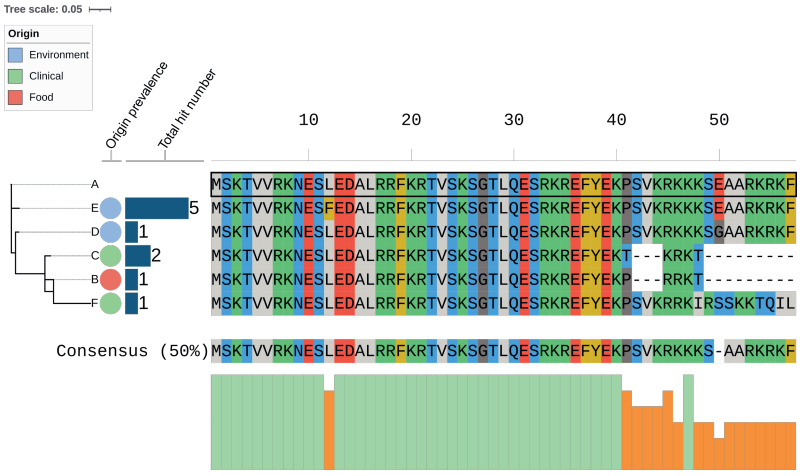

Supplemental Figure 6.1: **Neighbour-joining tree based on translated *rpsU* BLAST results.** Each tip of the tree represents one RpsU protein unique sequence type, and the type A is the same as EGDe RpsU protein sequence. For each RpsU protein unique sequence type except type A, isolation origin prevalence (pie chart) and total BLAST hit number (bar chart) are annotated next to the tree. The sequence alignment is also annotated with consensus and conservation graph below. The conservation graph is colored based on conservation value with green (>95%), orange (>30%) and red (<30%).

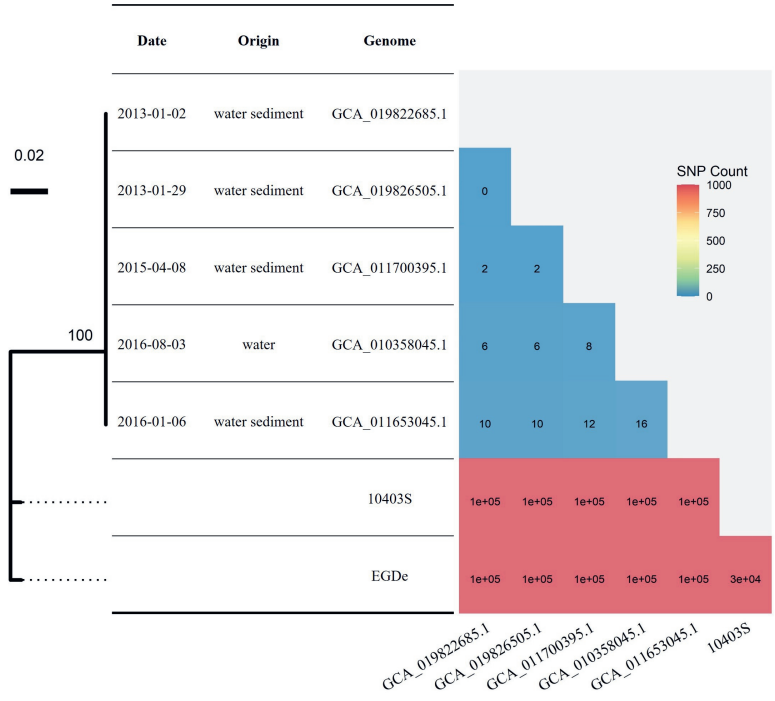

Supplemental Figure 6.2: **Phylogenetic analysis and core genome SNP matrix of EGDe, 10403S and five environmental isolated samples from Salinas, California, USA with the same mutation *rpsU*$^{\mathbf{C34T}}$.** Maximum likelihood phylogenetic tree was constructed by using the program RAxML (8.2.12) with GTRCAT model and 1,000 rapid bootstraps. Branch labels indicate support values in percentage for 1,000 bootstrap replicates. Bootstrap values less than 90% are not shown. The number and color in the core genome SNP matrix heatmap represent the amount of core genome SNP between the samples indicated at the row and column. The attribution data of each genome, except reference genome EGDe and 10403S, are annotated between the phylogenetic tree and the heatmap.

References

Abee, T., Koomen, J., Metselaar, K.I., Zwietering, M.H., Den Besten, H.M.W., 2016. Impact of pathogen population heterogeneity and stress-resistant variants on food safety. Annu. Rev. Food Sci. Technol. 7, 439–456. https://doi.org/10.1146/annurev-food-041715-033128

Abram, F., Starr, E., Karatzas, K.A.G., Matlawska-Wasowska, K., Boyd, A., Wiedmann, M., Boor, K.J., Connally, D., O'Byrne, C.P., 2008. Identification of components of the Sigma B regulon in *Listeria monocytogenes* that contribute to acid and salt tolerance. Appl. Environ. Microbiol. 74, 6848–6858. https://doi.org/10.1128/AEM.00442-08

Acosta-Reyes, F.J., Bhattacharjee, S., Gottesman, M., Frank, J., 2023. Structural insight into translation initiation of the λcl leaderless mRNA. bioRxiv 2023.09.02.556006. https://doi.org/10.1101/2023.09.02.556006

Afzal, M., Shafeeq, S., Ahmed, H., Kuipers, O.P., 2015. Sialic acid-mediated gene expression in *Streptococcus pneumoniae* and role of NanR as a transcriptional activator of the *nan* gene cluster. Appl. Environ. Microbiol. 81, 3121–3131. https://doi.org/10.1128/AEM.00499-15

Ahlmann-Eltze, C., Patil, I., 2021. ggsignif: R package for displaying significance brackets for 'ggplot2'. PsyArxiv. https://doi.org/10.31234/osf.io/7awm6

Aleksandrzak-Piekarczyk, T., Szatraj, K., Kosiorek, K., 2019. GlaR (YugA)-a novel RpiR-family transcription activator of the Leloir pathway of galactose utilization in *Lactococcus lactis* IL1403. Microbiologyopen 8, e00714. https://doi.org/10.1002/mbo3.714

Allenby, N.E.E., O'Connor, N., Prágai, Z., Ward, A.C., Wipat, A., Harwood, C.R., 2005. Genome-wide transcriptional analysis of the phosphate starvation stimulon of *Bacillus subtilis*. J. Bacteriol. 187, 8063–8080. https://doi.org/10.1128/JB.187.23.8063-8080.2005

Allende, A., Barbuddhe, S.B., Devleesschauwer, B., Dong, Q., Donnelly, C., Farber, J.M., Hansen, L.T., Latorre, A., Leclercq, A., Magwedere, K., Mahoney, D., Ross, T., Ryser, E., Zwietering, M.H., 2022. *Listeria monocytogenes* in ready-to-eat (RTE) foods: attribution, characterization and monitoring : Meeting report, Microbiological Risk Assessment Series No. 38. FAO/WHO, Rome. https://doi.org/10.4060/cc2400en

Allerberger, F., Wagner, M., 2010. Listeriosis: A resurgent foodborne infection. Clin. Microbiol. Infect. 16, 16–23. https://doi.org/10.1111/j.1469-0691.2009.03109.x

Amin, M.R., Yurovsky, A., Chen, Y., Skiena, S., Futcher, B., 2018. Re-annotation of 12,495 prokaryotic 16S rRNA 3' ends and analysis of Shine-Dalgarno and anti-Shine-Dalgarno sequences. PLoS ONE 13, e0202767. https://doi.org/10.1371/journal.pone.0202767

Anders, S., Pyl, P.T., Huber, W., 2015. HTSeq—a Python framework to work with high-throughput sequencing data. Bioinformatics 31, 166–169. https://doi.org/10.1093/bioinformatics/btu638

Andrews, S., n.d. FastQC A Quality Control tool for High Throughput Sequence Data.

Asahara, H., Magnelli, P., Shi, X., Tuckey, C., Zhou, Y., Samuelson, J.C., 2021. Chapter Fifteen - Guidelines for nucleic acid template design for optimal cell-free protein synthesis using an *Escherichia coli* reconstituted system or a lysate-based system, in: Kelman, Z., O'Dell, W.B. (Eds.), Methods in Enzymology, Recombinant Protein Expression: Prokaryotic Hosts and Cell-Free Systems. Academic Press, pp. 351–369. https://doi.org/10.1016/bs.mie.2021.07.005

Aseev, L.V., Chugunov, A.O., Efremov, R.G., Boni, I.V., 2013. A single missense mutation in a coiled-coil Domain of *Escherichia coli* ribosomal protein S2 confers a thermosensitive phenotype that can be suppressed by ribosomal protein S1. J. Bacteriol. 195, 95–104. https://doi.org/10.1128/jb.01305-12

Bannenberg, J.W., Abee, T., Zwietering, M.H., Den Besten, H.M.W., 2021. Variability in lag duration of *Listeria monocytogenes* strains in half Fraser enrichment broth after stress affects the detection efficacy using the ISO 11290-1 method. Int. J. Food Microbiol. 337, 108914. https://doi.org/10.1016/j.ijfoodmicro.2020.108914

Basco, M.D.S., Kothari, A., McKinzie, P.B., Revollo, J.R., Agnihothram, S., Azevedo, M.P., Saccente, M., Hart, M.E., 2019. Reduced vancomycin susceptibility and increased macrophage survival in *Staphylococcus aureus* strains sequentially isolated from a bacteraemic patient during a short course of antibiotic therapy. J. Med. Microbiol. 68, 848–859. https://doi.org/10.1099/jmm.0.000988

Bateman, A., 1999. The SIS domain: a phosphosugar-binding domain. Trends Biochem. Sci. 24, 94–95. https://doi.org/10.1016/S0968-0004(99)01357-2

Becker, L.A., Çetin, M.S., Hutkins, R.W., Benson, A.K., 1998. Identification of the gene encoding the alternative sigma factor sigma(B) from *Listeria monocytogenes* and its role in osmotolerance. J. Bacteriol. 180, 4547–4554. https://doi.org/10.1128/JB.180.17.4547-4554.1998

Berk, V., Zhang, W., Pai, R.D., Cate, J.H.D., 2006. Structural basis for mRNA and tRNA positioning on the ribosome. Proc. Natl. Acad. Sci. U.S.A. 103, 15830–15834. https://doi.org/10.1073/pnas.0607541103

Bidart, G.N., Rodríguez-Díaz, J., Pérez-Martínez, G., Yebra, M.J., 2018. The lactose operon from *Lactobacillus casei* is involved in the transport and metabolism of the human milk oligosaccharide core-2 N-acetyllactosamine. Sci. Rep. 8, 7152. https://doi.org/10.1038/s41598-018-25660-w

Bielow, C., Mastrobuoni, G., Kempa, S., 2016. Proteomics quality control: Quality control software for MaxQuant results. J. Proteome Res. 15, 777–787. https://doi.org/10.1021/acs.jproteome.5b00780

Biesta-Peters, E.G., Reij, M.W., Joosten, H., Gorris, L.G.M., Zwietering, M.H., 2010. Comparison of two optical-density-based methods and a plate count method for estimation of growth parameters of *Bacillus cereus*. Appl. Environ. Microbiol. 76, 1399–1405. https://doi.org/10.1128/AEM.02336-09

Brennan, R.G., Matthews, B.W., 1989. The helix-turn-helix DNA binding motif. J. Biol. Chem. 264, 1903–1906.

Brigulla, M., Hoffmann, T., Krisp, A., Völker, A., Bremer, E., Völker, U., 2003. Chill induction of the SigB-dependent general stress response in *Bacillus subtilis* and its contribution to low-temperature adaptation. J. Bacteriol. 185, 4305–4314. https:

//doi.org/10.1128/JB.185.15.4305-4314.2003
Bruhn, J.B., Vogel, B.F., Gram, L., 2005. Bias in the *Listeria monocytogenes* enrichment procedure: lineage 2 strains outcompete lineage 1 strains in University of Vermont selective enrichments. Appl. Environ. Microbiol. 71, 961–967. https://doi.org/10.1128/AEM.71.2.961-967.2005
Buchanan, R.L., Gorris, L.G.M., Hayman, M.M., Jackson, T.C., Whiting, R.C., 2017. A review of Listeria monocytogenes: An update on outbreaks, virulence, dose-response, ecology, and risk assessments. Food Control 75, 1–13. https://doi.org/10.1016/j.foodcont.2016.12.016
Buchanan, R.L., Whiting, R.C., Damert, W.C., 1997. When is simple good enough: A comparison of the Gompertz, Baranyi, and three-phase linear models for fitting bacterial growth curves. Food Microbiology 14, 313–326. https://doi.org/10.1006/fmic.1997.0125
Cao, T.N., Joyet, P., Aké, F.M.D., Milohanic, E., Deutscher, J., 2019. Studies of the *Listeria monocytogenes* cellobiose transport components and their impact on virulence gene repression. J. Mol. Microbiol. Biotechnol. 29, 10–26. https://doi.org/10.1159/000500090
Carlin, C.R., Liao, J., Hudson, L.K., Peters, T.L., Denes, T.G., Orsi, R.H., Guo, X., Wiedmann, M., 2022. Soil Collected in the Great Smoky Mountains National Park Yielded a Novel Listeria sensu stricto Species, L. swaminathanii. Microbiology Spectrum 10. https://doi.org/10.1128/spectrum.00442-22
Carrique-Mas, J.J., Hökeberg, I., Andersson, Y., Arneborn, M., Tham, W., Danielsson-Tham, M.L., Osterman, B., Leffler, M., Steen, M., Eriksson, E., Hedin, G., Giesecke, J., 2003. Febrile gastroenteritis after eating on-farm manufactured fresh cheese–an outbreak of listeriosis? Epidemiol. Infect. 130, 79–86. https://doi.org/10.1017/s0950268802008014
Castro, H., Douillard, F.P., Korkeala, H., Lindström, M., 2021. Mobile elements harboring heavy metal and bacitracin resistance genes are common among *Listeria monocytogenes* strains persisting on dairy farms. mSphere 6, 10.1128/msphere.00383–21. https://doi.org/10.1128/msphere.00383-21
Castro, H., Jaakkonen, A., Hakkinen, M., Korkeala, H., Lindström, M., 2018. Occurrence, persistence, and contamination routes of *Listeria monocytogenes* genotypes on three Finnish dairy cattle farms: a longitudinal study. Appl. Environ. Microbiol. 84, e02000–17. https://doi.org/10.1128/AEM.02000-17
Chakraborty, T., Leimeister-Wächter, M., Domann, E., Hartl, M., Goebel, W., Nichterlein, T., Notermans, S., 1992. Coordinate regulation of virulence genes in Listeria monocytogenes requires the product of the prfA gene. J. Bacteriol. 174, 568–574. https://doi.org/10.1128/jb.174.2.568-574.1992
Chen, L.-X., Jaffe, A.L., Borges, A.L., Penev, P.I., Nelson, T.C., Warren, L.A., Banfield, J.F., 2022. Phage-encoded ribosomal protein S21 expression is linked to late-stage phage replication. ISME Commun. 2, 1–10. https://doi.org/10.1038/s43705-022-00111-w
Cherifi, T., Carrillo, C., Lambert, D., Miniaï, I., Quessy, S., Larivière-Gauthier, G., Blais, B., Fravalo, P., 2018. Genomic characterization of *Listeria monocytogenes* isolates reveals that their persistence in a pig slaughterhouse is linked to the presence of benzalkonium chloride resistance genes. BMC Microbiol. 18, 220. https://doi.org/10.1186/s12866-018-1363-9
Chou, P.Y., Fasman, G.D., 1974. Prediction of protein conformation. Biochemistry

13, 222–245. https://doi.org/10.1021/bi00699a002
Cox, J., Hein, M.Y., Luber, C.A., Paron, I., Nagaraj, N., Mann, M., 2014. Accurate proteome-wide label-free quantification by delayed normalization and maximal peptide ratio extraction, termed MaxLFQ. Mol. Cell Proteomics 13, 2513–2526. https://doi.org/10.1074/mcp.M113.031591
Crespo Tapia, N., Dorey, A.L., Gahan, C.G.M., Den Besten, H.M.W., O'Byrne, C.P., Abee, T., 2020. Different carbon sources result in differential activation of sigma B and stress resistance in *Listeria monocytogenes*. Int. J. Food Microbiol. 320, 108504. https://doi.org/10.1016/j.ijfoodmicro.2019.108504
Culver, G.M., Kirthi, N., 2008. Assembly of the 30S ribosomal subunit. EcoSal Plus 3, 10.1128/ecosalplus.2.5.3. https://doi.org/10.1128/ecosalplus.2.5.3
D'Urso, G., Chat, S., Gillet, R., Giudice, E., 2023. Structural insights into the binding of bS1 to the ribosome. Nucleic Acids Res. 51, 3410–3419. https://doi.org/10.1093/nar/gkad126
Dagley, L.F., Infusini, G., Larsen, R.H., Sandow, J.J., Webb, A.I., 2019. Universal solid-phase protein preparation (USP3) for bottom-up and top-down proteomics. J. Proteome Res. 18, 2915–2924. https://doi.org/10.1021/acs.jproteome.9b00217
Dalet, K., Arous, S., Cenatiempo, Y., Héchard, Y., 2003. Characterization of a unique σ54–dependent PTS operon of the lactose family in *Listeria monocytogenes*. Biochimie 85, 633–638. https://doi.org/10.1016/S0300-9084(03)00134-2
Davidson, C.J., Surette, M.G., 2008. Individuality in Bacteria. Annu. Rev. Genet. 42, 253–268. https://doi.org/10.1146/annurev.genet.42.110807.091601
Den Besten, H.M.W., Mataragas, M., Moezelaar, R., Abee, T., Zwietering, M.H., 2006. Quantification of the effects of salt stress and physiological state on thermotolerance of *Bacillus cereus* ATCC 10987 and ATCC 14579. Appl. Environ. Microbiol. 72, 5884–5894. https://doi.org/10.1128/AEM.00780-06
Desai, A.N., Anyoha, A., Madoff, L.C., Lassmann, B., 2019. Changing epidemiology of Listeria monocytogenes outbreaks, sporadic cases, and recalls globally: A review of ProMED reports from 1996 to 2018. Int J Infect Dis 84, 48–53. https://doi.org/10.1016/j.ijid.2019.04.021
Dessaux, C., Guerreiro, D.N., Pucciarelli, M.G., O'Byrne, C.P., García-del Portillo, F., 2020. Impact of osmotic stress on the phosphorylation and subcellular location of *Listeria monocytogenes* stressosome proteins. Sci. Rep. 10, 20837. https://doi.org/10.1038/s41598-020-77738-z
Dorey, A.L., Lee, B.-H., Rotter, B., O'Byrne, C.P., 2019. Blue Light Sensing in Listeria monocytogenes Is Temperature-Dependent and the Transcriptional Response to It Is Predominantly SigB-Dependent. Front Microbiol 10. https://doi.org/10.3389/fmicb.2019.02497
Duval, M., Dar, D., Carvalho, F., Rocha, E.P.C., Sorek, R., Cossart, P., 2018. HflXr, a homolog of a ribosome-splitting factor, mediates antibiotic resistance. Proc. Natl. Acad. Sci. U.S.A. 115, 13359–13364. https://doi.org/10.1073/pnas.1810555115
Duval, M., Korepanov, A., Fuchsbauer, O., Fechter, P., Haller, A., Fabbretti, A., Choulier, L., Micura, R., Klaholz, B.P., Romby, P., Springer, M., Marzi, S., 2013. *Escherichia coli* ribosomal protein S1 unfolds structured mRNAs onto the ribosome for active translation initiation. PLoS Biol. 11, e1001731. https://doi.org/10.1371/journal.pbio.1001731
EFSA, ECDC, 2022. The European Union One Health 2021 Zoonoses Report. EFSA Journal 20, e07666. https://doi.org/10.2903/j.efsa.2022.7666

EFSA, ECDC, 2021. The European Union One Health 2020 Zoonoses Report. EFSA Journal 19, e06971. https://doi.org/10.2903/j.efsa.2021.6971

Elson, R., Awofisayo-Okuyelu, A., Greener, T., Swift, C., Painset, A., Amar, C.F.L., Newton, A., Aird, H., Swindlehurst, M., Elviss, N., Foster, K., Dallman, T.J., Ruggles, R., Grant, K., 2019. Utility of Whole Genome Sequencing To Describe the Persistence and Evolution of Listeria monocytogenes Strains within Crabmeat Processing Environments Linked to Two Outbreaks of Listeriosis. J Food Prot 82, 30–38. https://doi.org/10.4315/0362-028X.JFP-18-206

Espah Borujeni, A., Channarasappa, A.S., Salis, H.M., 2014. Translation rate is controlled by coupled trade-offs between site accessibility, selective RNA unfolding and sliding at upstream standby sites. Nucleic Acids Res. 42, 2646–2659. https://doi.org/10.1093/nar/gkt1139

European Commission, 2023. NOTIFICATION 2023.0500 Listeria monocytogenes in vegan organic cheese and foie gras alternative [WWW Document]. URL https://webgate.ec.europa.eu/rasff-window/screen/notification/591930 (accessed 11.20.2023).

Fagerlund, A., Idland, L., Heir, E., Møretrø, T., Aspholm, M., Lindbäck, T., Langsrud, S., 2022. Whole-Genome Sequencing Analysis of Listeria monocytogenes from Rural, Urban, and Farm Environments in Norway: Genetic Diversity, Persistence, and Relation to Clinical and Food Isolates. Appl Environ Microbiol 88, e0213621. https://doi.org/10.1128/aem.02136-21

FAO/WHO, 2004. Risk assessment of Listeria monocytogenes in ready-to-eat foods. Interpretative Summary. Microbiological Risk Assessment Series (MRA) 4, Microbiological Risk Assessment Series (FAO/WHO). FAO, Rome, Italy.

Faure, G., Ogurtsov, A.Y., Shabalina, S.A., Koonin, E.V., 2016. Role of mRNA structure in the control of protein folding. Nucleic Acids Res. 44, 10898–10911. https://doi.org/10.1093/nar/gkw671

Feng, Y., Bui, T.P.N., Stams, A.J.M., Boeren, S., Sánchez-Andrea, I., de Vos, W.M., 2022. Comparative genomics and proteomics of *Eubacterium maltosivorans*: functional identification of trimethylamine methyltransferases and bacterial microcompartments in a human intestinal bacterium with a versatile lifestyle. Environ Microbiol 24, 517–534. https://doi.org/10.1111/1462-2920.15886

Ferreira, A., Gray, M., Wiedmann, M., Boor, K.J., 2004. Comparative genomic analysis of the sigB operon in *Listeria monocytogenes* and in other Gram-positive bacteria. Curr. Microbiol. 48, 39–46. https://doi.org/10.1007/s00284-003-4020-x

Ferreira, V., Wiedmann, M., Teixeira, P., Stasiewicz, M.J., 2014. *Listeria monocytogenes* persistence in food-associated environments: epidemiology, strain characteristics, and implications for public health. J. Food Prot. 77, 150–170. https://doi.org/10.4315/0362-028X.JFP-13-150

Fleming, D.W., Cochi, S.L., MacDonald, K.L., Brondum, J., Hayes, P.S., Plikaytis, B.D., Holmes, M.B., Audurier, A., Broome, C.V., Reingold, A.L., 1985. Pasteurized milk as a vehicle of infection in an outbreak of listeriosis. N. Engl. J. Med. 312, 404–407. https://doi.org/10.1056/NEJM198502143120704

Gaballa, A., Guariglia-Oropeza, V., Wiedmann, M., Boor, K.J., 2019. Cross Talk between SigB and PrfA in Listeria monocytogenes Facilitates Transitions between Extra- and Intracellular Environments. Microbiol. Mol. Biol. Rev. 83. https://doi.org/10.1128/MMBR.00034-19

Galaxy Community, 2022. The Galaxy platform for accessible, reproducible

and collaborative biomedical analyses: 2022 update. Nucleic Acids Res. 50, W345–W351. https://doi.org/10.1093/nar/gkac247

Galinier, A., Deutscher, J., 2017. Sophisticated Regulation of Transcriptional Factors by the Bacterial Phosphoenolpyruvate: Sugar Phosphotransferase System. Journal of Molecular Biology 429, 773–789. https://doi.org/10.1016/j.jmb.2017.02.006

Garre, A., Koomen, J., Den Besten, H.M.W., Zwietering, M.H., 2023. Modeling population growth in R with the biogrowth package. J. Stat. Softw. 107, 1–51. https://doi.org/10.18637/jss.v107.i01

Genuth, N.R., Barna, M., 2018. The discovery of ribosome heterogeneity and its implications for gene regulation and organismal life. Mol. Cell 71, 364–374. https://doi.org/10.1016/j.molcel.2018.07.018

Gerst, J.E., 2018. Pimp my ribosome: Ribosomal protein paralogs specify translational control. Trends Genet. 34, 832–845. https://doi.org/10.1016/j.tig.2018.08.004

Gómez-Laguna, J., Cardoso-Toset, F., Meza-Torres, J., Pizarro-Cerdá, J., Quereda, J.J., 2020. Virulence potential of Listeria monocytogenes strains recovered from pigs in Spain. Vet Rec 187, e101. https://doi.org/10.1136/vr.105945

Gorski, L., Flaherty, D., Mandrell, R.E., 2006. Competitive fitness of *Listeria monocytogenes* serotype 1/2a and 4b strains in mixed cultures with and without food in the U.S. Food and Drug Administration enrichment protocol. Appl. Environ. Microbiol. 72, 776–783. https://doi.org/10.1128/AEM.72.1.776-783.2006

Gray, M.J., Zadoks, R.N., Fortes, E.D., Dogan, B., Cai, S., Chen, Y., Scott, V.N., Gombas, D.E., Boor, K.J., Wiedmann, M., 2004. Listeria monocytogenes Isolates from Foods and Humans Form Distinct but Overlapping Populations. Applied and Environmental Microbiology 70, 5833–5841. https://doi.org/10.1128/AEM.70.10.5833-5841.2004

Grif, K., Patscheider, G., Dierich, M.P., Allerberger, F., 2003. Incidence of fecal carriage of Listeria monocytogenes in three healthy volunteers: A one-year prospective stool survey. Eur J Clin Microbiol Infect Dis 22, 16–20. https://doi.org/10.1007/s10096-002-0835-9

Guariglia-Oropeza, V., Orsi, R.H., Guldimann, C., Wiedmann, M., Boor, K.J., 2018. The *Listeria monocytogenes* bile stimulon under acidic conditions is characterized by strain-specific patterns and the upregulation of motility, cell wall modification functions, and the PrfA regulon. Front. Microbiol. 9, 120. https://doi.org/10.3389/fmicb.2018.00120

Guerreiro, D.N., Arcari, T., O'Byrne, C.P., 2020a. The σB-mediated general stress response of *Listeria monocytogenes*: life and death decision making in a pathogen. Front. Microbiol. 11, 1505. https://doi.org/10.3389/fmicb.2020.01505

Guerreiro, D.N., Pucciarelli, M.G., Tiensuu, T., Gudynaite, D., Boyd, A., Johansson, J., Portillo, F.G., O'Byrne, C.P., 2022a. Acid stress signals are integrated into the σB-dependent general stress response pathway via the stressosome in the food-borne pathogen *Listeria monocytogenes*. PLOS Pathogens 18, e1010213. https://doi.org/10.1371/journal.ppat.1010213

Guerreiro, D.N., Wu, J., Dessaux, C., Oliveira, A.H., Tiensuu, T., Gudynaite, D., Marinho, C.M., Boyd, A., García-del Portillo, F., Johansson, J., O'Byrne, C.P., 2020b. Mild stress conditions during laboratory culture promote the proliferation of mutations that negatively affect Sigma B activity in *Listeria monocytogenes*. J. Bacteriol. 202, e00751–19. https://doi.org/10.1128/JB.00751-19

Guerreiro, D.N., Wu, J., McDermott, E., Garmyn, D., Dockery, P., Boyd,

A., Piveteau, P., O'Byrne, C.P., 2022b. *In vitro* evolution of *Listeria monocytogenes* reveals selective pressure for loss of SigB and AgrA function at different incubation temperatures. Appl. Environ. Microbiol. 88, e00330–22. https://doi.org/10.1128/aem.00330-22

Hain, T., Hossain, H., Chatterjee, S.S., Machata, S., Volk, U., Wagner, S., Brors, B., Haas, S., Kuenne, C.T., Billion, A., Otten, S., Pane-Farre, J., Engelmann, S., Chakraborty, T., 2008. Temporal transcriptomic analysis of the *Listeria monocytogenes* EGD-e σB regulon. BMC Microbiol. 8, 20. https://doi.org/10.1186/1471-2180-8-20

Hall, T.A., 1999. BioEdit: a user-friendly biological sequence alignment editor and analysis program for Windows 95/98/NT, in: Nucleic Acids Symposium Series. Oxford, pp. 95–98.

Harrand, A.S., Jagadeesan, B., Baert, L., Wiedmann, M., Orsi, R.H., 2020. Evolution of *Listeria monocytogenes* in a food processing plant involves limited single-nucleotide substitutions but considerable diversification by gain and loss of prophages. Appl. Environ. Microbiol. 86, e02493–19. https://doi.org/10.1128/AEM.02493-19

Havelaar, A.H., Kirk, M.D., Torgerson, P.R., Gibb, H.J., Hald, T., Lake, R.J., Praet, N., Bellinger, D.C., de Silva, N.R., Gargouri, N., Speybroeck, N., Cawthorne, A., Mathers, C., Stein, C., Angulo, F.J., Devleesschauwer, B., World Health Organization Foodborne Disease Burden Epidemiology Reference Group, 2015. World Health Organization Global Estimates and Regional Comparisons of the Burden of Foodborne Disease in 2010. PLoS Med 12, e1001923. https://doi.org/10.1371/journal.pmed.1001923

Holch, A., Webb, K., Lukjancenko, O., Ussery, D., Rosenthal, B.M., Gram, L., 2013. Genome Sequencing Identifies Two Nearly Unchanged Strains of Persistent Listeria monocytogenes Isolated at Two Different Fish Processing Plants Sampled 6 Years Apart. Applied and Environmental Microbiology 79, 2944–2951. https://doi.org/10.1128/AEM.03715-12

Holtmann, G., Brigulla, M., Steil, L., Schütz, A., Barnekow, K., Völker, U., Bremer, E., 2004. RsbV-independent induction of the SigB-dependent general stress regulon of *Bacillus subtilis* during growth at high temperature. J. Bacteriol. 186, 6150–6158. https://doi.org/10.1128/JB.186.18.6150-6158.2004

Hsieh, Y.-J., Wanner, B.L., 2010. Global regulation by the seven-component Pi signaling system. Curr. Opin. Microbiol., Cell regulation 13, 198–203. https://doi.org/10.1016/j.mib.2010.01.014

Huang, C., Lu, T.-L., Yang, Y., 2023. Mortality risk factors related to listeriosis — A meta-analysis. Journal of Infection and Public Health 16, 771–783. https://doi.org/10.1016/j.jiph.2023.03.013

Hunt, R., Hettiarachchi, G., Katneni, U., Hernandez, N., Holcomb, D., Kames, J., Alnifaidy, R., Lin, B., Hamasaki-Katagiri, N., Wesley, A., Kafri, T., Morris, C., Bouché, L., Panico, M., Schiller, T., Ibla, J., Bar, H., Ismail, A., Morris, H., Komar, A., Kimchi-Sarfaty, C., 2019. A Single Synonymous Variant (c.354G>A [p.P118P]) in ADAMTS13 Confers Enhanced Specific Activity. Int J Mol Sci 20, 5734. https://doi.org/10.3390/ijms20225734

Huntley, R.P., Sawford, T., Mutowo-Meullenet, P., Shypitsyna, A., Bonilla, C., Martin, M.J., O'Donovan, C., 2015. The GOA database: Gene Ontology annotation updates for 2015. Nucleic Acids Res. 43, D1057–1063. https:

//doi.org/10.1093/nar/gku1113

Hurley, D., Luque-Sastre, L., Parker, C.T., Huynh, S., Eshwar, A.K., Nguyen, S.V., Andrews, N., Moura, A., Fox, E.M., Jordan, K., Lehner, A., Stephan, R., Fanning, S., 2019. Whole-Genome Sequencing-Based Characterization of 100 Listeria monocytogenes Isolates Collected from Food Processing Environments over a Four-Year Period. mSphere 4, 10.1128/msphere.00252–19. https://doi.org/10.1128/msphere.00252-19

Impens, F., Rolhion, N., Radoshevich, L., Bécavin, C., Duval, M., Mellin, J., García del Portillo, F., Pucciarelli, M.G., Williams, A.H., Cossart, P., 2017. N-terminomics identifies Prli42 as a membrane miniprotein conserved in Firmicutes and critical for stressosome activation in Listeria monocytogenes. Nat Microbiol 2, 17005. https://doi.org/10.1038/nmicrobiol.2017.5

Iskandar, C.F., Cailliez-Grimal, C., Borges, F., Revol-Junelles, A.-M., 2019. Review of lactose and galactose metabolism in Lactic Acid Bacteria dedicated to expert genomic annotation. Trends Food Sci. Technol. 88, 121–132. https://doi.org/10.1016/j.tifs.2019.03.020

Jacquet, C., Doumith, M., Gordon, J.I., Martin, P.M.V., Cossart, P., Lecuit, M., 2004. A Molecular Marker for Evaluating the Pathogenic Potential of Foodborne Listeria monocytogenes. The Journal of Infectious Diseases 189, 2094–2100. https://doi.org/10.1086/420853

Jagannathan, I., Culver, G.M., 2003. Assembly of the central domain of the 30S ribosomal subunit: Roles for the primary binding ribosomal proteins S15 and S8. J. Mol. Biol. 330, 373–383. https://doi.org/10.1016/S0022-2836(03)00586-2

Jha, V., Roy, B., Jahagirdar, D., McNutt, Z.A., Shatoff, E.A., Boleratz, B.L., Watkins, D.E., Bundschuh, R., Basu, K., Ortega, J., Fredrick, K., 2021. Structural basis of sequestration of the anti-Shine-Dalgarno sequence in the Bacteroidetes ribosome. Nucleic Acids Res. 49, 547–567. https://doi.org/10.1093/nar/gkaa1195

Jiang, Y., Neti, S.S., Sitarik, I., Pradhan, P., To, P., Xia, Y., Fried, S.D., Booker, S.J., O'Brien, E.P., 2023. How synonymous mutations alter enzyme structure and function over long timescales. Nat. Chem. 15, 308–318. https://doi.org/10.1038/s41557-022-01091-z

Jumper, J., Evans, R., Pritzel, A., Green, T., Figurnov, M., Ronneberger, O., Tunyasuvunakool, K., Bates, R., Žídek, A., Potapenko, A., Bridgland, A., Meyer, C., Kohl, S.A.A., Ballard, A.J., Cowie, A., Romera-Paredes, B., Nikolov, S., Jain, R., Adler, J., Back, T., Petersen, S., Reiman, D., Clancy, E., Zielinski, M., Steinegger, M., Pacholska, M., Berghammer, T., Bodenstein, S., Silver, D., Vinyals, O., Senior, A.W., Kavukcuoglu, K., Kohli, P., Hassabis, D., 2021. Highly accurate protein structure prediction with AlphaFold. Nature 596, 583–589. https://doi.org/10.1038/s41586-021-03819-2

Karatzas, K.A.G., Bennik, M.H.J., 2002. Characterization of a Listeria monocytogenes Scott A Isolate with High Tolerance towards High Hydrostatic Pressure. Appl. Environ. Microbiol. 68, 3183–3189. https://doi.org/10.1128/AEM.68.7.3183-3189.2002

Karatzas, K.A.G., Wouters, J.A., Gahan, C.G.M., Hill, C., Abee, T., Bennik, M.H.J., 2003. The CtsR regulator of Listeria monocytogenes contains a variant glycine repeat region that affects piezotolerance, stress resistance, motility and virulence. Mol Microbiol 49, 1227–1238. https://doi.org/10.1046/j.1365-2958.2003.03636.x

Karp, P.D., Billington, R., Caspi, R., Fulcher, C.A., Latendresse, M., Kothari, A.,

Keseler, I.M., Krummenacker, M., Midford, P.E., Ong, Q., Ong, W.K., Paley, S.M., Subhraveti, P., 2019. The BioCyc collection of microbial genomes and metabolic pathways. Brief. Bioinform. 20, 1085–1093. https://doi.org/10.1093/bib/bbx085

Kazmierczak, M.J., Mithoe, S.C., Boor, K.J., Wiedmann, M., 2003. *Listeria monocytogenes* σB regulates stress response and virulence functions. J. Bacteriol. 185, 5722–5734. https://doi.org/10.1128/JB.185.19.5722-5734.2003

Keiler, K.C., 2015. Mechanisms of ribosome rescue in bacteria. Nat. Rev. Microbiol. 13, 285–297. https://doi.org/10.1038/nrmicro3438

Kim, S.W., Haendiges, J., Keller, E.N., Myers, R., Kim, A., Lombard, J.E., Karns, J.S., Kessel, J.A.S.V., Haley, B.J., 2018. Genetic diversity and virulence profiles of *Listeria monocytogenes* recovered from bulk tank milk, milk filters, and milking equipment from dairies in the United States (2002 to 2014). PLoS One 13, e0197053. https://doi.org/10.1371/journal.pone.0197053

Kint, C., Verstraeten, N., Hofkens, J., Fauvart, M., Michiels, J., 2014. Bacterial Obg proteins: GTPases at the nexus of protein and DNA synthesis. Crit. Rev. Microbiol. 40, 207–224. https://doi.org/10.3109/1040841X.2013.776510

Kiss, R., Tirczka, T., Szita, G., Bernáth, S., Csikó, G., 2006. *Listeria monocytogenes* food monitoring data and incidence of human listeriosis in Hungary, 2004. Int. J. Food Microbiol. 112, 71–74. https://doi.org/10.1016/j.ijfoodmicro.2006.06.013

Kohler, P.R.A., Choong, E.-L., Rossbach, S., 2011. The RpiR-like repressor IolR regulates inositol catabolism in *Sinorhizobium meliloti*. J. Bacteriol. 193, 5155–5163. https://doi.org/10.1128/JB.05371-11

Koller, T.O., Turnbull, K.J., Vaitkevicius, K., Crowe-McAuliffe, C., Roghanian, M., Bulvas, O., Nakamoto, J.A., Kurata, T., Julius, C., Atkinson, G.C., Johansson, J., Hauryliuk, V., Wilson, D.N., 2022. Structural basis for HflXr-mediated antibiotic resistance in *Listeria monocytogenes*. Nucleic Acids Res. 50, 11285–11300. https://doi.org/10.1093/nar/gkac934

Koomen, J., 2022. On the role of ribosomal proteins in stress resistance and fitness of *Listeria monocytogenes*: A laboratory evolution approach (PhD thesis). Wageningen University, Wageningen, the Netherlands.

Koomen, J., Den Besten, H.M.W., Metselaar, K.I., Tempelaars, M.H., Wijnands, L.M., Zwietering, M.H., Abee, T., 2018. Gene profiling-based phenotyping for identification of cellular parameters that contribute to fitness, stress-tolerance and virulence of *Listeria monocytogenes* variants. Int. J. Food Microbiol. 283, 14–21. https://doi.org/10.1016/j.ijfoodmicro.2018.06.003

Koomen, J., Huijboom, L., Ma, X., Tempelaars, M.H., Boeren, S., Zwietering, M.H., Den Besten, H.M.W., Abee, T., 2021. Amino acid substitutions in ribosomal protein RpsU enable switching between high fitness and multiple-stress resistance in *Listeria monocytogenes*. Int. J. Food Microbiol. 351, 109269. https://doi.org/10.1016/j.ijfoodmicro.2021.109269

Kuo, S., Demeler, B., Haldenwang, W.G., 2008. The growth-promoting and stress response activities of the *Bacillus subtilis* GTP binding protein Obg are separable by mutation. J. Bacteriol. 190, 6625–6635. https://doi.org/10.1128/jb.00799-08

Kuo, S.-T., Jahn, R.-L., Cheng, Y.-J., Chen, Y.-L., Lee, Y.-J., Hollfelder, F., Wen, J.-D., Chou, H.-H.D., 2020. Global fitness landscapes of the Shine-Dalgarno sequence. Genome Res. 30, 711–723. https://doi.org/10.1101/gr.260182.119

Lake, F.B., Van Overbeek, L.S., Baars, J.J.P., Koomen, J., Abee, T., Den Besten, H.M.W., 2021. Genomic characteristics of Listeria monocytogenes isolated during

mushroom (Agaricus bisporus) production and processing. Int J Food Microbiol 360, 109438. https://doi.org/10.1016/j.ijfoodmicro.2021.109438

Larsen, T., Moyes, K.M., 2015. Are free glucose and glucose-6-phosphate in milk indicators of specific physiological states in the cow? Animal 9, 86–93. https://doi.org/10.1017/S1751731114002043

Latino, L., Midoux, C., Vergnaud, G., Pourcel, C., 2019. Investigation of *Pseudomonas aeruginosa* strain PcyII-10 variants resisting infection by N4-like phage Ab09 in search for genes involved in phage adsorption. PLoS ONE 14, e0215456. https://doi.org/10.1371/journal.pone.0215456

Laursen, B.S., Sørensen, H.P., Mortensen, K.K., Sperling-Petersen, H.U., 2005. Initiation of protein synthesis in bacteria. Microbiol. Mol. Biol. 69, 101–123. https://doi.org/10.1128/mmbr.69.1.101-123.2005

Li, Z., Pérez-Osorio, A., Wang, Y., Eckmann, K., Glover, W.A., Allard, M.W., Brown, E.W., Chen, Y., 2017. Whole genome sequencing analyses of Listeria monocytogenes that persisted in a milkshake machine for a year and caused illnesses in Washington State. BMC Microbiology 17, 134. https://doi.org/10.1186/s12866-017-1043-1

Linnan, M.J., Mascola, L., Lou, X.D., Goulet, V., May, S., Salminen, C., Hird, D.W., Yonekura, M.L., Hayes, P., Weaver, R., 1988. Epidemic listeriosis associated with Mexican-style cheese. N. Engl. J. Med. 319, 823–828. https://doi.org/10.1056/NEJM198809293191303

Liu, Y., Orsi, R.H., Boor, K.J., Wiedmann, M., Guariglia-Oropeza, V., 2017. Home alone: Elimination of all but one alternative sigma factor in *Listeria monocytogenes* allows prediction of new roles for σB. Front. Microbiol. 8, 1910. https://doi.org/10.3389/fmicb.2017.01910

Liu, Y., Orsi, R.H., Gaballa, A., Wiedmann, M., Boor, K.J., Guariglia-Oropeza, V., 2019. Systematic review of the *Listeria monocytogenes* σB regulon supports a role in stress response, virulence and metabolism. Future Microbiol. 14, 801–828. https://doi.org/10.2217/fmb-2019-0072

Loveland, A.B., Korostelev, A.A., 2018. Structural dynamics of protein S1 on the 70S ribosome visualized by ensemble cryo-EM. Methods 137, 55–66. https://doi.org/10.1016/j.ymeth.2017.12.004

Lu, J., Boeren, S., de Vries, S.C., van Valenberg, H.J.F., Vervoort, J., Hettinga, K., 2011. Filter-aided sample preparation with dimethyl labeling to identify and quantify milk fat globule membrane proteins. J. Proteomics, A Proteomics Odyssey Towards Next Decade 75, 34–43. https://doi.org/10.1016/j.jprot.2011.07.031

Lucchini, R., Carraro, L., Pauletto, M., Gallo, M., Andreani, N.A., Weiss, G., Tessaro, C., Babbucci, M., Cardazzo, B., 2023. Molecular typing and genome sequencing allow the identification of persistent *Listeria monocytogenes* strains and the tracking of the contamination source in food environments. Int. J. Food Microbiol. 386, 110025. https://doi.org/10.1016/j.ijfoodmicro.2022.110025

MacDonald, P.D.M., Whitwam, R.E., Boggs, J.D., MacCormack, J.N., Anderson, K.L., Reardon, J.W., Saah, J.R., Graves, L.M., Hunter, S.B., Sobel, J., 2005. Outbreak of listeriosis among Mexican immigrants as a result of consumption of illicitly produced Mexican-style cheese. Clin. Infect. Dis. 40, 677–682. https://doi.org/10.1086/427803

Madeira, F., Pearce, M., Tivey, A.R.N., Basutkar, P., Lee, J., Edbali, O., Madhusoodanan, N., Kolesnikov, A., Lopez, R., 2022. Search and sequence

analysis tools services from EMBL-EBI in 2022. Nucleic Acids Res. 50, W276–W279. https://doi.org/10.1093/nar/gkac240

Marzi, S., Myasnikov, A.G., Serganov, A., Ehresmann, C., Romby, P., Yusupov, M., Klaholz, B.P., 2007. Structured mRNAs regulate translation initiation by binding to the platform of the ribosome. Cell 130, 1019–1031. https://doi.org/10.1016/j.cell.2007.07.008

Masi, A.C., Stewart, C.J., 2021. Untangling human milk oligosaccharides and infant gut microbiome. iScience 25, 103542. https://doi.org/10.1016/j.isci.2021.103542

Mattila, M., Somervuo, P., Korkeala, H., Stephan, R., Tasara, T., 2020. Transcriptomic and phenotypic analyses of the Sigma B-dependent characteristics and the synergism between Sigma B and Sigma L in *Listeria monocytogenes* EGD-e. Microorganisms 8, 1644. https://doi.org/10.3390/microorganisms8111644

Maury, M.M., Bracq-Dieye, H., Huang, L., Vales, G., Lavina, M., Thouvenot, P., Disson, O., Leclercq, A., Brisse, S., Lecuit, M., 2019. Hypervirulent *Listeria monocytogenes* clones' adaption to mammalian gut accounts for their association with dairy products. Nat. Commun. 10, 2488. https://doi.org/10.1038/s41467-019-10380-0

Maury, M.M., Tsai, Y.-H., Charlier, C., Touchon, M., Chenal-Francisque, V., Leclercq, A., Criscuolo, A., Gaultier, C., Roussel, S., Brisabois, A., Disson, O., Rocha, E.P.C., Brisse, S., Lecuit, M., 2016. Uncovering *Listeria monocytogenes* hypervirulence by harnessing its biodiversity. Nature Genet. 48, 308–313. https://doi.org/10.1038/ng.3501

McLauchlin, J., 1990. Distribution of serovars ofListeria monocytogenes isolated from different categories of patients with listeriosis. Eur. J. Clin. Microbiol. Infect. Dis. 9, 210–213. https://doi.org/10.1007/BF01963840

McLauchlin, J., Mitchell, R.T., Smerdon, W.J., Jewell, K., 2004. Listeria monocytogenes and listeriosis: A review of hazard characterisation for use in microbiological risk assessment of foods. International Journal of Food Microbiology 92, 15–33. https://doi.org/10.1016/S0168-1605(03)00326-X

McNutt, Z.A., Roy, B., Gemler, B.T., Shatoff, E.A., Moon, K.-M., Foster, L.J., Bundschuh, R., Fredrick, K., 2023. Ribosomes lacking bS21 gain function to regulate protein synthesis in *Flavobacterium johnsoniae*. Nucleic Acids Res. 51, 1927–1942. https://doi.org/10.1093/nar/gkad047

Mellefont, L.A., McMeekin, T.A., Ross, T., 2008. Effect of relative inoculum concentration on *Listeria monocytogenes* growth in co-culture. Int. J. Food Microbiol. 121, 157–168. https://doi.org/10.1016/j.ijfoodmicro.2007.10.010

Metselaar, K.I., 2016. Quantitative and ecological aspects of *Listeria monocytogenes* population heterogeneity (PhD thesis). Wageningen University, Wageningen, the Netherlands.

Metselaar, K.I., Abee, T., Zwietering, M.H., Den Besten, H.M.W., 2016. Modeling and validation of the ecological behavior of wild-type *Listeria monocytogenes* and stress-resistant variants. Appl. Environ. Microbiol. 82, 5389–5401. https://doi.org/10.1128/AEM.00442-16

Metselaar, K.I., Den Besten, H.M.W., Abee, T., Moezelaar, R., Zwietering, M.H., 2013. Isolation and quantification of highly acid resistant variants of *Listeria monocytogenes*. Int. J. Food Microbiol. 166, 508–514. https://doi.org/10.1016/j.ijfoodmicro.2013.08.011

Metselaar, K.I., Den Besten, H.M.W., Boekhorst, J., Van Hijum, S.A.F.T., Zwietering,

M.H., Abee, T., 2015. Diversity of acid stress resistant variants of *Listeria monocytogenes* and the potential role of ribosomal protein S21 encoded by *rpsU*. Front. Microbiol. 6, 422. https://doi.org/10.3389/fmicb.2015.00422

Mizuno, C.M., Guyomar, C., Roux, S., Lavigne, R., Rodriguez-Valera, F., Sullivan, M.B., Gillet, R., Forterre, P., Krupovic, M., 2019. Numerous cultivated and uncultivated viruses encode ribosomal proteins. Nat. Commun. 10, 752. https://doi.org/10.1038/s41467-019-08672-6

Moura, A., Lefrancq, N., Wirth, T., Leclercq, A., Borges, V., Gilpin, B., Dallman, T.J., Frey, J., Franz, E., Nielsen, E.M., Thomas, J., Pightling, A., Howden, B.P., Tarr, C.L., Gerner-Smidt, P., Cauchemez, S., Salje, H., Brisse, S., Lecuit, M., LISTERIA CC1 STUDY GROUP, 2021. Emergence and global spread of Listeria monocytogenes main clinical clonal complex. Science Advances 7, eabj9805. https://doi.org/10.1126/sciadv.abj9805

Muchaamba, F., Eshwar, A.K., Stevens, M.J.A., von Ah, U., Tasara, T., 2019. Variable Carbon Source Utilization, Stress Resistance, and Virulence Profiles Among Listeria monocytogenes Strains Responsible for Listeriosis Outbreaks in Switzerland. Front. Microbiol. 10. https://doi.org/10.3389/fmicb.2019.00957

Müller-Herbst, S., Wüstner, S., Mühlig, A., Eder, D., M. Fuchs, T., Held, C., Ehrenreich, A., Scherer, S., 2014. Identification of genes essential for anaerobic growth of *Listeria monocytogenes*. Microbiology 160, 752–765. https://doi.org/10.1099/mic.0.075242-0

Murray, E.G.D., Webb, R.A., Swann, M.B.R., 1926. A disease of rabbits characterised by a large mononuclear leucocytosis, caused by a hitherto undescribed bacillus Bacterium monocytogenes (n.sp.). The Journal of Pathology and Bacteriology 29, 407–439. https://doi.org/10.1002/path.1700290409

NicAogáin, K., O'Byrne, C.P., 2016. The role of stress and stress adaptations in determining the fate of the bacterial pathogen *Listeria monocytogenes* in the food chain. Front. Microbiol. 7, 1865. https://doi.org/10.3389/fmicb.2016.01865

Nightingale, K.K., Milillo, S.R., Ivy, R.A., Ho, A.J., Oliver, H.F., Wiedmann, M., 2007. *Listeria monocytogenes* F2365 carries several authentic mutations potentially leading to truncated gene products, including *inlB*, and demonstrates atypical phenotypic characteristics. J. Food Prot. 70, 482–488. https://doi.org/10.4315/0362-028x-70.2.482

Nystrom, T., 2004. Growth versus maintenance: A trade-off dictated by RNA polymerase availability and sigma factor competition? Mol. Microbiol. 54, 855–862. https://doi.org/10.1111/j.1365-2958.2004.04342.x

O'Brien, E.P., Vendruscolo, M., Dobson, C.M., 2014. Kinetic modelling indicates that fast-translating codons can coordinate cotranslational protein folding by avoiding misfolded intermediates. Nat Commun 5, 2988. https://doi.org/10.1038/ncomms3988

O'Byrne, C.P., Karatzas, K.A.G., 2008. Chapter 5 - The role of Sigma B (σB) in the stress adaptations of *Listeria monocytogenes*: Overlaps between stress adaptation and virulence, in: Laskin, A.I., Sariaslani, S., Gadd, G.M. (Eds.), Advances in Applied Microbiology. Academic Press, pp. 115–140. https://doi.org/10.1016/S0065-2164(08)00605-9

O'Donoghue, B., NicAogáin, K., Bennett, C., Conneely, A., Tiensuu, T., Johansson, J., O'Byrne, C., 2016. Blue-light inhibition of *Listeria monocytogenes* growth Is mediated by reactive oxygen species and is influenced by σB and the blue-light

sensor Lmo0799. Appl. Environ. Microbiol. 82, 4017–4027. https://doi.org/10.1128/AEM.00685-16

Ohlsson, J.A., Johansson, M., Hansson, H., Abrahamson, A., Byberg, L., Smedman, A., Lindmark-Månsson, H., Lundh, Å., 2017. Lactose, glucose and galactose content in milk, fermented milk and lactose-free milk products. Int. Dairy J. 73, 151–154. https://doi.org/10.1016/j.idairyj.2017.06.004

Oliveira, A.H., Tiensuu, T., Guerreiro, D.N., Tükenmez, H., Dessaux, C., García-Del Portillo, F., O'Byrne, C., Johansson, J., 2022. *Listeria monocytogenes* requires the RsbX protein to prevent SigB activation under nonstressed conditions. J Bacteriol 204, e0048621. https://doi.org/10.1128/JB.00486-21

Oliver, H.F., Orsi, R.H., Wiedmann, M., Boor, K.J., 2010. *Listeria monocytogenes* σB has a small core regulon and a conserved role in virulence but makes differential contributions to stress tolerance across a diverse collection of strains. Appl. Environ. Microbiol. 76, 4216–4232. https://doi.org/10.1128/AEM.00031-10

Ollinger, J., Bowen, B., Wiedmann, M., Boor, K.J., Bergholz, T.M., 2009. *Listeria monocytogenes* sigmaB modulates PrfA-mediated virulence factor expression. Infect. Immun. 77, 2113–2124. https://doi.org/10.1128/IAI.01205-08

Ondrusch, N., Kreft, J., 2011. Blue and Red Light Modulates SigB-Dependent Gene Transcription, Swimming Motility and Invasiveness in Listeria monocytogenes. PLOS ONE 6, e16151. https://doi.org/10.1371/journal.pone.0016151

Orsi, R.H., Den Bakker, H.C., Wiedmann, M., 2011. Listeria monocytogenes lineages: Genomics, evolution, ecology, and phenotypic characteristics. Int. J. Med. Microbiol. 301, 79–96. https://doi.org/10.1016/j.ijmm.2010.05.002

Österberg, S., Peso-Santos, T. del, Shingler, V., 2011. Regulation of alternative sigma factor use. Annu. Rev. Microbiol. 65, 37–55. https://doi.org/10.1146/annurev.micro.112408.134219

Palma, F., Brauge, T., Radomski, N., Mallet, L., Felten, A., Mistou, M.-Y., Brisabois, A., Guillier, L., Midelet-Bourdin, G., 2020. Dynamics of mobile genetic elements of *Listeria monocytogenes* persisting in ready-to-eat seafood processing plants in France. BMC Genomics 21, 130. https://doi.org/10.1186/s12864-020-6544-x

Paterson, J.S., 1940. The Antigenic Structure of Organisms of the Genus Listerella. Journal of Pathology and Bacteriology 51, 427–36.

Pathak, D., Jin, K.S., Tandukar, S., Kim, J.H., Kwon, E., Kim, D.Y., 2020. Structural insights into the regulation of SigB activity by RsbV and RsbW. IUCrJ 7, 737–747. https://doi.org/10.1107/S2052252520007617

Perez-Riverol, Y., Bai, J., Bandla, C., García-Seisdedos, D., Hewapathirana, S., Kamatchinathan, S., Kundu, D.J., Prakash, A., Frericks-Zipper, A., Eisenacher, M., Walzer, M., Wang, S., Brazma, A., Vizcaíno, J.A., 2022. The PRIDE database resources in 2022: A hub for mass spectrometry-based proteomics evidences. Nucleic Acids Research 50, D543–D552. https://doi.org/10.1093/nar/gkab1038

Piffaretti, J.C., Kressebuch, H., Aeschbacher, M., Bille, J., Bannerman, E., Musser, J.M., Selander, R.K., Rocourt, J., 1989. Genetic characterization of clones of the bacterium Listeria monocytogenes causing epidemic disease. Proc. Natl. Acad. Sci. U.S.A. 86, 3818–3822. https://doi.org/10.1073/pnas.86.10.3818

Pightling, A.W., Pettengill, J.B., Luo, Y., Baugher, J.D., Rand, H., Strain, E., 2018. Interpreting whole-genome sequence analyses of foodborne bacteria for regulatory applications and outbreak investigations. Front. Microbiol. 9, 1482. https://doi.org/doi.org/10.3389/fmicb.2018.01482

Pine, L., Malcolm, G.B., Brooks, J.B., Daneshvar, M.I., 1989. Physiological studies on the growth and utilization of sugars by *Listeria* species. Can. J. Microbiol. 35, 245–254. https://doi.org/10.1139/m89-037

Quereda, J.J., Morón-García, A., Palacios-Gorba, C., Dessaux, C., García-del Portillo, F., Pucciarelli, M.G., Ortega, A.D., 2021. Pathogenicity and virulence of Listeria monocytogenes: A trip from environmental to medical microbiology. Virulence 12, 2509–2545. https://doi.org/10.1080/21505594.2021.1975526

Radoshevich, L., Cossart, P., 2018. *Listeria monocytogenes*: towards a complete picture of its physiology and pathogenesis. Nat. Rev. Microbiol. 16, 32–46. https://doi.org/10.1038/nrmicro.2017.126

Raengpradub, S., Wiedmann, M., Boor, K.J., 2008. Comparative analysis of the σB-dependent stress responses in *Listeria monocytogenes* and *Listeria innocua* strains exposed to selected stress conditions. Appl. Environ. Microbiol. 74, 158–171. https://doi.org/10.1128/AEM.00951-07

Ragon, M., Wirth, T., Hollandt, F., Lavenir, R., Lecuit, M., Monnier, A.L., Brisse, S., 2008. A New Perspective on Listeria monocytogenes Evolution. PLOS Pathogens 4, e1000146. https://doi.org/10.1371/journal.ppat.1000146

Rajkovic, A., Smigic, N., Uyttendaele, M., Medic, H., de Zutter, L., Devlieghere, F., 2009. Resistance of Listeria monocytogenes, Escherichia coli O157:H7 and Campylobacter jejuni after exposure to repetitive cycles of mild bactericidal treatments. Food Microbiol 26, 889–895. https://doi.org/10.1016/j.fm.2009.06.006

Rasmussen, O.F., Skouboe, P., Dons, L., Rossen, L., Olsen, J.E., 1995. Listeria monocytogenes exists in at least three evolutionary lines: Evidence from flagellin, invasive associated protein and listeriolysin O genes. Microbiology 141, 2053–2061. https://doi.org/10.1099/13500872-141-9-2053

Ribot, E.M., Freeman, M., Hise, K.B., Gerner-Smidt, P., 2019. PulseNet: Entering the Age of Next-Generation Sequencing. Foodborne Pathog Dis 16, 451–456. https://doi.org/10.1089/fpd.2019.2634

Roberts, A., Nightingale, K., Jeffers, G., Fortes, E., Kongo, J.M., Wiedmann, M., 2006. Genetic and phenotypic characterization of Listeria monocytogenes lineage III. Microbiology 152, 685–693. https://doi.org/10.1099/mic.0.28503-0

Ryall, B., Eydallin, G., Ferenci, T., 2012. Culture history and population heterogeneity as determinants of bacterial adaptation: The adaptomics of a single environmental transition. Microbiol. Mol. Biol. Rev. 76, 597–625. https://doi.org/10.1128/MMBR.05028-11

Rychli, K., Wagner, E., Guinane, C.M., Daly, K., Hill, C., Cotter, P.D., 2021. Generation of nonpolar deletion mutants in *Listeria monocytogenes* using the "SOEing" method, in: Fox, E.M., Bierne, H., Stessl, B. (Eds.), Listeria Monocytogenes: Methods and Protocols, Methods in Molecular Biology. Springer US, New York, NY, pp. 165–175. https://doi.org/10.1007/978-1-0716-0982-8_13

Santos-Beneit, F., 2015. The Pho regulon: A huge regulatory network in bacteria. Front. Microbiol. 6, 402. https://doi.org/10.3389/fmicb.2015.00402

Sashital, D.G., Greeman, C.A., Lyumkis, D., Potter, C.S., Carragher, B., Williamson, J.R., 2014. A combined quantitative mass spectrometry and electron microscopy analysis of ribosomal 30S subunit assembly in *E. coli*. eLife 3, e04491. https://doi.org/10.7554/eLife.04491

Sasindran, S.J., Saikolappan, S., Scofield, V.L., Dhandayuthapani, S., 2011. Biochemical and physiological characterization of the GTP-binding protein

Obg of *Mycobacterium tuberculosis*. BMC Microbiol. 11, 43. https://doi.org/10.1186/1471-2180-11-43

Sauders, B.D., D'Amico, D.J., 2016. *Listeria monocytogenes* cross-contamination of cheese: risk throughout the food supply chain. Epidemiol. Infect. 144, 2693–2697. https://doi.org/10.1017/S0950268816001503

Schlech, W.F., Lavigne, P.M., Bortolussi, R.A., Allen, A.C., Haldane, E.V., Wort, A.J., Hightower, A.W., Johnson, S.E., King, S.H., Nicholls, E.S., Broome, C.V., 1983. Epidemic listeriosis–evidence for transmission by food. N Engl J Med 308, 203–206. https://doi.org/10.1056/NEJM198301273080407

Scott, J.M., Haldenwang, W.G., 1999. Obg, an essential GTP binding protein of *Bacillus subtilis*, is necessary for stress activation of transcription factor ςB. J. Bacteriol. 181, 4653–4660. https://doi.org/10.1128/JB.181.15.4653-4660.1999

Seeliger, H.P.R., Höhne, K., 1979. Chapter II Serotyping of Listeria monocytogenes and Related Species, in: Bergan, T., Norris, J.R. (Eds.), Methods in Microbiology. Academic Press, pp. 31–49. https://doi.org/10.1016/S0580-9517(08)70372-6

Shah, P., Ding, Y., Niemczyk, M., Kudla, G., Plotkin, J.B., 2013. Rate-limiting steps in yeast protein translation. Cell 153, 1589–1601. https://doi.org/10.1016/j.cell.2013.05.049

Shi, L., Pigeonneau, N., Ravikumar, V., Dobrinic, P., Macek, B., Franjevic, D., Noirot-Gros, M.-F., Mijakovic, I., 2014. Cross-phosphorylation of bacterial serine/threonine and tyrosine protein kinases on key regulatory residues. Front. Microbiol. 5, 495. https://doi.org/10.3389/fmicb.2014.00495

Shin, J.-H., Brody, M.S., Price, C.W., 2010. Physical and antibiotic stresses require activation of the RsbU phosphatase to induce the general stress response in *Listeria monocytogenes*. Microbiology 156, 2660–2669. https://doi.org/10.1099/mic.0.041202-0

Shine, J., Dalgarno, L., 1974. The 3'-terminal sequence of *Escherichia coli* 16S ribosomal RNA: complementarity to nonsense triplets and ribosome binding sites. Proc. Natl. Acad. Sci. U.S.A. 71, 1342–1346. https://doi.org/10.1073/pnas.71.4.1342

Sigrist, C.J.A., de Castro, E., Cerutti, L., Cuche, B.A., Hulo, N., Bridge, A., Bougueleret, L., Xenarios, I., 2013. New and continuing developments at PROSITE. Nucleic Acids Res. 41, D344–D347. https://doi.org/10.1093/nar/gks1067

Simmons, C., Stasiewicz, M.J., Wright, E., Warchocki, S., Roof, S., Kause, J.R., Bauer, N., Ibrahim, S., Wiedmann, M., Oliver, H.F., 2014. *Listeria monocytogenes* and *Listeria* spp. Contamination patterns in retail delicatessen establishments in three U.S. states. J. Food Prot. 77, 1929–1939. https://doi.org/10.4315/0362-028X.JFP-14-183

Smaczniak, C., Immink, R.G.H., Muiño, J.M., Blanvillain, R., Busscher, M., Busscher-Lange, J., Dinh, Q.D.P., Liu, S., Westphal, A.H., Boeren, S., Parcy, F., Xu, L., Carles, C.C., Angenent, G.C., Kaufmann, K., 2012. Characterization of MADS-domain transcription factor complexes in *Arabidopsis* flower development. Proc. Natl. Acad. Sci. U.S.A. 109, 1560–1565. https://doi.org/10.1073/pnas.1112871109

Smith, K., Youngman, P., 1992. Use of a new integrational vector to investigate compartment-specific expression of the *Bacillus subtilis spollM* gene. Biochimie 74, 705–711. https://doi.org/10.1016/0300-9084(92)90143-3

Smits, W.K., Kuipers, O.P., Veening, J.-W., 2006. Phenotypic variation in bacteria:

The role of feedback regulation. Nat. Rev. Microbiol. 4, 259–271. https://doi.org/10.1038/nrmicro1381

Sohmen, D., Chiba, S., Shimokawa-Chiba, N., Innis, C.A., Berninghausen, O., Beckmann, R., Ito, K., Wilson, D.N., 2015. Structure of the *Bacillus subtilis* 70S ribosome reveals the basis for species-specific stalling. Nat. Commun. 6, 6941. https://doi.org/10.1038/ncomms7941

Solopova, A., Bachmann, H., Teusink, B., Kok, J., Neves, A.R., Kuipers, O.P., 2012. A specific mutation in the promoter region of the silent *cel* cluster accounts for the appearance of lactose-utilizing *Lactococcus lactis* MG1363. Appl. Environ. Microbiol. 78, 5612–5621. https://doi.org/10.1128/AEM.00455-12

Sørensen, K.I., Hove-Jensen, B., 1996. Ribose catabolism of *Escherichia coli*: characterization of the *rpiB* gene encoding ribose phosphate isomerase B and of the *rpiR* gene, which is involved in regulation of *rpiB* expression. J. Bacteriol. 178, 1003–1011. https://doi.org/10.1128/jb.178.4.1003-1011.1996

Stasiewicz, M.J., Oliver, H.F., Wiedmann, M., Den Bakker, H.C., 2015. Whole genome sequencing allows for improved identification of persistent *Listeria monocytogenes* in food associated environments. Appl. Environ. Microbiol. AEM.01049–15. https://doi.org/10.1128/AEM.01049-15

Stoll, R., Goebel, W., 2010. The major PEP-phosphotransferase systems (PTSs) for glucose, mannose and cellobiose of *Listeria monocytogenes*, and their significance for extra- and intracellular growth. Microbiology 156, 1069–1083. https://doi.org/10.1099/mic.0.034934-0

Takada, H., Morita, M., Shiwa, Y., Sugimoto, R., Suzuki, S., Kawamura, F., Yoshikawa, H., 2014. Cell motility and biofilm formation in *Bacillus subtilis* are affected by the ribosomal proteins, S11 and S21. Biosci. Biotechnol. Biochem. 78, 898–907. https://doi.org/10.1080/09168451.2014.915729

Taylor, C.M., Beresford, M., Epton, H.A.S., Sigee, D.C., Shama, G., Andrew, P.W., Roberts, I.S., 2002. *Listeria monocytogenes relA* and *hpt* mutants are impaired in surface-attached growth and virulence. J. Bacteriol. 184, 621–628. https://doi.org/10.1128/jb.184.3.621-628.2002

Thomas, J., Govender, N., McCarthy, K.M., Erasmus, L.K., Doyle, T.J., Allam, M., Ismail, A., Ramalwa, N., Sekwadi, P., Ntshoe, G., Shonhiwa, A., Essel, V., Tau, N., Smouse, S., Ngomane, H.M., Disenyeng, B., Page, N.A., Govender, N.P., Duse, A.G., Stewart, R., Thomas, T., Mahoney, D., Tourdjman, M., Disson, O., Thouvenot, P., Maury, M.M., Leclercq, A., Lecuit, M., Smith, A.M., Blumberg, L.H., 2020. Outbreak of Listeriosis in South Africa Associated with Processed Meat. N Engl J Med 382, 632–643. https://doi.org/10.1056/NEJMoa1907462

Toledo-Arana, A., Dussurget, O., Nikitas, G., Sesto, N., Guet-Revillet, H., Balestrino, D., Loh, E., Gripenland, J., Tiensuu, T., Vaitkevicius, K., Barthelemy, M., Vergassola, M., Nahori, M.-A., Soubigou, G., Régnault, B., Coppée, J.-Y., Lecuit, M., Johansson, J., Cossart, P., 2009. The *Listeria* transcriptional landscape from saprophytism to virulence. Nature 459, 950–956. https://doi.org/10.1038/nature08080

Torsten, S., 2015. Snippy: fast bacterial variant calling from NGS reads.

Trabelsi, H., Dhali, D., Yaseen, Y., Leclère, V., Jacques, P., Coutte, F., 2021. Chapter 9 - *Bacillus subtilis*-based microbial cell factories, in: Singh, V. (Ed.), Microbial Cell Factories Engineering for Production of Biomolecules. Academic Press, pp. 139–164. https://doi.org/10.1016/B978-0-12-821477-0.00002-7

Tran, B.M., Linnik, D.S., Punter, C.M., Śmigiel, W.M., Mantovanelli, L., Iyer, A., O'Byrne, C., Abee, T., Johansson, J., Poolman, B., 2023. Super-resolving microscopy reveals the localizations and movement dynamics of stressosome proteins in Listeria monocytogenes. Commun Biol 6, 1–15. https://doi.org/10.1038/s42003-023-04423-y

Trautmann, H.S., Ramsey, K.M., 2022. A ribosomal protein homolog governs gene expression and virulence in a bacterial pathogen. J. Bacteriol. 204, e00268–22. https://doi.org/10.1128/jb.00268-22

Trautmann, H.S., Schmidt, S.S., Gregory, S.T., Ramsey, K.M., Comstock, L.E., 2023. Ribosome heterogeneity results in leader sequence-mediated regulation of protein synthesis in *Francisella tularensis*. J. Bacteriol. 205, e0014023. https://doi.org/10.1128/jb.00140-23

Tyanova, S., Temu, T., Sinitcyn, P., Carlson, A., Hein, M.Y., Geiger, T., Mann, M., Cox, J., 2016. The Perseus computational platform for comprehensive analysis of (prote)omics data. Nat. Methods. 13, 731–740. https://doi.org/10.1038/nmeth.3901

UN Committee on Economic, S. and C.R.(CESCR)., 1999. General Comment No. 12: The right to adequate food (art. 11).

United Nations (General Assembly), 1966. International covenant on economic, social, and cultural rights. Treaty Series 999, 171.

Utratna, M., Cosgrave, E., Baustian, C., Ceredig, R.H., O'Byrne, C.P., 2014. Effects of growth phase and temperature on σB activity within a *Listeria monocytogenes* population: Evidence for RsbV-independent activation of σB at refrigeration temperatures. Biomed Res. Int. 2014, 641647. https://doi.org/10.1155/2014/641647

Utratna, M., Cosgrave, E., Baustian, C., Ceredig, R., O'Byrne, C., 2012. Development and optimization of an EGFP-based reporter for measuring the general stress response in *Listeria monocytogenes*. Bioengineered 3, 93–103. https://doi.org/10.4161/bbug.19476

Vaestermark, A., Saier, M.H., 2014. The involvement of transport proteins in transcriptional and metabolic regulation. Curr. Opin. Microbiol. 18, 8–15. https://doi.org/10.1016/j.mib.2014.01.002

Van Boeijen, I.K.H., Francke, C., Moezelaar, R., Abee, T., Zwietering, M.H., 2011. Isolation of highly heat-resistant *Listeria monocytogenes* variants by use of a kinetic modeling-based sampling scheme. Appl. Environ. Microbiol. 77, 2617–2624. https://doi.org/10.1128/AEM.02617-10

Van Boeijen, I.K.H., Moezelaar, R., Abee, T., Zwietering, M.H., 2008. Inactivation kinetics of three *Listeria monocytogenes* strains under high hydrostatic pressure. J. Food Prot. 71, 2007–2013. https://doi.org/10.4315/0362-028x-71.10.2007

Van Duin, J., Wijnands, R., 1981. The function of ribosomal protein S21 in protein synthesis. Eur. J. Biochem. 118, 615–619. https://doi.org/10.1111/j.1432-1033.1981.tb05563.x

Varadi, M., Anyango, S., Deshpande, M., Nair, S., Natassia, C., Yordanova, G., Yuan, D., Stroe, O., Wood, G., Laydon, A., Žídek, A., Green, T., Tunyasuvunakool, K., Petersen, S., Jumper, J., Clancy, E., Green, R., Vora, A., Lutfi, M., Figurnov, M., Cowie, A., Hobbs, N., Kohli, P., Kleywegt, G., Birney, E., Hassabis, D., Velankar, S., 2022. AlphaFold Protein Structure Database: massively expanding the structural coverage of protein-sequence space with high-accuracy models.

Nucleic Acids Res. 50, D439–D444. https://doi.org/10.1093/nar/gkab1061
Verstraeten, N., Fauvart, M., Versées, W., Michiels, J., 2011. The universally conserved prokaryotic GTPases. Microbiol. Mol. Biol. Rev. 75, 507–542. https://doi.org/10.1128/MMBR.00009-11
Vijay, K., Brody, M.S., Fredlund, E., Price, C.W., 2000. A PP2C phosphatase containing a PAS domain is required to convey signals of energy stress to the sigma(B) transcription factor of *Bacillus subtilis*. Mol. Microbiol. 35, 180–188. https://doi.org/10.1046/j.1365-2958.2000.01697.x
Vongkamjan, K., Roof, S., Stasiewicz, M.J., Wiedmann, M., 2013. Persistent *Listeria monocytogenes* subtypes isolated from a smoked fish processing facility included both phage susceptible and resistant isolates. Food Microbiol. 35, 38–48. https://doi.org/10.1016/j.fm.2013.02.012
Walker, B.J., Abeel, T., Shea, T., Priest, M., Abouelliel, A., Sakthikumar, S., Cuomo, C.A., Zeng, Q., Wortman, J., Young, S.K., Earl, A.M., 2014. Pilon: An integrated tool for comprehensive microbial variant detection and genome assembly improvement. PLoS One 9, e112963. https://doi.org/10.1371/journal.pone.0112963
Walker, S.j., Archer, P., Banks, J.g., 1990. Growth of Listeria monocytogenes at refrigeration temperatures. Journal of Applied Bacteriology 68, 157–162. https://doi.org/10.1111/j.1365-2672.1990.tb02561.x
Walsh, I.M., Bowman, M.A., Soto Santarriaga, I.F., Rodriguez, A., Clark, P.L., 2020. Synonymous codon substitutions perturb cotranslational protein folding in vivo and impair cell fitness. Proc. Natl. Acad. Sci. U.S.A. 117, 3528–3534. https://doi.org/10.1073/pnas.1907126117
Wang, W., Li, W., Ge, X., Yan, K., Mandava, C.S., Sanyal, S., Gao, N., 2020. Loss of a single methylation in 23S rRNA delays 50S assembly at multiple late stages and impairs translation initiation and elongation. Proc. Natl. Acad. Sci. U.S.A. 117, 15609–15619. https://doi.org/10.1073/pnas.1914323117
Ward, T.J., Ducey, T.F., Usgaard, T., Dunn, K.A., Bielawski, J.P., 2008. Multilocus Genotyping assays for single nucleotide polymorphism-based subtyping of *Listeria monocytogenes* isolates. Applied and Environmental Microbiology 74, 7629–7642. https://doi.org/10.1128/AEM.01127-08
Watson, Z.L., Ward, F.R., Méheust, R., Ad, O., Schepartz, A., Banfield, J.F., Cate, J.H., 2020. Structure of the bacterial ribosome at 2 Å resolution. eLife 9, e60482. https://doi.org/10.7554/eLife.60482
Wen, J.-D., Kuo, S.-T., Chou, H.-H.D., 2021. The diversity of Shine-Dalgarno sequences sheds light on the evolution of translation initiation. RNA Biol. 18, 1489–1500. https://doi.org/10.1080/15476286.2020.1861406
Wendrich, J.R., Boeren, S., Möller, B.K., Weijers, D., De Rybel, B., 2017. *In vivo* identification of plant protein complexes using IP-MS/MS, in: Kleine-Vehn, J., Sauer, M. (Eds.), Plant Hormones: Methods and Protocols, Methods in Molecular Biology. Springer, New York, NY, pp. 147–158. https://doi.org/10.1007/978-1-4939-6469-7_14
Williams, A.H., Redzej, A., Rolhion, N., Costa, T.R.D., Rifflet, A., Waksman, G., Cossart, P., 2019. The cryo-electron microscopy supramolecular structure of the bacterial stressosome unveils its mechanism of activation. Nat. Commun. 10, 1–10. https://doi.org/10.1038/s41467-019-10782-0
Wiśniewski, J.R., Zougman, A., Nagaraj, N., Mann, M., 2009. Universal sample

preparation method for proteome analysis. Nat. Methods 6, 359–362. https://doi.org/10.1038/nmeth.1322

Wu, J., McAuliffe, O., O'Byrne, C.P., 2023. Trehalose transport occurs via TreB in Listeria monocytogenes and it influences biofilm development and acid resistance. International Journal of Food Microbiology 394, 110165. https://doi.org/10.1016/j.ijfoodmicro.2023.110165

Wu, T., Hu, E., Xu, S., Chen, M., Guo, P., Dai, Z., Feng, T., Zhou, L., Tang, W., Zhan, L., Fu, X., Liu, S., Bo, X., Yu, G., 2021. clusterProfiler 4.0: A universal enrichment tool for interpreting omics data. The Innovation 2, 100141. https://doi.org/10.1016/j.xinn.2021.100141

Xia, Y., Xin, Y., Li, X., Fang, W., 2016. To modulate survival under secondary stress conditions, *Listeria monocytogenes* 10403S employs RsbX to downregulate sigma(B) activity in the poststress recovery stage or stationary phase. Appl. Environ. Microbiol. 82, 1126–1135. https://doi.org/10.1128/AEM.03218-15

Yamamoto, H., Serizawa, M., Thompson, J., Sekiguchi, J., 2001. Regulation of the *glv* operon in *Bacillus subtilis*: YfiA (GlvR) is a positive regulator of the operon that is repressed through CcpA and *cre*. J. Bacteriol. 183, 5110–5121. https://doi.org/10.1128/JB.183.17.5110-5121.2001

Yu, C.-H., Dang, Y., Zhou, Z., Wu, C., Zhao, F., Sachs, M.S., Liu, Y., 2015. Codon usage influences the local rate of translation elongation to regulate co-translational protein folding. Mol Cell 59, 744–754. https://doi.org/10.1016/j.molcel.2015.07.018

Zhang, Y., Chen, W., Wu, D., Liu, Y., Wu, Z., Li, J., Zhang, S.-Y., Ji, Q., 2022. Molecular basis for cell-wall recycling regulation by transcriptional repressor MurR in *Escherichia coli*. Nucleic Acids Res. 50, 5948–5960. https://doi.org/10.1093/nar/gkac442

Zilelidou, E.A., Rychli, K., Manthou, E., Ciolacu, L., Wagner, M., Skandamis, P.N., 2015. Highly invasive *Listeria monocytogenes* strains have growth and invasion advantages in strain competition. PLoS ONE 10, e0141617. https://doi.org/10.1371/journal.pone.0141617

Zilelidou, E., Karmiri, C.-V., Zoumpopoulou, G., Mavrogonatou, E., Kletsas, D., Tsakalidou, E., Papadimitriou, K., Drosinos, E., Skandamis, P., 2016a. *Listeria monocytogenes* strains underrepresented during selective enrichment with an ISO method might dominate during passage through simulated gastric fluid and *in vitro* infection of Caco-2 cells. Appl. Environ. Microbiol. 82, 6846–6858. https://doi.org/10.1128/AEM.02120-16

Zilelidou, E., Manthou, E., Skandamis, P., 2016b. Growth differences and competition between *Listeria monocytogenes* strains determine their predominance on ham slices and lead to bias during selective enrichment with the ISO protocol. Int. J. Food Microbiol. 235, 60–70. https://doi.org/10.1016/j.ijfoodmicro.2016.07.016

Appendices

Summary

Acknowledgements

Affiliations of co-authors

About the author

Overview of completed training activities

Summary

To ensure the right to safe food, efficient strategies are required to control foodborne pathogens throughout the food supply chain. Among these pathogens, *Listeria monocytogenes* is particularly notable due to its low incidence but high case-fatality rates, ranging from 12 to 41 percent . This organism is ubiquitous, capable of being isolated from a wide range of environments including natural habitats, farms, silage, decaying vegetables, food production facilities, refrigerators, as well as human and animal feces. To adapt and survive the challenging conditions it encounters from soil to human hosts, *L. monocytogenes* employs a variety of protective strategies, one of which is population heterogeneity. Population heterogeneity, encompassing both genetic and non-genetic variability, generates phenotypic variation within a population, contributing to its fitness, adaptation, and survival. During the process of pathogen inactivation, variations in stress resistance among individual cells can cause deviations from expected linear inactivation patterns, resulting in a higher-than-expected number of surviving cells and selection of stress-resistant variants.

Previously, 23 stable stress resistance *L. monocytogenes* variants have been isolated upon acid treatment of *L. monocytogenes* strain LO28, and 11 of the 23 variants had mutations in the *rpsU* gene locus, which encodes the ribosome 30S small sub-unit protein S21 (RpsU) These stress-resistant *rpsU* variants showed a trade-off between increased resistance and reduced growth rates. Further studies of the *rpsU* deletion variant V14 and the $rpsU^{G50C}$ variant V15 showed that both variants shared similar gene expression profiles and phenotypes compared to the WT. These findings suggest that *rpsU* deletion and the $rpsU^{G50C}$ mutation may impact the phenotype through a similar mechanism. Evolutionary experiments of variant V15 revealed that single amino acid substitutions in RpsU can facilitate a switch between states of high fitness and high stress resistance in *L. monocytogenes*, rising questions if variant V14 with complete *rpsU* deletion could also undergo a similar switching between multi-stress resistant and high fitness states.

In **Chapter 2**, we explored the potential for V14 to revert to a WT-like phenotype by employing an experimental evolution protocol selecting for increased fitness. This led to the discovery of evolved variants 14EV1 and 14EV2, exhibiting WT-like fitness and stress sensitivity. Genotyping of 14EV1 and 14EV2 provided evidence for unique point-mutations in the ribosomal *rpsB* gene causing amino acid substitutions at the same protein sequence position in RpsB. Combined with data obtained with constructed mutants in the V14 background, we provided evidence that loss of RpsU resulting in the multiple stress resistant and reduced fitness phenotype could be reversed by single point mutations in *rpsB* leading to arginine substitutions in RpsB.

In **Chapter 3**, we focused on the molecular mechanism of SigB activation in the *L. monocytogenes* $rpsU^{G50C}$ mutants. We introduced the $rpsU^{G50C}$ mutation into the *L. monocytogenes* EGDe wild type and the Δ*sigB*, Δ*rsbV* and Δ*rsbR1* mutant strains and investigated the acid and heat stress resistance, growth rate, and SigB activation with a combination of a phenotype and proteomics approach. We found that the increased stress resistance in the $rpsU^{G50C}$ mutant resulted from SigB activation through an unknown mechanism distinct from the classical stressosome and RsbV/RsbW partner switching model. Moreover, the reduced maximum specific growth rate of the $rpsU^{G50C}$ mutant was unrelated to SigB activation and potentially linked to impaired ribosomal function.

In **Chapter 4**, our investigation into the *rpsU* gene variation within the NCBI *L. monocytogenes* genome database revealed an extraordinarily high level of conservation. To determine whether the detection chance of *rpsU* variants differs from that of WT strains when using enrichment-based detection methods, we conducted a comprehensive analysis, including growth kinetics analysis, co-culture prediction, and subsequent qPCR validation. These experiments were performed using the LO28 WT, along with the V14 and V15 variants, and two commonly employed enrichment-based procedures. The results indicated that the detection chances for *rpsU* mutants were notably reduced during the enrichment process when the LO28 WT was present. This finding suggested the selective enrichment procedures inadequately represented the genotypic diversity present in a sample. Consequently, the enrichment bias during the *L. monocytogenes* isolation procedure might contribute to the observed underrepresentation of the *rpsU* mutation in *L. monocytogenes* isolates deposited in publicly available genome databases.

In **Chapter 5**, following a screening of a collection of *L. monocytogenes* strains for the capacity to use lactose as a growth substrate, the cheese outbreak-associated F2365 strain with low lactose utilization efficiency has been identified, which had a frameshift mutation ($lacR^{887del}$) resulting in a truncated LacR. Via experimental evolution of the ancestral strain, an evolved isolate F2365 EV was obtained, which showed enhanced growth and metabolism of lactose. An additional point mutation $lmo2766^{C415T}$ was identified in F2365 EV, resulting in an amino acid substitution in the putative regulator Lmo2766. Together with additional growth and HPLC experiments using mutants constructed in lactose-positive *L. monocytogenes* EGDe, this chapter demonstrated that an amino acid substitution in the Lmo2766 regulator activates a previously silent lactose utilization pathway encoded by operon *lmo2761-2765*, facilitating the growth and metabolism of *L. monocytogenes* with lactose as a substrate. This finding enhances our understanding of the metabolic capabilities and adaptability of *L. monocytogenes*, offering a broader view of the lactose utilization of this pathogen.

Finally, **Chapter 6** revisited key findings of this thesis and hypotheses regarding RsbV-independent SigB activation in *L. monocytogenes* are proposed. The persistence of *rpsU* mutants of *L. monocytogenes* and other pathogens including *Staphylococcus aureus* in specific environments is explored and possible impact on contamination and safety of food is discussed. In addition, investigating the prevalence of truncated LacR in the *L. monocytogenes* genome database revealed an association between truncated LacR and dairy isolates.

In conclusion, this thesis highlights the genetic diversity and adaptation capabilities of

L. monocytogenes stress resistance, growth performance, and carbon source utilization using isolates from different origins, evolved variants and constructed mutants. A deeper mechanistic understanding of these adaptations can contribute to better controlling of this foodborne pathogen, thereby enhancing food safety and quality.

Acknowledgements

Since I was a child, I've harbored the dream of becoming a scientist. Now, thanks to all these generous supports and pivotal opportunities, I've realized this dream by earning my PhD. I want to express my heartfelt gratitude to everyone who has been part of my PhD journey. Without your support and companionship, I wouldn't have reached this significant milestone in my life and career.

First of all, I would like to thank my promotors and supervisors, **Prof. Tjakko Abee**, **Prof. Heidy den Besten**, and **Prof. Marcel Zwietering**. Your willingness to guide me through the interesting and challenging PhD topic is invaluable, helping me forge my path as an independent scientist. **Tjakko**, I always feel so grateful to be your student since my master study. No matter what kind of challenges I met, in research and in life, you could always bring great ideas and solutions with your vast knowledge and kindness. Your enthusiasm for science has inspired me to passionately explore nature, while your critical mindset has grounded me in making sound conclusions. **Heidy**, your expertise in food safety and project management is exemplary. When I lost in big data and complex questions, you could always steer me towards clarity and efficiency Your guidance has been crucial in teaching me the art of balancing the infinite scientific questions with the finite research time, a skill essential for contributing meaningful knowledge to our society. **Marcel**, you have not only helped me in refining the details of my work with keen insights but also provided me broad and long-term suggestions from a high vantage point. Moreover, your kindness and leadership, particularly during the challenging times of COVID, made me feel so many supports from our group. I will always remember the positive and collaborative atmosphere in FHM.

I also extend my sincere gratitude to **Prof. Michiel Kleerebezem**, **Prof. Colin Hill**, **Dr. Masja Nierop Groot** and **Dr. Aldert Zomer** for accepting the invitation to be on the thesis committee. Thank you for taking your time to meticulously review my thesis.

I also thank all the co-authors from other department at Wageningen University or other organizations involved in this thesis. A special thanks to **Prof. Conor O'Byrne** from the University of Galway for your invaluable expertise in *Listeria* and your timely responses that greatly assisted my research. I would also like to thank **Sjef Boeren** for the Laboratory of Biochemistry for proteomics analysis. Sjef, your exceptional teaching skills, patience, and positivity have not only enhanced my learning experience but have also greatly contributed to the success of my research. I also extend my gratitude to **Jingjie Chen** from Yunnan University for your invaluable assistance in bioinformatics analysis.

I have spent five years at the Laboratory of Food Microbiology, a period filled with cherished memories thanks to my wonderful colleagues. From weekly VrijMiBo, Thursday running, sports events to annually lab outings, PhD weekends, BBQs, cleaning days, department dinners and PhD trip, each moment has contributed to an unforgettable journey. I'd like to take a moment to walk through each office and extend my personal thanks to each one.

A heartfelt thanks to my dear office mates in X2111. **Maren**, you've been like a sister, always looking out for me and creating countless wonderful memories. From PhD weekends in Stevensbeek to sharing delicious cookies during Christmas, enjoying PlayStation games, and tackling escape rooms in Athens, your joyful laughter will always make me happy. **Jasper B.**, you know how I love to take photos of you. This is not only because you are handsome, but also for the joy and laughter you bring to our surroundings **Pjotr**, thank you for all the nice talks about games, life and mandarin. Thanks to your help, I could managed to keep a plant alive in my room. **Johanna**, your vibrant energy and spirit have a way of brightening everyone's day. Your presence has added color and vitality to our office. **Clara**, your dedication and hard working are truly inspiring. I have no doubt that your PhD journey will be marked by remarkable achievements. **Thelma**, thank you for your kind words when I got sick. Sharing wine beside Lake Geneva is an unforgettable memory. And to **Xing**, my old classmate, dear friend, and paranymph, your unwavering support, especially in the final year of my PhD, has been a pillar of strength. Having you as my paranymph was an honor. I wish you all the success in your PhD journey and know that I'll always be there to support you as well.

Gerda, over the past few years, I've reached out to you countless times through emails seeking assistance. You've consistently addressed every issue with perfect solutions. Your unwavering support has been invaluable, and for that, I am truly grateful.

Marcel T., your support as a colleague has been invaluable. Your expertise and willingness to assist in the lab have significantly eased my workload. Outside of work, you've been a wonderful friend. Our table tennis games, beer after sports, and conversations about life and the future have been truly enjoyable. Your unique table tennis skills will always be a cherished memory. **Dennis**, I'm grateful for your insightful advice on molecular biology and your support in setting up the workstation (after scavenger hunt). Conversations with you are always enlightening, thanks to your extensive knowledge. **Anne**, thank you for taking over the GitLab group, and I wish you collect more interesting glasses.

Eddy, your constant gentle smile is a source of joy. Thank you for enriching our coffee breaks with your fascinating stories.

Oscar, I'm deeply appreciative of your assistance with my HPLC analysis and for sharing the wonderful foods you've fermented or harvested from your garden. The night we spent enjoying homemade pizza and cheering for the Dutch national team during the World Cup is a memory I'll always treasure. **Jeroen**, I am grateful for all the invaluable skills you taught me throughout my master's and PhD studies. It has been an honor to continue your project and to stand with you during your PhD defence. **Frank**, working in the same lab with you has brought me so much joy. Your passion for work, humility, and kindness set an example I strive to follow. You are truly a role model to me! **Alex**, I'm grateful for the proteomics analysis scripts and the

guidance on thesis writing via Rmarkdown you shared with me. **Soundarya**, thank you for all your assistance with ISO standard questions. Your expertise has been invaluable in navigating those complexities. **Jasper Z.**, your table soccer skills are truly fascinating. Watching you play is always a highlight. **Cristina**, your laughter and humorous stories bring so much joy to our coffee room. Your presence always brightens the atmosphere.

Andy, the breadth of knowledge I've gained from you is immense. From conducting experiments in the lab and performing data analysis on the computer, to networking with other scientists and planning my career, your guidance has been always invaluable. Your insightful suggestions have consistently brought clarity to my thoughts. Thank you for everything. **Sylviani**, you are such a hospitable person. I'm grateful for the delightful meals you've prepared, from rendang to hotpot and kimchi, and for the memorable New Year celebrations you've hosted. Your culinary skills are truly exceptional. **Angela**, your empathy shines through in every interaction. Our conversations during coffee breaks and VrijMiBo have been a source of comfort and joy. **George**, my charismatic friend, our endless discussions on coding, AI, and gastronomy have been incredibly enriching. And let's not forget your impressive dance moves when you are slightly tipsy—they're absolutely amazing! **Yingzhe**, thanks for sharing so many hilarious stories with me. Your humor was a much-needed relief during the intense final year of my studies.

James, my running coach, I'm grateful for your encouragement to step away from my desk. Thank you for helping me find a balance between work and life.

Wilma, I'm deeply thankful for your assistance and kindness during our time co-supervising lab courses. Your expertise in student supervision and lab management has been incredibly educational for me. **Judith**, your guidance on data management and consistent encouragement from my very first year have been invaluable. Thank you for your support and kindness. **Martine**, thank you for the guidance you've provided since my master's studies. Your knowledge of food safety and hygiene has significantly broadened my understanding of my PhD topic. **Yue L.**, I regard you as a true role model. Your dedication, emotional intelligence, and zest for life are truly inspirational. Thank you for your care and support during the challenging times brought on by COVID. The memories of sharing jianbing guozi, youtiao, hotpot, congee, and dancing moments are unforgettable. **Zhiwei**, I appreciate your help with the FHM news. Wish you have a great PhD journey too.

Claire, I'm truly grateful for your insightful suggestions regarding the SigB activation pathway, as well as for all the wonderful times we've shared including playing tennis, during PhD weekends, PhD trip, and the Veluweloop. I'm looking forward to hearing about your success with the tofu experiment soon. **Alberto G.**, I'm grateful for your assistance with coding and statistical analysis. The sausages you brought from Spain were truly amazing. **Richard**, I appreciated our engaging conversation during the department dinner.

Denja, thank you for your assistance in teaching. The PhD weekend in Stevensbeek was unforgettable. **Gamze**, your ability to make our work more interesting through comics is greatly appreciated. **Pol**, your passion for fermentation and education is truly inspiring. **Mark**, working alongside an old friend since our master's studies has been a pleasure. **Jori**, organizing such an nice lab outing activity deserves a special

thank you. **Carol**, the Brazilian snacks you prepared were delightful. Thank you for adding a taste of Brazil to our coffee break.

Linda, your representation of us in the PhD council and priet, along with your excellent organization of our PhD trip in 2022, is deeply appreciated. You truly embody the spirit of a heartfelt group leader. Additionally, your homemade cakes and stamppot are incredibly delicious. I wish you all the best in the final stages of your PhD journey. **Alberto B.**, thank you for the countless funny memories we've shared, from the Netherlands and Germany to Switzerland and Greece. Your sense of humor has been a beacon of light throughout my PhD journey. **Rebecca**, you are such a nice friend and wonderful chef. Your carbonara is the finest Italian dish I've ever had. **Domi**, working with you in the same lab has been a true pleasure. I'm grateful for all the wonderful memories we've created, from the city hunt in Zurich to making dumplings, playing table tennis, solving escape rooms, and celebrating New Year's Eve. **Tamara**, collaborating with you, particularly in organizing lab outings, has been a true delight. Sharing photos of adorable animals, especially cats, and attending the warm and hospitable parties at your place have added so much joy to my PhD journey. Wish you also enjoy your final year of your PhD journey. And **Kais**, although not officially part of our lovely team, you've felt like an integral member. Your conversations and advice on coding have been invaluable, and the snacks from your hometown are truly delicious.

Ingrid, thank you for keeping our lab so well-organized. The meticulous ordering and maintenance of media, chemicals, disposables, and equipment you handle lay the foundation for our daily work. Without your efforts, my work would not have progressed as smoothly.

Theo, thank you for consistently bringing interesting and delightful snacks to us. Your karaoke parties are truly unforgettable. **Luuk**, though your visits are infrequent, each one enriches me with intriguing ideas through our conversations.

I would like to thank MSc students **Chendi**, **Kirsten**, **Ziye** and **Danai**, who conducted their thesis under my PhD project.

I'm grateful to **Yvonne**, **Vesna**, and **Jochem** for their excellent organization of the VLAG courses and activities and for the support they've provided from VLAG.

I extend my special thanks to **Dr. Lucas Wijnands** and **Dr. Indra Bergval**. The research techniques and insights you imparted during my master's internship have been invaluable. And your ongoing encouragement throughout my PhD journey is deeply appreciated.

My thanks go to **Jochem**, **Tiny**, **Kasper**, **Deniz**, **Pieter**, **Frances**, and **Daniel** from the Bayesian peer consultation group. Exploring the new realms of statistics together has been an enjoyable journey.

I would also like to extend my heartfelt thanks to all my wonderful friends. Your support, especially during the challenging times of COVID, has meant a lot to me.

My friends from Dijkgraaf 4-16B, your companionship made the lockdown period far less daunting. **Juan**, amigo, thank you to be my paranymph. Your unwavering support whenever I've needed is invaluable. I'm truly fortunate to have you as my friend. Our memories in Dijkgraaf, Earth House, and Haarlem are treasures I will always hold.

Dan, your passion in life is incredibly inspiring. You embody the essence of "世上无难事，只怕有心人". Veel succes in het Verenigd Koninkrijk met je PhD. **Xilong**, finding someone with almost identical interests and hobbies is rare, but you are that person for me. I hope that one day in the future, we'll be able to enjoy frequent hangouts once again. **Cleo**, thank you for always being so considerate and thoughtful towards all your friends. I am deeply grateful for all the wonderful moments you've brought into my master and PhD life. **Wenjiao**, thank you for sharing your fascinating ideas about life and the future with me. I greatly admire your courage and passion for exploring the world. **Zhaoxiang**, you sense of responsibility and bravery are qualities I admire. I wish you enjoyment and fulfillment in the final stage of your PhD journey.

Guisheng, even though we haven't met in person for four years, your unwavering support from China has always been a strong source of encouragement for me. Thank you for always being there. **Wenjie**, **Xiaobing**, **Dengke**, **Taojun**, and **Chen**, you have been exemplary models for a successful PhD journey. I'm thankful for the valuable lessons and insights you've shared with me. **Tiantong** and **Ruobin**, collaborating with you during the One Health challenge of WFF has been a true pleasure. Thank you for the enjoyable times spent at parties, playing board games, and cycling together. **Shuo** and **Jingxuan**, thank you for the unforgettable moments during the Moon Festival, playing Mahjong, and enjoying homemade noodles. I wish you both the best in your new journeys. **Yifeng**, thank you for the engaging discussions about my research. The Guandan parties you organized were always fun. **Qimeng**, **Weiwei**, **Yifan L.**, **Shuchun** and **Yuting**, it has been an honor to meet such a fantastic group of new friends in the final year of my PhD. Thank you for all the wonderful activities we've shared, and I wish you all the best of luck in your studies and careers.

I extend my deepest gratitude to my girlfriend, **Qing Ren**, who is one of my most valued treasures and my strongest support during my PhD journey. Thank you for standing by my side and lifting my spirits during challenging times. You are my anchor, ensuring I never lose my way in the storm. Your love adds a profound layer of meaning to my achievements. Let us continue to grow and support each other in the journey of life ahead.

最后也是最重要的，我衷心地感谢故乡的父母和家人。你们是我最坚实的后盾，让我能追逐梦想。

As I reflect on reaching this milestone in my journey, I believe this is not an end but a continuation of the science adventure that lies before me. As the words from J.R.R. Tolkien:

"The road goes ever on and on,
down from the door where it began.
Now far ahead the road has gone,
and I must follow, if I can."

A

Affiliations of co-authors *

Jeroen Koomen, Alberto Bombelli, Marcel H. Tempelaars, Marcel H. Zwietering, Heidy M.W. den Besten, Tjakko Abee, Natalia Crespo Tapia, Oscar van Mastrigt

Food Microbiology, Wageningen University & Research, Wageningen, the Netherlands

Sjef Boeren

Laboratory of Biochemistry, Wageningen University & Research, Wageningen, the Netherlands

Conor O'Byrne

Bacterial Stress Response Group, Microbiology, Ryan Institute, School of Biological and Chemical Sciences, University of Galway, Ireland

Jingjie Chen

State Key Laboratory for Conservation and Utilization of Bio-Resources, School of Life Sciences, Center for Life Sciences, Yunnan University, Kunming, China

*Affiliations at the time of collaboration.

About the author

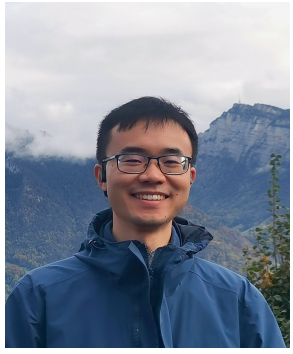

Xuchuan Ma (马虚船) was born on November 13, 1994, in Kunming, China. After graduating from the High School Affiliated to Yunnan Normal University, he went to the China Agricultural University for his Bachelor of Science (BSc) in Food Safety and Quality.

During his BSc, Xuchuan undertook a research training project under the National Innovation and Entrepreneurship Training Program at the Key Laboratory of Functional Dairy. This experience provided him with valuable skills in molecular biology and microbiology. He concluded his BSc with a thesis in the College of Food Science & Nutritional Engineering, which was recognized with an Outstanding Thesis Report award.

In 2017, Xuchuan moved to the Netherlands to start his Master of Science (MSc) in Food Safety at Wageningen University (WUR), specializing in Applied Food Safety. His thesis project at the Laboratory of Food Microbiology (WUR) focused on the phenotypic and genotypic characterization of *Listeria monocytogenes* variants, supervised by Dr. Jeroen Koomen and Prof. Tjakko Abee. Following his thesis, he completed an internship at the National Institute for Public Health and the Environment (RIVM), working on the virulence capacity of various *L. monocytogenes* strains, supervised by Dr. Indra Bergval, Dr. Lucas Wijnands, and Prof. Tjakko Abee.

In 2019, Xuchuan started a PhD project at the Laboratory of Food Microbiology (WUR), supported by a grant from the China Scholarship Council. His research, titled "Adaptive strategies of *Listeria monocytogenes*: evolved variants with altered stress resistance and fitness", is presented in this thesis.

Mail: xuchuan.ma@gmail.com

LinkedIn: linkedin.com/in/xuchuan-ma OR scan QR-code

Overview of completed training activities

Discipline specific activities

Name of the course/meeting	Organizing institute (s)	City	Year
Annual Fall KNVM Microbial Ecology Symposium	KNVM	Wageningen (NL)	2019
Wageningen Food Science Symposium	VLAG	Wageningen (NL)	2020
Annual Fall KNVM General and Molecular Microbiology Division	KNVM	Wageningen (NL)	2020
Alternative approaches to the risk management of *Listeria monocytogenes* in low risk foods	AFFI	Online	2020
EuroMicropH 6th Acidic Friday	EuroMicropH	Online	2021
Update on Food Safety	ICMSF	Online	2021
World Microbe Forum	ASM/FEMS	Online	2021
Big Data Analysis in the Life Sciences	VLAG	Wageningen (NL)	2021
Ecophysiology of food-associated micro-organisms: Roles in health and disease	VLAG	Wageningen (NL)	2021
Symposium "Foodborne pathogens revisited"	KNVM	Wageningen (NL)	2022
Diving deeper into the ICMSF approach to microbiological food safety management now and in the future	ICMSF	Online	2022
Advanced Course Microscopy and Spectroscopy in Food and Plant Sciences	EPS/VLAG	Wageningen (NL)	2022
FoodMicro 2022	ICFMH	Athens (Greece)	2022
Advanced Proteomics 8th edition	VLAG	Wageningen (NL)	2023
Intestinal microbiome of humans and animals 6th edition	VLAG	Wageningen (NL)	2023
Microbiome, metagenomics, and health implications	GGI	Online	2023
WHO Global Strategy for Food Safety 2022-2030	IAFP	Online	2023
Healthy and sustainable diets: synergies and trade-offs	VLAG	Wageningen (NL)	2023
KNVM Symposium Food Safety Risks of our Future Food	KNVM	Wageningen (NL)	2023
UNLOCK Symposium	UNLOCK	Wageningen (NL)	2023
KNVM General & Molecular Microbiology Fall Meeting	KNVM	Nijmegen (NL)	2023

General courses

Name of the course/meeting	Organizing institute (s)	City	Year
VLAG PhD week	VLAG	Baarlo (NL)	2020
Philosophy and Ethics of Food Science and Technology	VLAG	Wageningen (NL)	2020
Reviewing a Scientific Manuscript	WGS	Wageningen (NL)	2020
Using Python for Research	edX	Online	2020
Scientific Writing	WGS	Wageningen (NL)	2022
Bayesian Statistics	PE&RC	Wageningen (NL)	2023

Other activities

Name of the course/meeting	Organizing institute (s)	City	Year
Preparation of research proposal	FHM	Wageningen (NL)	2020
PhD study tour to Germany and Switzerland (Including organization)	FHM	DE & CH	2022
Department seminars	FHM	Wageningen (NL)	2019 - 2024

The research described in this thesis was performed at the Laboratory of Food Microbiology, Wageningen University & Research. Xuchuan Ma was supported by a grant from the China Scholarship Council (File No. 201907720086).

Financial support from Wageningen University for printing this thesis is gratefully acknowledged.

Cover design and thesis layout by Xuchuan Ma.

Printed by Proefschrifmaken.